

# **Investigations into Drug Delivery to the Eye: Nanoparticle Comparisons**

Yousef Al-ebini

Submitted to the University of Hertfordshire in partial  
fulfilment of the requirements of the degree of PhD

January 2014

## Abstract

Eye disorders are on the rise as a result of an ageing population, an increasing obesity problem and a growth in the number of diabetic patients. Conventional ophthalmic formulations do not maintain therapeutic drug concentration in the target tissues for a long duration due to the physiological and anatomical eye barriers. Novel delivery systems such as nanoparticles have been explored to enhance the delivery of therapeutic agents to the eye. These delivery systems have in general been assessed using *in-vivo* animal models, despite ethical concerns for animal wellbeing.

The aims of this thesis were to synthesise and characterise four amphiphilic polymers, subsequently prepare and characterise four nano sized polymeric self-assemblies loaded with triamcinolone acetonide (TA), develop an *in-vitro* porcine eye model and to evaluate the permeation of nano sized self-assemblies using the developed model.

Four comb-shaped amphiphilic polymers (Pa<sub>5</sub>, Pa<sub>5</sub>-MPEG, Ch<sub>5</sub> and Da<sub>10</sub>) were synthesised with a high yield (>81%) and good reproducibility. These polymers formed spontaneous positive self-assemblies in aqueous media (114-314 nm). The mean hydrodynamic diameters of the positive spontaneous self-assemblies entrapping TA were in the range of 200–334 nm loading high concentrations (455-1263 µg mL<sup>-1</sup>) of TA, much greater than the TA inherent aqueous solubility or concentrations achieved using conventional solubilisers.

A porcine *in-vitro* eye model was developed to assess drug permeation through anterior and posterior ocular tissues. The model was partially validated using tritiated water and a series of hydrophilic markers with increasing molecular weights. The integrity of porcine ocular tissue was checked by monitoring the

permeation of tritiated water to ensure the membrane intactness. Tritiated water permeation at 15 min was exploited as a potential method to normalise drug flux, as tritiated water percentage permeation at 15 min had an inverse relationship with tissue thickness ( $R^2 = 0.66$ ), to reduce the inherent variability between tissue samples thus increasing the accuracy of the *in-vitro* eye model. Four markers (fluorescein sodium salt, 4, 10 and 20 kDa FITC-dextran) were used for the purpose of investigating the effect of increasing molecular weight on ocular tissue permeability. The permeability of the markers displayed an inverse relationship and abrupt decline with Mw in terms of the permeability through scleral and corneal tissues of human and porcine and the molecular weight of the markers. The developed porcine *in-vitro* eye model showed good correlation with the human *in-vitro* model providing strong evidence it can be used to screen potential formulations before testing *in-vivo*.

The TA loaded self-assemblies and a few chemical enhancers (glutamic acid, tween 80, chitosan, Pa<sub>5</sub> and elevate temperature (45 °C)), selected to assist drug delivery via two routes (paracellular and transcellular), were tested using the developed *in-vitro* eye model. The results showed there was no marker permeation enhancement effect in porcine and human ocular tissues using chemical enhancers.

In summary, a porcine *in-vitro* eye model was developed to assess hydrophobic and hydrophilic penetrant permeation across anterior and posterior ocular tissues. The porcine *in-vitro* eye model showed good correlation with the human *in-vitro* model providing strong evidence that the porcine *in-vitro* eye model can be used to screen potential formulations before testing *in-vivo* using the porcine model which ultimately might correlate well with the *in-vivo* human responses. Although TA self-assemblies did not significantly increase drug flux through human or porcine

scleral tissues, it might be of interest for ophthalmic topically administered formulations due to their positive charge and small nano size.

## **Acknowledgment**

In the name of Allah the most beneficent the most merciful, I bear witness that there is no deity worthy of worship except Allah without any partners or peers, praise to Allah whom without his guidance and bounties won't reached this far in my life.

My sincere thanks goes to my family (especially mum, Samera, Waleed and Mais) for their continuous love, Doaa and their support financially and emotionally, whom without I could not have made it to this level.

I would like to express my sincere gratitude to my supervisory team Prof Marc Brown, Dr Matthew Traynor and Dr Woei Ping Cheng for the continuous support during my PhD, for their insightful comments, patience, motivation, and immense knowledge. Their guidance helped me at every stage of this research and during the writing up of this thesis. I could not asked for a better advisors and mentors for my PhD.

I thank my fellow co-workers at UH: Mr Caserta, Miss Osoba, Mr Shetage, Dr Owen and Mr Edwards for the stimulating discussions, restless days and nights we were working together ahead of deadlines, and for all the fun we had in the last couple of years. Also I thank my friends Dr Shoaee at UCL, Mr Caserta and Miss Osoba for their enlightening ideas in writing the first draft of this work, helping me think rationally and listening to my problems and moaning.

Unfortunately, I could not thank everyone by name in this brief acknowledgment, and therefore I would like to thank everyone who helped me physically or emotionally over the duration of this work, in particular the technicians team at UH.

## Table of Contents

<b>1</b>	<b>Chapter One: General Introduction.....</b>	<b>1</b>
1.1	Introduction.....	2
1.2	Human Eye Structure .....	3
1.2.1	Anterior Eye Segment .....	5
1.2.1.1	The Conjunctiva.....	5
1.2.1.2	The Cornea.....	5
1.2.1.3	Aqueous Humour.....	7
1.2.1.4	The Iris and Ciliary Body.....	8
1.2.2	Posterior Segment.....	8
1.2.2.1	The Sclera .....	8
1.2.2.2	The Choroid.....	9
1.2.2.3	The Retina.....	10
1.2.2.4	Vitreous Humour.....	12
1.3	Eye Diseases.....	12
1.3.1	Anterior Eye Diseases.....	13
1.3.1.1	Glaucoma .....	13
1.3.1.2	Endophthalmitis .....	13
1.3.2	Posterior Eye Diseases .....	14
1.3.2.1	Age Related Macular Degeneration (AMD) .....	14
1.3.2.2	Macular Oedema .....	15
1.3.2.3	Diabetic Macular Oedema .....	15

1.3.3	Ocular Drug Delivery Routes.....	17
1.3.3.1	Topical Drug Delivery .....	18
1.3.3.2	Systemic Drug Delivery .....	19
1.3.3.3	Transscleral Drug Delivery.....	19
1.3.3.4	Intravitreal Drug Delivery .....	21
1.4	The Ocular Physiological Barriers .....	21
1.4.1	Lacrimal Fluid and Eye Movement (Precorneal) Barriers .....	21
1.4.2	Corneal and Conjunctival Barriers.....	22
1.4.3	Blood Retinal Barriers .....	24
1.5	Ocular Drug Permeation Pathways .....	25
1.5.1	Anterior Segment .....	25
1.5.2	Posterior Segment.....	28
1.6	Conventional Ophthalmic Drug Delivery Systems .....	29
1.6.1	Anterior Segment .....	29
1.6.1.1	Topical Formulations (Eye Drops, Suspensions, Ointments and Gels) .....	29
1.6.1.2	Cul-de-sac Inserts.....	32
1.6.1.3	Implants .....	32
1.6.2	Posterior Segment.....	33
1.6.2.1	Systemic, Intravitreal and Transscleral formulations.....	33
1.6.2.2	Implants .....	34
1.7	Novel Drug Delivery Systems and Methods .....	34

1.7.1	Novel Drug Delivery Systems in Clinical Trials.....	35
1.7.1.1	Anterior Segment.....	35
1.7.1.2	Posterior Segment.....	36
1.7.2	Novel Drug Delivery Methods.....	38
1.7.2.1	Anterior Segment.....	38
1.7.2.1.1	Drug Loaded Contact Lenses .....	38
1.7.2.1.2	Capsule Drug Ring.....	38
1.7.2.2	Posterior Segment.....	39
1.7.2.2.1	Drug Delivery through Suprachoroidal Space.....	39
1.7.2.2.2	Intrascleral Drug Delivery through Hollow Microneedles.....	39
1.8	Nano Size Drug Delivery Systems.....	40
1.9	NDDS in Ocular Drug Delivery .....	42
1.9.1	Polymeric Self-Assemblies (SA).....	44
1.9.1.1	Polymer Architecture and SA Formation.....	44
1.9.1.2	SA Drug Loading Methods.....	46
1.9.1.3	SA in Drug Delivery .....	49
1.9.1.4	SA in Ocular Delivery.....	49
1.10	Aims and Objectives .....	51
<b>2</b>	<b>Chapter Two: Polymer Synthesis and Characterisation .....</b>	<b>52</b>
2.1	Introduction.....	53
2.1.1	Elemental Analysis .....	56
2.1.2	Nuclear Magnetic Resonance .....	57

2.1.3	Differential Scanning Calorimetry .....	59
2.1.4	Aim and Objectives .....	60
2.2	Materials and Methods .....	60
2.2.1	Polymer Synthesis.....	61
2.2.1.1	Conversion and Purification of PAA-HCl.....	61
2.2.1.2	Synthesis of Palmitoyl Poly(allylamine) (Pa <sub>5</sub> ) .....	63
2.2.1.3	Synthesis of Methoxypolyethylene Glycol Palmitoyl Poly(allylamine) (Pa <sub>5</sub> -MPEG) .....	64
2.2.1.4	Synthesis of Cholesteryl Poly(allylamine) (Ch <sub>5</sub> ).....	65
2.2.1.5	Synthesis of Dansyl Poly(allylamine) (Da <sub>10</sub> ) .....	66
2.2.2	Characterisation of Polymers .....	67
2.2.2.1	Elemental Analysis .....	67
2.2.2.2	Nuclear Magnetic Resonance (NMR) .....	68
2.2.2.3	Differential Scanning Calorimetry (DSC) .....	68
2.3	Results.....	68
2.3.1	Physical Appearance and Reaction Yield Percentage .....	68
2.3.2	Elemental Analysis of PAA and Modified PAA .....	69
2.3.2.1	PAA Calculations .....	69
2.3.2.2	Percentage Mole Modification of Modified Polymers .....	70
2.3.2.2.1	Calculation of Percentage Mole Modification of Pa <sub>5</sub> & Ch <sub>5</sub> .....	70
2.3.2.2.2	Calculation of Percentage Mole Modification of Pa <sub>5</sub> -MPEG.....	71
2.3.2.2.3	Calculation of Percentage Mole Modification of Da <sub>10</sub> .....	72

2.3.3	NMR Spectra and Calculation of PAA and Modified PAA .....	74
2.3.3.1	PAA <sup>1</sup> H NMR Spectra and Calculation.....	74
2.3.3.2	Modified polymers <sup>1</sup> H NMR Spectra and Calculation.....	76
2.3.3.2.1	Pa <sub>5</sub> <sup>1</sup> H NMR Spectra and Calculation .....	77
2.3.3.2.2	Pa <sub>5</sub> -MPEG <sup>1</sup> H NMR Spectra and Calculation.....	79
2.3.3.2.3	Ch <sub>5</sub> <sup>1</sup> H NMR Spectra and Calculation .....	80
2.3.3.2.4	Da <sub>10</sub> <sup>1</sup> H NMR Spectra and Calculation.....	82
2.3.4	Differential Scanning Calorimetry (DSC) .....	83
2.4	Discussion .....	85
2.5	Conclusion.....	90
<b>3</b>	<b>Chapter Three: Triamcinolone Acetonide Loading into Self-Assemblies and Release from Triamcinolone Acetonide-Self-Assemblies .....</b>	<b>91</b>
3.1	Introduction.....	92
3.1.1	Photon Correlation Spectroscopy.....	96
3.1.2	Fluorescence Spectroscopy .....	98
3.1.3	Transmission Electron Microscopy.....	100
3.1.4	High Performance Liquid Chromatography .....	101
3.1.5	Model Hydrophobic Drug.....	102
3.1.6	Aim and Objectives .....	104
3.2	Materials and Methods .....	104
3.2.1	Preparation and Characterisation of SA.....	105
3.2.1.1	Preparation of SA .....	105

3.2.1.2	Characterisation of SA using PCS .....	105
3.2.1.3	Characterisation of SA using TEM.....	105
3.2.1.4	Determination of SA CAC .....	106
3.2.2	Preparation and Characterisation of TA-SA Formulations.....	107
3.2.2.1	Preparation of TA-SA Formulations .....	107
3.2.2.2	Characterisation of TA-SA Formulations using PCS and TEM .	107
3.2.2.3	LC of TA-SA Formulations .....	108
3.2.3	TA Solubility .....	108
3.2.4	<i>In-vitro</i> TA Release from TA-SA Formulations .....	108
3.2.5	HPLC Analysis Methods.....	109
3.2.5.1	Solid Phase Extraction.....	109
3.2.5.2	TA Extraction Recovery from TA-SA .....	110
3.2.5.3	Chromatographic System .....	110
3.2.5.4	Chromatographic Conditions .....	111
3.2.5.5	Calibration Standards .....	111
3.2.5.6	Validation and Suitability of HPLC Methods .....	111
3.2.6	Statistical Evaluation .....	113
3.3	Results.....	114
3.3.1	Photon Correlation Spectroscopy.....	114
3.3.2	Determination of SA CAC.....	117
3.3.3	TEM of SA and TA-SA Formulations.....	118
3.3.4	Partial Validation and Suitability of HPLC methods.....	123

3.3.5	TA Entrapped and Solubility .....	126
3.3.6	<i>In-Vitro</i> TA Release from TA-SA Formulation .....	128
3.4	Discussion .....	130
3.5	Conclusion.....	138
<b>4</b>	<b>Chapter Four: The Development of a Porcine <i>In-Vitro</i> Eye Model for Investigating Potential Ophthalmic Formulation .....</b>	<b>139</b>
4.1	Introduction.....	140
4.1.1	Existing <i>In-Vitro</i> Eye Models .....	140
4.1.2	Human, Porcine and Rabbit Ocular Tissues .....	143
4.1.3	Liquid Scintillation Counting .....	145
4.2	Aims and Objectives .....	145
4.3	Materials and Methods .....	146
4.3.1	Materials.....	146
4.3.2	Franz Cells Setup.....	147
4.3.2.1	Franz Cell Size .....	148
4.3.3	Ocular Tissues Preparation and Storage .....	149
4.3.3.1	Porcine Tissue Preparation.....	149
4.3.3.2	Porcine Tissue Storage .....	150
4.3.3.3	Human Corneal Tissue Preparation.....	151
4.3.3.4	Human Scleral Tissue Preparation .....	151
4.3.3.5	Human and Rabbit Corneal Tissue Preparation .....	151
4.3.4	Thickness Measurement of Posterior Porcine Ocular Tissues .....	152

4.3.5	Development of Suitable Receiver Fluids.....	152
4.3.6	TA and Marker Stability in Receiver Fluids.....	153
4.3.7	Tritiated Water Studies.....	153
4.3.8	Tritiated Water Correlation with TA and FSS .....	154
4.3.9	Marker Permeation Studies.....	154
4.3.10	TA Permeation Studies .....	155
4.3.10.1	TA Permeation Study across Posterior Porcine Ocular Tissues .... .....	155
4.3.10.2	TA Permeation Study through Human Scleral Tissue.....	155
4.3.11	Permeation Enhancer Studies .....	156
4.3.12	Analytical Methods.....	156
4.3.12.1	HPLC Analytical Method .....	157
4.3.12.2	Fluorescence Analysis Method .....	157
4.3.12.3	Liquid Scintillation Counter Method.....	157
4.3.13	Permeation Parameters .....	158
4.3.14	Statistical Evaluation.....	158
4.4	Results.....	159
4.4.1	Analytical Methods .....	159
4.4.2	Porcine Ocular Tissue Thickness .....	159
4.4.3	<i>In-Vitro</i> Porcine Eye Model Development.....	160
4.4.3.1	Development of Suitable Receiver Fluids .....	160
4.4.3.2	TA and Marker Stability in Receiver Fluid.....	162

4.4.4	Partial Validation of the In-Vitro Porcine Eye Model.....	163
4.4.4.1	Franz Cell Size Effect .....	163
4.4.4.2	Ocular Tissue Integrity.....	164
4.4.4.2.1	Tritiated Water Permeation .....	164
4.4.4.2.2	TA and FSS Permeation across Fresh and Stored Tissues....	167
4.4.4.3	Tritiated Water Correlation with TA and FSS Flux .....	168
4.4.4.4	Tritiated Water Permeation and Posterior Porcine Ocular Tissue Thickness .....	170
4.4.4.5	<i>In-Vitro</i> Marker Permeability Studies .....	170
4.4.4.6	Human, Rabbit and Porcine FSS Corneal Tissues Permeability Comparison.....	172
4.4.5	<i>In-Vitro</i> TA-SA Permeability Studies.....	173
4.4.6	Enhancer Permeation Studies.....	175
4.5	Discussion .....	177
4.6	Conclusion.....	189
<b>5</b>	<b>Chapter Five: <i>In-Vitro</i> Cytotoxicity of Modified Amphiphilic Polymers</b>	<b>191</b>
5.1	Introduction.....	192
5.1.1	Human Retinal Pigment Epithelial Cell line .....	198
5.1.2	Human Corneal Epithelial Cell Line.....	199
5.1.3	MTT Assay .....	200
5.1.4	PrestoBlue <sup>®</sup> Assay .....	201
5.1.5	Aims and Objectives.....	201

5.2	Materials and Methods .....	202
5.2.1	Materials.....	202
5.2.2	Cell Resuscitation and Freezing.....	202
5.2.3	Heat-inactivation of Fetal Bovine Serum .....	203
5.2.4	H1RPE7 Cell Growth Medium.....	203
5.2.4.1	H1RPE7 Cell Growth and Sub-culture .....	203
5.2.5	MTT and Glycine Buffer Preparation .....	204
5.2.6	L-glutamic acid and tween 80 Solution Preparation .....	204
5.2.7	H1RPE7 Cell Viability Test.....	205
5.2.8	HCE-S Cell Growth Medium.....	206
5.2.8.1	HCE-S Cell Growth and Cell Viability Test.....	206
5.2.9	Statistical Evaluation .....	207
5.3	Results.....	207
5.3.1	Polymer Cytotoxicity Studies.....	207
5.3.2	Permeation Enhancer Cytotoxicity Studies .....	210
5.4	Discussion .....	211
5.5	Conclusion.....	214
<b>6</b>	<b>Chapter Six: General Discussion .....</b>	<b>216</b>
6.1	Discussion .....	217
6.2	Future Work.....	228
	References .....	231
	Appendixes .....	254

## List of Abbreviations

Age related macular degeneration (AMD)  
Anti-vascular endothelial growth factor (anti-VEGF)  
Blood retinal barrier (BRB).  
Cholesteryl Poly(allylamine) (Ch5)  
Critical aggregation concentration (CAC)  
Critical micelle concentration (CMC)  
Cyclosporin A (CsA)  
Dansyl Poly(allylamine) (Da10)  
Dexamethasone (Dex)  
Diabetic macular oedema (DMO)  
Differential scanning calorimetry (DSC).  
Elemental analysis (EA)  
Fluorescein sodium salt (FSS)  
Food and Drug Administration (FDA)  
Glass transition (T<sub>g</sub>)  
High performance liquid chromatography (HPLC).  
Human Retinal Pigment Epithelial Cell line (H1RPE7)  
Human Corneal Epithelial Cell Line (HCE-S)  
Hyaluronic acid (HA)  
Intraocular pressure (IOP).  
Lactate dehydrogenase (LDH)  
Liquid scintillation counting (LCS)  
Loading capacity (LC)  
Macular oedema (MOD)  
Melting temperature (T<sub>m</sub>)  
Methoxypolyethylene Glycol Palmitoyl Poly(allylamine) (Pa5-MPEG)  
Methylthiazole tetrazolium (MTT)  
Nano-size drug delivery systems (NDDS)  
National Institute for Health and Clinical Excellence (NICE)  
Nuclear magnetic resonance (NMR)  
Palmitoyl Poly(allylamine) (Pa5)

Photon correlation spectroscopy (PCS)  
 Poly(allylamine) (PAA)  
 Poly(D,L-lactide-co-glycolide) (PLGA)  
 Polydispersity index (PDI)  
 Polyethylene glycol (PEG)  
 Polymeric Self-Assemblies (SA)  
 Retinal pigmented epithelium (RPE)  
 Solid phase extraction (SPE)  
 Transmission electron microscopy (TEM)  
 Triamcinolone acetonide (TA)

## List of Figures

**Figure 1.1:** Human eye structure and main components. The anterior segment consists mainly of the cornea, iris, ciliary body and the lens. The posterior segment consists of sclera, choroid and the retina (Myles, Neumann & Hill, 2005). ..... 4

**Figure 1.2:** Cross sectional view of the corneal tissue depicting the five layers of the cornea adapted from Willoughby et al (Willoughby *et al.*, 2010). ..... 7

**Figure 1.3:** A schematic diagram illustrating the layer structure of the retina (neural retina and RPE). ..... 11

**Figure 1.4:** Schematic representation of drug distribution pathways from the four drug delivery routes. Colour code: Blue line = transscleral route, Red line = intravitreal route, Green line = corneal route, Black line = conjunctival and systemic route. .... 18

**Figure 1.5:** Schematic representation of periocular routes of administration (Janoria, Gunda, Boddu & Mitra, 2007). ..... 20

**Figure 1.6:** Schematic presentation of the inner and the outer blood–retinal barrier (BRB) (Hornof, Toropainen & Urtti, 2005). ..... 24

**Figure 1.7:** Types of nano-size delivery systems used in drug delivery. .... 42

<b>Figure 1.8:</b> The self-assembly of amphiphiles into: polymeric micelles, polymeric vesicles and polymeric solid nanospheres.....	46
<b>Figure 1.9:</b> Methods of SA drug encapsulation. A) oil in water emulsion B) dialysis and C) sonication.....	48
<b>Figure 2.1:</b> Schematic diagram of an elemental analyser.....	57
<b>Figure 2.2:</b> The schematic diagram of NMR spectrometer.....	59
<b>Figure 2.3:</b> Schematic of a heat flux differential scanning calorimeter.....	60
<b>Figure 2.4:</b> The chemical structure of the free-base PAA monomer.....	61
<b>Figure 2.5:</b> The preparation of palmitoyl poly(allylamine).....	64
<b>Figure 2.6:</b> The preparation of methoxypolyethylene glycol (MPEG) palmitoyl Poly(allylamine) (Pa <sub>5</sub> -MPEG).....	65
<b>Figure 2.7:</b> The preparation of cholesterol Poly(allylamine) (Ch <sub>5</sub> ).....	66
<b>Figure 2.8:</b> The preparation of dansyl poly(allylamine) (Da <sub>10</sub> ).....	67
<b>Figure 2.9:</b> <sup>1</sup> H NMR spectrum of PAA in CD <sub>3</sub> OD carried out using 600 MHz spectrometer at 25 °C.....	75
<b>Figure 2.10:</b> <sup>1</sup> H NMR spectrum of PAA in D <sub>2</sub> O carried out using 600 MHz spectrometer at 25 °C.....	75
<b>Figure 2.11:</b> <sup>1</sup> H NMR spectrum of Pa <sub>5</sub> in CD <sub>3</sub> OD carried out using 600 MHz spectrometer at 25 °C.....	78
<b>Figure 2.12:</b> <sup>1</sup> H NMR spectrum of Pa <sub>5</sub> in D <sub>2</sub> O carried out using 600 MHz spectrometer at 25 °C.....	78
<b>Figure 2.13:</b> <sup>1</sup> H NMR spectrum of Pa <sub>5</sub> -MPEG in CD <sub>3</sub> OD carried out using 600 MHz spectrometer at 25 °C.....	79
<b>Figure 2.14:</b> <sup>1</sup> H NMR spectrum of Pa <sub>5</sub> -MPEG in D <sub>2</sub> O carried out using 600 MHz spectrometer at 25 °C.....	80

<b>Figure 2.15:</b> $^1\text{H}$ NMR spectrum of $\text{Ch}_5$ in $\text{CD}_3\text{OD}$ carried out using 600 MHz spectrometer at 25 °C.....	81
<b>Figure 2.16:</b> $^1\text{H}$ NMR spectrum of $\text{Ch}_5$ in $\text{D}_2\text{O}$ carried out using 600 MHz spectrometer at 25 °C.....	81
<b>Figure 2.17:</b> $^1\text{H}$ NMR spectrum of $\text{Da}_{10}$ in $\text{CD}_3\text{OD}$ carried out using 600 MHz spectrometer at 25 °C.....	82
<b>Figure 2.18:</b> $^1\text{H}$ NMR spectrum of $\text{Da}_{10}$ in $\text{D}_2\text{O}$ carried out using 600 MHz spectrometer at 25 °C.....	83
<b>Figure 2.19:</b> Differential scanning calorimetry thermogram of PAA, Pa5, Ch5 and Da10. Colour code: Blue line = PAA, Red line = Pa5, Green line = Ch5, Purple line = Da10. ....	84
<b>Figure 2.20:</b> Differential scanning calorimetry thermogram of Pa5-MPEG (Red line) and Methoxypolyethylene glycol p-nitrophenyl carbonate (Blue line).....	84
<b>Figure 3.1:</b> Schematic diagram of intramolecular and intermolecular SA.....	93
<b>Figure 3.2:</b> Schematic diagram of photon correlation spectroscopy analyser. ....	97
<b>Figure 3.3:</b> Schematic diagram of fluorescence spectrophotometer. ....	98
<b>Figure 3.4:</b> The chemical structure of pyrene.....	99
<b>Figure 3.5:</b> The fluorescence vibronic peaks of pyrene in aqueous medium (polar environment).....	100
<b>Figure 3.6:</b> Schematic diagram of a transmission electron microscope. ....	101
<b>Figure 3.7:</b> Schematic diagram of a HPLC.....	102
<b>Figure 3.8:</b> Triamcinolone acetonide structure (434.5 Mw, 21 $\mu\text{g mL}^{-1}$ solubility in water at 28 °C, $\log p = 2.53$ ). ....	103
<b>Figure 3.9:</b> Photon correlation spectroscopy size correlation chart for $\text{Pa}_5$ SA. .	115

<b>Figure 3.10:</b> Photon correlation spectroscopy size correlation chart for Da <sub>10</sub> SA.	115
<b>Figure 3.11:</b> The fluorescence vibronic peak ratio ( $I_3/I_1$ ) of pyrene at various Pa <sub>5</sub> , Pa <sub>5</sub> -MPEG and Ch <sub>5</sub> concentrations (Data represented as mean, error bars represent range, n = 3).	117
<b>Figure 3.12:</b> TEM micrographs of Pa <sub>5</sub> SA (Scale bar A = 100 nm, B = 200 nm).	118
<b>Figure 3.13:</b> TEM micrographs of Pa <sub>5</sub> -MPEG SA (Scale bar A = 1 μm, B = 2 μm).	119
<b>Figure 3.14:</b> TEM micrographs of Ch <sub>5</sub> SA (Scale bar A = 200 nm, B = 1 μm)....	119
<b>Figure 3.15:</b> TEM micrographs of Da <sub>10</sub> SA (Scale bar A = 100 nm, B = 200 nm).	120
<b>Figure 3.16:</b> TEM micrographs of Pa <sub>5</sub> TA-SA formulation (Scale bar A = 200 nm, B = 200 nm).	121
<b>Figure 3.17:</b> TEM micrographs of Pa <sub>5</sub> -MPEG TA-SA formulation (Scale bar A = 500 nm, B = 500 nm).	121
<b>Figure 3.18:</b> TEM micrographs of Ch <sub>5</sub> TA-SA formulation (Scale bar A = 200 nm, B = 200 nm).	122
<b>Figure 3.19:</b> TEM micrographs of Da <sub>10</sub> TA-SA formulation (Scale bar A = 100 nm, B = 200 nm).	122
<b>Figure 3.20:</b> High performance liquid chromatogram of TA (50 μg mL <sup>-1</sup> ) in 40: 60 v/v acetonitrile: water.	123
<b>Figure 3.21:</b> High performance liquid chromatography calibration curve for triamcinolone acetonide in 40: 60 v/v acetonitrile: water for drug loading studies (Data represented as mean, error bars represented as S.D., n = 6).	124

**Figure 3.22:** High performance liquid chromatography calibration curve for triamcinolone acetonide in 40: 60 v/v acetonitrile: water for drug release studies (Data represented as mean, error bars represented as S.D., n = 6)..... 124

**Figure 3.23:** Maximum TA concentration solubilised by TA-SA formulations at 1:5 initial TA: polymer loading ratio determined by HPLC, compared to the intrinsic solubility and other solubilising agents (Data represented as mean, error bars represent S.D., n = 5. All TA solubility and loading experiment were carried out at room temperature at approximately 22 °C). ..... 127

**Figure 3.24:** Release profiles of TA from TA suspension (1000 µg mL<sup>-1</sup>), Da<sub>10</sub> (1238 µg mL<sup>-1</sup>), Pa<sub>5</sub>-MPEG (830 µg mL<sup>-1</sup>), Pa<sub>5</sub> (468 µg mL<sup>-1</sup>), and Ch<sub>5</sub> (762 µg mL<sup>-1</sup>) TA-SA formulations (Data represented as mean, error bars represent range, n = 4)..... 129

**Figure 4.1:** Schematic representation of Franz cell set-up..... 148

**Figure 4.2:** TA permeation profiles from TA suspension (donor solution, 500 µg mL<sup>-1</sup>) across posterior porcine ocular tissues using 0, 5, 10 and 30% ethanol receiver fluids (Data represented as mean, error bars represented as S.D., n = 6). ..... 161

**Figure 4.3:** TA permeation profiles from TA solution (ethanol: water (50: 50), 500 µg mL<sup>-1</sup>) across posterior porcine ocular tissues using 0, 5, 10 and 30% ethanol receiver fluids (Data represented as mean, error bars represented as S.D., n = 6). ..... 161

**Figure 4.4:** Fluorescein sodium salt (5 mg mL<sup>-1</sup>) permeation profiles through one week stored porcine corneal tissues using PBS and 5% 500 kDa Dextran in PBS as receiver fluids. (Data represented as mean, error bars represent range, n = 4) ..... 162

<b>Figure 4.5:</b> Fluorescein sodium salt (5 mg mL <sup>-1</sup> ) permeation profiles through two week stored porcine corneal tissues using 5% (w/v) 500 kDa Dextran as receiver fluids. (Data represented as mean, error bars represent range, n = 4). .....	163
<b>Figure 4.6:</b> TA suspension (500 µg mL <sup>-1</sup> ) permeation profiles through posterior porcine ocular tissues using 5% (v/v) ethanol as receiver fluids (Data represented as mean, error bars represent range, n = 4). .....	164
<b>Figure 4.7:</b> <sup>3</sup> H <sub>2</sub> O permeation profiles across porcine posterior tissues (n=14) and corneal tissue (n=9) (Data represented as mean, error bars represent S.D.). ....	165
<b>Figure 4.8:</b> FSS (5% w/v) permeation profiles across fresh porcine corneal tissue, stored corneal tissues for one and two weeks and at -80 °C (Data represented as mean, error bars represent range., n = 4). .....	168
<b>Figure 4.9:</b> Correlation between TA flux and <sup>3</sup> H <sub>2</sub> O percentage permeation (15 min) across posterior porcine ocular tissues. ....	169
<b>Figure 4.10:</b> Correlation between FSS (1 mg mL <sup>-1</sup> ) flux and <sup>3</sup> H <sub>2</sub> O percentage permeation (15 min) across posterior porcine ocular tissues. ....	169
<b>Figure 4.11:</b> Correlation between posterior porcine ocular tissues thickness and <sup>3</sup> H <sub>2</sub> O percentage permeation (15 min) across the tissues. ....	170
<b>Figure 4.12:</b> The permeability coefficients of FSS, 4, 10 and 20 kDa FITC-Dextran across human corneal and scleral tissues (Data represented as mean, error bars represent range, n= 4). .....	171
<b>Figure 4.13:</b> The permeability coefficients of fluorescein sodium salt, 4, 10 and 20 kDa FITC-Dextran across porcine scleral and corneal tissues (Data represented as mean, error bars represent range, n= 4). .....	172

<b>Figure 4.14:</b> Comparative permeation profiles of FSS (5% w/v) across human, porcine and rabbit corneal tissues (Data represented as mean, error bars represent S.D., n = 6).....	173
<b>Figure 4.15:</b> TA suspension (1000 $\mu\text{g mL}^{-1}$ ) and Da <sub>10</sub> TA-SA permeation profiles through human scleral tissue (Data represented as mean, error bars represent range. n = 4). .....	174
<b>Figure 4.16:</b> TA suspension (500 $\mu\text{g mL}^{-1}$ ) and TA-SA permeation profiles through posterior porcine ocular tissues (Data represented as mean, error bars represent range, n = 4). .....	174
<b>Figure 4.17:</b> The flux of 10 kDa FITC-Dextran added to various enhancers and at elevated temperature through human corneal and scleral tissues (Data represented as mean, error bars represent range, n = 4). .....	176
<b>Figure 4.18:</b> The flux of 10 kDa FITC-Dextran added to various enhancers and at elevated temperature across porcine scleral tissues (Data represented as mean, error bars represent range, n = 4).....	176
<b>Figure 4.19:</b> The flux of fluorescein sodium salt added to various enhancers and at elevated temperature across porcine scleral tissues (Data represented as mean, error bars represent range, n = 4). .....	177
<b>Figure 5.1:</b> Phase contrast image of H1RPE7 cells grown in culture medium at day three.....	199
<b>Figure 5.2:</b> Image of HCE-S cells grown in culture medium at day two. ....	200
<b>Figure 5.3:</b> MTT results for percentage cell viability of RPE cells exposed to PAA, Pa <sub>5</sub> , Pa <sub>5</sub> -MPEG, Ch <sub>5</sub> and Da <sub>10</sub> (Data represented as mean, error bars represent range, n = 4). .....	208

<b>Figure 5.4:</b> PrestoBlue <sup>®</sup> results for percentage cell viability of corneal epithelial cells (HCE-S) exposed to PAA, Pa <sub>5</sub> , Pa <sub>5</sub> -MPEG and Da <sub>10</sub> (Data represented as mean, error bars represent range, n = 4). .....	209
<b>Figure 5.5:</b> MTT results for percentage cell viability of RPE cells exposed to Tween 80 and L-Glutamine acid (Data represented as mean, error bars represent range, n = 4). .....	210
<b>Figure 6.1:</b> Schematic diagram showing the formation of the polymeric SA's from amphiphilic polymers in aqueous media. ....	219

## List of Tables

<b>Table 2-1:</b> The synthesised polymer names and their corresponding abbreviations.....	63
<b>Table 2-2:</b> Yield percentages and physical appearance of PAA and modified polymers. ....	69
<b>Table 2-3:</b> The calculations of the empirical formula of the PAA monomer. ....	70
<b>Table 2-4:</b> The calculation of the percentage mole modification of palmitoyl in Pa <sub>5</sub> . .....	71
<b>Table 2-5:</b> The calculation of the percentage mole modification of palmitoyl in Pa <sub>5</sub> -MPEG. ....	72
<b>Table 2-6:</b> The calculation of the percentage mole modification of dansyl in Da <sub>10</sub> . .....	73
<b>Table 2-7:</b> Elemental analysis results for PAA and modified polymers, with their corresponding percentage mole modification. ....	74
<b>Table 2-8:</b> Assignment of the corresponding chemical shifts in <sup>1</sup> H NMR spectra of Pa <sub>5</sub> , Pa <sub>5</sub> -MPEG, Ch <sub>5</sub> and Da <sub>10</sub> amphiphilic polymers. ....	76

<b>Table 2-9:</b> The percentage mole modification of modified polymers obtained using EA and NMR.....	85
<b>Table 3-1:</b> Average hydrodynamic size, PDI and zeta potential of the SA (Data represented as mean and standard deviation (S.D.), n = 5). .....	114
<b>Table 3-2:</b> Average hydrodynamic size, PDI and zeta potential of TA-SA formulations (Data represented as mean and standard deviation (S.D.), n = 5). .....	116
<b>Table 3-3:</b> HPLC TA methods validation and suitability for the both TA loading and <i>in-vitro</i> release methods.....	126
<b>Table 3-4:</b> Loading capacity of TA-SA formulations and number of folds of TA entrapped within the TA-SA formulations in comparison to conventional solubilisers. ....	128
<b>Table 3-5:</b> <i>In-vitro</i> release data fit to kinetic models. ....	130
<b>Table 4-1:</b> The TA donor vehicles used in permeation studies.....	155
<b>Table 4-2:</b> Parameters of FSS and FITC-dextran calibration graphs.....	159
<b>Table 4-3:</b> <sup>3</sup> H <sub>2</sub> O% permeating at 15 minutes through fresh and frozen posterior porcine ocular tissues. ....	166
<b>Table 4-4:</b> <sup>3</sup> H <sub>2</sub> O% permeating at 15 minutes through fresh and one week stored porcine corneal tissues. ....	166
<b>Table 4-5:</b> TA flux through fresh and frozen posterior porcine ocular tissues.....	167
<b>Table 5-1:</b> Most common <i>in-vitro</i> ocular cell culture models.....	193
<b>Table 5-2:</b> IC <sub>50</sub> values for RPE cells treated with PAA and modified PAA polymers (3.9 x 10 <sup>-4</sup> - 0.4 mg mL <sup>-1</sup> ) for 24 h.....	208
<b>Table 5-3:</b> IC <sub>50</sub> values for RPE and HCE cells treated with PAA and modified PAA polymers. ....	209

## **Chapter One: General Introduction**

---

## 1.1 Introduction

Profound changes in modern life style over the past decades have led to an increase in the prevalence of obesity, diabetes and an ageing population (Amos, McCarty & Zimmet, 1997; Office for National Statistics, 2002; The NHS Information Centre, 2012). A significant risk factor to major eye diseases such as age related macular degeneration (AMD, posterior eye disease) and glaucoma (anterior eye disease) are associated with obesity (Cheung & Wong, 2007; Habet-Wilner & Belkin, 2005), diabetes (Bonovas, Peponis & Filioussi, 2004; Chronopoulos, Trudeau, Roy, Huang & Vinore, 2011; Wong, Bui & Vingrys, 2011) and ageing (Cedrone, Mancino, Cerulli, Cesareo & Nucci, 2008; Klein *et al.*, 2010). In the United States alone, due to a rapidly ageing population, the number of people affected by AMD is estimated to increase by 50% to three million by 2020 (Yorio, Clark & Wax, 2011). Worldwide there are 70 million patients who are suffering from AMD or glaucoma (Yorio, Clark & Wax, 2011). In 2010 it was estimated that the medicines targeting these eye diseases have a projected market of 1.8 and 4 billion US dollars, respectively (Yorio, Clark & Wax, 2011).

Anterior and posterior eye diseases such as glaucoma, proliferative diabetic retinopathy and AMD are the main causes of visual impairment, deterioration in visual acuity and blindness in developed countries (Antonetti *et al.*, 2006). Patients with anterior or posterior eye diseases are commonly treated by surgery, laser treatment and medicines (Del Amo & Urtti, 2008). However, these treatments, especially those targeting posterior eye diseases are associated with many complications such as inflammation, toxicity, side effects and pain (Del Amo & Urtti, 2008).

Despite the accessibility of the eye and the ease of instilling topical dosage forms, the delivery pathways of drugs through ocular tissues is undoubtedly a complicated process in which drugs encounter many barriers (Willoughby *et al.*, 2010). These barriers hinder the delivery of drugs to the targeted tissue through the most convenient route i.e. the trans-corneal route (Willoughby *et al.*, 2010). To understand the barriers and how to improve ocular drug delivery, it is crucially important to be familiar with the structure of the eye.

### **1.2 Human Eye Structure**

The human eye is composed of two different sized anterior and posterior spherical segments that are connected by circular tissue called the limbus (Moore, Dalley & Agur, 2009). A schematic diagram of the main components of the human eye is shown in Figure 1.1.

The anterior segment is the smaller of the two (one-sixth of the whole eye, 8 mm radius) with an outer focal component that is a multilayer transparent tissue called the cornea. The posterior segment is the larger of the two segments (12 mm radius) with an outer white opaque collagen layer called the sclera. The eye weight in a human adult is approximately 7.5 grams, has a volume of 6.5 cm<sup>3</sup> and a 24 mm vertical diameter which is usually less than the horizontal diameter (Rogers, 2010). The aqueous humour is a solution filling the anterior and posterior chambers (anterior: space between the cornea and the iris, posterior: space between the iris and the lens), whereas the vitreous humour is a clear gel filling the vitreous chamber (space between the retina and the lens) (Rogers, 2010). The anterior segment of the eye consists mainly of the cornea, iris, ciliary body and the lens while the posterior segment consists of sclera, choroid and the retina (Yanoff, Duker & Augsburger, 2004). The retina (inner component of the posterior

segment) consists mainly of light sensitive photocells which are responsible for converting observed light to electrical signals (Yanoff, Duker & Augsburger, 2004).

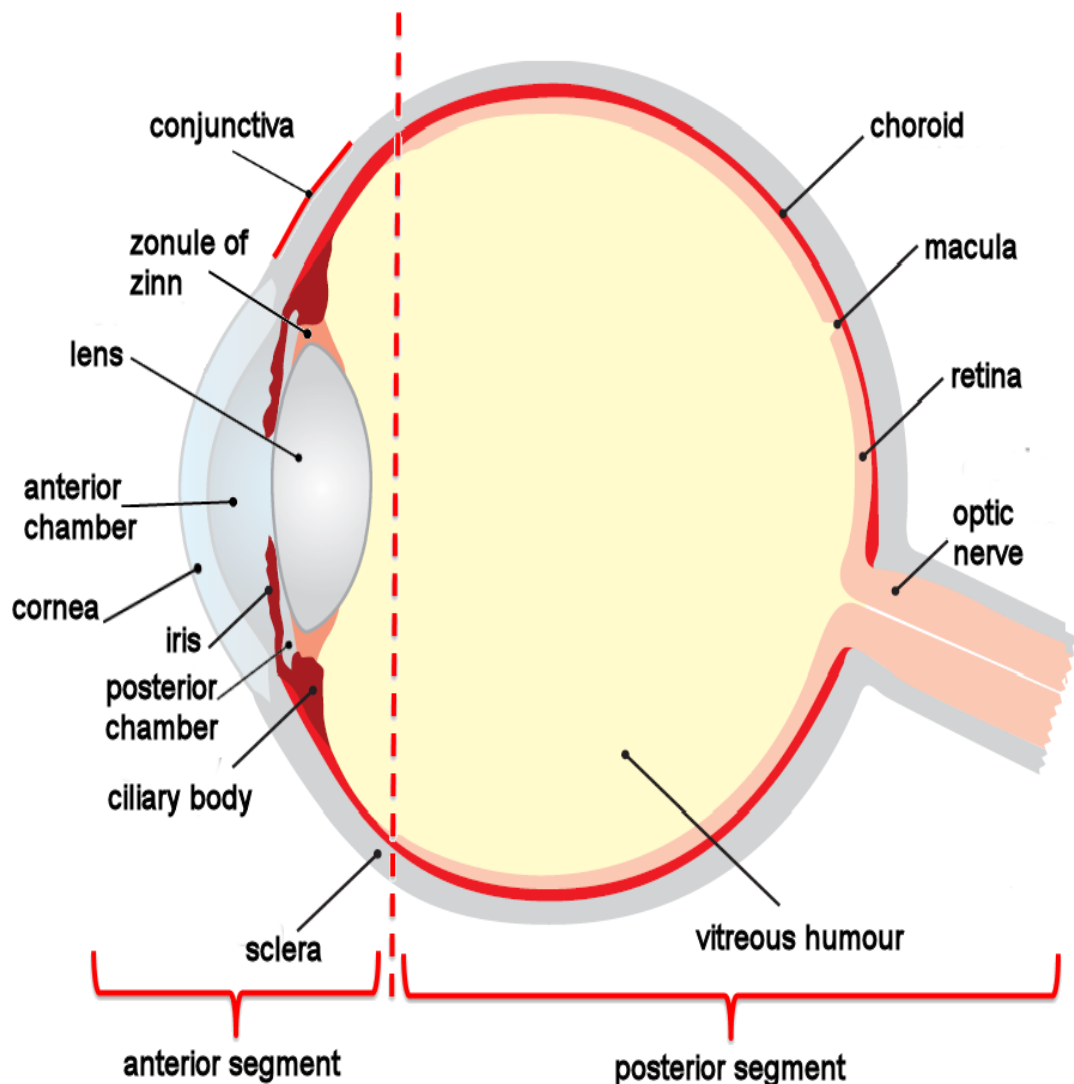


**Figure 1.1:** Human eye structure and main components. The anterior segment consists mainly of the cornea, iris, ciliary body and the lens. The posterior segment consists of sclera, choroid and the retina (Myles, Neumann & Hill, 2005).

The eye is a complex collective organ, composed of many tissues, each designed to perform a specific function. Detailed description of each tissue is beyond the scope of this general introduction, hence, some of the tissues and layers have been briefly mentioned (sections 1.2.1.4 and 1.2.2.2).

## **1.2.1 Anterior Eye Segment**

### **1.2.1.1 The Conjunctiva**

The conjunctiva is a transparent vascularised mucous membrane covering the anterior surface of the eyeball and the inner surface of the eyelids (Figure 1.1, (Cummings, 2012). The conjunctiva can be divided into three morphologically distinct areas: bulbar (covering the anterior part of the eyeball), palpebral (covering the inside of the eyelids) and fovea or the conjunctival cul-de-sac (a transition zone between the bulbar and the palpebral conjunctivas) (Hoang-Xuan, Baudouin & Creuzot-Garcher, 1998; Lens, Nemeth & Ledford, 2008). The conjunctival tissue consists of two to three layers of epithelial cells with tight junctions only on the apical surface layer and cuboidal basal cells (Hornof, Toropainen & Urtti, 2005). The conjunctival tissue also contains mucous goblet cells which are responsible for secreting the mucus required for the tear film stability and corneal transparency (Holland, Mannis & Lee, 2013). This tissue has a rich supply of blood vessels, and plays a significant role in systemic clearance of topically administered formulations (Hamalainen, Kananen, Auriola, Kontturi & Urtti, 1997).

### **1.2.1.2 The Cornea**

The cornea is an avascular transparent tissue covering approximately 15% of the surface area of the eye (Pathak & Thassu, 2009). It is primarily responsible for focusing light and protecting internal ocular tissues from xenobiotics (foreign materials) (Thassu & Chader, 2013). Due to the absence of vasculature in the cornea, the corneal tissue receives nourishment from the tear film, aqueous humour and limbal vessels (Wilson, Semenova, Hughes & Olejnik, 2006). The cornea in an adult human has an average dimension of 11.5 mm horizontally, 10.5

mm vertically (Rufer, Schroder & Erb, 2005) and an average central corneal thickness of 0.53 mm (Doughty & Zaman, 2000).

The cornea is composed of five layers (Figure 1.2) namely the corneal epithelium (the outer layer), Bowman's layer, corneal stroma, Descemet's membrane and corneal endothelium (Li *et al.*, 1997; Yanoff & Duker, 2008). The epithelium layer consists of 5-7 layers of superficial, wing and basal epithelial cells (Hao, Li, Kao & Liu, 2010) that form a major barrier to ophthalmic topical formulation due to the tight junctions between the cells; especially in the superficial cells (Willoughby *et al.*, 2010). The thickness of the human epithelial layer is approximately 50  $\mu\text{m}$  (Li *et al.*, 1997; Patel, McLaren, Hodge & Bourne, 2001). The stroma mainly consists of an extracellular matrix, stromal cells and approximately 4% glycosaminoglycans (Akhtar *et al.*, 2002) with an approximate thickness of 500  $\mu\text{m}$  which accounts for >90% of the corneal thickness (Willoughby *et al.*, 2010). The endothelium layer consists of a monolayer of cuboidal cells with an approximate thickness of 5  $\mu\text{m}$  (Wilson, Semenova, Hughes & Olejnik, 2006). The main function of this monolayer is to regulate fluid and solute transport between the aqueous humour and the corneal stroma. In contrast to the corneal epithelium the endothelium cells do not regenerate (Bourne, Nelson & Hodge, 1997) and upon cell death in the endothelium layer the cells flatten and enlarge in volume, covering the space occupied by the dead cell (Bourne, Nelson & Hodge, 1997).

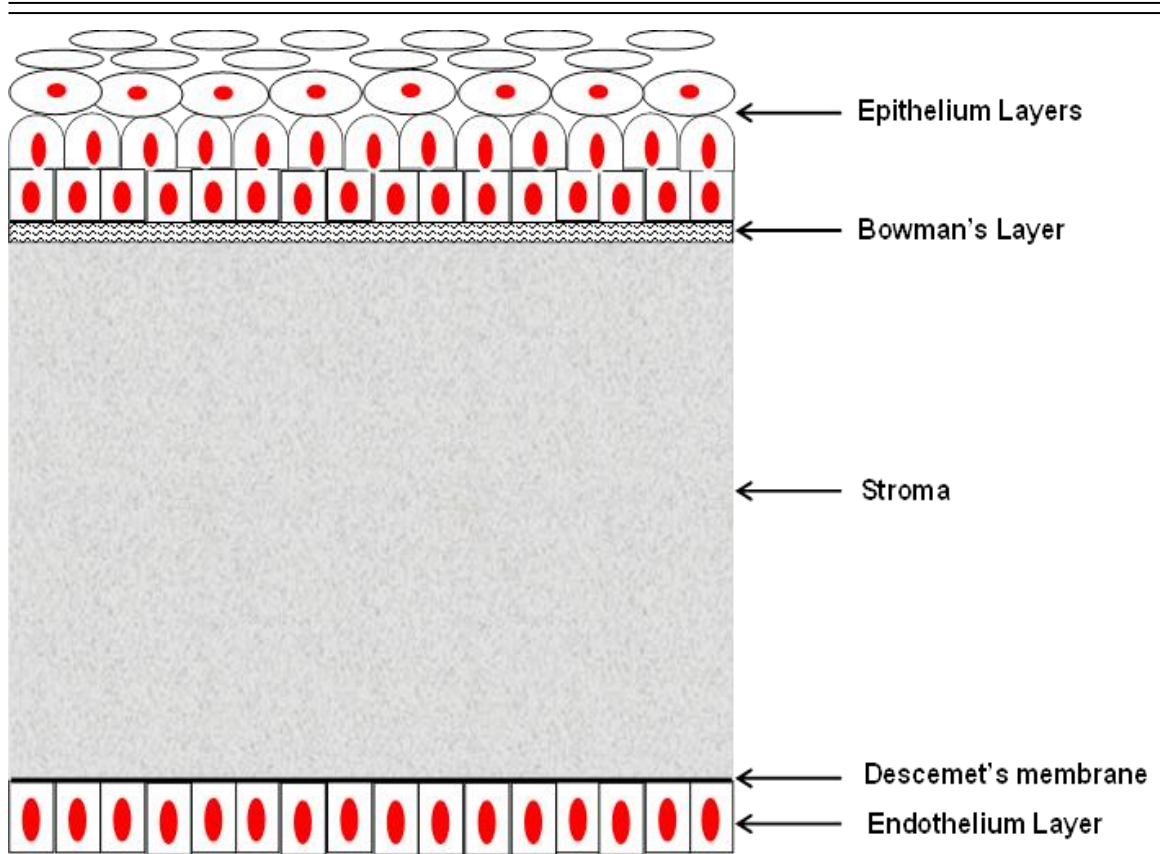


**Figure 1.2:** Cross sectional view of the corneal tissue depicting the five layers of the cornea adapted from Willoughby et al (Willoughby *et al.*, 2010).

### 1.2.1.3 Aqueous Humour

Aqueous humour is a clear fluid filling the anterior inner space of the eyeball (approximately 250  $\mu\text{L}$ ); it is contained in the anterior and posterior chambers. The aqueous humour has a pH of 7.2 and it contains low levels of proteins, glucose, various ions and high levels of ascorbic acid and lactic acid in comparison to the blood plasma (Crooke, Guzman-Aranguez, Peral, Abdurrahman & Pintor, 2008). This fluid nourishes the cornea and the lens and gives the front of the eye (cornea) its shape. The aqueous humour drains out of the anterior chamber by the trabecular meshwork (spongy tissue near the ciliary body) through a set of channels called Schlemm's canal to the episcleral venous system (Thassu & Chader, 2013). The turnover and drainage of the aqueous humour ( $2.75 \mu\text{L}\cdot\text{min}^{-1}$

(To, Kong, Chan, Shahidullah & Do, 2002)) plays an important role in the clearance of instilled topical formulations (Thassu & Chader, 2013).

#### **1.2.1.4 The Iris and Ciliary Body**

The iris is a circular tissue which controls the amount of light entering the eye by regulating the diameter of the pupil (an aperture at the centre of the iris) and divides the anterior and posterior chambers (Lens, Nemeth & Ledford, 2008). The ciliary body is responsible for the production of the aqueous humour and for changing the shape of the lens through a connective tissue called the zonule of Zinn (Figure 1.1) (To, Kong, Chan, Shahidullah & Do, 2002).

### **1.2.2 Posterior Segment**

#### **1.2.2.1 The Sclera**

The sclera is a vascular, tough and opaque white-yellow protective layer consisting of collagen, elastic fibres and proteoglycan (Watson & Young, 2004). The main purpose of the sclera is to maintain the shape of the eyeball and to provide resistance to internal and external forces (Lens, Nemeth & Ledford, 2008). The sclera is composed of four layers; 1) Tenon's capsule, 2) episclera, 3) scleral stroma and 4) lamina fusca layers (Maza, Tauber & Foster, 2012). The Tenon's capsule layer is a hypocellular layer which contains arranged compact collagen bundles (Maza, Tauber & Foster, 2012). The episclera layer is a well-vascularised layer which contains elastic tissue and macrophages (Maza, Tauber & Foster, 2012). The scleral stroma has interwoven dense collagen fibre bundles and lamellae with scattered elastic fibres present within (Watson & Young, 2004). The innermost layer of the sclera (lamina fusca) has collagen bundles smaller than those that exist in the scleral stroma and branch extensively to blend with the

underlying choroidal tissue (Curtin, 1969; Komai & Ushiki, 1991a). This layer has a noticeable increase in cell numbers (sclerocytes and melanocytes) in comparison to the scleral stroma (Watson & Young, 2004).

The sclera covers approximately 80% of the eye surface and varies in thickness (Maza, Tauber & Foster, 2012; Olsen, Aaberg, Geroski & Edelhauser, 1998). The thickness of sclera in an adult human is thickest at the posterior pole (1-1.18 mm), decreasing progressively to the equator (0.4-0.6 mm) and progressively increasing towards the limbs (0.8 mm). The thinnest part of the sclera is immediately behind the recti muscles (0.3 mm) (Maza, Tauber & Foster, 2012; Norman *et al.*, 2010; Vannas & Teir, 1960; Watson & Young, 2004). Besides not having epithelium and endothelium cell layers, the scleral tissue differs primarily from the corneal tissue in the uniformity of the arrangement of the collagen fibres and the degree of hydration (Watson & Young, 2004). Relative to the cornea, the sclera has irregular collagen fibres (scleral collagen fibrils diameter 25-230 nm, corneal collagen fibrils diameter approximately 25 nm) and a four fold lower concentration of proteoglycans resulting in a lower water content (68% in comparison to 78% in the corneal stroma) (Komai & Ushiki, 1991b; Watson & Young, 2004). In addition, the sclera is perforated by blood vessels and has an extensive nerve supply (Watson & Young, 2004).

### **1.2.2.2 The Choroid**

The choroid, ciliary body and iris form the vascular middle layer of the human eyeball. The choroid is a dark reddish brown layer, which lies between the sclera and retina. The choroid thickness in human eyes is approximately 220  $\mu\text{m}$  at the posterior pole and 100  $\mu\text{m}$  at the anterior (Touitou & Barry, 2007). Within this vascular layer, large vessels are located near the sclera (vascular lamina) and

extended smaller vessels (choriocapillaris) are pressed against the light sensitive layer of the retina. These capillaries provide oxygen and nourishment to the outer layers of the retina (Lens, Nemeth & Ledford, 2008; Touitou & Barry, 2007).

### **1.2.2.3 The Retina**

The innermost layer of the posterior segment of the eyeball consists of the retina (approximately 32 mm diameter, (Kolb, Fernandez & Nelson, 2007)). The retina is a complex part of the eye and consists of ten layers which are depicted in Figure 1.3. The retinal tissue is divided into two segments namely, the retinal pigmented epithelium (RPE) and the neural retina (the rest of the cell layers). The RPE is a tight barrier separating the neural retina from the choroidal circulation (Kolb, Fernandez & Nelson, 2007). It regulates nutrients supply to the retina and removes metabolic end products from the retina (Yanoff, Duker & Augsburger, 2004).

The innermost layer (inner limiting membrane) of the retina is in contact with the vitreous body, while the outermost layer (RPE) is in contact with the choroid. The retinal thickness across mammalian species has been reported to be around 217  $\mu\text{m}$  (Buttery, Hinrichsen, Weller & Haight, 1991; Duong *et al.*, 2008). In humans the retina is thinnest at the fovea centre (approximately 178  $\mu\text{m}$ ) and thickest at the foveal rim (approximately 320  $\mu\text{m}$ ), beyond the fovea the retina progressively thins until the equator (approximately 120  $\mu\text{m}$ ) (Landau, Schneidman, Jacobovitz & Rozenman, 1997). The retina is packed with photosensitive cells called rods and cones (photoreceptor outer segment in Figure 1.3). There are three kinds of cone cells each responding to different wavelengths of light, namely, red, green and blue. Rod cells are responsible for

nocturnal vision and are sensitive to light but insensitive to colour (Yanoff, Duker & Augsburger, 2004).

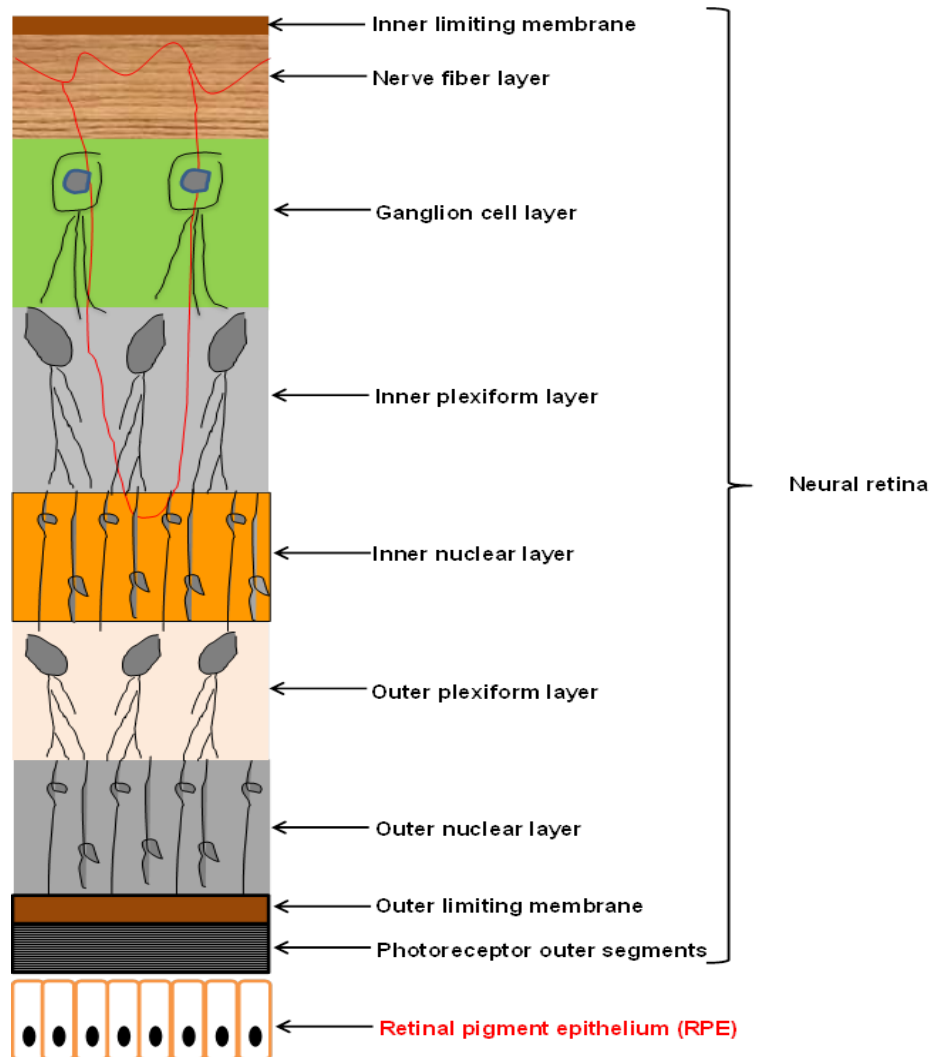


**Figure 1.3:** A schematic diagram illustrating the layer structure of the retina (neural retina and RPE).

Near the centre of the retina there is a highly pigmented yellow spot called the macula. Close to the macula centre is the fovea, the fovea is a small pit (5-6 mm in diameter (Rogers, 2010)) dominated by tightly packed cone cells responsible for central vision. The rest of the retina (peripheral) consists of rod cells responsible for nocturnal vision (Yanoff, Duker & Augsburger, 2004). The retina is considered as one of the most metabolically active tissues in the body

(Yanoff, Duker & Augsburger, 2004). Therefore, the functional integrity of the retina depends on the supply of nutrients and the removal of waste. This is achieved through the inner retinal blood and choroidal circulations (Yanoff, Duker & Augsburger, 2004).

#### **1.2.2.4 Vitreous Humour**

The vitreous humour is an acellular (apart from a few phagocyte cells) transparent gel (approximately 4 mL) that fills the space between the lens and the retina (vitreous chamber). The constituents of the vitreous body are approximately 98-99% water (the water percentage increases with age), collagen and natural macromolecules such as hyaluronic acid (HA) (Yanoff, Duker & Augsburger, 2004). The collagen confers the gel-like property of the vitreous, whereas the HA stabilises the collagen network (Bos *et al.*, 2001). Unlike the aqueous humour which is continuously secreted and drained, the vitreous humour is undynamic. Therefore, any haemorrhage and inflammation in the vitreous cavity will cause vision obstruction and surgical intervention might be necessary to remove the debris (blood and cells). The vitreous humour is targeted as a drug depot for retinal drug delivery.

### **1.3 Eye Diseases**

There are a number of diseases concerned with the eye varying in severity, prevalence and in duration. A brief description of some of the common eye diseases (anterior and posterior), pathogenesis and treatments are discussed in sections 1.3.1.1-1.3.2.3.

### **1.3.1 Anterior Eye Diseases**

#### **1.3.1.1 Glaucoma**

Glaucoma is a condition where the eye trabecular meshwork becomes slightly blocked resulting in an increased intraocular pressure (IOP) (Edward & Vajaranant, 2012). Untreated glaucoma might causes damage to the optic nerve (Edward & Vajaranant, 2012). There are two types of glaucoma (chronic and acute glaucoma), both types can be considered as a type of optic neuropathy (Rogers, 2010). The increased IOP can be reduced by means of medical intervention such as laser or surgery and by drugs. The drugs work by increasing the flow of aqueous humour (prostaglandin analogues e.g. tafluprost), decreasing the production of aqueous humour (beta-blockers and carbonic anhydrase inhibitors) or opening up the blocked trabecular meshwork (miotics e.g. pilocarpine) (Edward & Vajaranant, 2012; Fogagnolo & Rossetti, 2011).

#### **1.3.1.2 Endophthalmitis**

Endophthalmitis is an inflammatory condition of the internal ocular structure caused by bacterial or fungal microorganisms (Scott, Loo, Flynn & Miller, 2003; Shen, Wang, Tsai & Lee, 2010). It often occurs due to complications in intraocular surgery, particularly cataract surgery or intravitreal injections (Shen, Wang, Tsai & Lee, 2010). Endophthalmitis is often accompanied by severe pain, and in extreme cases it can result in vision loss (Scott, Loo, Flynn & Miller, 2003). Endophthalmitis can be treated using antibiotic (intravitreal or topical) and corticosteroids (intravitreal or topical) reducing the inflammation and swelling to the affected tissues (Das, Jalali, Gothwal, Sharma & Naduvilath, 1999; Pijl, Theelen, Tilanus, Rentenaar & Crama, 2010).

## **1.3.2 Posterior Eye Diseases**

### **1.3.2.1 Age Related Macular Degeneration (AMD)**

Age related macular degeneration (AMD) is a disease that affects the photoreceptor cells in the retina, especially the macula; the exact cause of this disorder is still unknown (Prasad, Schwartz & Hubschman, 2010). Generally AMD is painless, and progresses slowly until the central vision is lost due to the degeneration of photoreceptor cells and RPE (Birch & Liang, 2007). There are two types of macular degeneration, namely atrophic or non-exudative (dry form) and neovascular or exudative (wet form) (Prasad, Schwartz & Hubschman, 2010). The wet form is the most severe of the two and the least common (Prasad, Schwartz & Hubschman, 2010). The vision of patients suffering from this form degenerates more rapidly than the dry form (Prasad, Schwartz & Hubschman, 2010). In the wet form, abnormal blood vessels grow behind the retina resulting in bleeding and scarring that lead to the distortion or loss of central vision (Prasad, Schwartz & Hubschman, 2010). The dry form is less severe and it develops very slowly (gradual cell death of the cone and rod cells) causing gradual loss of central vision (Birch & Liang, 2007).

Currently, there is no conclusive evidence to demonstrate that medical treatment can reverse the damage caused by this disease. Nevertheless, in 2008 the National Institute for Health and Clinical Excellence (NICE) ("National Institute for Health and Care Excellence," 2013) approved the use of an anti-vascular endothelial growth factor (anti-VEGF) drug, ranibizumab (Lucentis<sup>®</sup>, Genentech) for the treatment of AMD ("National Institute for Health and Care Excellence," 2013). The approved treatment does not reverse the damage but slows the progression of the disease by selectively binding with VEGF and inhibiting the

vascular leakage and growth of blood vessels ("National Institute for Health and Care Excellence," 2013). The wet form of the disease can also be treated with laser photocoagulation, photodynamic therapy and surgical intervention (Prasad, Schwartz & Hubschman, 2010).

### **1.3.2.2 Macular Oedema**

Macular oedema (MOD) is a painless disease, in which swelling or thickening of the macula occurs, due to an increase in retinal blood vessel permeability (Cummings, 2012). This leads to the retention of fluid and protein deposits collected on or under the macula (Cummings, 2012). Macular oedema is a common posterior eye disease causing blurred and/or distorted vision (Dartt, Dana, D'Amore & Niederkorn, 2011). It can be classified as macular oedema caused by systemic diseases such as diabetes or chronic renal failure, or macular oedema caused by vein occlusion or surgical procedure e.g. cataract or retinal surgery. The standard treatment of macular oedema is laser photocoagulation, in which the laser cauterises the abnormal ocular blood vessels and thus reduces the swelling and improves the visual acuity in some cases. Other treatments include vitreous surgery, anti-VEGF and the use of corticosteroids (Jonas, Kreissig & Degenring, 2002; Kuppermann *et al.*, 2007; Sivaprasad, McCluskey & Lightman, 2006).

### **1.3.2.3 Diabetic Macular Oedema**

Diabetic macular oedema (DMO) retinopathy is a condition caused by complications of diabetes mellitus. Diabetic retinopathy is the most common diabetic eye disease and is a leading cause of severe vision loss or even blindness (Dartt, Dana, D'Amore & Niederkorn, 2011). Hyperglycemia leads to high intracellular levels of glucose, oxidative stress (formation of free radicals), and

the activation of protein kinase C; these factors ultimately disrupt the blood retinal barrier (BRB) (Antonetti *et al.*, 2006; Bhagat, Grigorian, Tutela & Zarbin, 2009). In non-proliferative diabetic retinopathy, blood vessels may swell and leak fluid whereas in proliferative diabetic retinopathy abnormal new blood vessels grow on the surface of the retina (Cunha-Vaz, 2010).

Diabetic retinopathy has four stages mild, moderate, severe non-proliferative retinopathy and proliferative retinopathy (Cunha-Vaz, 2010). The earliest stage is the mild non-proliferative retinopathy in which a microscopic aneurysm occurs. These microscopic aneurysms are blood-filled dilatations of blood vessels (balloon-like swelling) in the retina. The second stage of this condition is the moderate non-proliferative retinopathy where some blood vessels nourishing the retina are blocked (Cunha-Vaz, 2010). These blocked blood vessels lead to blood supply deprivation in several areas of the retina, which triggers signals to the body to grow new blood vessels, this is the last stage before the proliferative stage (Severe non-proliferative) (Cunha-Vaz, 2010). The disease progresses to the proliferative retinopathy as the starved retina triggers VEGF to grow new blood vessels to supply nutrients (Cunha-Vaz, 2010). These new blood vessels are abnormal; they are fragile and grow along the retina and into the vitreous body. The newly grown blood vessels do not cause symptoms or vision loss (Cunha-Vaz, 2010). However if blood leaks out of these vessels, this may cause severe vision loss and even blindness in some cases (Cunha-Vaz, 2010). The main way of treating proliferative retinopathy is by laser surgery and vitrectomy (removal of the vitreous humour). This laser surgery is called scatter laser photocoagulation treatment where the laser is used to shrink the abnormal blood vessels by placing burns in the areas of the retina away from the macula,

causing them to shrink. In recent years, anti-VEGF and corticosteroids have been shown to be effective in treating diabetic retinopathy (Avery *et al.*, 2006; Isaac, Abud, Frantz, Rassi & Avila, 2012).

### **1.3.3 Ocular Drug Delivery Routes**

There are four ocular drug delivery routes, namely topical, systemic, transscleral and intravitreal which have been employed to treat various eye diseases (Mitra, 2003). A summary of the four ocular drug delivery routes is illustrated in Figure 1.4. The most effective and convenient route of drug delivery to the anterior segment of the eye is the topical route (section 1.3.3.1) (Wilson, Zhu, Kurmala, Rao & Dhillon, 2001). However, this is not an effective way of delivering drugs to the posterior segment of the eye due to the obstructive nature of the eye barriers toward xenobiotics (foreign materials) (Wilson, Zhu, Kurmala, Rao & Dhillon, 2001). The systemic, transscleral and intravitreal routes (sections 1.3.3.2-1.3.3.4) are used in treating posterior eye segment diseases.

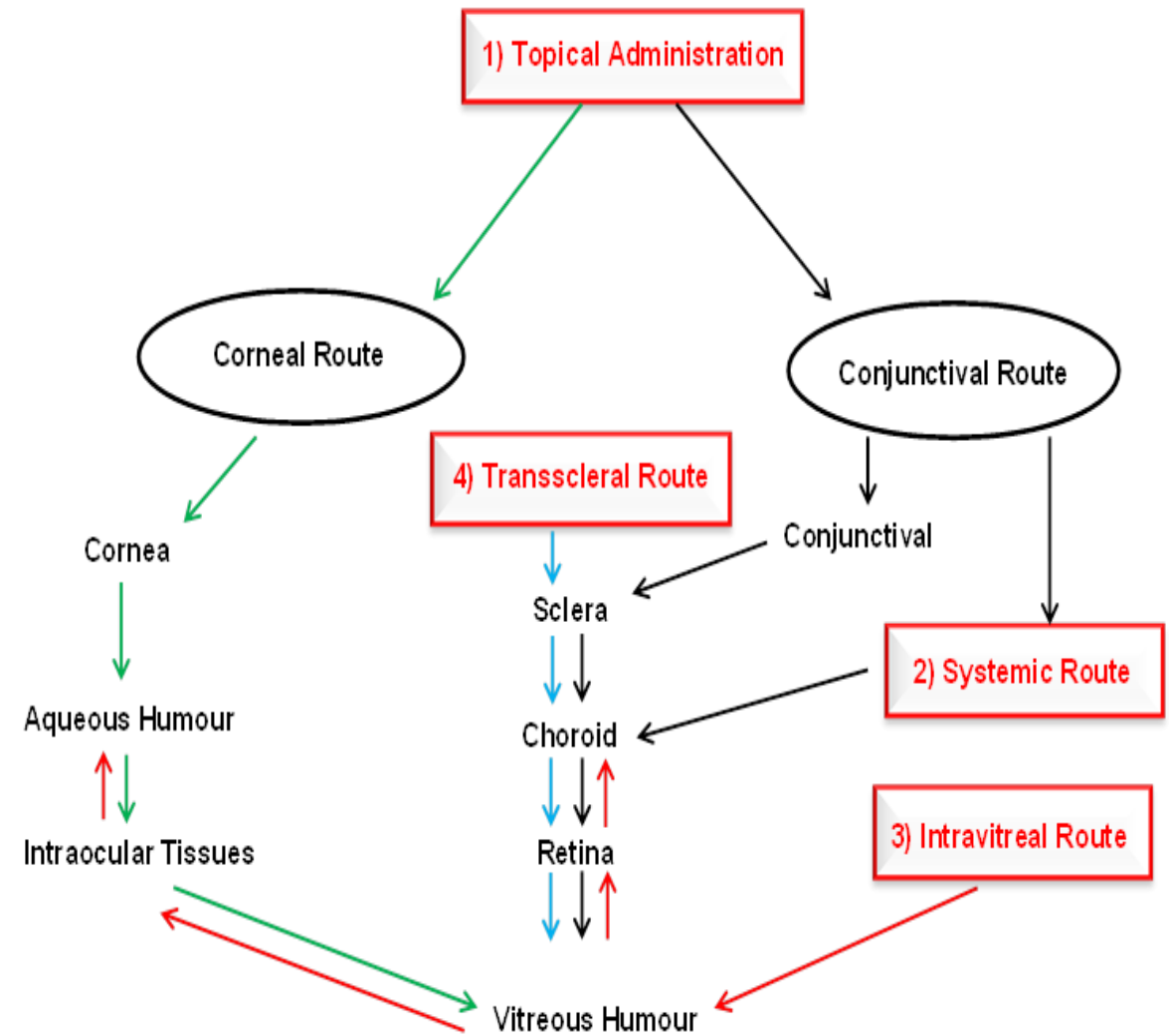


**Figure 1.4:** Schematic representation of drug distribution pathways from the four drug delivery routes. Colour code: Blue line = transscleral route, Red line = intravitreal route, Green line = corneal route, Black line = conjunctival and systemic route.

### 1.3.3.1 Topical Drug Delivery

This is the most convenient route, due to the accessibility of the eye and ease of instilling the dosage form. However, this route suffers from many disadvantages such as vision distortion, systemic clearance and frequent application that may cause inconvenience and disruption to the patient's daily life (Wilson, Zhu, Kurmala, Rao & Dhillon, 2001). In addition, it is an ineffective route for chronic and posterior segment diseases due to the short drug contact time with the cornea (precorneal barriers). In addition to the corneal barrier, the aqueous

humour circulation and the long distance between the anterior segment and the retina (approximately 23 mm) are some of the main barriers limiting the access of topically applied drugs to posterior segments of the eye (Urtti, 2006).

### **1.3.3.2 Systemic Drug Delivery**

Ophthalmic drugs delivered through the systemic route are generally delivered via intravenous injection (e.g. Visudyne<sup>®</sup>, Novartis AG (Prasad, Schwartz & Hubschman, 2010)). This route is the least desirable route in ophthalmology due to the high drug concentrations needed to overcome the blood retinal barriers and due to the toxicity that might occur in other organs in the body (Wilson, Zhu, Kurmala, Rao & Dhillon, 2001).

### **1.3.3.3 Transscleral Drug Delivery**

In recent years, scleral drug delivery for various posterior disorders has attracted attention among academics and the pharmaceutical industry. The transscleral delivery route offers many advantages over other routes such as the corneal route: relative high scleral surface area (potential drug depot), high degree of hydration (enhanced diffusion of hydrophilic molecules), metabolically inactive and relatively high permeability to macromolecules (Ambati *et al.*, 2000; Ayalasomayajula & Kompella, 2004; Bourges *et al.*, 2006; Kim *et al.*, 2009; Olsen, Edelhauser, Lim & Geroski, 1995).

Drug delivery through the transscleral route is normally achieved via periocular injections. Periocular Injections (subconjunctival, subtenon, peribulbar and retrobulbar) are administered in the cavities around the eye or under the conjunctiva (Janoria, Gunda, Boddu & Mitra, 2007). Figure 1.5 illustrates the periocular injection positions around the eye. Periocular injections can provide high retinal and vitreous humour drug levels (approximately 0.01–0.1% of the

applied dose) in comparison to topically administered eye drops (approximately 0.001% or less) (Thassu & Chader, 2013).

Subconjunctival injections (volume up to 500  $\mu$ L) are used to deliver drug to the anterior (through systemic circulation, transcorneal and transscleral diffusion) and posterior segment of the eye (through transscleral route). The subtenon (1-5 mL), peribulbar (8-10 mL), retrobulbar (2-3 mL) and posterior juxtасcleral (0.5 mL) injections are mainly used to deliver injected drug to the posterior segments through the transscleral route. These injections allow the dosing of large volumes and can be repeated as necessary (Thassu & Chader, 2013).

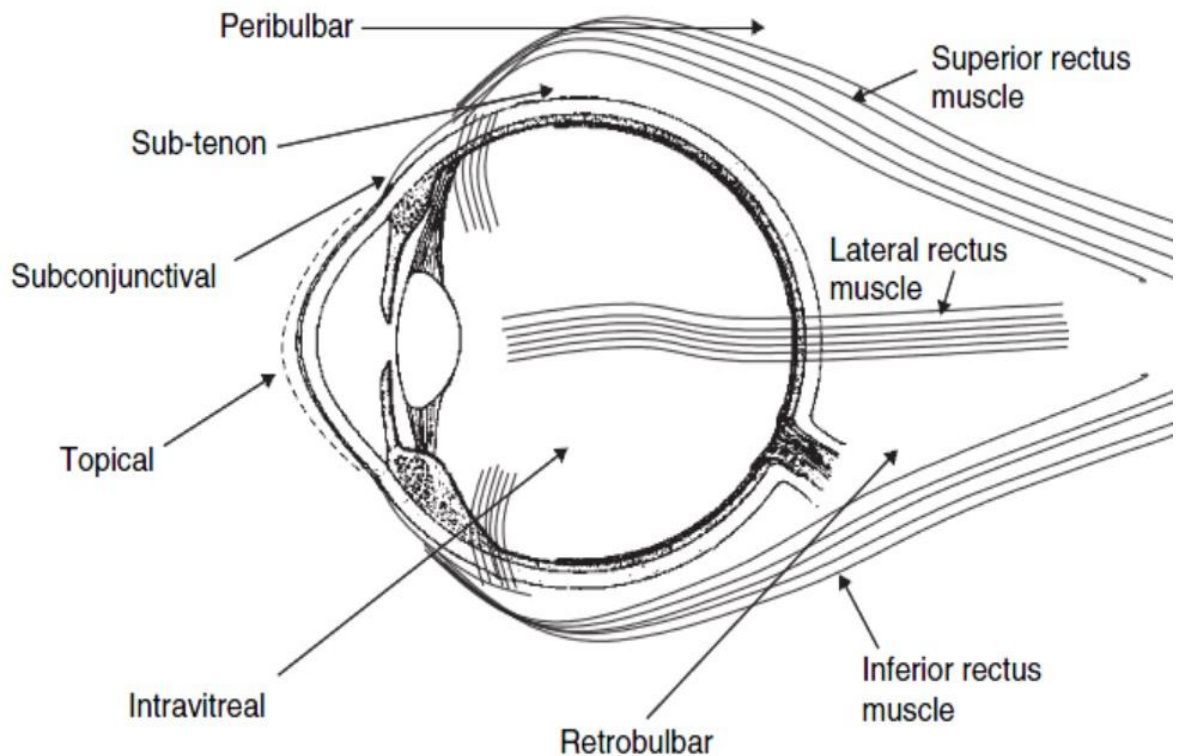


**Figure 1.5:** Schematic representation of periocular routes of administration (Janoria, Gunda, Boddu & Mitra, 2007).

#### **1.3.3.4 Intravitreal Drug Delivery**

The intravitreal injection (maximum 0.2 mL volume) penetrates the sclera, choroid and retina, this route delivers the drugs directly to the vitreous humour (Figure 1.5). However, it is associated with many disadvantages such as endophthalmitis, retinal detachment, haemorrhage and the need for repetitive treatments. The puncture point of the needle is usually at the par planar which is about 1.5 mm from the limbus. The par planar is the ideal point for intravitreal injections and implants as the peripheral retina is less vascular at this point and it enables the needle to deliver the drug/implant deep in the vitreous humour (Kompella & Edelhauser, 2011). Despite all the associated disadvantages of the intravitreal technique, it is the most common route of delivery to the posterior segment of the eye (Kompella & Edelhauser, 2011).

### **1.4 The Ocular Physiological Barriers**

In order to understand the challenges and formidable obstacles facing ocular drug delivery to the anterior and posterior segments of the human eye, the eyes physiological barriers must be explained. The next two sections (1.4.1 and 1.4.2) describe the precorneal and corneal barriers that any drug applied to the anterior segment of the eye must overcome, whereas sections 1.4.2 and 1.4.3 detail the conjunctival and systemic barriers associated with drug delivery to the posterior segment of the eye.

#### **1.4.1 Lacrimal Fluid and Eye Movement (Precorneal) Barriers**

The tear film and eye lids are the first defensive barrier against any foreign materials entering the eye. Tear film (lacrimal fluid) is composed of three layers namely, lipid, aqueous and mucin, it has an approximate 3  $\mu\text{m}$  thickness, 6-8  $\mu\text{L}$

volume and  $1.2 \mu\text{L min}^{-1}$  turnover volume (Järvinen, Järvinen & Urtti, 1995; Thassu & Chader, 2013). The lipid layer is the superficial layer consists of wax esters, diglycerides, triglycerides and hydrocarbons. This layer reduces the surface friction related to blinking and eye movement and prevents the evaporation of the aqueous layer (Thassu & Chader, 2013). The aqueous layer consists of mainly water, proteins, glycoprotein, electrolytes and peptides (Touitou & Barry, 2007). The mucin layer consists of glycoproteins which prevent bacterial adhesion, provide lubrication and function as antioxidants (Touitou & Barry, 2007).

The eye cul-de-sac can accommodate approximately  $30 \mu\text{L}$  of administered drug without overflow. Drugs applied topically to the surface of the eye (typical eye drop volume  $25\text{-}56 \mu\text{L}$  (Brown & Lynch, 1986)) are subjected to rapid elimination via the lacrimal fluid and eye lid movement. The lacrimal fluid shows a quick restoration time (typically  $2\text{-}3 \text{ min}$ ) to its original volume ( $6\text{-}8 \mu\text{L}$ ) (Maurice, 1973), and the majority of the topically administered dose is washed away within just  $15\text{-}30 \text{ s}$  after instillation due to lacrimal turn over, blinking (every  $2\text{-}10 \text{ s}$  (Rogers, 2010)) and induced lacrimation (Gaudana, Ananthula, Parenky & Mitra, 2010; Thassu & Chader, 2013).

### **1.4.2 Corneal and Conjunctival Barriers**

Topically administered drugs to the front of the eye can penetrate by two routes, namely the corneal and non-corneal pathways. The non-corneal route involves drug penetration across the conjunctival and scleral tissues before permeation into the inner intraocular tissues (Thassu & Chader, 2013). Drugs penetrating through the corneal route encounter the lipophilic corneal epithelial and endothelial layers and the hydrophilic stroma layer (Wilson, Zhu, Kurmala, Rao & Dhillon, 2001). The epithelium and endothelium cell layers contain a  $100\text{-}$

fold higher lipid content per unit mass than the corneal stroma (Cogan & Hirsch, 1944) and the apical corneal epithelial cells have tight junctions (the estimated intercellular pore size is 60 Å or less (Lee, 1990)). The epithelial layer is a rate limiting barrier for transcorneal diffusion of small ionic and hydrophilic drugs, as a result of the presence of tight junctions which retard paracellular drug permeation of these molecules (Klyce & Crosson, 1985). The endothelium layer is not a rate limiting barrier as it is approximately 200 times more permeable than the epithelium (Touitou & Barry, 2007). After the epithelial layer drugs encounter the stroma (500 µm thick) which is hydrophilic in nature and acts as a major barrier for highly lipophilic drugs (Urtti, 2006).

The conjunctiva has 5-15 layers of epithelia cells with tight junctions at the apical end (Aulton & Cooper, 1988). Although the conjunctival tissue have more epithelia cell layers than the corneal tissue, it has two times larger pores and sixteen times higher pore density than the cornea (Hamalainen, Kananen, Auriola, Kontturi & Urtti, 1997). Hence, the conjunctiva is more leaky and permeable to hydrophilic and large molecules than the cornea and allows drugs to permeate through both paracellular and transcellular routes (Mitra, Velagaleti & Grau, 2010). In humans, the conjunctiva possesses a relatively large surface area (16-18 cm<sup>2</sup>) in comparison to the cornea (1 cm<sup>2</sup>) (Järvinen, Järvinen & Urtti, 1995). Due to the large surface area, the high vascularisation and lymphatics of the conjunctiva, topically applied drugs are quickly cleared into the blood circulation resulting in systemic distribution of the drug away from the eye (Mitra, 2003).

The precorneal barriers and the short drug-cornea contact time is considered to be the primary reason for the low percentage (typically 1%) of the

topically administered drug to reach the intraocular tissues (Lee & Robinson, 1986).

### 1.4.3 Blood Retinal Barriers

This barrier affects drug delivery targeting the posterior segment of the eye. Passive diffusion of materials into the retinal tissue is restricted by the blood retinal barrier (BRB) (Ranta *et al.*, 2010). The BRB can be divided into an inner and an outer BRB as depicted in Figure 1.6. The inner BRB is located near the vitreous humour and is formed by endothelial capillary cells which have tight junctions. The outer BRB consists of the RPE and choroidal circulation.

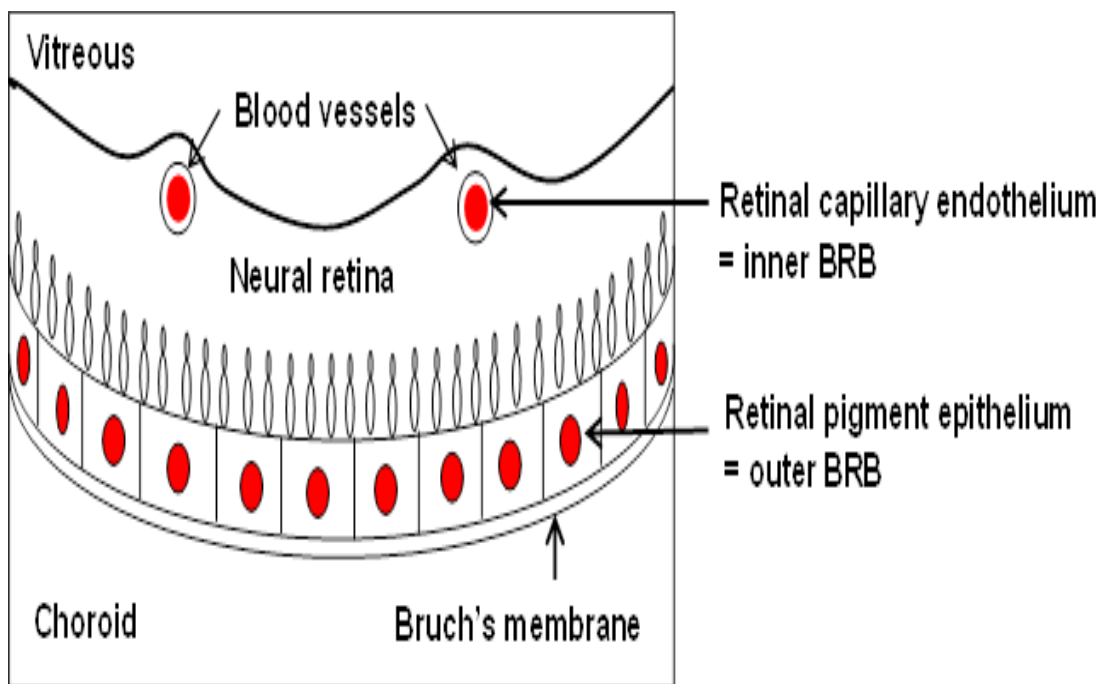


**Figure 1.6:** Schematic presentation of the inner and the outer blood–retinal barrier (BRB) (Hornof, Toropainen & Urtti, 2005).

The inner two thirds of the retina obtains nourishment from the retinal blood vessels which branch from the ophthalmic artery (inner BRB). These blood vessels are not fenestrated, similar to the vessels of the brain and have tight junctions in between retinal capillary endothelial cells. The other third of the retina obtains its

nourishment from the choroidal circulation (outer BRB). The choroidal capillaries (choriocapillaries) have fenestrations of approximately 60 nm in diameter. They are leaky and relatively permeable allowing the exchange of nutrients and waste products (Thassu & Chader, 2013).

Despite the high blood flow of the retinal and choroid (the average rate of the entire retina blood flow is  $80 \text{ mL min}^{-1}$ , whereas the choroidal flow is ten times the retinal blood flow (Thassu & Chader, 2013; Yanoff, Duker & Augsburger, 2004)). The tight junctions in the RPE and in the retinal capillaries restrict the movement of many substances and form a formidable barrier for drugs administered systemically or periorcularly (injections in the cavities between the eyeball and the eye orbit, Figure 1.5) (Urtti, 2006).

## **1.5 Ocular Drug Permeation Pathways**

### **1.5.1 Anterior Segment**

Drug transport across corneal epithelial cells occurs via two pathways namely, transcellular and paracellular. The transcellular involves cell membrane diffusion, channel diffusion and carrier-mediated transport through the cells. The paracellular involves diffusion through intercellular spaces and tight junctions. The passive transcellular pathway, in which molecules diffuse through the lipid matrix of the epithelial cells membrane, is believed to be the major mechanism of corneal absorption of topically applied ocular drugs (Macha & Mitra, 2003). The molecules' ability to diffuse across epithelial cells through the transcellular pathway depends upon the molecules interaction with the constituents of the cell plasma membrane (lipids, cell receptors). The partitioning of molecules into the cornea is a crucial step to enter the cell. Consequently, the partition coefficient is a major factor in

determining the transport across the epithelium and stroma. A parabolic relationship between the partition coefficient (octanol/water) and the corneal permeability has been reported for many molecules (Kishida & Otori, 1980; Mosher & Mikkelsen, 1979; Schoenwald & Huang, 1983; Schoenwald & Ward, 1978). As a result of the lipophilic and hydrophilic nature of the corneal barriers (corneal epithelium and stroma), the optimal corneal permeability was reported to be in the range of 1-3 log partition coefficient (Lee, 1990; Mitra, 2003; Mosher & Mikkelsen, 1979) indicating the absorption of neither extremely hydrophilic nor extremely lipophilic compounds is favoured. Nonetheless, other factors such as molecular size and charge influence the corneal permeability (Lee, Carson & Takemoto, 1986; Mitra, 2003). Liaw *et. al.* reported cationic molecules such as L-lysine and benzylamine had 2-3 fold higher rabbit corneal permeability than negatively charged molecules such as L-glutamic acid and salicylic acid (Liaw, Rojanasakul & Robinson, 1992). The author also reported a decrease in polyethylene glycol (200-1000 Da) rabbit corneal permeability with increasing molecular weight (Liaw & Robinson, 1992).

The paracellular pathway is the preferred route of diffusion for small hydrophilic molecules through the corneal epithelium. However, the existence of three forms of junctional complexes namely, tight junctions (zonula occludens), intermediate junctions and spot desmosomes hinders the transport of the hydrophilic molecules (Macha & Mitra, 2003).

The two major barriers encountered in topical ocular drug delivery are the precorneal short residence time and the poor permeability of the cornea. Prolonged topical drug residence time is achieved using inserts (Jain, Carvalho & Banerjee, 2010; Salminen, Urtti, Kujari & Juslin, 1983), bioadhesives (Kaur &

Smitha, 2002) and via vehicle modification (Diebold *et al.*, 2007). Reportedly the poor corneal permeability can be altered by modifying the integrity of the corneal epithelium either by using chemical penetration enhancers or physical enhancement techniques (e.g. iontophoresis) or by altering the physicochemical properties of the drug (prodrug) (Hao, Li, Liu & Kao, 2009; Järvinen & Järvinen, 1996).

Ocular penetration enhancers used topically affect either the paracellular or the transcellular route. The paracellular enhancers alter reversibly the corneal epithelial tight junction, increasing paracellular transport. Many ocular paracellular enhancers have been reported in the literature, most commonly calcium chelating agents and cytochalasins (group of small molecules which bind to the actin microfilaments rendering the permeability of the tight junctions). The chemical transcellular enhancers disrupt the cell membrane lipids and protein components, increasing drug transcellular permeability (Mitra, 2003; Zambito, Zaino & Di Colo, 2006).

A prodrug is an inactive form of the drug, which is enzymatically metabolised (esterases, ketone reductase, and steroid 6-hydroxylase) to the active parent compound in ocular tissues (Patel, Shastri, Shelat & Shukla, 2010). The prodrug approach has been reported to enhance corneal permeation. For example dipivefrine a prodrug of epinephrine (used in the treatment of glaucoma) was shown to have 17 fold higher corneal permeability than epinephrine in human (Järvinen & Järvinen, 1996; Mandell, Stentz & Kitabchi, 1978). The disadvantage of the prodrug approach is that it is considered as a new drug entity and hence extensive pharmacokinetic information is required.

### 1.5.2 Posterior Segment

As scleral tissue is acellular and does not have epithelium and endothelium cell layers, the transcellular drug permeation pathway is absent. Scleral drug permeation can occur via the perivascular and the collagen network spaces and via the aqueous media of the mucopolysaccharides (Wilson, Zhu, Kurmala, Rao & Dhillon, 2001). Due to the structure of the scleral tissue (mainly the absence of the tight junctions), large molecules can passively diffuse via the tissue. Molecules of size up to 120 kDa have been reported to diffuse into human sclera (Nicoli *et al.*, 2009). Due to the porous nature of the sclera and the passive diffusion of penetrants in between the free spaces of the collagen bundles, scleral drug permeability is influenced by drug properties such as lipophilicity and solubility (Thakur, Kadam & Kompella, 2011). An inverse correlation between the drug lipophilicity of six corticosteroids (triamcinolone, prednisolone, dexamethasone, fluocinolone acetonide, triamcinolone acetonide, and budesonide) and bovine scleral transport has been reported (Thakur, Kadam & Kompella, 2011). The latter study also reported a strong positive correlation between drug solubility and tissue concentration, which affected free drug levels and scleral drug transport.

Similar to the cornea, the drug permeability through the sclera can be enhanced using the prodrug approach. Malik *et al.* reported the permeation of celecoxib prodrug (celecoxib succinamidic acid) to be eight fold higher than celecoxib through bovine scleral tissue due to the increase in the solubility of the prodrug (the aqueous solubility of the prodrug was 300 fold higher than celecoxib) (Malik, Kadam, Cheruvu & Kompella, 2012). The alteration of the BRB permeability is another method to enhance posterior drug delivery. The BRB permeability can be altered using a hyperosmotic solution (e.g. mannitol) which

prompts shrinkage of the RPE cells and retinal capillaries ultimately causing the opening of tight junctions (Mitra, 2003). However, the aforesaid method is non-specific, prompting shrinkage to all blood capillaries and hence rendering them more permeable, making this method unsuitable for specifically enhancing ocular drug delivery (Mitra, 2003).

## **1.6 Conventional Ophthalmic Drug Delivery Systems**

There are various conventional ophthalmic formulations that have been developed to overcome the ocular barriers and target the internal tissues of the eye. The following sections (1.6.1 and 1.6.2) will briefly describe the most common formulations used in treating anterior and posterior segment diseases.

### **1.6.1 Anterior Segment**

#### **1.6.1.1 Topical Formulations (Eye Drops, Suspensions, Ointments and Gels)**

The current treatment for most anterior segment diseases is topically administered drugs. The topically applied formulations can be liquids, suspensions, creams or gels.

Examples of eye drops solutions are antibiotics (e.g. Chloramphenicol 0.5% w/v), antihistamines (e.g. Azelastin Hydrochloride 0.05% w/v) and lubricants (e.g. Hypromellose 0.5% w/v) (*British National Formulary* 2013). Despite the ease and convenience of self-application of eye drops, conventional eye drops are inefficient (Siepmann, 2012) as they suffer from rapid elimination through the precorneal barriers (i.e. eye blinking and tear flow) resulting in a short duration of drug effect and hence the requirement for a more frequent dosing regimen (Siepmann, 2012). The actual dose penetrating into the eye from topical eye drops is estimated to be

less than 5% of the total administered dose (Urtti, 2006). To improve drug contact time, permeation and bioavailability; viscosity enhancers, such as methylcellulose, polyvinyl alcohol, polyvinylpyrrolidone and carbomers can be added to topical eye drops (Bartlett & Jaanus, 2008). Viscosity enhancers improve precorneal residence time and bioavailability by enhancing formulation viscosity resulting in a slower dose elimination from the precorneal area and hence a greater transcorneal penetration of the drug into the anterior chamber (Bartlett & Jaanus, 2008).

Ophthalmic suspensions contain solid micron sized particles of hydrophobic drugs suspended in aqueous medium (e.g. Betaxolol Hydrochloride 0.5% w/v, 99.5% of the particles are less than 25  $\mu\text{m}$  in size) (*British National Formulary* 2013; "British Pharmacopoeia Volume III," 2012). The solid micron sized particles are retained in the precorneal pocket and thus improve drug contact time and duration of action relative to drug solution. The drug contact time and duration of action for a suspension is particle size dependent in which larger sized particles can be retained in the precorneal area for longer time and show slower drug dissolution compared to smaller size particles (Remington, Troy & Beringer, 2006). The disadvantages of ophthalmic suspensions include coagulation and disturbance in vision.

Ophthalmic ointments are composed of a mixture of solid hydrocarbons (paraffin) which have a melting point close to the physiological ocular temperature (34 °C) (Bartlett & Jaanus, 2008). The drug is added to the ointment mixture either as a solution or as a micro sized powder. Upon administration to the precorneal area, the ointment can break up into small droplets forming a depot of drug in the cul-de-sac for extended periods. Ophthalmic ointments, such as betamethasone

sodium phosphate 0.1% w/v (*British National Formulary* 2013), are indicated for a range of inflammatory conditions of the eye, such as blepharitis (inflammation of the eyelid). Due to the viscous nature of such formulations, they provide prolonged therapeutic action relative to eye drops. This can be particularly beneficial for nocturnal use and may also enhance patient compliance due to a reduced number of applications. The main disadvantage of ointments is that they cause blurred vision due to the refractive index difference between tears and the non-aqueous ointment (Bartlett & Jaanus, 2008).

Ophthalmic gels form as a result of high concentration of viscosity enhancers (e.g. carbomers). Viscotears<sup>®</sup> and GelTears<sup>®</sup> are two examples of ophthalmic gels containing carbomer 980 (*British National Formulary* 2013). The main advantage of ophthalmic gels is that they prolong precorneal residence time and reduce systemic clearance (Bartlett & Jaanus, 2008). Despite the high viscosity, a gel achieves only a limited improvement in bioavailability, and the administration frequency can be reduced to once a day at most. The high viscosity gel might result in blurred vision and matted eyelids, which reduce patient compliance (Bartlett & Jaanus, 2008). A newer development in ophthalmic gels is the use of polymers that exhibit solution-gel phase transition in the precorneal area (mainly cul-de-sac) in response to environmental stimuli such as pH, ion strength or temperature. This new development allows ophthalmic gel formulation to be applied using eye drops, which is simple, convenient and able to dispense precise volume. Timoptol<sup>®</sup> LA (*British National Formulary* 2013) and Lizmon TG<sup>®</sup> (Shibuya, Kashiwagi & Tsukahara, 2003; Yamamoto, Kitazawa, Azuma, Tsukahara & Nakashima, 1997) are two commercially marketed gel-forming ophthalmic solutions, the first changes to gel in the presence of sodium ions (ion

strength), whereas the latter forms gel upon changes in temperature (thermosetting gel) (Shibuya, Kashiwagi & Tsukahara, 2003).

#### **1.6.1.2 Cul-de-sac Inserts**

The cul-de-sac of the eye is situated between the palpebral or bulbar conjunctiva and either the lower or the upper eyelid (Lens, Nemeth & Ledford, 2008). Ocusert<sup>®</sup> is a cul-de-sac non-bioerodible (ethylene–vinyl ester) insert developed for glaucoma. It provides uniform controlled release of pilocarpine over a seven day period (20 or 40 µg/h of pilocarpine). This product was introduced to the market in 1974 (Macoul & Pavanlangston, 1975), but soon after, Ocusert<sup>®</sup> was shown to have unsatisfactory intraocular pressure (IOP) control due to difficulty of insertion, irritation of the eye and displacement of the device (Sihvola & Puustjarvi, 1981). The insert is no longer marketed due to side effects of pilocarpine, such as a miosis and brow ache (Molokhia, Thomas, Garff, Mandell & Wirostko, 2013).

Lacrisert<sup>®</sup> is a rod shaped (1.27 mm diameter, 3.5 mm long) water soluble cul-de-sac insert introduced in 1981 (Lee, Hughes, Ross & Robinson, 2010). It is composed of 5 mg of hydroxypropyl cellulose without any additives (McDonald *et al.*, 2009). The insert is designed to treat moderate to severe dry eye syndrome. It works by breaking down into cellulose, which stabilizes and prolongs the tear film breakup time, it also serves as an eye lubricant (Lee, Hughes, Ross & Robinson, 2010).

#### **1.6.1.3 Implants**

Surodex<sup>™</sup> is a rod shaped biodegradable poly(D,L-lactide-co-glycolide) (PLGA) anterior chamber implant. The implant is inserted into position (anterior chamber) after cataract surgery to control postoperative inflammation (Lee, Chee, Balakrishnan, Farzavandi & Tan, 2003). It is a matrix implant consisting of

dexamethasone (60 µg) and PLGA with hydroxypropyl methylcellulose. The implant has 1.0 x 0.5 mm dimension and provides sustained dexamethasone release over 7-10 d at a constant rate (Lee, Hughes, Ross & Robinson, 2010).

## 1.6.2 Posterior Segment

### 1.6.2.1 Systemic, Intravitreal and Transscleral formulations

Currently, the treatment of posterior segment disease is still significantly limited to intravitreal and periocular injections. However, there are treatments which use other delivery routes (i.e. systemic) such as Visudyne<sup>®</sup>. Visudyne<sup>®</sup> is a photodynamic therapy (photosensitizer) developed as an alternative to thermal laser photocoagulation for the treatment of subfoveal choroidal neovascularization due to AMD. The photodynamic therapy is a two phase treatment and employs photosensitizer (verteporfin<sup>®</sup>) administered intravenously (systemic) followed by activation with a laser which emits light having the same wavelength of light absorption as the photosensitizer. Unlike thermal laser photocoagulation, the photodynamic therapy allows selective damage of tissue containing the photosensitizer (Prasad, Schwartz & Hubschman, 2010).

Periocular corticosteroid injections for control of intraocular inflammation (e.g. uveitis) are well established clinical practice. For example TA sub-Tenon's injections have been reported to be effective in the treatment of uveitis (Salek *et al.*, 2013).

More recently the majority of treatments have shifted in favour of intravitreal injections. Lucentis<sup>®</sup> (anti-VEGF drug) became the first-line therapeutics in wet AMD treatment. It is an intravitreal injection approved in the United Kingdom in

January 2013. NICE also approved Lucentis<sup>®</sup> for the treatment of diabetic macular oedema (DMO) ("National Institute for Health and Care Excellence," 2013).

### **1.6.2.2 Implants**

Posterior implants are often too big to be delivered through needles and surgical operations have to be performed. However, recently smaller injectable implants have been commercialised (Sanford, 2013). Vitrasert<sup>®</sup> is a Food and Drug Administration (FDA) approved implant for the treatment of AIDS-related cytomegalovirus infection. It requires a 4-5 mm sclerotomy (surgical incision of the sclera) to implant inside the human eye. It releases ganciclovir (4.5 mg) over a 6 month period (Choonara, Pillay, Danckwerts, Carmichael & Du Toit, 2010). Another implant named Retisert<sup>®</sup> is an FDA approved treatment for chronic non-infectious posterior uveitis (an inflammation of the interior tissues of the eye). Retisert<sup>®</sup> is surgically implanted in the eye through a small 3-4 mm incision. The implant is a reservoir insert (disc shaped 3 x 2 x 5 mm) containing 0.49 mg of fluocinolone which releases the drug over 30 months (Nicholson, Singh, Sears, Lowder & Kaiser, 2012). Similarly, Iluvien<sup>®</sup> is also an intravitreal implant providing a sustained dose of fluocinolone acetonide to treat diabetic macular oedema. It has been approved in several European countries including the United Kingdom (Sanford, 2013). This implant is delivered through an applicator employing a 25-gauge needle and the implant can last up to 36 months (Sanford, 2013).

## **1.7 Novel Drug Delivery Systems and Methods**

Topical and conventional ophthalmic formulations do not maintain therapeutic drug concentration in the target tissues for a long duration due to the unique physiological and anatomical eye barriers (Kompella & Edelhauser, 2011).

Researchers and the pharmaceutical industry are still in pursuit of novel drug delivery systems to overcome ocular barriers and to provide prolonged drug therapeutic concentration by the least invasive method possible. The following two sections (1.7.1 and 1.7.2) describe novel drug delivery systems in various clinical stages and novel ocular drug delivery methods.

### **1.7.1 Novel Drug Delivery Systems in Clinical Trials**

For the treatment of chronic eye diseases, various formulations are at different stages of clinical trial to prolong and maintain therapeutic drug concentration in the target tissues. The urgent need to develop novel ophthalmic drug delivery systems for chronic diseases arises from the necessity to increase the convenience for the patient, reduce the dosing frequency of both anterior and posterior formulations and to reduce the invasiveness of treatment targeting the posterior segment.

#### **1.7.1.1 Anterior Segment**

A subconjunctival insert developed by Pfizer, Inc. containing latanoprost (glaucoma treatment) is in Phase I clinical trials. The insert is composed of a latanoprost core contained in a poly (DL-lactide-co-glycolide) (PLGA) tube. An impermeable polymer caps one end of the tube, whilst a permeable polymer caps the other. Latanoprost is released across the permeable end and the drug release duration is designed to be 3-6 months (ClinicalTrials.gov Identifier: NCT01180062).

IBI-10090 is a dexamethasone biodegradable product for injection into the anterior chamber to treat inflammation associated with cataract surgery (ClinicalTrials.gov Identifier: NCT01606735). IBI-10090 will be Icon's first product

to reach the market using the Verisome<sup>®</sup> technology (a novel drug delivery system in which the final product can be manufactured in a biodegradable solid, gel or liquid form capable of releasing drug in a controlled manner for extended periods of time). Icon Bioscience also plans on using Verisome<sup>®</sup> technology for the delivery of therapeutic levels of latanoprost to the anterior chamber (IBI-60089) as a Phase I/II clinical trial will be launched in the second quarter of 2013 ("Icon Bioscience, Inc. (IBI)," 2013).

### **1.7.1.2 Posterior Segment**

Eye drops to target the posterior segment of the eye have not yet been commercially introduced. However, a few eye drop formulations targeting posterior eye diseases are in clinical trials.

A topical dexamethasone cyclodextrin microparticle eye drop was applied topically into DMO patients three or six times a day for 4 weeks. Interestingly, the eye drops have been shown to decrease central macular thickness and improve visual acuity after 4 weeks (Tanito *et al.*, 2011). A Phase II/III clinical trial for DMO is currently undergoing (ClinicalTrials.gov Identifier: NCT01523314).

Triamcinolone acetonide (TA) has been used extensively in treating various posterior ocular disorders such as: macular oedema, DMO and AMD using intravitreal or periocular injection. Despite the apparent established efficacy of corticosteroids, disadvantages such as the relative short half-life of drugs in their free form for intravitreal use and frequent dosage related problems (inconvenience, vitreous hemorrhage, endophthalmitis, and retinal detachment) has led researchers to develop a variety of sustained release drug delivery systems to overcome the aforementioned drawbacks.

Cardillo *et al.* designed PLGA microspheres encapsulating TA (RETAAC system). The efficacy of intravitreally RETAAC (1 mg) was compared to a TA suspension (4 mg) in DMO patients. RETAAC demonstrated a superior performance compared to the TA suspension in decreasing the retinal thickness and improving visual acuity after 12 months (Cardillo, Souza-Filho & Oliveira, 2006). The formulation is currently undergoing Phase I/II (ClinicalTrials.gov, NCT00407849).

Icon Bioscience, Inc. is also using Verisome<sup>®</sup> drug delivery platform technology to deliver TA via intravitreal injection (IBI-20089). The IBI-20089 is designed to last up to six months (6.9 mg, 25 µL) or one year (13.8 mg, 50 µL). A Phase I study of IBI-20089 for chronic cystoid macular oedema has been completed ("Icon Bioscience, Inc. (IBI)," 2013). Cohort 1 and 2 (five patients each) received an intravitreal injection of 6.9 and 13.8 mg of TA, respectively. The central subfield thickness (CST) decreased significantly from the baseline in cohort 1 and 2 at day 1, 30 and 360 after receiving the TA intravitreal injection (Lim, Fung, Wieland, Hung & Wong, 2011). The IBI-20089 is now being tested in a Phase II clinical study adjunctively with 0.5 mg of ranibizumab (Lucentis<sup>®</sup>) for choroidal neovascular AMD (ClinicalTrials.gov Identifier: NCT01175395).

Cortiject<sup>®</sup> is a preservative and solvent free emulsion encapsulating a target tissue-activated corticosteroid prodrug developed by Novagali Pharma ("Cortiject<sup>®</sup>," 2013). Although a Phase I study is currently ongoing in the United States in patients suffering from diabetic retinopathy, to date there are no details disclosed about the efficacy of the trial nor about the duration of the drug release from the formulation (ClinicalTrials.gov Identifier: NCT00665106).

## 1.7.2 Novel Drug Delivery Methods

### 1.7.2.1 Anterior Segment

#### 1.7.2.1.1 Drug Loaded Contact Lenses

Recently, a drug loaded contact lens has been investigated as a potential technology for delivering drugs to the anterior segment of the eye. This route has the advantage of minimising the frequency of administration and is non-invasive. Costa *et al.* showed the possibility of impregnating commercially available silicon-based contact lenses with two anti-glaucoma drugs without altering important features of the contact lenses, such as O<sub>2</sub> permeability (Costa *et al.*, 2010). A silicone hydrogel contact lens loaded (pre-soaked) with ketotifen fumarate (allergic conjunctivitis treatment) sustained the drug release for more than 24 h in rabbits eyes (Xu, Li & Sun, 2011).

#### 1.7.2.1.2 Capsule Drug Ring

The capsule drug ring (13 mm outside diameter, 0.1 mm thickness and volume of 50 µL) is a novel intraocular insert inserted in to the lens capsule during cataract surgery (placed on the empty circumferential space around the intraocular lens) (Molokhia *et al.*, 2010). This implant is a non-biodegradable refillable reservoir capable of delivering multiple drugs to either the anterior or posterior segment of the eye. Molokhia *et al.* produced prototypes using poly methyl methacrylate sheets as the reservoir material with silicon valves for refilling. The device has shown near-zero-order release kinetics of Avastin as a model drug in *in-vitro* studies (Molokhia *et al.*, 2010).

### **1.7.2.2 Posterior Segment**

#### **1.7.2.2.1 Drug Delivery through Suprachoroidal Space**

The suprachoroidal space is a virtual space between the choroids and sclera. This space becomes real when fluid accumulates resulting of detachment of the choroid from the sclera. Delivery to the suprachoroidal space via microcannulation is a prospective route of drug delivery to the posterior segment of the human eye, especially to target the macular region and optic nerve (Olsen *et al.*, 2006). A research team reported the use of microcannulation to deliver TA to the suprachoroidal space (Olsen *et al.*, 2006). It is shown to be safe and reproducible in primates and pigs. Furthermore, the study demonstrated steady delivery of triamcinolone acetonide to the posterior tissue for at least 120 days with the advantage of very low systemic levels of TA, thus reducing side effects (Olsen *et al.*, 2006).

#### **1.7.2.2.2 Intrasccleral Drug Delivery through Hollow Microneedles**

A novel approach has been attempted where hollow microneedles are used to deliver drugs to the sclera. Microneedles can penetrate into scleral tissue without completely crossing or rupturing the sclera and hence they can diminish the side effects associated with intravitreal injections, such as pain, retinal detachment and haemorrhage. Microneedles can be coated with a therapeutic agent or used to deliver a therapeutic agent in a solution form (Jiang, Moore, Edelhauser & Prausnitz, 2009). The novel approach of intrasccleral drug delivery through individual microneedles has been shown to deliver 10-35  $\mu$ L of solutions to an approximate circular area of diameter 1-10 mm in human cadaver scleral tissue (Jiang, Moore, Edelhauser & Prausnitz, 2009). This novel approach

bypasses the conjunctival and episcleral barriers (well-vascularised tissue) and deposit drugs directly in the scleral tissue.

## 1.8 Nano Size Drug Delivery Systems

The European commission define nano-materials as “A natural, incidental or manufactured material containing particles, in an unbound state or as an aggregate or as an agglomerate and where, for 50 % or more of the particles in the number size distribution, one or more external dimensions is in the size range 1 nm - 100 nm.” (“European Commission”, 2013). However, the range of nano-size drug delivery systems (NDDS) in nano-pharmaceuticals according to the European Science Foundation ranges from 1 to 1000 nm (“Nanomedicine,” 2005; Volker, Bärbel & Sibylle, 2008). NDDS, broadly referred to as nanocarriers, have a number of exploitable properties for drug delivery, due to their small relative size such as, high surface area to volume ratio, the effects of Brownian motion and low settling velocity (Gupta & Kompella, 2006). Aqueous NDDS below 1000 nm in size have higher Brownian motion velocity (a 1000 nm particle has a speed of 1716 nm.s<sup>-1</sup>) than the settling velocity (a 1000 nm particle has a speed of 430 nm.s<sup>-1</sup>) and hence the colloidal solutions are stable and have a long shelf-life (Gupta & Kompella, 2006). Colloidal solutions precipitate upon agglomeration or the formation of particles larger than 2 µm (Hsu, 2007; Yasukawa *et al.*, 2004).

NDDS have been prepared from various materials such as synthetic polymers (e.g. PLGA), natural polymers (e.g. chitosan), proteins (e.g. human albumine serum), lipids and even metals (e.g. gold). The variation of used materials and different preparation methods results in numerous types of NDDS such as liposomes, solid lipid nanoparticles, dendrimers, polyelectrolyte complexes, nanoemulsions, and polymeric nanoparticles, nanospheres or micelles

(Badawi, El-Laithy, Qidra, Mofty & Dally, 2008; Bakkour, Darcos, Coumes, Li & Coudane, 2013; Chaiyasan, Srinivas & Tiyaboonchai, 2013; Hippalgaonkar, Adelli, Hippalgaonkar, Repka & Majumdar, 2013; Sinha, Bansal, Kaushik, Kumria & Trehan, 2004; Vandamme & Brobeck, 2005). Figure 1.7 illustrates a few types of the NDDS used in ocular drug delivery. The explanation of all the different NDDS systems is beyond the scope of this thesis but the reader is direct to read previous reviews (Diebold & Calonge, 2010; Lehner, Wang, Marsch & Hunziker, 2013). Special attention will be focused on polymeric self-assemblies (SA) as a consequence of their thermodynamic stability, ease of preparation and the possibility of eliminating organic solvents from the preparations method.

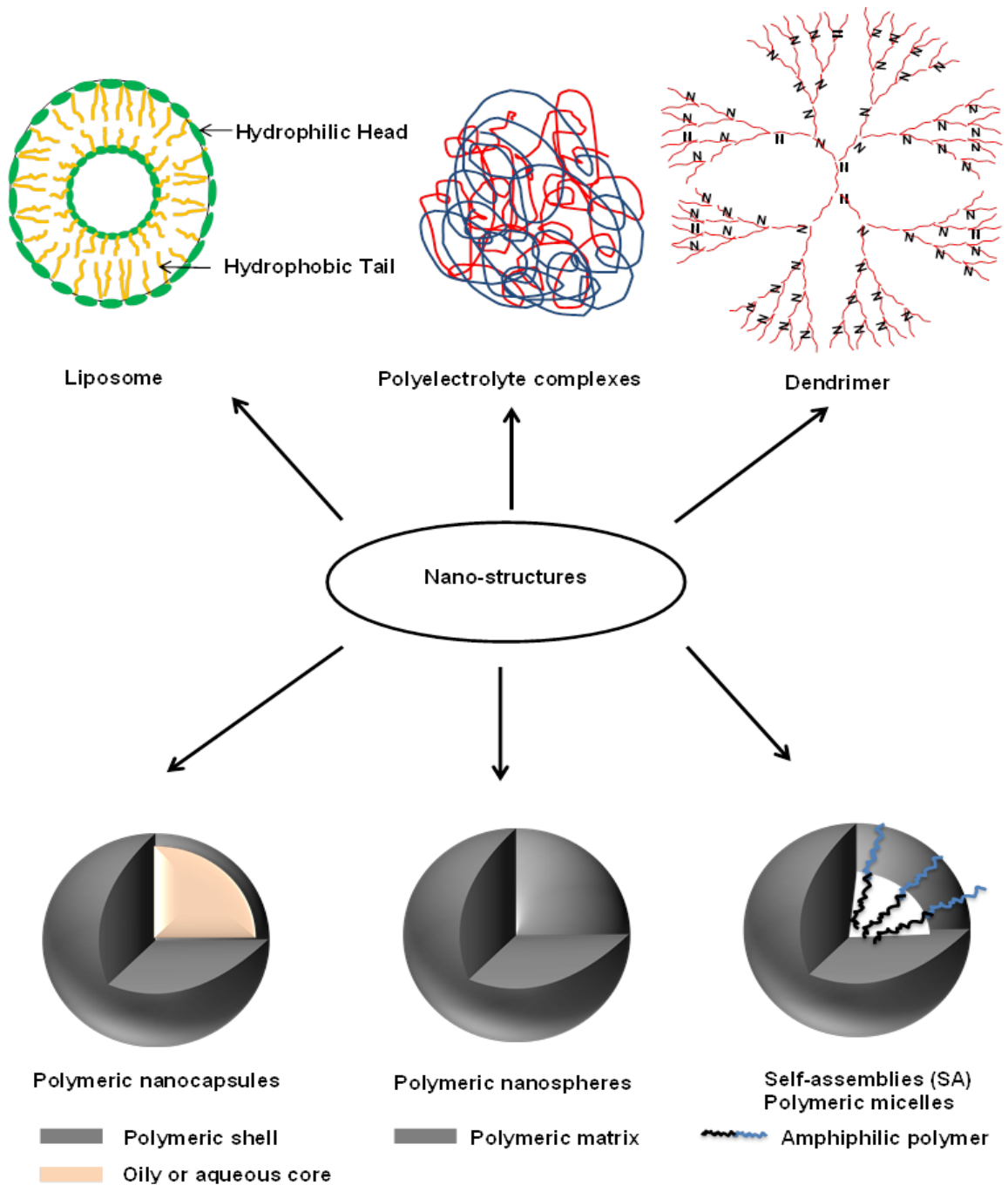


Figure 1.7: Types of nano-size delivery systems used in drug delivery.

## 1.9 NDDS in Ocular Drug Delivery

The use of nano-sized delivery systems is an emerging concept with promising potential to allow ophthalmic drugs to overcome the eye's physiological barriers by enhancing penetration, prolonging drug residence time and allowing

the delivery of high drug concentrations to ocular tissues, with relatively fewer side effects such as toxicity in comparison to drug suspension and conventional formulations (Macha & Mitra, 2003; Mitra, 2003). NDDS are of special interest in ocular drug delivery due to their small size (typically 20-500 nm), which not only enables the foreign body sensation in the eye to be avoided but also influences their permeation through ocular barriers. For example the uptake of small PLGA nanospheres (100 nm) was found to be higher than larger particles (800 nm and 10  $\mu$ m) in primary cultured rabbit conjunctival epithelial cells (Qaddoumi *et al.*, 2004). Similarly, the size of the NDDS influenced their penetration into rabbit retinal tissue after intravitreal injection, wherein 200 and 50 nm nanospheres were observed in the retina unlike 2  $\mu$ m spheres which were unable to penetrate the retina (Sakurai, Ozeki, Kunou & Ogura, 2001).

NDDS have been reported to enhance drug bioavailability in the eye compared to drug alone solutions/suspensions. For example after topical instillation of an indomethacin chitosan nano-emulsion in rabbits the levels of indomethacin in the aqueous humour were found to be 30 times higher than topical administration of an indomethacin solution (Badawi, El-Laithy, Qidra, Mofty & Dally, 2008). Similarly, the levels of prednisolone in the aqueous humour of a rabbit eye following topical administration of polymeric micelles were similar to those found after administration of a tenfold dose of a commercial suspension of the drug (Qu *et al.*, 2006). NDDS not only offer enhanced corneal permeation and high drug entrapment, but can also reduce drug related side effects. Poly- $\epsilon$ -caprolactone nanocapsules with oily core containing metipranolol evaluated in rabbits eyes lowered the cardiovascular side effects in comparison to commercial drops (Torchilin, 2006).

Due to the high Brownian motion velocity and low settling velocity of NDDS in comparison to microparticles, NDDS can offer prolonged vitreal half-life. NDDS injected in the vitreous humour (static fluid) stays suspended for a prolonged period in comparison to microparticles before coming in contact with the surrounding tissue (retina) and hence limits contact of the drug with cells capable of engulfing and clearing the NDDS. Sakurai *et al.* reported decreased fluorescein vitreal half-life with an increase in size of polystyrene nanospheres containing fluorescein. The author reported fluorescein vitreal half-life of  $5.4 \pm 0.8$ ,  $8.6 \pm 0.7$  and  $10.1 \pm 1.8$  days for 2  $\mu\text{m}$ , 200 nm and 50 nm particles, respectively (Sakurai, Ozeki, Kunou & Ogura, 2001).

A plethora of reports demonstrated the capability of NDDS to sustain drug release in the posterior segment (Araujo, Nikolic, Egea, Souto & Garcia, 2011; Kompella & Edelhauser, 2011; Yang *et al.*, 2013; Zhang, Li, Zhang, Wang & Song, 2009) and to enhance corneal permeability, via transcellular, paracellular routes or by a combination of both (Baba *et al.*, 2011; Contreras-Ruiz *et al.*, 2011; De Campos, Diebold, Carvalho, Sanchez & Alonso, 2004; De la Fuente, Seijo & Alonso, 2008; Jain *et al.*, 2011).

### **1.9.1 Polymeric Self-Assemblies (SA)**

#### **1.9.1.1 Polymer Architecture and SA Formation**

Self-assembly is a spontaneous process at which disordered amphiphiles (molecules consisting of hydrophobic and hydrophilic segments) organize into supramolecular aggregates (self-assemblies), typically in the nano size range (Chen, Cheng & Zhuo, 2011). The type and shape of these self-assemblies (SA) depends on the architecture of the amphiphiles (Letchford & Burt, 2007;

Thompson *et al.*, 2008). Amphiphiles such as block co-polymers typically self-assemble into polymeric micelles with dimension smaller than 100 nm (Kataoka, Harada & Nagasaki, 2012), whereas comb-shaped polymers (graft polymers) self-assemble into polymeric micelles, vesicles or solid nanospheres as depicted in Figure 1.8 (Cheng *et al.*, 2006; Hoskins, Lin & Cheng, 2012; Wang, Qu, Gray, Tetley & Uchegbu, 2004). At low concentrations amphiphiles remain as single molecules in solution, until reaching a critical concentration known as the critical aggregation concentration (CAC), at which molecules start to spontaneously assemble. The self-assembly process of the amphiphiles is driven by the entropy gain associated with the dehydration of the hydrophobic core. Freeing water molecules from the hydrophobic environment, facilitates the formation of hydrogen bonding between the unfettered water molecules and hence results in an increase in system entropy.

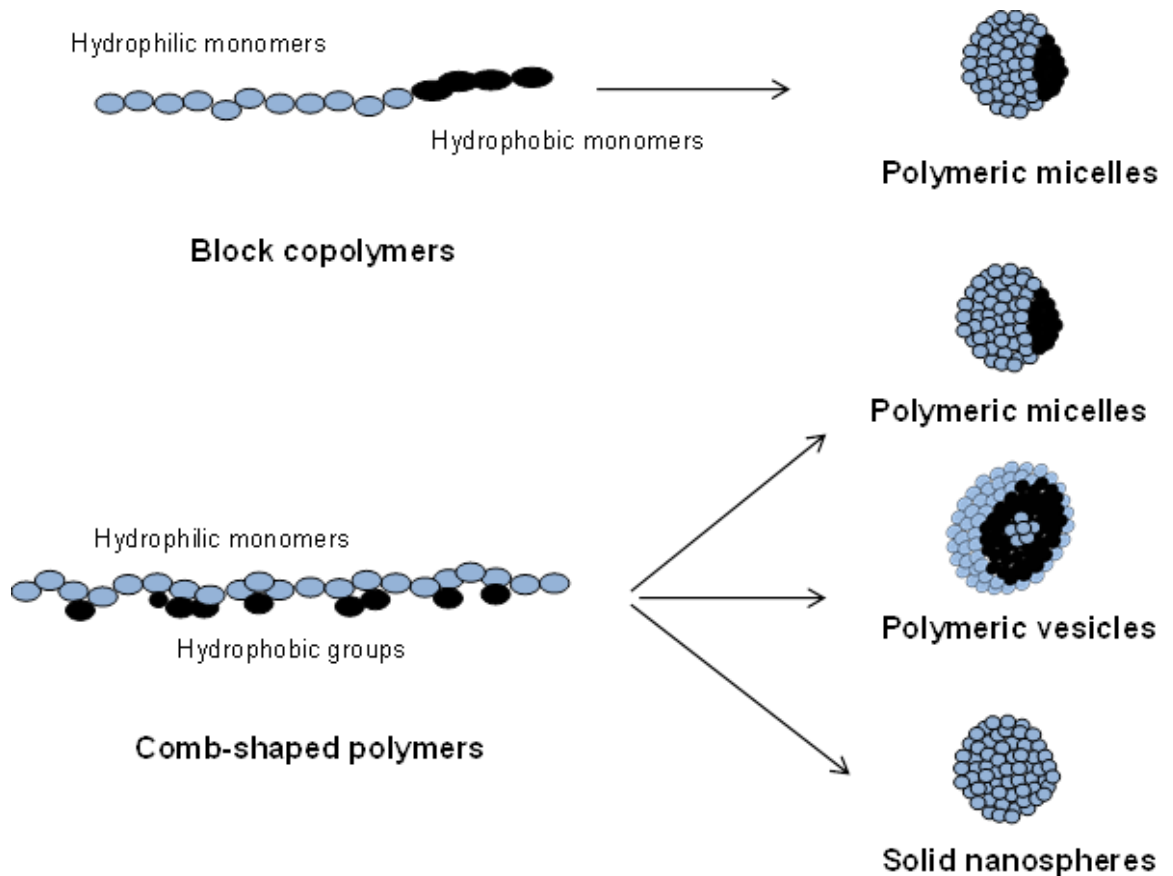


**Figure 1.8:** The self-assembly of amphiphiles into: polymeric micelles, polymeric vesicles and polymeric solid nanospheres.

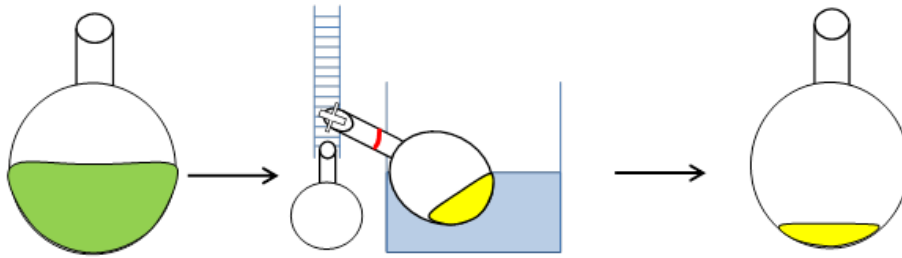
### 1.9.1.2 SA Drug Loading Methods

SA may encapsulate drugs by chemical, physical or electrostatic means. A physical means is the most common; occurring via various drug loading methods such as oil in water emulsion, dialysis and sonication (Figure 1.9). The oil in water emulsion method involves preparing an aqueous solution of the amphiphilic polymer to which the solution of drug in water-miscible volatile organic solvent (e.g. chloroform) is added. An oil in water emulsion is formed by continuous magnetic stirring followed by evaporation of the volatile solvent. In this method it is almost impossible to completely eliminate the organic solvent which is potentially toxic, and hence this renders this method unsuitable for the preparation intended for ocular drug delivery (Pathak & Thassu, 2009).

In the dialysis method, both the polymer and drug are dissolved in an organic solvent; the polymer-drug solution is then dialysed against an aqueous based solvent. The passive diffusion of the organic solvent from the dialysis bag into the aqueous based solvent drives the formation of self-assemblies with the drug becoming encapsulated as a result of decrease in polymer/drug solubility with the decrease of concentration of the organic solvent. The organic solvent used in dissolving the drug and the polymer affects the morphology and particle size distribution of the nanoparticles (Rao & Geckeler, 2011). In order to ensure the removal of the organic solvent the dialysis has to be extended over several days, which is inconvenient from an industrial scale point of view.

The direct dissolution method consists of equilibrating the drug and amphiphilic polymer in aqueous media. Despite this method being spontaneous, the aggregation of the molecules can be facilitated using sonication (Cheng *et al.*, 2006; Hoskins, 2010; Hoskins, Lin, Tetley & Cheng, 2012b). This method has the advantages over other methods of not using organic solvent and producing thermodynamically stable SA where the size and shape of these SA can be controlled by the polymer architecture (Thompson *et al.*, 2008).

A-

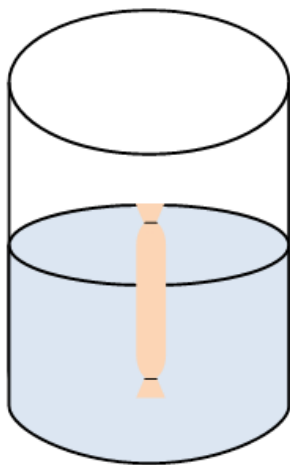


Oil in water emulsion

Solvent removed

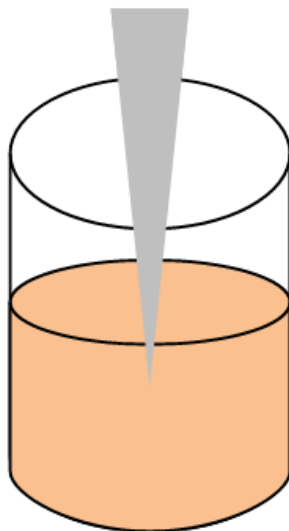
Residue formulation re-dissolved  
in water and filtered

B-

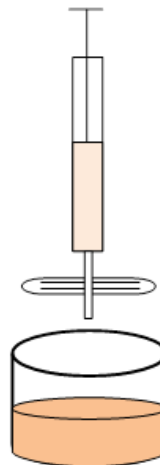


Polymer and drug dissolved in organic solvent and  
dialysed against water

C-



Polymer and drug probe sonicated in aqueous  
environment



Resultant solution filtered to  
remove free drug

**Figure 1.9:** Methods of SA drug encapsulation. A) oil in water emulsion B) dialysis and C) sonication.

### 1.9.1.3 SA in Drug Delivery

SA usually exhibit a much lower critical micelle concentration (CMC) or CAC compared to low molecular weight surfactants (Kedar, Phutane, Shidhaye & Kadam, 2010). The CAC of amphiphiles is typically in the order of  $10^{-6}$  to  $10^{-7}$  M, which is approximately a thousand times lower than the CMC of low molecular weight surfactants ( $10^{-3}$  to  $10^{-4}$  M) (Douroumis & Fahr, 2012). Due to their low CMC/CAC, SA are relatively unaffected by dilution and remain stable at very low polymer concentrations (Nishiyama & Kataoka, 2006). The SA stability result in an enhanced circulation time compared to surfactant micelles especially when the formulation is applied intravenously (the ideal route for anticancer drugs and tumour targeting) (Cheng *et al.*, 2010; Nishiyama & Kataoka, 2006; Oerlemans *et al.*, 2010). The use of SA incorporating anticancer drugs avoids the use of adjuvants, such as ethanol or cremophor EL, which often have toxic side effects (Hamaguchi *et al.*, 2007). SA have also been shown to be excellent solubilisers for poorly water-soluble drugs (Gu *et al.*, 2011; Hoskins, Lin & Cheng, 2012) and this has resulted in great interest in their use in oral route (Hoskins, Lin, Tetley & Cheng, 2012b; Kedar, Phutane, Shidhaye & Kadam, 2010; Thompson, Tetley, Uchegbu & Cheng, 2009).

### 1.9.1.4 SA in Ocular Delivery

In recent years, a few reports have emerged wherein SA have been investigated for ocular drug delivery. Di Tommaso *et al.* prepared spherical polymeric micelles which enhanced the aqueous solubility of the very hydrophobic drug cyclosporin A (CsA) by approximately 400 times (Di Tommaso *et al.*, 2012). The latter study also demonstrated the topical effectiveness and tolerability of the formulation in rat eyes as an alternative to the systemic treatment of CsA for the

prevention of corneal graft rejection. Another polymeric micelle system reported by Pepic *et al.* increased the bioavailability of dexamethasone (Dex) in rabbit eye by 2.4 fold compared to commercial Dex eye drops despite the micellar system having a fourfold lower dose concentration (Pepic, Hafner, Lovric, Pirkic & Filipovic-Grcic, 2010). Qu *et al.* have shown prednisolone polymeric micelles produced a 10-fold increase in aqueous humour prednisolone levels in rabbit eyes when compared to prednisolone suspension after topical ocular application (Qu *et al.*, 2006). Other research groups also have demonstrated improved drug permeation and bioavailability in the eye by polymeric micelles (Civiale, Licciardi, Cavallaro, Giammona & Mazzone, 2009; Mitra, Velagaleti & Grau, 2010). There have been limited publications investigating SA made from comb-shaped amphiphilic polymers designed for ocular drug delivery (Qu *et al.*, 2006; Yuan, Li & Yuan, 2006) despite the ease of preparation and the high hydrophobic drug encapsulation efficiency (Gu *et al.*, 2011; Hoskins, Lin, Tetley & Cheng, 2012b). SA made from comb-shaped amphiphilic polymers have shown promising potential in protein delivery (Cheng *et al.*, 2010) and intravenous hydrophobic drug delivery (Hoskins *et al.*, 2010). They have also been shown to open tight junctions, facilitate transcellular transport in gut epithelial cell line and demonstrate an improved oral bioavailability *in-vivo* (Hoskins, Lin, Tetley & Cheng, 2012b; Thompson *et al.*, 2011). Therefore in this work four SA spontaneously formed from comb-shaped amphiphilic polymers based on poly(allylamine) were synthesised and the effect on the different polymer architecture of these amphiphilic polymers in influencing their potential in ocular delivery was evaluated.

## 1.10 Aims and Objectives

The overall aim of this research project was to investigate drug delivery to the eye using novel polymeric nanoparticles as drug carriers. As such, the objectives of this work were:

- To synthesise four amphiphilic polymers by attaching hydrophobic and hydrophilic moieties onto Poly(allylamine) (PAA) backbone.
- To characterise the synthesised amphiphilic polymers.
- To prepare and characterise polymeric SA formed by the amphiphilic polymers in aqueous media.
- To prepare and optimize polymeric SA loaded with Triamcinolone Acetonide (TA) and to determine the TA content, and TA release from the SA.
- To develop an *in-vitro* eye model.
- To test and compare the permeability of the synthesised TA-SA using the developed *in-vitro* eye model.
- To test the *In-vitro* toxicity of the synthesised amphiphilic polymers on a human cell culture line.

## **Chapter Two: Polymer Synthesis and Characterisation**

---

## 2.1 Introduction

Amphiphilic polymers are composed of hydrophobic and hydrophilic moieties. The different arrangement of these moieties within the macromolecule produces various architectures such as block copolymers (Gaucher *et al.*, 2005; Yao *et al.*, 2011), comb-shaped polymers (Cheng *et al.*, 2006) and star-shaped polymers (Li *et al.*, 2011). In aqueous media where the concentrations of amphiphilic polymers are lower than the critical aggregation concentration (CAC) they saturate the air/water interface in order to attain a state of minimal energy (Lee, 2008). Above the CAC threshold, the amphiphilic polymeric chains spontaneously self-assemble into a core-shell structure as a result of aggregation of the hydrophobic moieties, stabilised by the hydrophilic corona (Kedar, Phutane, Shidhaye & Kadam, 2010). Amphiphilic polymers are known to form different types of aggregates with nano-scale size such as polymeric micelles (Gu *et al.*, 2007; Thompson *et al.*, 2008), vesicles (Sarkar, El Khoury, Lopina & Hu, 2007; Wang, McConaghy, Tetley & Uchegbu, 2001; Zhu, Zhao, Qu & Yang, 2012) and nanoparticles (Cheng *et al.*, 2006; Thompson, Tetley & Cheng, 2010).

In recent years, there has been an increase in interest in the use of polymeric self-assemblies (SA) as a drug delivery vehicle (Gupta, Agrawal & Vyas, 2013). The amphiphilic polymeric SA have several advantages over other vehicles (i.e. liposomes, niosomes and conventional formulations) such as 1) mild preparation conditions without the need of organic solvents or stabilisers which are potentially toxic 2) an inherent low CAC which is approximately a thousand times lower than the critical micelle concentration (CMC) of low molecular weight surfactant (Kedar, Phutane, Shidhaye & Kadam, 2010) 3) high hydrophobic drug

loading capacity (Xiong, Binkhathlan, Molavi & Lavasanifar, 2012) and 4) ease of surface functionalisation to achieve active targeting (Zhu *et al.*, 2011).

Effective ophthalmic drug delivery still remains a challenge due to clearance mechanisms of xenobiotics and the protecting nature of the ocular barriers (section 1.4). In recent years there has been an increased interest in the use of SA based drug delivery systems to overcome the challenges faced by the conventional ocular formulations (Gupta *et al.*, 2010; Nagarwal, Kant, Singh, Maiti & Pandit, 2009). The permeability of positively charged molecules through the corneal epithelium cells is favoured owing to the transport of these molecules through active pump and carrier-mediated systems (Liaw, Rojanasakul & Robinson, 1992). Furthermore, positively charged molecules have a longer residence time on the surface of the eye as the corneal epithelial cells possess a negative charge at physiological pH (Rabinovich-Guilatt, Couvreur, Lambert & Dubernet, 2004). It has been demonstrated that the transcorneal permeation of cationic liposomes resulted in a higher permeation compared to anionic and neutral liposomes (Hathout, Mansour, Mortada & Guinedi, 2007; Schaeffer & Krohn, 1982). Similar behaviour is also predicted and observed for other drug vehicles such as cationic nanoparticles (De Campos *et al.*, 2003; Fitzgerald, Hadgraft, Kreuter & Wilson, 1987) and cationic SA (Thompson *et al.*, 2011). One example is a SA formed by hydrophobically modified Poly(allylamine) (PAA). PAA (Figure 2.4) is a cationic water soluble homo-polymer, which has primary amine groups. Previous reports have shown that hydrophobically modified PAA-insulin nano-complexes were able to reversibly open tight junctions as well as increasing the gene transfer efficacy in comparison to commercial transfecting agents and the native polymer (Nimesh, Kumar & Chandra, 2006; Pathak *et al.*, 2007; Thompson

*et al.*, 2011). Furthermore, PAA hydrophobically modified polymers offer stable aggregates at low modification percentages (2.5 and 5 %mole) in comparison to other polymers such as poly(ethylenimine) (Thompson *et al.*, 2008). However, to date SA formed by these hydrophobically modified PAA have not been explored in ocular drug delivery.

Therefore, in this study four hydrophobically modified PAA polymers; containing 1) palmitoyl 2) cholesteryl 3) polyethylene glycol and 4) dansyl residues were synthesised. Palmitoyl groups have been shown to reduce the cytotoxicity of PAA by 2-3 fold and to form stable self-assemblies at low molar grafting percentages (Thompson, Tetley, Uchegbu & Cheng, 2009). Cholesterol is a naturally occurring sterol within the body and is a vital component of cell the membrane for regulating membrane fluidity. The introduction of a cholesteryl moiety to polymers has been reported to increase the biological compatibility of the polymer and to induce spontaneous formation of SA (Liu, Wang, Zhuang, Yang & Yang, 2012; Yu, Li, Qiu & Jin, 2008; Yusa, Kamachi & Morishima, 1998). A dansyl moiety has a bicyclic naphthalene ring which absorbs light in the UV-visible range and undergoes fluorescence, these phenomena makes the dansyl modified polymer detectable by various analytical techniques. Additionally, previous work by Hoskins *et al.* has shown that the SA of PAA modified with a dansyl group (10% mole modification) significantly improved the solubility of three hydrophobic drugs by at least 145 fold (Hoskins, Lin, Tetley & Cheng, 2012b). Although, positively charged SA are preferred for topical ocular drug delivery, they tend to aggregate in the vitreous humour due to electrostatic interaction with the negatively charged hyaluronic acid (Koo *et al.*, 2012). The addition of a hydrophilic polyethylene glycol (PEG) moiety can significantly minimize protein adsorption

onto SA, consequently reducing the aggregation of SA (José Alonso, 2004; Peeters *et al.*, 2005; Roberts, Bentley & Harris, 2002). Additionally, PEG coated nanocapsules have also been reported to migrate deeper across the corneal epithelium than chitosan coated nanocapsules (De Campos *et al.*, 2003). Therefore, it was planned to synthesise PEG-palmitoyl PAA and compare to the cationic PAA.

The analytical methods used in characterising the PAA and modified polymers were elemental analysis, nuclear magnetic resonance (NMR) and differential scanning calorimetry (DSC).

### 2.1.1 Elemental Analysis

Elemental analysis (EA) is a useful tool for determining the elemental composition of an unknown sample. The most common elements are carbon (C), hydrogen (H), nitrogen (N) and sulphur (S). The quantitative measurement of elements in the material under study enables the determination of the empirical formula of the material. The empirical formula is the smallest set of integer ratio of elements constituting the unknown compound.

The C, H, N and S weight percentages are determined using an elemental analyser as shown in Figure 2.1. An accurate weighed sample is instantaneously oxidised at an elevated temperature (flash combustion), usually about 1000 °C, in the presence of excess oxygen and helium (gas carrier). A complete oxidation of the elements in the presence of a catalyst produces CO<sub>2</sub>, H<sub>2</sub>O, NO<sub>2</sub> and SO<sub>2</sub> gases. The gaseous mixture is then passed over copper to reduce the nitrogen oxides to nitrogen and to remove excess oxygen. The gaseous mixture is then directed into a gas chromatography column where individual components are separated and eluted as N<sub>2</sub>, CO<sub>2</sub>, H<sub>2</sub>O and SO<sub>2</sub>. The eluted gases are detected by

a thermal conductivity detector producing a signal proportional to the concentration of the element.

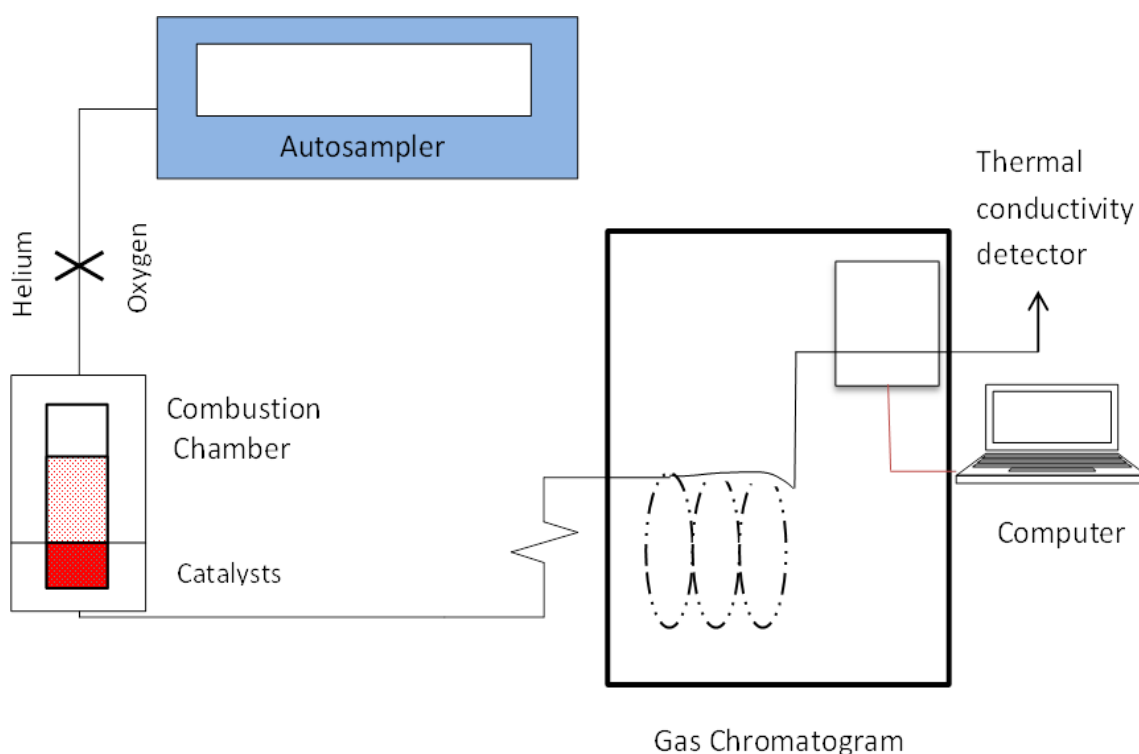


**Figure 2.1:** Schematic diagram of an elemental analyser.

### 2.1.2 Nuclear Magnetic Resonance

Nuclear magnetic resonance (NMR) is a powerful and useful analytical tool used in elucidating the structure and interactions of unknown compounds. The NMR phenomenon is based on the fact that some nuclei have magnetic spin properties. These nuclei resonate at a certain wavelength upon being placed in a magnetic field and excited by an electromagnetic radiation. The resonating wavelength corresponds to the radio frequency range in the electromagnetic radiation spectrum. The difference between the lower and higher energy levels in the resonating nuclei is proportional to the strength of the applied magnetic field. Different protons within a chemical structure resonate at slightly different frequencies, thereby producing a distinctive electromagnetic radiation (ER) signal.

The measured signal is recorded and processed to yield an NMR spectrum for the nucleus concerned. The chemical shift in the NMR spectrum is the frequency of the resonance expressed with reference to a standard compound, the chemical shift is expressed as parts per million (ppm, or  $\delta$ ).

The different chemical environments surrounding the nuclei such as the presence of methyl/ethyl groups or electronegative atoms (e.g. O, Cl) give rise to different chemical shifts. The electronegative atoms have the ability to de-shield the nucleus by withdrawing the electron cloud thus influencing their nuclear resonance frequencies. De-shielded protons appear downfield in a NMR spectrum in comparison to shielded protons, as the de-shielded protons require less applied magnetic field to change their spin state. The spinning of nearby atoms can affect the magnetic field of the nucleus. This phenomenon is called spin-spin coupling and occurs as duplets, triplets or multiplets depending on the number of neighbouring magnetic nuclei. A schematic representation of an NMR spectrometer is shown in Figure 2.2.

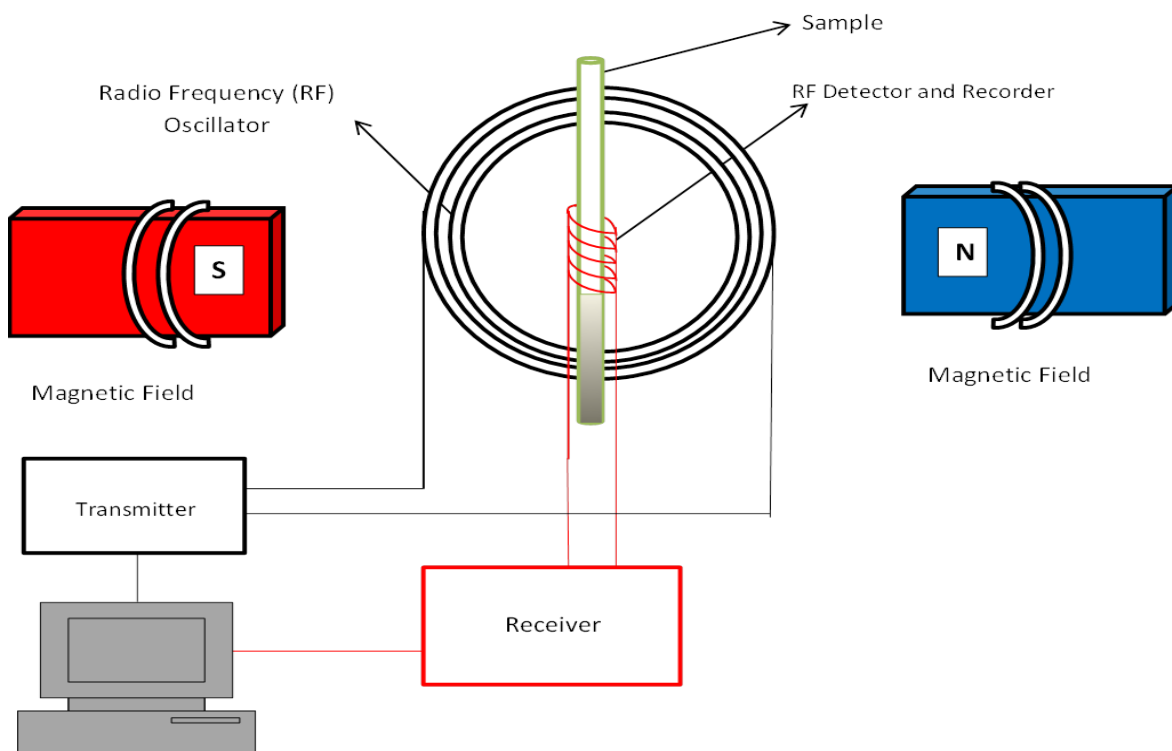


**Figure 2.2:** The schematic diagram of NMR spectrometer.

### 2.1.3 Differential Scanning Calorimetry

Differential scanning calorimeter (DSC) is a highly sensitive analytical tool, used mainly in the investigation of thermal events associated with phase transitions such as the melting point and glass transition ( $T_g$ ) of polymeric materials. The polymeric material is contained in an aluminium pan and an empty pan is used as a reference. Both pans are subjected to the same heat profile and the difference in the heat flow between the sample and the reference is recorded. At phase transition events more or less heat flows to the sample pan than the reference to maintain both pans at the same temperature. The recorded difference is plotted against temperature and this produces peaks in the thermogram corresponding to the thermal events. Figure 2.3 shows a schematic representation of the main components of a differential scanning calorimeter.

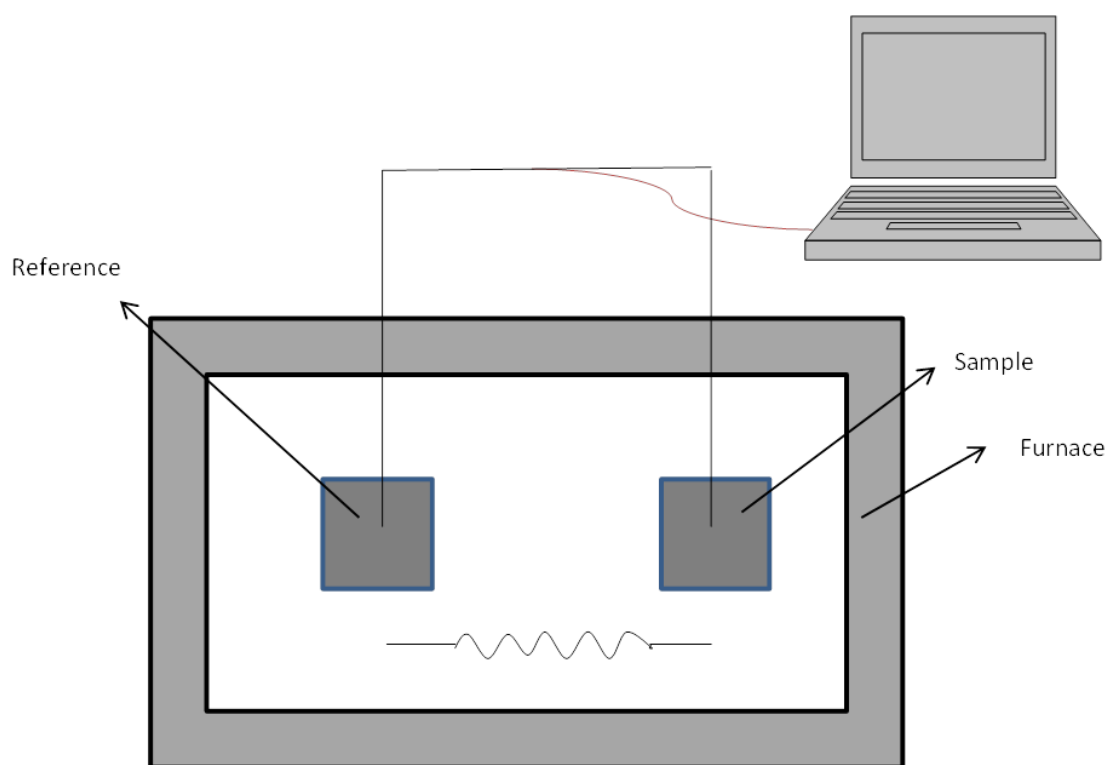


**Figure 2.3:** Schematic of a heat flux differential scanning calorimeter.

### 2.1.4 Aim and Objectives

The aim of the work in this chapter was to synthesise and characterise the hydrophobically and hydrophilically modified PAA. The objectives were:

- To covalently attach palmitoyl, cholesteryl, dansyl and PEG moieties onto PAA backbone to form four different amphiphilic polymers.
- To characterise the synthesised amphiphilic polymers using EA, NMR and DSC techniques.
- To calculate the percentage mole modification of the attached moieties on the synthesised polymers.

## 2.2 Materials and Methods

Poly(allylamine hydrochloride) (PAA-HCl, average  $M_w = 15$  kDa), palmitic acid N-hydroxysuccinimide ester (98%), cholesteryl chloroformate (97%),

methoxypolyethylene glycol p-nitrophenyl carbonate (average Mw = 5 kDa), dansyl chloride, triethylamine, tris (hydroxymethyl) aminomethane and deuterated solvents (D<sub>2</sub>O and CD<sub>3</sub>OD) were all purchased from Sigma Aldrich, United Kingdom. Sodium hydrogen carbonate, sodium hydroxide, sodium carbonate and all solvents (HPLC grade) were acquired from Fisher, United Kingdom. Dialysis tubing membranes (Mw cut-off = 7 and 12-14 kDa) were purchased from Medicell International Ltd, United Kingdom.

## 2.2.1 Polymer Synthesis

### 2.2.1.1 Conversion and Purification of PAA-HCl

PAA-HCl was converted to PAA by dissolving PAA-HCl (10 g) in deionised water (100 mL) followed by the addition of sodium hydroxide pellets (8.5 g) under stirring until pH 13 was reached (pH meter 209, HANNA<sup>®</sup> Instruments, United Kingdom). The resulting solution was stirred for 1 h, and then dialysed in dialysis tube (Mw cut-off = 7 kDa) against deionised water (5 L) with six changes. The dialysate was then lyophilised for 24 h as described below to obtain PAA. Figure 2.4 illustrates the PAA structure based on the empirical formula of PAA monomer.

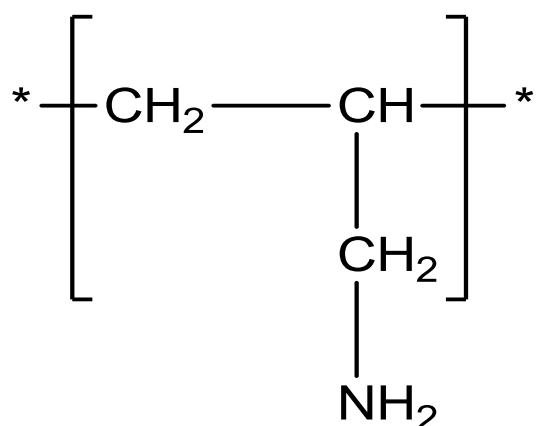


**Figure 2.4:** The chemical structure of the free-base PAA monomer.

The lyophilisation process was performed as outlined below:

The dialysate was cooled to  $-40\text{ }^{\circ}\text{C}$  at a rate of  $1^{\circ}\text{ min}^{-1}$  using a freeze dryer (LSB40 Freeze Dryer, MechaTech Systems Ltd, United Kingdom) and maintained for 60 min under normal atmospheric pressure. This was followed by heating the solution at a rate of  $1^{\circ}\text{ min}^{-1}$  (LSB40 Freeze Dryer, MechaTech Systems Ltd, United Kingdom) and keeping the temperature at  $-30\text{ }^{\circ}\text{C}$  for 180 min under low pressure (typically  $5 \times 10^{-1}$  mbar). Subsequently, the dialysate was further heated at a rate of  $1^{\circ}\text{ min}^{-1}$  and maintained at  $-10\text{ }^{\circ}\text{C}$  for 180 min under low pressure (typically  $9 \times 10^{-1}$  mbar). Finally, the lyophilised material was heated to  $20\text{ }^{\circ}\text{C}$  at a rate of  $1^{\circ}\text{ min}^{-1}$  and maintained for 860 min under low pressure (typically  $7.2 \times 10^{-2}$  mbar).

The same lyophilisation protocol for PAA was used for all synthesised polymers reported in sections 2.2.1.1-2.2.1.5.

Hydrophobic and hydrophilic pendant groups were attached on the PAA backbone using various initial feed molar ratios as described in sections 2.2.1.2 to 2.2.1.5. The numerals in the polymer abbreviations indicate the initial feed mole percentage of the hydrophobic pendant groups as summarised in Table 2-1. The 5% initial feed molar ratio was the highest that could be achieved with  $\text{Ch}_5$  and  $\text{Pa}_5$ , attempts to modify the initial feed mole ratio of dansyl to 20% were not successful (due to the polymer being insoluble in water), so 10% was the highest that could be achieved.

**Table 2-1:** The synthesised polymer names and their corresponding abbreviations.

Polymer Name	Abbreviation	Initial Percentage Feed Molar
Palmitoyl Poly(allylamine)	Pa <sub>5</sub>	5%
Methoxypolyethylene glycol Palmitoyl Poly(allylamine)	Pa <sub>5</sub> -MPEG	5% Palmitoyl 3.6% MPEG
Cholesteryl Poly(allylamine)	Ch <sub>5</sub>	5%
Dansyl Poly(allylamine)	Da <sub>10</sub>	10%

### 2.2.1.2 Synthesis of Palmitoyl Poly(allylamine) (Pa<sub>5</sub>)

The method for the synthesis of palmitoyl poly(allylamine) (Figure 2.5) was adapted from Thompson and colleagues (Thompson *et al.*, 2008; Thompson, Tetley, Uchegbu & Cheng, 2009). Pa<sub>5</sub> was synthesised by dissolving PAA (1 g) and NaHCO<sub>3</sub> (1.18 g) in deionised water (100 mL) for 5 min at room temperature. Palmitic acid-N-hydroxysuccinimide ester (310 mg) was dissolved in ethanol (100 mL). The latter solution was added to the PAA solution drop-wise over 1 h whilst stirring using magnetic flea and stirrer. The reaction was carried out for 72 h at room temperature. Solvents were evaporated using a rotary evaporator and the residue was washed with diethyl ether (3 x 50 mL). The residue was subsequently dissolved in deionised water (100 mL) and dialysed for two days using dialysis tubing (Mw cut-off = 12-14 kDa) with six changes of deionised water (5 L). The dialysate was lyophilised for 24 h and Pa<sub>5</sub> was obtained as cotton like solid.

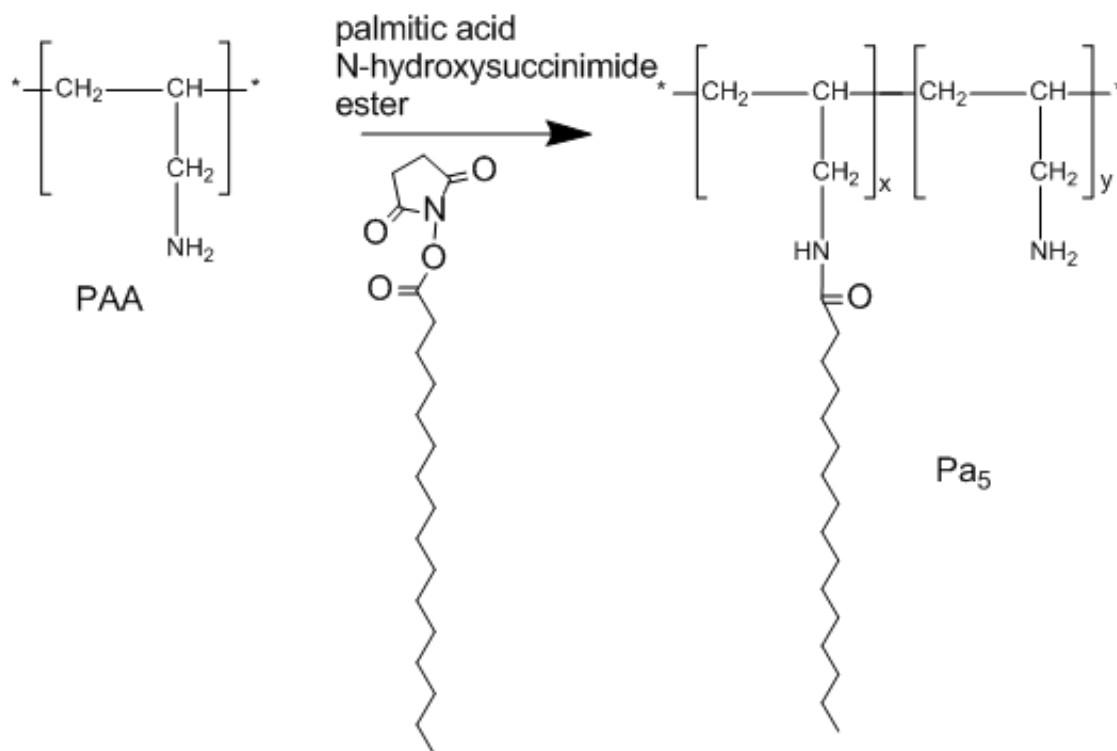
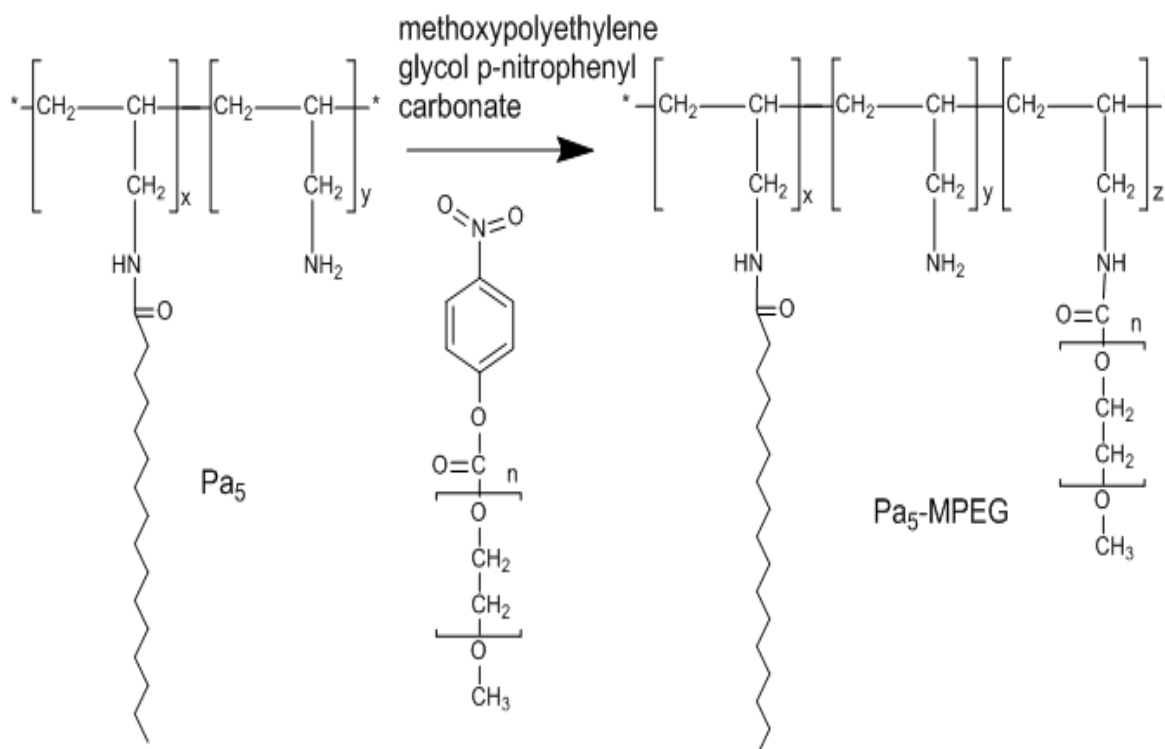


Figure 2.5: The preparation of palmitoyl poly(allylamine).

### 2.2.1.3 Synthesis of Methoxypolyethylene Glycol Palmitoyl Poly(allylamine) (Pa<sub>5</sub>-MPEG)

The synthesis method was adapted from Brown and colleagues (Brown *et al.*, 2000). Pa<sub>5</sub>-MPEG was synthesised by dissolving Pa<sub>5</sub> (300 mg) in Tris-HCl buffer (0.2 M, 100 mL). Methoxypolyethylene glycol p-nitrophenyl carbonate (600 mg) was then added to the polymer solution in 3 portions over 3 h intervals (200 mg every 1 h) while stirring using magnetic flea and stirrer. The mixture was stirred for a further 18-20 h at room temperature while protected from light. The solution was dialysed in dialysis tubing (Mw cut-off = 12-14 kDa) for four days against twelve changes of deionised water (5 L). Pa<sub>5</sub>-MPEG was obtained after lyophilising the dialysate for 24 h. Figure 2.6 illustrates the synthetic route of Pa<sub>5</sub>-MPEG polymer.



**Figure 2.6:** The preparation of methoxypolyethylene glycol (MPEG) palmitoyl Poly(allylamine) (Pa<sub>5</sub>-MPEG).

#### 2.2.1.4 Synthesis of Cholesteryl Poly(allylamine) (Ch<sub>5</sub>)

The method for the synthesis of cholesteryl poly(allylamine) was adapted from Thompson and colleagues (Thompson *et al.*, 2008). Ch<sub>5</sub> was synthesised by first dissolving PAA (2 g) in chloroform:methanol (1:1 (v/v), 100 mL). Triethylamine (2 mL) was then added to the solution and stirred for 0.5 h. Cholesteryl chloroformate (787 mg) was dissolved in chloroform:methanol (1:1 (v/v), 50 mL) and this solution was then added drop wise to the PAA solution over 2 h at 37 °C with continuous stirring using magnetic flea and stirrer. The reaction was then left stirring for an additional 24 h at 37 °C. Solvents were evaporated using a rotary evaporator and the residue was washed with diethyl ether (3 x 50 mL). The residue was then dissolved in deionised water (100 mL) and dialysed in dialysis tube (Mw cut-off = 12 kDa) for two days against deionised water (5 L) with six

changes. Ch<sub>5</sub> was obtained as a white solid after lyophilising the dialysate for 24 h.

The synthetic route of Ch<sub>5</sub> is illustrated in Figure 2.7.

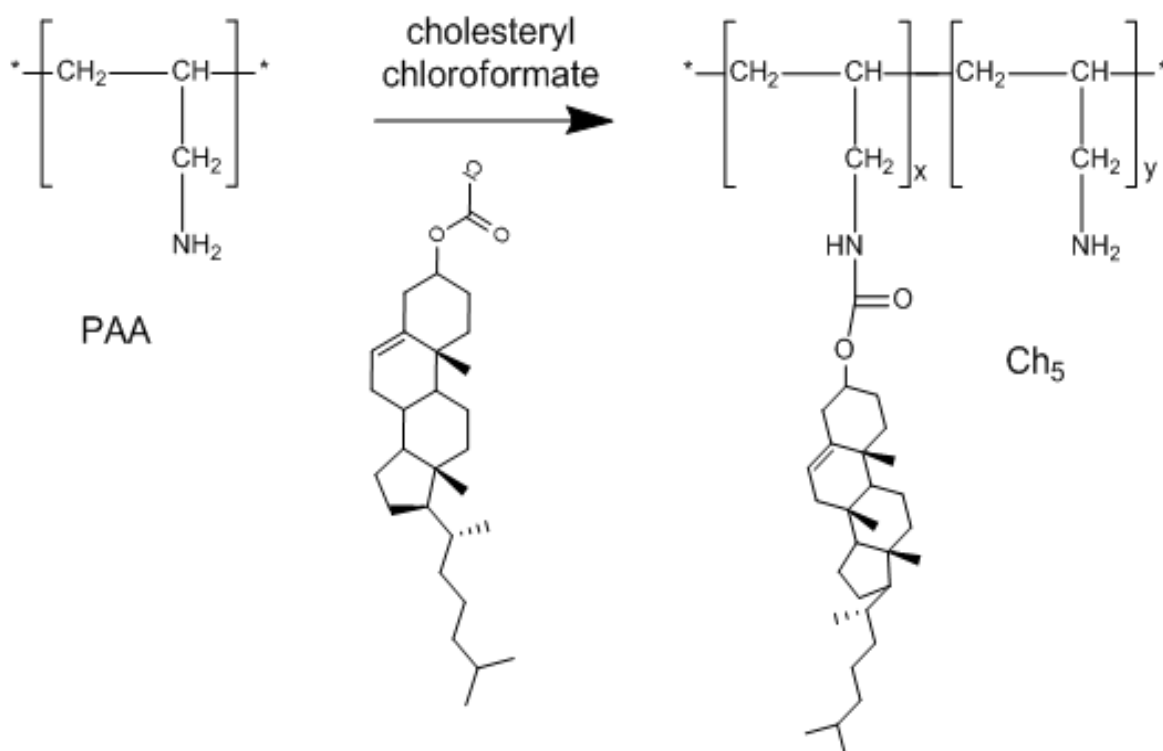


**Figure 2.7:** The preparation of cholesterol Poly(allylamine) (Ch<sub>5</sub>).

### 2.2.1.5 Synthesis of Dansyl Poly(allylamine) (Da<sub>10</sub>)

The synthesis of Da<sub>10</sub> was carried out as described by Hoskins *et.al* (Hoskins, Lin, Tetley & Cheng, 2012a) (Figure 2.8). Da<sub>10</sub> was synthesised by dissolving PAA (2 g) in dioxane:water (1:1 (v/v)) (150 mL). Sodium carbonate (185 mg) was then added to the solution and stirred until completely dissolved in the solution. Dansyl chloride (847 mg) was dissolved in dioxane (90 mL) and the solution was added drop-wise to the PAA solution over 2 h at 0 °C whilst stirring using magnetic flea and stirrer. The resulting solution was stirred continuously for 4 h at 0 °C and followed by 14 h at room temperature. A solid was obtained after solvents were evaporated using a rotary evaporator. The residue was then washed with diethyl ether (3 x 50 mL) before dissolving in deionised water (100

mL) and dialysing in dialysis tubing (Mw cut-off = 12-14 kDa) for two days against deionised water (5 L, six changes). A yellow cotton like solid was obtained after lyophilising the dialysate for 24 h.

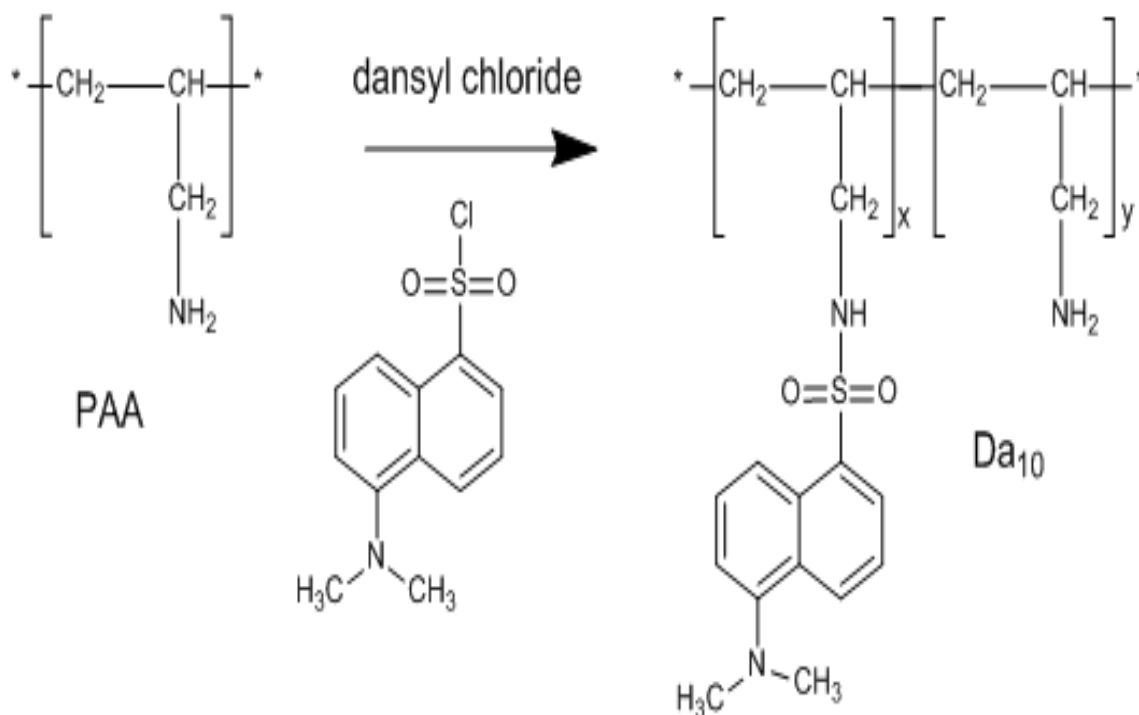


**Figure 2.8:** The preparation of dansyl poly(allylamine) (Da<sub>10</sub>).

## 2.2.2 Characterisation of Polymers

### 2.2.2.1 Elemental Analysis

The abundance of carbon (C), hydrogen (H), nitrogen (N) was determined in all modified polymers and PAA freebase. Additionally to C, H and N the abundance of sulphur (S) was determined for Da<sub>10</sub>. Samples (1 mg) were accurately weighed in a tin capsule and placed inside the auto-sampler drum. The determined weight percentage of C, H, N and S was performed using a FlashEA® 1112 Elemental Analyzer based on the quantitative dynamic flash combustion method provided by Medac Ltd, United Kingdom. The instrument was calibrated with the analysis of standard compounds (i.e. Acetanilide, Aspartic acid, Benzoic

acid or Sulphanilimide) using the K factors calculation or linear regression method incorporated in the EAGER300™ software.

### **2.2.2.2 Nuclear Magnetic Resonance (NMR)**

Approximately 7-15 mg of PAA and the modified polymers were probe sonicated (Hielscher UP200S, Germany) in CD<sub>3</sub>OD or D<sub>2</sub>O for 2 min at 100% amplitude on full cycle. The Pa<sub>5</sub> and Ch<sub>5</sub> suspensions were filtered into a NMR tube through cotton, to remove any insoluble particles. The <sup>1</sup>H NMR spectra were obtained using a 600 MHz Ultrashield spectrometer (JEOL, Japan) at 25 °C. Samples were spanned at 16 Hz, locking and shimming was performed manually for each individual sample before acquiring 64 <sup>1</sup>H NMR scan.

### **2.2.2.3 Differential Scanning Calorimetry (DSC)**

Thermal analysis of polymeric samples was performed using a DSC Q200 (TA Instruments, UK) attached to a refrigerated cooling system (TA Instruments, UK). Indium standards were used to calibrate the DSC temperature and the enthalpy prior to use. Samples (3-10 mg) were weighed into standard aluminium pans (TA Instruments, UK). The pans were heated from -30 to 250 °C in a heat-cool-heat cycle at a linear heating/cooling rate of 10 °C min<sup>-1</sup>. An inert atmosphere was maintained by purging nitrogen gas at a flow rate of 50 mL min<sup>-1</sup>.

## **2.3 Results**

### **2.3.1 Physical Appearance and Reaction Yield Percentage**

The yield percentage of each polymer and modified PAA was calculated according to Equation 2.1 (Brown, 2006) and is shown along with a description of their physical appearance in Table 2-2. Different batches of each polymer were synthesised to ensure batch uniformity/repeatability.

$$\text{Yield Percentage} = \frac{\text{Modified Polymer Yield}}{\text{Theoretical Yield}} \times 100\% \quad \text{Equation 2.1}$$

**Table 2-2:** Yield percentages and physical appearance of PAA and modified polymers.

Polymer	Yield Percentage (mean $\pm$ SD (n>3) or individual values (n=2))	Number of Batches	Physical Appearance
PAA	78.5 $\pm$ 5.8	5	Transparent glassy viscous material
Pa <sub>5</sub>	81.3 $\pm$ 4.6	4	White cotton like solid
Pa <sub>5</sub> -MPEG	94.3 $\pm$ 3.5	4	White cotton like solid
Ch <sub>5</sub>	(91.1, 93.5)	2	White powder
Da <sub>10</sub>	89.1 $\pm$ 2.1	3	Yellow cotton like solid

## 2.3.2 Elemental Analysis of PAA and Modified PAA

### 2.3.2.1 PAA Calculations

Elemental analysis was performed as an initial characterisation method to obtain the percentage mole modification of the PAA backbone. The empirical formula of the PAA free-base was calculated using Equation 2.2 & 2.3 and the result was tabulated in Table 2-3.

$$\frac{\text{The Element's molar ratio} = \text{The Element's weight percentage obtained from elemental analysis}}{\text{The Element's atomic weight}} \quad \text{Equation 2.2}$$

$$\text{Element's molar ratio relative to N} = \frac{\text{Element's molar ratio}}{\text{Element's molar ratio of N}} \quad \text{Equation 2.3}$$

**Table 2-3:** The calculations of the empirical formula of the PAA monomer.

	Elements in Unmodified PAA		
	C	H	N
Elements weight percentage obtained from elemental analysis	59.0	12.0	24.0
Element's molar ratio (Equation 2.2)	4.9	12.0	1.7
Element's molar ratio relative to N (Equation 2.3)	2.9	7.0	1.0

The calculated molar ratios of C and H relative to the N atom based on the elemental analysis of PAA freebase was 2.9:7.0:1.0 (Table 2-3), which is in good agreement with the predicted structure of PAA monomer (3 C atoms: 7 H atoms: 1 N atom (Figure 2.4)) (Thompson *et al.*, 2008).

### 2.3.2.2 Percentage Mole Modification of Modified Polymers

#### 2.3.2.2.1 Calculation of Percentage Mole Modification of Pa<sub>5</sub> & Ch<sub>5</sub>

The mole percentages of the cholesterol and palmitoyl groups attached to the PAA backbone were calculated using Equation 2.2 & 2.2 (2.3.2.1) followed by Equation 2.32.4 & 2.5. An example of the calculation of the percentage mole modification of palmitoyl groups is tabulated in Table 2-4.

$$\text{Moles of each element from the attached moiety} = \frac{\text{Element molar ratio relative to N} - \text{Element molar ratio relative to N (PAA)}}{\text{Element molar ratio relative to N (PAA)}} \quad \text{Equation 2.4}$$

$$\text{Percentage mole modification} = \frac{\text{Moles of the element from the attached moiety}}{\text{Number of element's atom present in the moiety}} \times 100 \% \quad \text{Equation 2.5}$$

**Table 2-4:** The calculation of the percentage mole modification of palmitoyl in Pa<sub>5</sub>.

	Elements in Pa <sub>5</sub>		
	C	H	N
<b>Element's weight percentage obtained from elemental analysis</b>	56.3	10.6	14.9
<b>Element's molar ratio (Equation 2.2)</b>	4.7	10.6	1.1
<b>Element's molar ratio relative to N (Equation 2.3)</b>	4.4	10.0	1.0
<b>Moles of each element from attached moiety (Error! Reference source not found.)</b>	1.5	3.0	0.0
<b>Percentage mole modification (Equation 2.5)</b>	9.7	9.6	-

Elemental analysis of Pa<sub>5</sub> revealed a carbon: hydrogen: nitrogen ratio of 4.4: 10.0: 1, higher than the expected theoretical ratio of the empirical formula of Pa<sub>5</sub> (3.8: 8.5: 1). On the contrary, the carbon: hydrogen: nitrogen ratio in the modified Ch<sub>5</sub> was 4.6: 10.1: 1, concordant with the expected theoretical ratio of 4.4: 9.2: 1. The percentage mole modification of Pa<sub>5</sub> based on carbon (9.7%) was approximately double the initial feed molar ratio (5%). In contrast the percentage mole modification of Ch<sub>5</sub> (6.1%) was close to the initial feed molar ratio (5%).

#### 2.3.2.2.2 Calculation of Percentage Mole Modification of Pa<sub>5</sub>-MPEG

The mole percentage of the MPEG moiety attached to Pa<sub>5</sub> was calculated using Equation 2.2 - Equation 2.5, with a modification in **Error! Reference source not found.** where the element molar ratio relative to N in PAA was replaced with the element molar ratio relative to N in Pa<sub>5</sub>, the reason being that Pa<sub>5</sub> is the starting material. Table 2-5 shows an example of the calculation of the percentage mole modification of MPEG moiety onto Pa<sub>5</sub>. The carbon: hydrogen: nitrogen ratio in the modified Pa<sub>5</sub>-MPEG was 12.4: 26.7: 1, equating to 3.6% mole modification

of MPEG which correlates well with the expected theoretical modification ratio of 3.5% (theoretical C: H: N is 11.6: 24: 1).

**Table 2-5:** The calculation of the percentage mole modification of palmitoyl in Pa<sub>5</sub>-MPEG.

	Elements in Pa <sub>5</sub> -MPEG		
	C	H	N
<b>Element's weight percentage obtained from elemental analysis</b>	53.4	9.6	5.0
<b>Element's molar ratio (Equation 2.2)</b>	4.5	9.6	0.4
<b>Element's molar ratio relative to N (Equation 2.3)</b>	12.4	26.7	1.0
<b>Moles of each element from attached moiety (Error! Reference source not found.)</b>	8.0	16.7	0.0
<b>Percentage mole modification (Equation 2.5)</b>	3.6	3.8	-

### 2.3.2.2.3 Calculation of Percentage Mole Modification of Da<sub>10</sub>

The mole percentage of the dansyl group in Da<sub>10</sub> was determined using similar calculations as to those described in sections 2.3.2.1 and 2.3.2.2.1 (Equation 2.2 - Equation 2.5), with the addition of an extra step (Equation 2.2A) between Equation 2.2 & Equation 2.3. This is due to the presence of a nitrogen atom in the dansyl moiety (Figure 2.8) which will contribute to the total nitrogen weight percentage of the PAA monomer. Since the molar ratio of N:S in the dansyl moiety is 1:1 (Figure 2.8), subtraction of the sulphur molar ratio from the total N molar ratio results in the corrected N molar ratio contributed by PAA monomer only (Equation 2.2A).

$$\text{Corrected N molar ratio} = \text{N atom's molar ratio} - \text{S atom's molar ratio}$$

Equation 2.2A

The calculation of the mole percentage of dansyl moiety in Da<sub>10</sub> is outlined in Table 2-6. The carbon: hydrogen: sulphur: nitrogen ratio in the modified Da<sub>10</sub> was 4.3: 8.2: 1: 0.1, this ratio is in agreement with the expected theoretical ratio of 4.2: 8.2: 1: 0.1.

**Table 2-6:** The calculation of the percentage mole modification of dansyl in Da<sub>10</sub>.

	Elements in Da <sub>10</sub>			
	C	H	N	S
<b>Element's weight percentage obtained from elemental analysis</b>	53.2	8.6	16.0	3.2
<b>Element's molar ratio (Equation 2.2)</b>	4.4	8.6	1.1	0.1
<b>Corrected N molar ratio (Equation 2.2A)</b>	4.4	8.6	1.0	0.1
<b>Element's molar ratio relative to N (Equation 2.3)</b>	4.3	8.2	1	0.1
<b>Element molar ratio relative to N in PAA</b>	2.9	7.0	1.0	-
<b>Moles of each element from attached moiety (Equation 2.4)</b>	1.4	1.2	-	0.1
<b>Percentage mole modification (Equation 2.5)</b>	11.5	10.2	-	9.6

Table 2-7 summarises the percentage mole modification for all modified polymers, and shows the small variation in percentage mole modification between batch to batch for each polymer. The calculated percentage mole modification of Pa<sub>5</sub>-MPEG, Ch<sub>5</sub> and Da<sub>10</sub> were close to the initial mole feed ratio, in contrast to Pa<sub>5</sub> which had approximately double the initial mole feed ratio.

**Table 2-7:** Elemental analysis results for PAA and modified polymers, with their corresponding percentage mole modification.

Polymer	Element weight percentage obtained from elemental analysis				Percentage mole modification Mean (n) (range)
	C Mean (n) (range)	H Mean (n) (range)	N Mean (n) (range)	S Mean (n) (range)	
PAA	57.8 (2) (59.0,56.6)	12.2 (2) (12.0,12.3)	23.6 (2) (24.0,23.2)	-	-
Pa <sub>5</sub>	53.9 (3) (52.1-56.3)	10.3 (3) (10.0-10.6)	14.6 (3) (14.2-14.9)	-	8.9 (3) (8.2-9.7)
MPEG	52.4 (3) (51.3-53.4)	9.4 (3) (8.8-9.8)	5.4 (3) (5.0-5.7)	-	3.4 (3) (3.2-3.6)
Ch <sub>5</sub>	62.8 (2) (65.1,60.5)	11.6 (2) (12.1,11.1)	15.8 (2) (16.3,15.3)	-	6.2 (2) (6.3,6.1)
Da <sub>10</sub>	53.2 (3) (52.0-54.3)	8.7 (3) (8.6-8.9)	15.6 (3) (15.1-16.0)	3.1 (3) (3.0-3.2)	9.6 (3) (9.2-10.0)

### 2.3.3 NMR Spectra and Calculation of PAA and Modified PAA

#### 2.3.3.1 PAA <sup>1</sup>H NMR Spectra and Calculation

The peaks in the <sup>1</sup>H NMR spectrum of PAA in CD<sub>3</sub>OD (Figure 2.9) were assigned to the CH<sub>2</sub> (Figure 2.9, peak A), CH (Figure 2.9, peak B) and CH<sub>2</sub>-N (Figure 2.9, peak C) protons in the PAA monomer at  $\delta_{1.15-1.35}$ ,  $\delta_{1.54}$  and  $\delta_{2.59-3.02}$ , respectively (Thompson *et al.*, 2008). The integration ratio of the peaks at  $\delta_{1.15-1.35}$  = CH<sub>2</sub> (A),  $\delta_{1.54}$  = CH (B) and  $\delta_{2.59-3.02}$  = CH<sub>2</sub> (C) was 97:53:100 respectively. This ratio corresponds well to the theoretical 2:1:2 proton ratio in the PAA monomer structure. Similar results were obtained from the <sup>1</sup>H NMR spectrum of PAA in D<sub>2</sub>O (Figure 2.10), the integration ratio of the peaks at  $\delta_{1.06-1.22}$  = CH<sub>2</sub> (A),  $\delta_{1.44}$  = CH (B) and  $\delta_{2.50-2.88}$  = CH<sub>2</sub> (C) was 105:50:100 respectively. The two hydrogen atoms

attached to the nitrogen atom are invisible in the NMR spectra, due to the fast exchange with deuterium from the deuterated solvent (Kleckner & Foster, 2011).

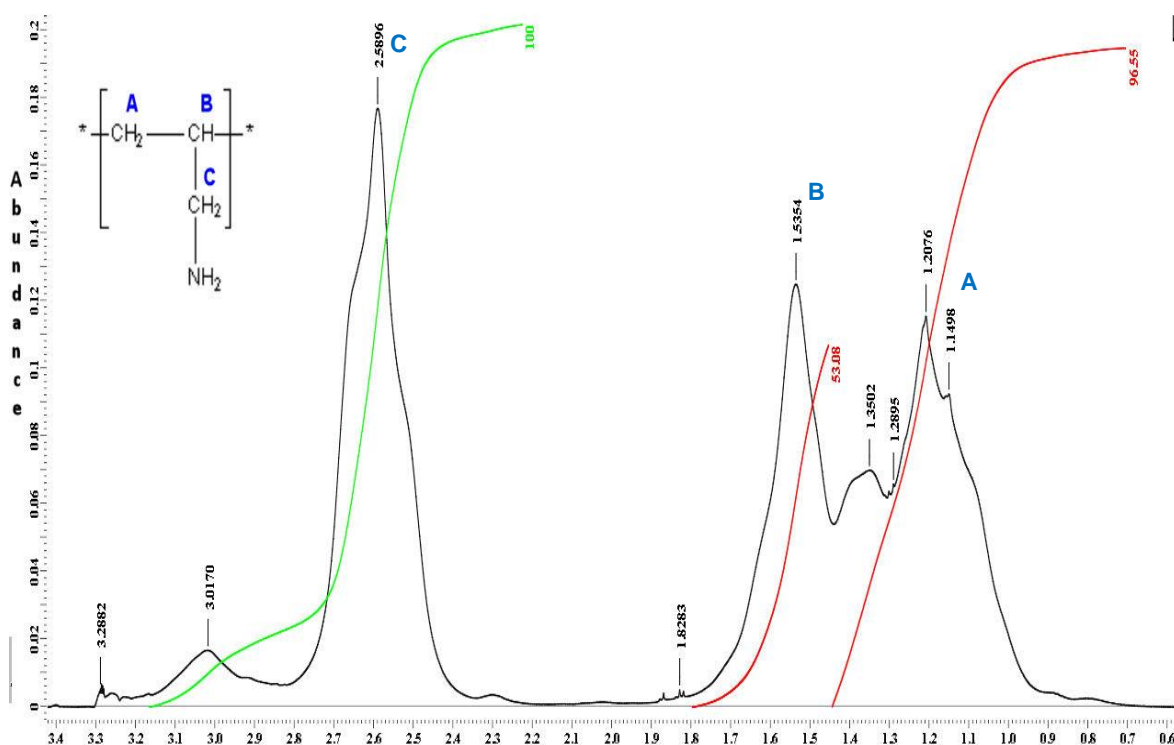


Figure 2.9:  $^1\text{H}$  NMR spectrum of PAA in  $\text{CD}_3\text{OD}$  carried out using 600 MHz spectrometer at 25 °C.

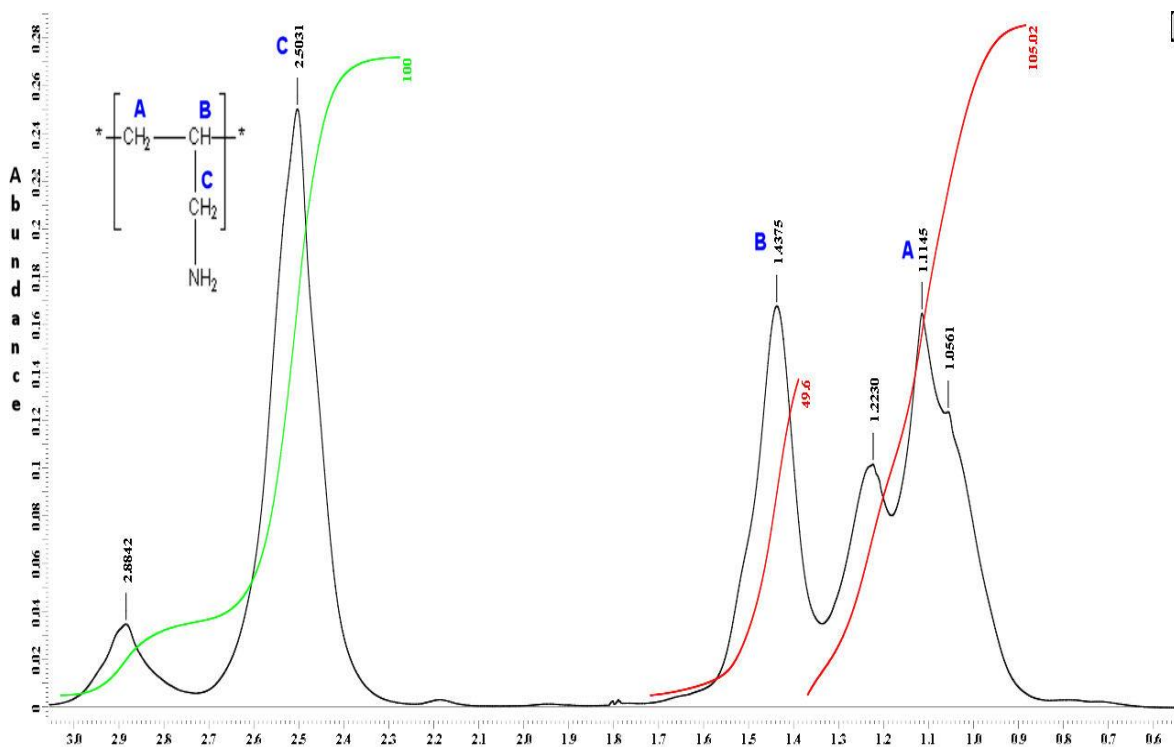


Figure 2.10:  $^1\text{H}$  NMR spectrum of PAA in  $\text{D}_2\text{O}$  carried out using 600 MHz spectrometer at 25 °C.

### 2.3.3.2 Modified polymers <sup>1</sup>H NMR Spectra and Calculation

The <sup>1</sup>H NMR spectra of all modified polymers in CD<sub>3</sub>OD and D<sub>2</sub>O were presented in Figures 2.11-2.18. The extra peaks alongside the PAA peaks corresponding to the attached modified groups were assigned and labelled in the corresponding <sup>1</sup>H NMR spectrum. The mole percentage of modified groups was calculated using Equation 2.6, where the CH<sub>2</sub> PAA peak at approximately δ<sub>2.5</sub> was used as reference peak of PAA backbone. This peak was chosen due to the fact it does not overlap with other peaks and can be easily and accurately integrated. A summary of the corresponding chemical shifts for each attached hydrophobic / hydrophilic groups and the percentage mole modification calculated using Equation 2.6 is tabulated in Table 2-8.

*Percentage mole modification*

$$= \frac{\left( \frac{\text{Integration value of the peak}_i}{\text{number of protons}_i} \right)}{\left( \frac{\text{Integration value of CH}_2 \text{ PAA peak at } \delta_{2.5}}{\text{number of protons of CH}_2 \text{ PAA}} \right)} \times 100\% \quad \text{Equation 2.6}$$

**Table 2-8:** Assignment of the corresponding chemical shifts in <sup>1</sup>H NMR spectra of Pa<sub>5</sub>, Pa<sub>5</sub>-MPEG, Ch<sub>5</sub> and Da<sub>10</sub> amphiphilic polymers.

Polymer	D <sub>2</sub> O			CD <sub>3</sub> OD		
	Peak i (δ)	No. of protons i	Percentage Mole Modification	Peak i (δ)	No. of protons i	Percentage Mole Modification
<b>Pa<sub>5</sub></b>	δ <sub>0.73</sub>	3	5.7%	δ <sub>0.7</sub>	3	3.5%
<b>Pa<sub>5</sub>- MPEG</b>	δ <sub>3.5</sub>	439	4.9%	δ <sub>3.6</sub>	439	5.7%
	δ <sub>3.2</sub>	3	4.9%	δ <sub>3.3</sub>	3	5.0%
<b>Ch<sub>5</sub></b>	δ <sub>0.63</sub>	3	1.2%	δ <sub>0.70</sub>	3	6.2%
<b>Da<sub>10</sub></b>	δ <sub>6.9-8.4</sub>	6	5.5%	δ <sub>7.1-8.5</sub>	6	8.8%

### 2.3.3.2.1 Pa<sub>5</sub> <sup>1</sup>H NMR Spectra and Calculation

In CD<sub>3</sub>OD solvent all PAA peaks were still evident in Pa<sub>5</sub> <sup>1</sup>H NMR spectrum (Figure 2.11). In addition, a peak at  $\delta_{0.75}$  was observed corresponding to the terminal CH<sub>3</sub> from the attached palmitoyl group (peak D in Figure 2.11) (Jiang, Quan, Liao & Wang, 2006; Thompson *et al.*, 2008). The peaks corresponding to the CH<sub>2</sub> from the palmitoyl group were overlapping with the CH<sub>2</sub> peak from PAA (peak E in Figure 2.11).

The calculated percentage mole modification of palmitoyl moiety using the CH<sub>3</sub> peak at  $\delta_{0.75}$  was calculated using Equation 2.7.

$$\text{Percentage mole of palmitoyl} = \frac{\left(\frac{\text{Integration value of the } \delta_{0.73}}{\text{number of protons of CH}_3}\right)}{\left(\frac{\text{Integration value of } \delta_{2.5}}{\text{number of protons of CH}_2 \text{ PAA}}\right)} \times 100\% =$$

Equation 2.7

$$\left[\frac{5.3}{3}\right] / \left[\frac{100}{2}\right] = 3.5\%$$

Similarly for the D<sub>2</sub>O solvent, the CH<sub>3</sub> peak ( $\delta_{0.73}$ ) (Figure 2.12) was used, the calculated percentage mole of palmitoyl modification was 5.7%. The increase in the mole percentage attachment in D<sub>2</sub>O compared to CD<sub>3</sub>OD is partially due to the overlapping of the CH<sub>3</sub> peak from Pa<sub>5</sub> with the PAA CH<sub>2</sub>.

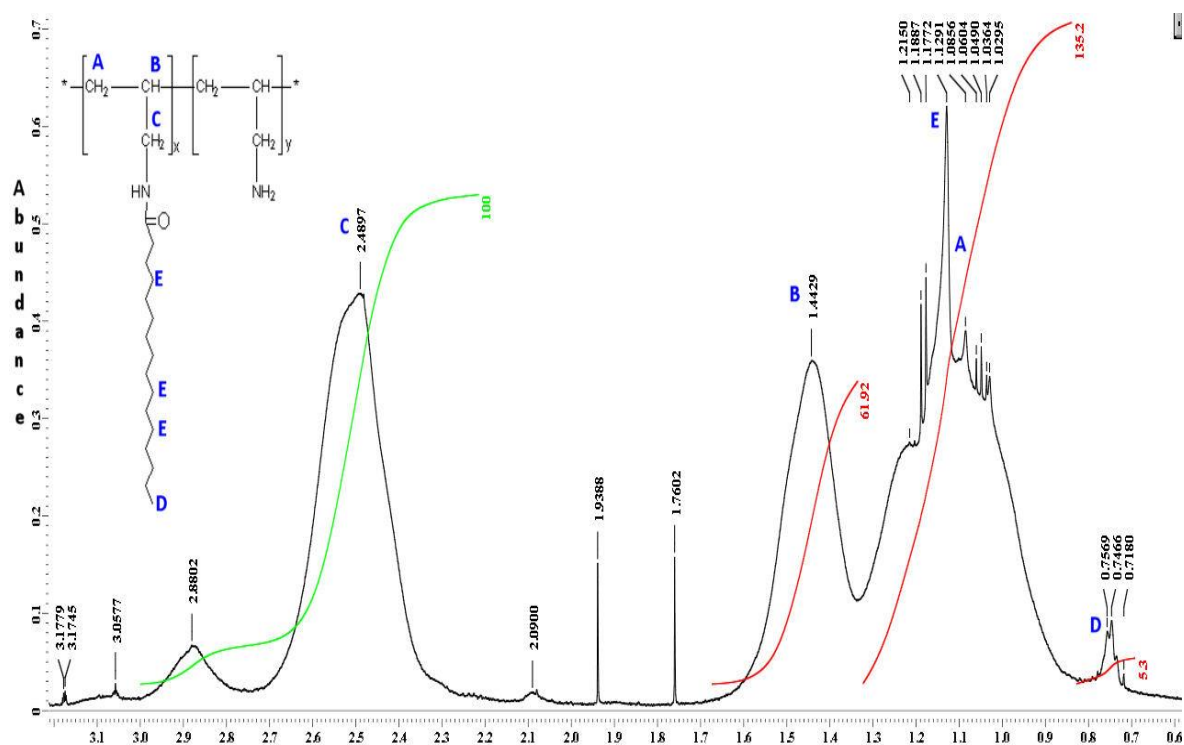


Figure 2.11:  $^1\text{H}$  NMR spectrum of  $\text{Pa}_5$  in  $\text{CD}_3\text{OD}$  carried out using 600 MHz spectrometer at  $25^\circ\text{C}$ .

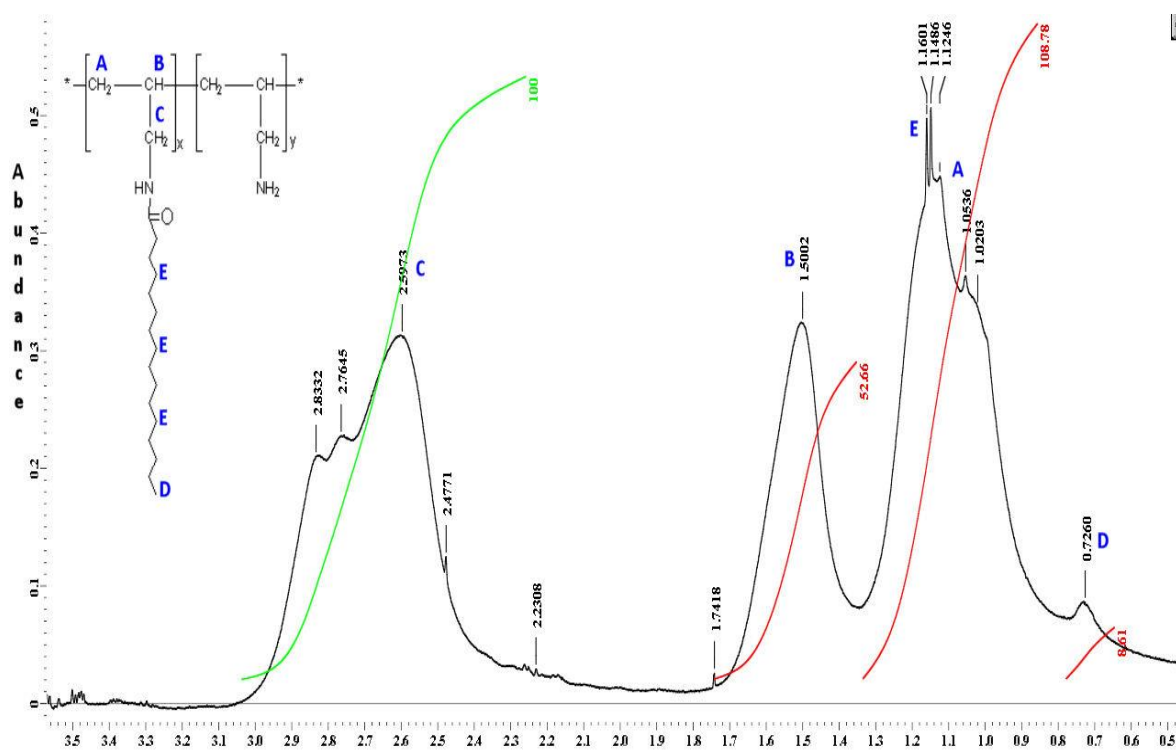
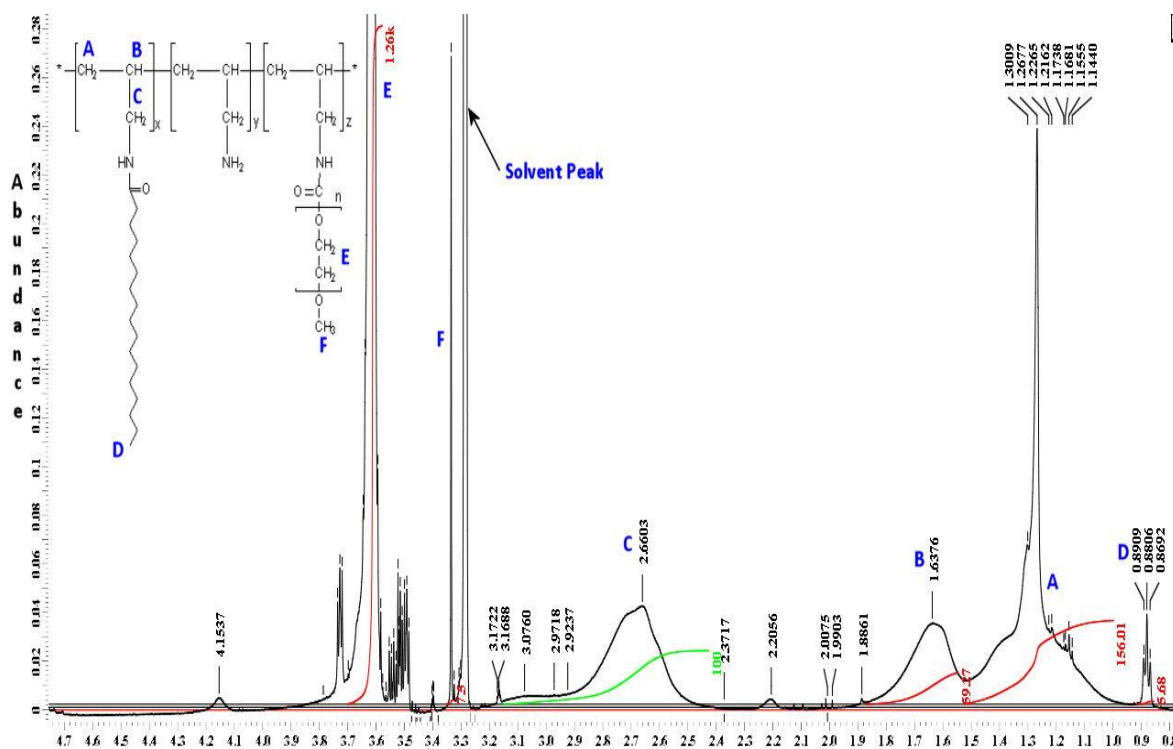


Figure 2.12:  $^1\text{H}$  NMR spectrum of  $\text{Pa}_5$  in  $\text{D}_2\text{O}$  carried out using 600 MHz spectrometer at  $25^\circ\text{C}$ .

2.3.3.2.2 Pa<sub>5</sub>-MPEG <sup>1</sup>H NMR Spectra and Calculation

The peaks at  $\delta_{3.3}$  (F) and  $\delta_{3.6}$  (E) in the Pa<sub>5</sub>-MPEG spectrum using CD<sub>3</sub>OD as a solvent (Figure 2.13), correspond to the terminal methoxy protons and MPEG OCH<sub>2</sub>, respectively (Chang *et al.*, 2012; Sun, Du, Wang & Liu, 2011; Zhang, Jackson & Burt, 1996). The calculated percentage mole modification of MPEG moiety using  $\delta_{3.6}$  and  $\delta_{3.3}$  peaks (Figure 2.13) were 5.7 and 5.0%, respectively. The peak at  $\delta_{3.28}$  in Figure 2.13 is due to an unsuppressed solvent peak. Conversely, the calculated percentage mole modification of MPEG in D<sub>2</sub>O (Figure 2.14) based on  $\delta_{3.5}$  and  $\delta_{3.2}$  peaks were both 4.9%.



**Figure 2.13:** <sup>1</sup>H NMR spectrum of Pa<sub>5</sub>-MPEG in CD<sub>3</sub>OD carried out using 600 MHz spectrometer at 25 °C.

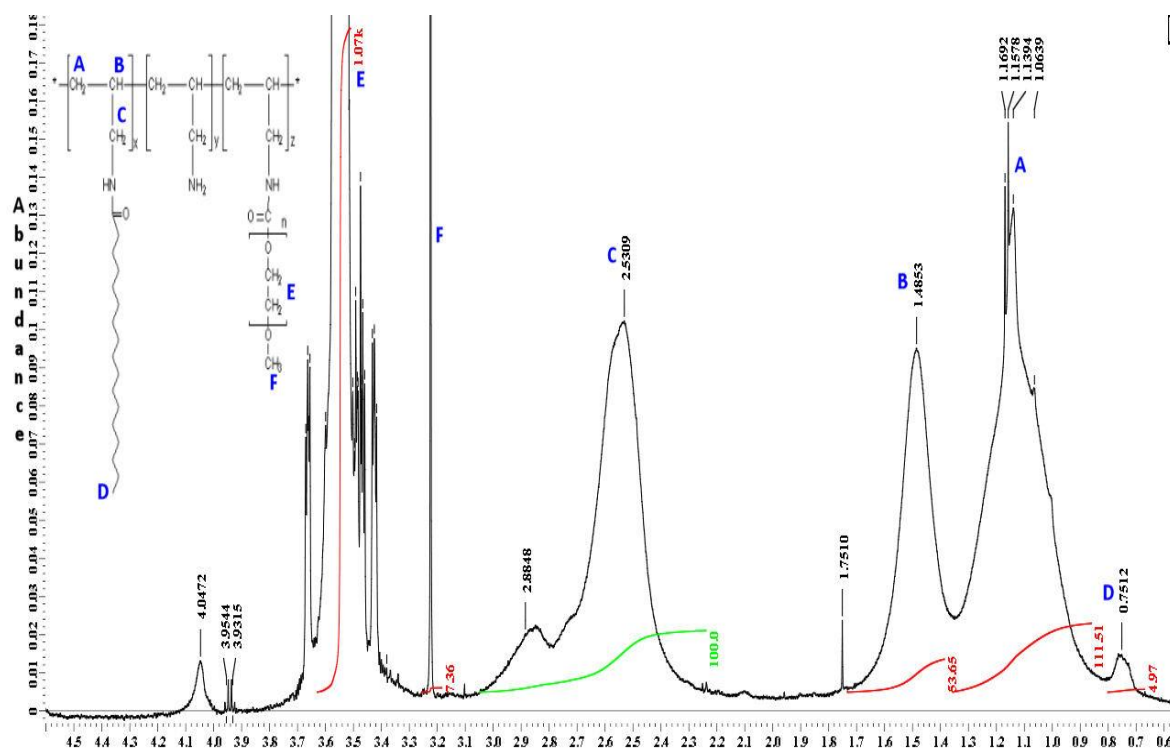


**Figure 2.14:**  $^1\text{H}$  NMR spectrum of  $\text{Pa}_5\text{-MPEG}$  in  $\text{D}_2\text{O}$  carried out using 600 MHz spectrometer at 25  $^\circ\text{C}$ .

### 2.3.3.2.3 $\text{CH}_5$ $^1\text{H}$ NMR Spectra and Calculation

The  $^1\text{H}$  NMR spectrum of  $\text{CH}_5$  in  $\text{CD}_3\text{OD}$  (Figure 2.15) showed extra peaks at  $\delta_{0.70}$ ,  $\delta_{0.85}$ ,  $\delta_{0.92}$ ,  $\delta_{1.01}$ ,  $\delta_{4.35}$ , and  $\delta_{5.36}$  in comparison to the PAA spectrum. These peaks were assigned to the  $\text{CH}_3$ ,  $\text{CH-O}$  and  $\text{C=CH}$  in the cholesterol moiety as shown in Figure 2.15 (Bagheri & Bigdeli, 2013; Chen *et al.*, 2013; Kuang, Liu, Liu & Zhuo, 2012). The percentage mole modification of cholesterol attached onto PAA backbone was calculated using the  $\text{CH}_3$  peaks at  $\delta_{0.70}$  and  $\delta_{0.63}$  in the  $\text{CD}_3\text{OD}$  and  $\text{D}_2\text{O}$  spectra (Figures 2.15 and 2.16). The calculated percentage mole modification was very different depending on the solvent, as demonstrated by the 6.2% and 1.2% obtained from the  $\text{CD}_3\text{O}$  and  $\text{D}_2\text{O}$  spectra, respectively.

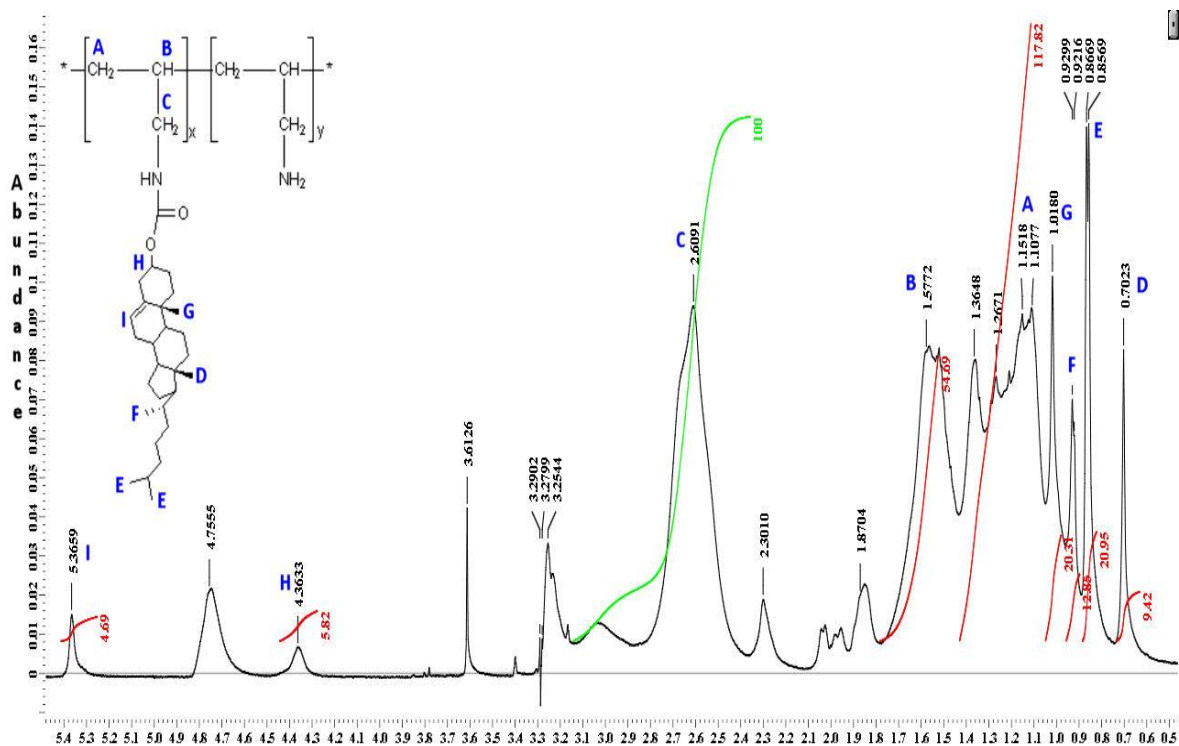


Figure 2.15:  $^1\text{H}$  NMR spectrum of  $\text{Ch}_5$  in  $\text{CD}_3\text{OD}$  carried out using 600 MHz spectrometer at 25 °C.

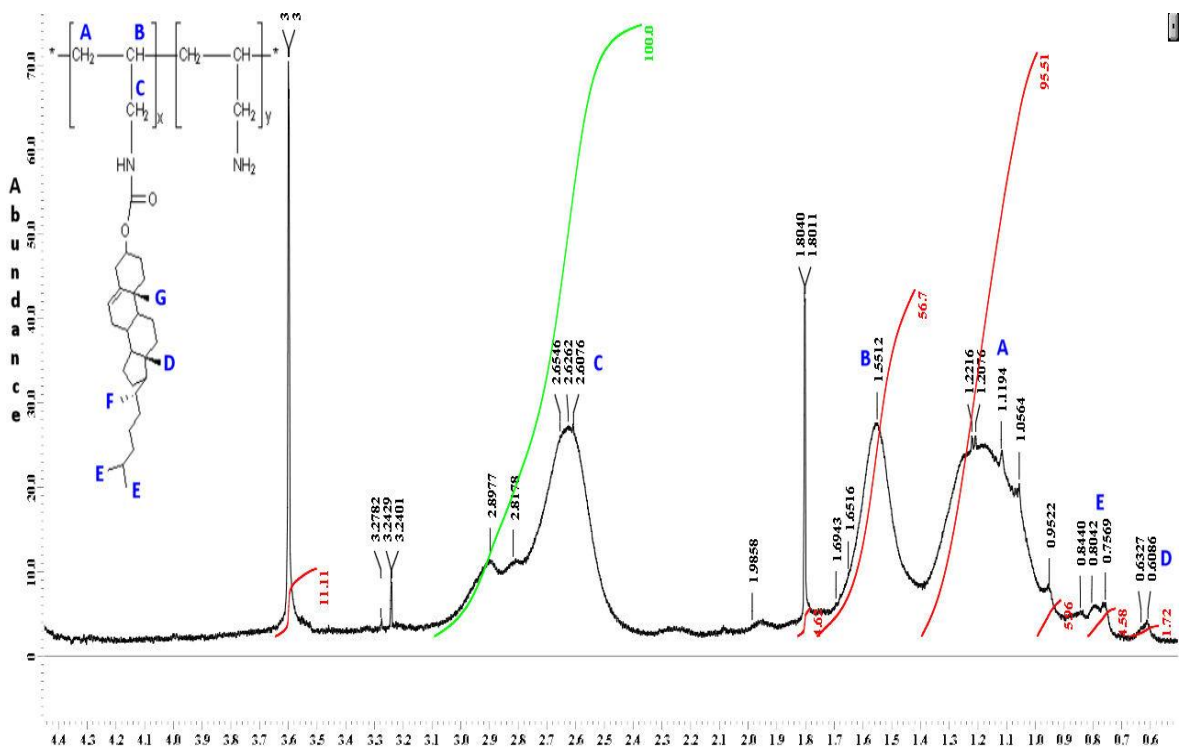
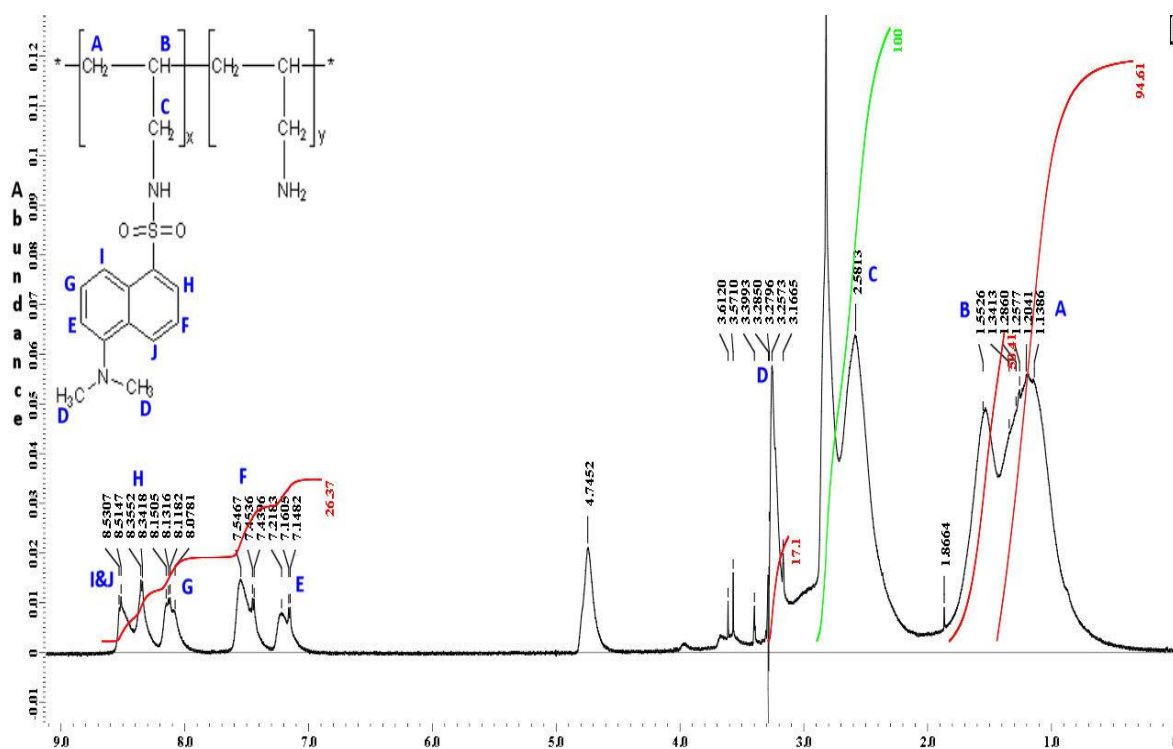


Figure 2.16:  $^1\text{H}$  NMR spectrum of  $\text{Ch}_5$  in  $\text{D}_2\text{O}$  carried out using 600 MHz spectrometer at 25 °C.

2.3.3.2.4 Da<sub>10</sub> <sup>1</sup>H NMR Spectra and Calculation

The <sup>1</sup>H NMR spectrum of Da<sub>10</sub> in CD<sub>3</sub>OD (Figure 2.17) showed extra peaks at  $\delta_{3.25}$  and at  $\delta_{7.2-8.5}$  in comparison to the PAA spectrum. The  $\delta_{3.25}$  peak corresponds to the six protons from CH<sub>3</sub> groups attached to the nitrogen atom in the dansyl moiety (atom D in Figure 2.17) (Buruiana, Chibac & Buruiana, 2010; Hoskins, Lin, Tetley & Cheng, 2012a), whereas the  $\delta_{7.1-8.5}$  peaks correspond to the protons of the naphthalene ring (atoms E-J in Figure 2.17) (Hoskins, Lin, Tetley & Cheng, 2012a). The percentage mole modification of dansyl attached to the PAA backbone was calculated using the peaks at  $\delta_{7.2-8.5}$  (peaks E-J in Figure 2.17) resulting in 8.8% mole modification. Conversely, the calculated percentage mole modification of dansyl from the <sup>1</sup>H NMR spectra in D<sub>2</sub>O (Figure 2.18) was 5.5%. The peaks at  $\delta_{4.7}$  and  $\delta_{4.6}$  in Figure 2.17 and Figure 2.18 respectively are due to absorbed H<sub>2</sub>O and a partially unsuppressed solvent peak.



**Figure 2.17:** <sup>1</sup>H NMR spectrum of Da<sub>10</sub> in CD<sub>3</sub>OD carried out using 600 MHz spectrometer at 25 °C.

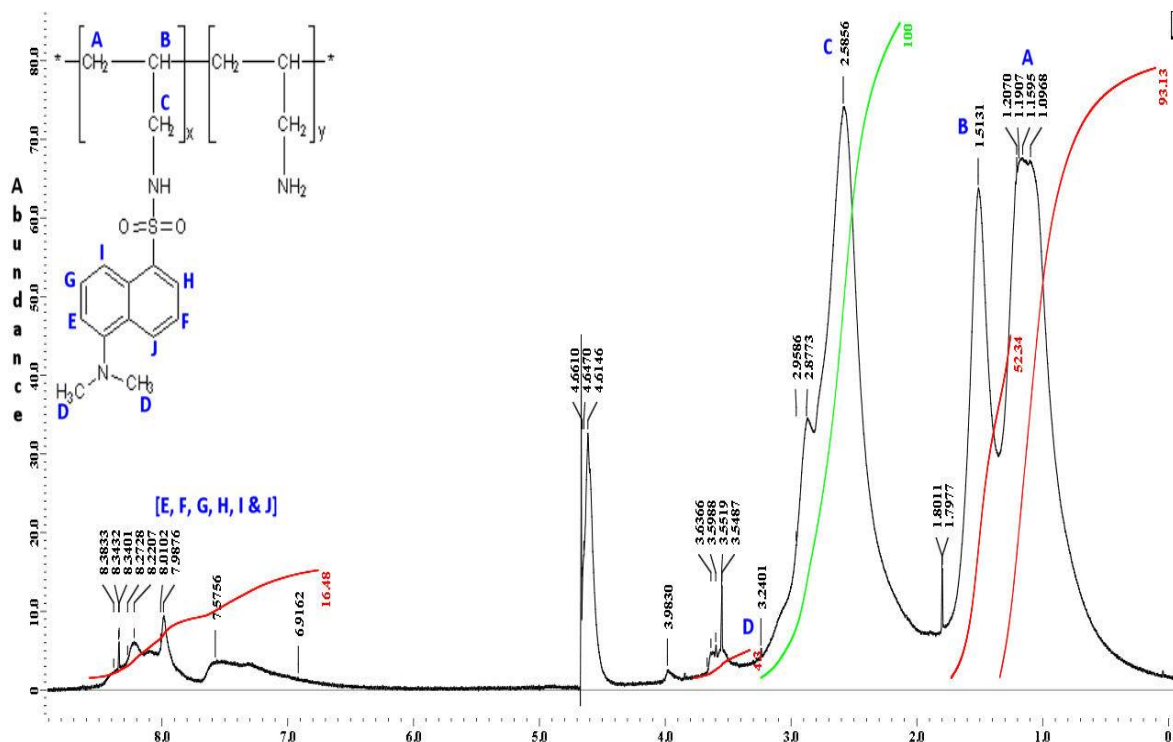
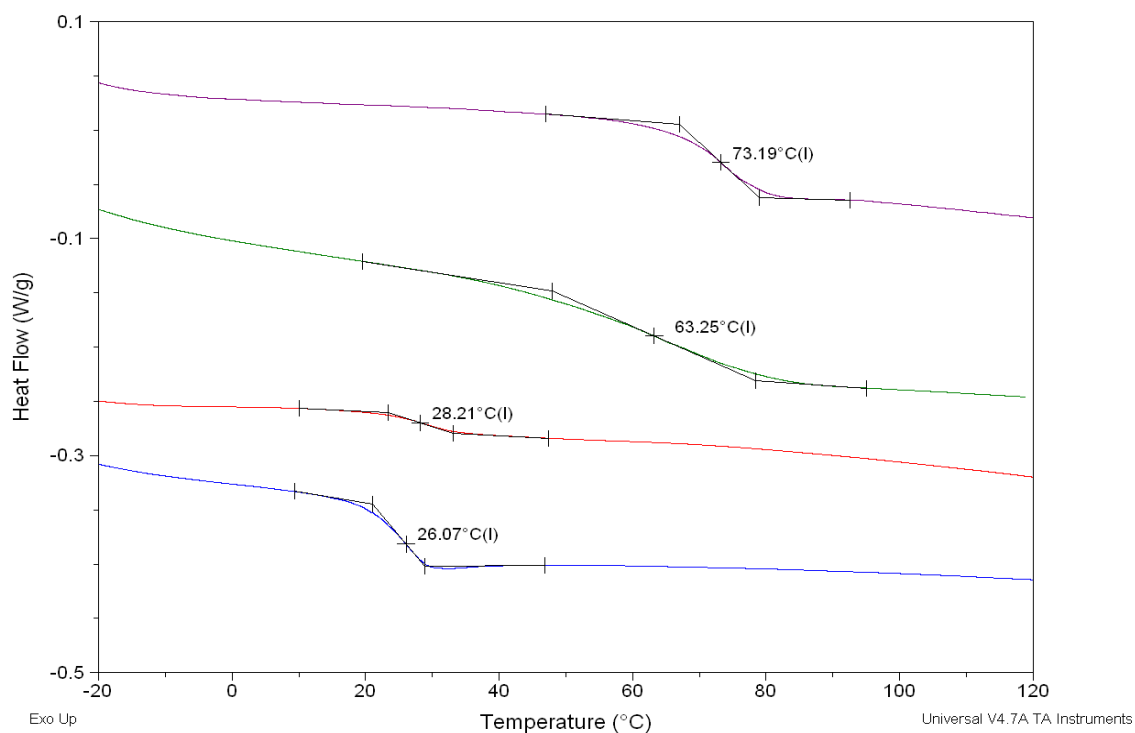


Figure 2.18:  $^1\text{H}$  NMR spectrum of  $\text{Da}_{10}$  in  $\text{D}_2\text{O}$  carried out using 600 MHz spectrometer at  $25^\circ\text{C}$ .

### 2.3.4 Differential Scanning Calorimetry (DSC)

Figure 2.19 shows the enlarged sections of the DSC thermograms for PAA and the hydrophobically modified polymers. The thermogram shows the  $T_g$  of PAA at  $26.1^\circ\text{C}$ . The modification of the palmitoyl moieties on the PAA backbone increased the  $T_g$  by two degrees from  $26.1$  to  $28.2^\circ\text{C}$ . When a cholesteryl moiety was attached onto the PAA backbone the  $T_g$  further increased to  $63.3^\circ\text{C}$  whereas dansyl moieties increased the  $T_g$  of PAA even more to  $73.2^\circ\text{C}$ . Interestingly, the  $T_g$  of  $\text{Pa}_5$ -MPEG polymer was absent, instead the polymer had melting temperature ( $T_m$ ) at  $56.8^\circ\text{C}$  as shown in Figure 2.20. The melting point at  $56.8^\circ\text{C}$  in  $\text{Pa}_5$ -MPEG polymer is due to the presence of the MPEG polymeric chains, this was confirmed by the DSC thermogram of the methoxypolyethylene glycol p-nitrophenyl carbonate where the material had the same melting point ( $56.48^\circ\text{C}$ ).



**Figure 2.19:** Differential scanning calorimetry thermogram of PAA, Pa5, Ch5 and Da10. Colour code: Blue line = PAA, Red line = Pa5, Green line = Ch5, Purple line = Da10.

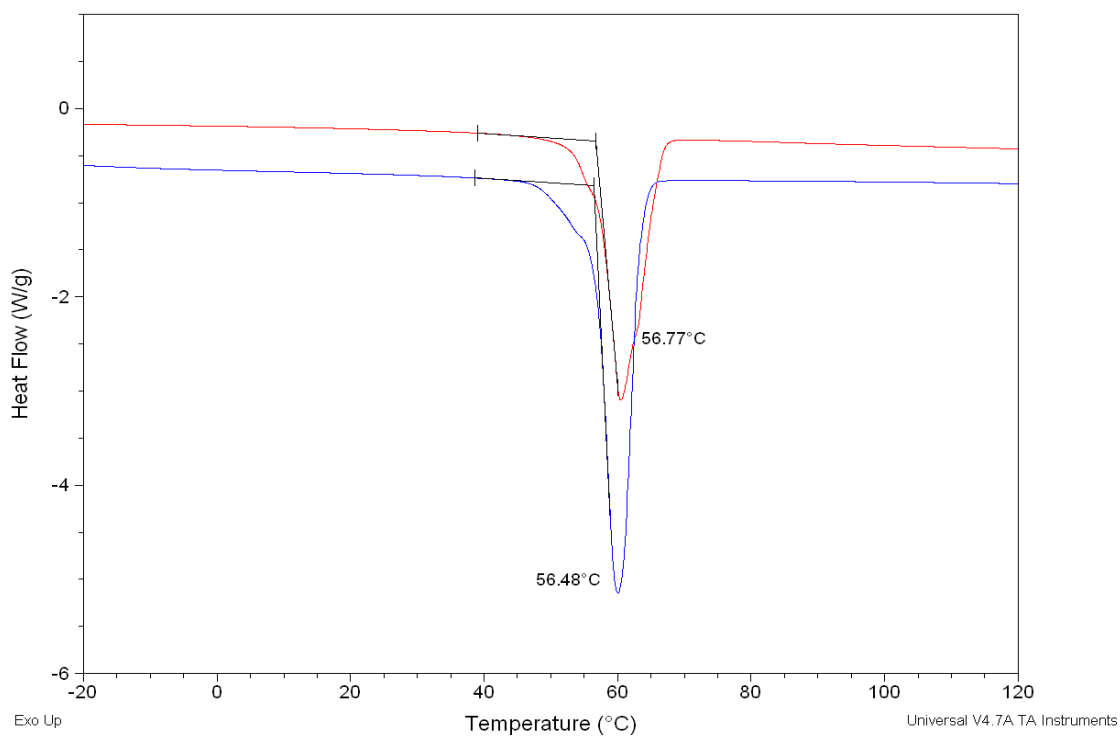


**Figure 2.20:** Differential scanning calorimetry thermogram of Pa5-MPEG (Red line) and Methoxypolyethylene glycol p-nitrophenyl carbonate (Blue line).

## 2.4 Discussion

In this study, three hydrophobic (Pa, Ch and Da) and one hydrophilic (MPEG) pendant groups were successfully attached onto the PAA backbone, to form four different amphiphilic polymers.

The modification of the PAA polymer with the four groups was successful. This was apparent from the differences in the physical appearance of all modified polymers (Pa<sub>5</sub>, Pa<sub>5</sub>-MPEG, Ch<sub>5</sub> and Da<sub>10</sub>) in comparison to PAA (Table 2-2) and the confirmation obtained using data from EA, NMR and DSC. The yield percentage was high for all the modified polymers ranging from 81% (Pa<sub>5</sub>) to 94% (Pa<sub>5</sub>-MPEG). The percentage mole modification of attached groups was quantified using EA and NMR (Table 2-9).

**Table 2-9:** The percentage mole modification of modified polymers obtained using EA and NMR.

Polymer	Percentage Mole Modification		
	NMR		EA
	D <sub>2</sub> O	CD <sub>3</sub> OD	
Pa <sub>5</sub>	5.7	3.5	8.9
Pa <sub>5</sub> -MPEG	4.9 ( $\delta_{3.5}$ ) 4.9 ( $\delta_{3.2}$ )	5.7 ( $\delta_{3.6}$ ) 5.0 ( $\delta_{3.3}$ )	3.4
Ch <sub>5</sub>	1.2	6.2	6.2
Da <sub>10</sub>	5.5	8.8	9.6

The successful attachment of palmitoyl group onto the PAA backbone was confirmed using elemental analysis. The calculations based on carbon abundance

of Pa<sub>5</sub> revealed 8.9% mole modification of palmitoyl group onto PAA, which is higher than the initial molar feed ratio of 5%. This trend was reported by Thompson *et al.* where the author reported  $4.2 \pm 4.4\%$  and  $6.6 \pm 7.8\%$  mole percentage attachment for the 2.5 and 5% initial molar feed ratio (Pa<sub>2.5</sub> and Pa<sub>5</sub>), respectively (Thompson *et al.*, 2008; Thompson, Tetley, Uchegbu & Cheng, 2009). Wang *et al.* (Wang, Qu, Gray, Tetley & Uchegbu, 2004) proposed that the higher than expected percentage mole modification may be explained in terms of the coil expansion of the polymers. Polymeric chains with lower percentage mole modification are thought to escape from the dialysis tube due to the limited coil expansion in comparison to the higher percentage mole modified chains (Wang, Qu, Gray, Tetley & Uchegbu, 2004).

In contrast to Pa<sub>5</sub>, elemental analysis results showed that the actual percentage mole attachment of MPEG onto Pa<sub>5</sub> was  $3.4 \pm 0.2\%$ , which is in good agreement with the initial molar feed ratio (3.5%). The approximate 110 repeating units in the MPEG group (polymeric chain), and the branching of the modified polymer chains (Pa<sub>5</sub>-MPEG) seem to prevent the loss of polymeric chains with lower attachment percentages from the dialysis tube, resulting in an accurate percentage mole modification results.

The percentage mole modification of cholesteryl groups attached onto PAA was 6.2%. Whilst this value is higher than the expected 5%, it is in good agreement with previously published work by both Hoskins and Thompson co-workers (Hoskins, Lin, Tetley & Cheng, 2012a; Thompson *et al.*, 2008), where the authors reported 6 and 6.3% mole modification, respectively. For Da<sub>10</sub> the elemental analysis calculation based on the sulphur abundance for Da<sub>10</sub> resulted in  $9.6 \pm 0.4\%$  as an actual percentage mole modification of dansyl group onto

PAA. This is in good agreement with the  $9.3 \pm 0.4\%$  percentage mole modification of Da<sub>10</sub> reported by Hoskins *et al.* (Hoskins, Lin, Tetley & Cheng, 2012a).

The <sup>1</sup>H NMR data in D<sub>2</sub>O for the hydrophobically modified polymers are indicative of the formation of hydrophobic interactions as a result of the amphiphiles aggregation in aqueous medium (Chen *et al.*, 2004; Zhang, Jackson & Burt, 1996). The calculated percentage mole attachment of Pa<sub>5</sub>, Ch<sub>5</sub> and Da<sub>10</sub> in CD<sub>3</sub>OD and D<sub>2</sub>O were different (Table 2-9). The different percentage mole modification obtained in different solvents is not an unfamiliar phenomenon (Xu, Ji, Chen & Shen, 2005), as amphiphilic polymers form solvent dependent aggregates. These aggregates affect the mobility of a certain part of the amphiphile. Chen *et al.* reported a difference in the relaxation time (<sup>1</sup>H NMR longitudinal relaxation time (T<sub>1</sub>)) of the hydrophobic chain protons attached to an amphiphilic polyethylene glycol based polymer in D<sub>2</sub>O and CDCl<sub>3</sub> (Chen *et al.*, 2004). A decrease in relaxation time of the hydrophobic side chain protons in D<sub>2</sub>O was observed by the author, in contrast to no change in the relaxation time in CDCl<sub>3</sub> (Chen *et al.*, 2004). The relaxation time in D<sub>2</sub>O decreased with the increase in polymer concentration, followed by subtle decreases above the CMC. The subtle decrease of the relaxation above CMC occurred due to the aggregation of the hydrophobic groups in the core of nanospheres (Chen *et al.*, 2004). The large size of the MPEG chain (109 unit) might enforce a partial motional restriction on the PAA backbone, resulting in lower intensities of the PAA peaks, and thus a higher calculated percentage mole modification of MPEG (approximately 5%) in both solvents (D<sub>2</sub>O and CD<sub>3</sub>OD) in comparison to theoretical 3.5% molar attachment of the MPEG.

The <sup>1</sup>H NMR spectrum of Ch<sub>5</sub> in D<sub>2</sub>O revealed much broader peaks and lower integration values in comparison to the peaks in the CD<sub>3</sub>OD spectrum.

Furthermore, in the D<sub>2</sub>O spectrum two expected characteristic peaks of the cholesteryl moiety were not observed at around  $\delta_{4.4}$  and  $\delta_{5.4}$ . Similarly, Xu *et al.* (Xu, Ji, Chen & Shen, 2005) showed all peaks corresponding to the cholesteryl group and phosphorylcholine group in CD<sub>3</sub>OD <sup>1</sup>H NMR spectrum of cholesteryl containing amphiphilic polyelectrolytes, whereas the peaks corresponding cholesteryl group either diminished or disappeared in the D<sub>2</sub>O <sup>1</sup>H NMR spectrum of the polymer. Likewise, Brown *et al.* (Brown *et al.*, 2000) reported the absence of peaks corresponding to the amino acid polymer backbone in <sup>1</sup>H NMR spectrum of the palmitoyl and PEG modified poly-L-lysine at normal temperature using CDCl<sub>3</sub>. However, it should be noted that Brown *et al.* observed the peaks at elevated temperature (48 °C). The author stated that the observed peaks at elevated temperatures were due to the increase in the mobility of the polymer backbone. The broadening effect observed in D<sub>2</sub>O spectrum and the low intensity of the previously mentioned peaks might be another reason for the absence of these two peaks. The broadening of the peaks in D<sub>2</sub>O is indicative of the restricted mobility of the cholesteryl groups as a result of the formation of tight self-assemblies. Similar findings were reported by Yusa *et al.* in a study which the authors investigated the <sup>1</sup>H NMR of cholesterol modified polyelectrolytes in D<sub>2</sub>O and deuterated dimethyl sulfoxide at room temperature (Yusa, Kamachi & Morishima, 1998). In D<sub>2</sub>O, the author observed a considerable peak broadening in contrast to corresponding peaks in deuterated dimethyl sulfoxide. The earlier study attributed the peak broadening in D<sub>2</sub>O to the highly restricted motion of cholesteryl moieties, as a direct result of the hydrophobic self-association of cholesteryl groups. The calculated percentage mole modification of cholesteryl from the <sup>1</sup>H NMR spectrum in CD<sub>3</sub>OD was 6.2 %, this is in good agreement with the theoretical value and the

results obtained from the elemental analysis. This was in contrast to the low 1.2% mole modification of cholesteryl obtained from the D<sub>2</sub>O spectrum.

Similar to Ch<sub>5</sub>, the <sup>1</sup>H NMR spectrum of Da<sub>10</sub> showed broader peaks in D<sub>2</sub>O in comparison to the CD<sub>3</sub>OD spectrum. The calculated mole percentage attachment based on the CD<sub>3</sub>OD <sup>1</sup>H NMR spectrum was 8.8%, which correlates well with both EA and initial mole feed ratio. A lower mole percentage was calculated from the D<sub>2</sub>O <sup>1</sup>H NMR which was found to be 5.5%. This phenomenon is similar to the one observed in Ch<sub>5</sub>, in which the lower mole percentage attachment in Da<sub>10</sub> is an outcome of restricted mobility of the dansyl groups as a result of the formation of tight self-assemblies in water.

The modification of homo-polymer by pendant groups affects the thermal properties such as the melting point (T<sub>m</sub>) and glass transition temperature (T<sub>g</sub>). The absence of T<sub>m</sub> and the presence of T<sub>g</sub> in the DSC thermogram of PAA revealed the amorphous nature of the polymer. Given the structure of the modified polymers, the addition of the hydrophobic/hydrophilic pendant groups resulted in an acquired rigidity of the PAA backbone which ultimately restricts the motion of the PAA chains (Brydson, 1999; Gedde, 2001). The DSC thermograms revealed an increase in T<sub>g</sub> of Pa<sub>5</sub>, Ch<sub>5</sub> and Da<sub>10</sub> in comparison to that of PAA. This increase in T<sub>g</sub> seems to increase with the increasing moiety size and percentage mole modification of the attached group (dansyl > cholesteryl > palmitoyl). The trend is in agreement with the fact that T<sub>g</sub> of hydrocarbon polymers (CH<sub>2</sub>-CH<sub>2</sub>) increases with the increasing size of the attached group (cholesteryl > palmitoyl) (Gedde, 2001) and percentage mole modification (Halary, Lauprêtre & Monnerie, 2011). No T<sub>m</sub> was detected for Pa<sub>5</sub>, Ch<sub>5</sub> and Da<sub>10</sub>, indicating the amorphous nature of these polymers. However, the T<sub>g</sub> could not be determined for the Pa<sub>5</sub>-MPEG

polymer, instead the thermogram revealed a  $T_m$  at approximately 56.8 °C revealing the crystalline nature of the modified polymer. A similar finding has been reported by Huang *et al.* where the  $T_g$  of chitosan was suppressed in a chitosan based amphiphile modified with MPEG groups (Huang, Yu, Guo & Huang, 2010).

## 2.5 Conclusion

The hydrophobic (Pa, Ch and Da) and hydrophilic (MPEG) moieties were successfully attached on the PAA backbone. The presence of the attached moieties was confirmed and quantified using elemental analysis and NMR spectroscopy. The  $^1\text{H}$  NMR and elemental analysis results showed that the percentage mole modification of the attached moieties was close to the initial feed ratios. The NMR data of the hydrophobically modified polymers suggest the aggregation of these amphiphiles in aqueous environment. The presence of the attached moieties was further confirmed using DSC. The DSC thermograms demonstrated the attached moieties have an impact on the  $T_m$  and  $T_g$  of the modified polymers.

The ability of the synthesised polymers to form spontaneous self-assemblies (SA) and the capability of these SA to entrap hydrophobic drug is investigated in the next chapter. The SA size, surface charge, loading capacity and drug release time was also determined in order to study the effect of the aforementioned variables on ocular tissues permeation.

**Chapter Three: Triamcinolone Acetonide Loading into Self-Assemblies and Release from Triamcinolone Acetonide-Self-Assemblies**

---

### 3.1 Introduction

An ideal ophthalmic formulation should be able to 1) overcome the ocular barriers and deliver the drug to the target site 2) achieve the desired therapeutic levels at the site of action and 3) sustain the therapeutic level for the required duration of the treatment. Many novel nano-sized drug delivery systems (DDS) such as nanoparticles, liposomes and dendrimers have been explored in pursuit of these criteria (Gaudana, Ananthula, Parenky & Mitra, 2010; Liu, Wang, Zhuang, Yang & Yang, 2012; Nagarwal, Kumar & Pandit, 2012). These DDS have shown advantages compared with that attained using conventional formulations such as enhancement in the drug concentration reaching the targeted ocular tissue and prolonged action of the drug over conventional formulations. In recent years, some researchers have started to investigate the use of polymeric self-assemblies (SA) for ophthalmic drug delivery (Di Tommaso *et al.*, 2012; Yuan, Li & Yuan, 2006). In the work described in this chapter, the SA have been investigated because of their high stability resulting from their low critical aggregation concentration (CAC), high entrapment efficiency of hydrophobic drugs, nano-scale size which does not cause vision blurring and most importantly the absence of organic solvents or stabilisers, which can cause undesirable effects *in-vivo* (i.e. toxicity), from the preparation method (Aksungur *et al.*, 2011; Branco & Schneider, 2009; Hoskins, Lin & Cheng, 2012; Hoskins, Lin, Tetley & Cheng, 2012b).

Self-assembly is an entropy driven physical process wherein disordered molecules establish themselves into regulated nano-scale structures (Gruen & Haydon, 1980). Amphiphilic polymers can self-assemble into either intramolecular or intermolecular structures. Intramolecular SA are formed from one amphiphilic molecule undergoing an intramolecular association resulting in small unimers

(Yusa, Hashidzume & Morishima, 1999). Intermolecular SA emanates from the ability of polymeric chains to form multipolymer aggregates (supramolecular) such as polymeric micelles or nanoparticles (Wu, Qiao, Yang & Wang, 2010). Depictions of the intramolecular and intermolecular SA's are shown in Figure 3.1.

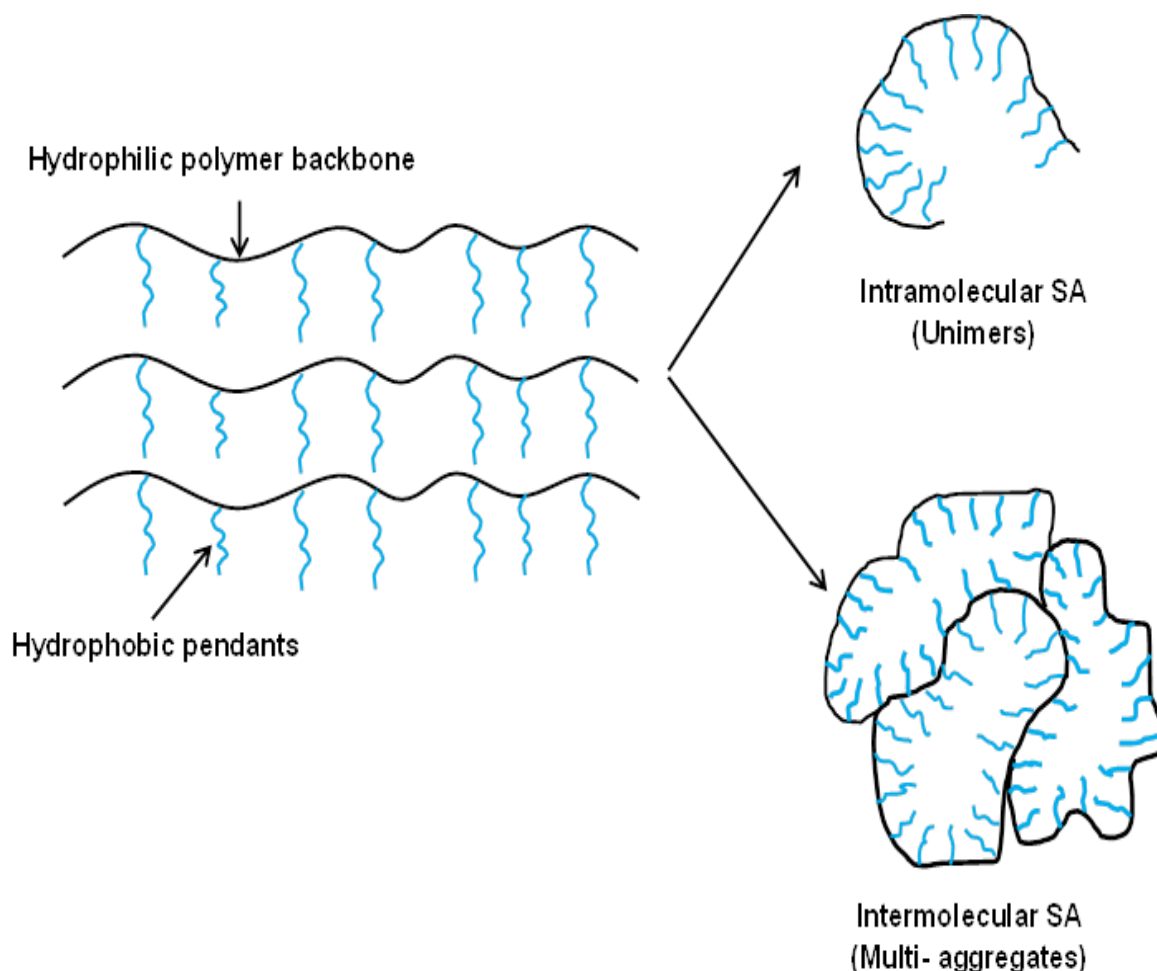


**Figure 3.1:** Schematic diagram of intramolecular and intermolecular SA.

The formation of SA in aqueous medium results in a decrease in the Gibbs free energy, due to the removal of hydrophobic groups from the aqueous environment and the formation of a SA hydrophobic core, which results in an increase in entropy. The creation of the SA is dependent on the concentration of the amphiphilic polymers in the aqueous solution, as SA are only formed above the CAC. The CAC of comb-shaped amphiphilic polymers is generally affected by

the type of the attached hydrophobic groups (Hoskins, Lin, Tetley & Cheng, 2012a; Thompson *et al.*, 2008) and decreases both with the increase in the chain length of the hydrophobic group ((Wu, Qiao, Yang & Wang, 2010) and the level of the hydrophobic attachment (Thompson *et al.*, 2008). The most frequent measurement techniques of the CAC are 1) surface tension (Hoskins, Lin, Tetley & Cheng, 2012a) 2) solvatochromic probes (Thompson *et al.*, 2008) 3) NMR (Barhoum & Yethiraj, 2010) and 4) fluorescent probes (Wu, Qiao, Yang & Wang, 2010). Each technique has its own drawbacks, however in the literature the fluorescent probe techniques are the most commonly used, due to the ease of measurement, accuracy in determining the CAC and the advantage of providing more information about the hydrophobicity of the core.

The comb-shaped amphiphilic polymers can form various types of SA with the most common being micelles and nanoparticles. Hydrophobic drugs can be physically entrapped within the hydrophobic core of a micelle or within the nanoparticle matrix mainly via hydrophobic interactions. A high drug loading capacity (LC) is preferred in DDS as it reduces the amount of polymer required for administration. The LC is dependent on many factors, one of which is the drug loading method used in the preparation of the SA. Generally, there are three major drug loading methods, namely solvent evaporation, dialysis and probe sonication.

In the solvent evaporation method the polymer and hydrophobic drug are dissolved in an organic solvent (e.g. dichloromethane). The organic solvent is then evaporated and the drug-polymer SA is collected after centrifugation. The SA is then reconstituted in water (Danhier *et al.*, 2012; Pignatello *et al.*, 2002).

In the dialysis method the polymer and drug are dissolved in water and a water miscible organic solvent. The solution is transferred into a dialysis

membrane and then exhaustively dialysed against water (Kim *et al.*, 2012; Sinha, Bansal, Kaushik, Kumria & Trehan, 2004). The exchange of the organic solvent and water molecules through the dialysis membrane drives the formation of drug-polymer SA. The dialysate is then filtered to remove any excess un-encapsulated drug. These two methods have a common disadvantage in that the use of organic solvent is essential. Some organic solvents can be toxic and hence any residual organic solvents entrapped within the drug-polymer SA may lead to undesirable effects *in-vivo*.

Ultrasonic probe sonication has been used recently to entrap hydrophobic drugs within SA (Cheng *et al.*, 2006; Hoskins, Lin, Tetley & Cheng, 2012a; Thompson *et al.*, 2008; Thompson, Tetley & Cheng, 2010). In this method, both the drug and the amphiphilic polymer are dispersed in an aqueous solution and the solution is probe sonicated to encourage and accelerate the drug-polymer SA formation. The colloidal solution is then filtered to remove excess free drug. This method is safe, simple, cost effective and most importantly it does not require the use of organic solvents in the preparation method.

The entrapped drug in the SA must be released at an appropriate rate in order to provide a prolonged therapeutic effect and controlled release. The drug release from the SA depends on the type of the SA. For example, drug released from the polymer matrix of nanoparticle SA occurs through diffusion, erosion or a combination of both (Zhang *et al.*, 2012). Whereas drug released from micelle SA occurs through diffusion. The determination of the drug release profile is crucial as it provides information about release kinetics and the mechanism by which the drug is being released from the SA. Generally drug release profiles of SA can be described as a mono- or bi-phasic release pattern (Li, Zhuang, Wang, Sui & Pan,

2012; Suen & Chau, 2013). The biphasic pattern is usually characterized by an initial burst release of the drug followed by a slower continuous release. The initial burst is usually due to the release of un-entrapped drug adsorbed on the surface of the nanoparticles.

The analytical methods used in characterising the SA were photon correlation spectroscopy (PCS), fluorescence spectroscopy and transmission electron microscopy (TEM). The drug content in the SA was determined using high performance liquid chromatography (HPLC).

### 3.1.1 Photon Correlation Spectroscopy

Photon correlation spectroscopy (PCS) or dynamic light scattering (DLS) is a technique that is used to determine the hydrodynamic size distribution of nano-sized colloidal particles (Figure 3.2). The size of dispersed particles is measured by passing a beam of monochromatic and coherent light (laser) through the colloidal dispersion. The incident light is scattered in all directions upon impact with the dispersed particle. As particles move randomly in solutions due to the Brownian motion the distance between the particles in solution is constantly changing with time. The scattering intensity varies dependent on time due to the distance variation of the particles. This time-dependent variation carries information about the diffusion coefficient of the particles (Collins, 2012). The hydrodynamic size of the particle can be determined using the Stokes-Einstein equation (Equation 3.1) (Collins, 2012):

$$D_h = \frac{k_b T}{3\pi\eta D}$$

Equation 3.1

### Chapter 3: Triamcinolone Acetonide Loading into Self-Assemblies and Release from Triamcinolone Acetonide-Self-Assemblies

---

Where  $D_h$  is the hydrodynamic diameter,  $k_B$  is Boltzmann's constant,  $T$  is the temperature (Kelvin),  $\eta$  is the viscosity of solvent medium and  $D$  is the diffusion coefficient.

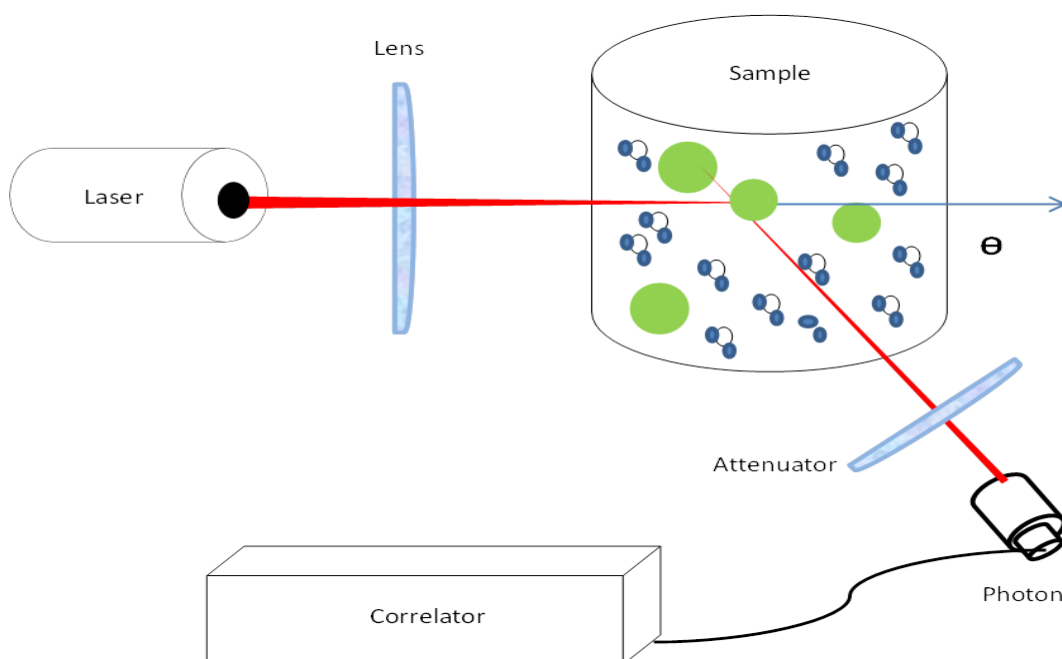


**Figure 3.2:** Schematic diagram of photon correlation spectroscopy analyser.

The observed time-dependent fluctuation at short time delays (usually nano-seconds intervals) is compared to an autocorrelation function. Smaller size particles have faster time-dependent fluctuation decay in comparison to the autocorrelation function of larger particles. The rate of change of light fluctuation is then used to determine the size distribution. The size distribution of a colloidal sample is presented by the polydispersity index (PDI) which can have any value between 0 and 1. A low PDI indicates a uniform particulate size (monodispersed) in the sample, whereas a high PDI indicates non-uniformity in particulate size (polydispersed).

### 3.1.2 Fluorescence Spectroscopy

Fluorescence spectroscopy (Figure 3.3) is a technique used to measure the emission and excitation spectra of fluorophores (fluorescent compound). Fluorescence spectroscopy is based on exciting the ground level electrons, by electromagnetic waves (usually UV) to the excited state (Albani, 2007). Collisions between molecules and thermal loss cause the excited electrons to occupy a lower vibrational state in the excited electronic state than in the ground state. The excited electrons migrate to one of the various vibrational levels at the ground electronic state, emitting a photon in the process. The emitted photons will have different energies, usually lower than the incident exciting light (visible light), due to the migration to different vibrational states.

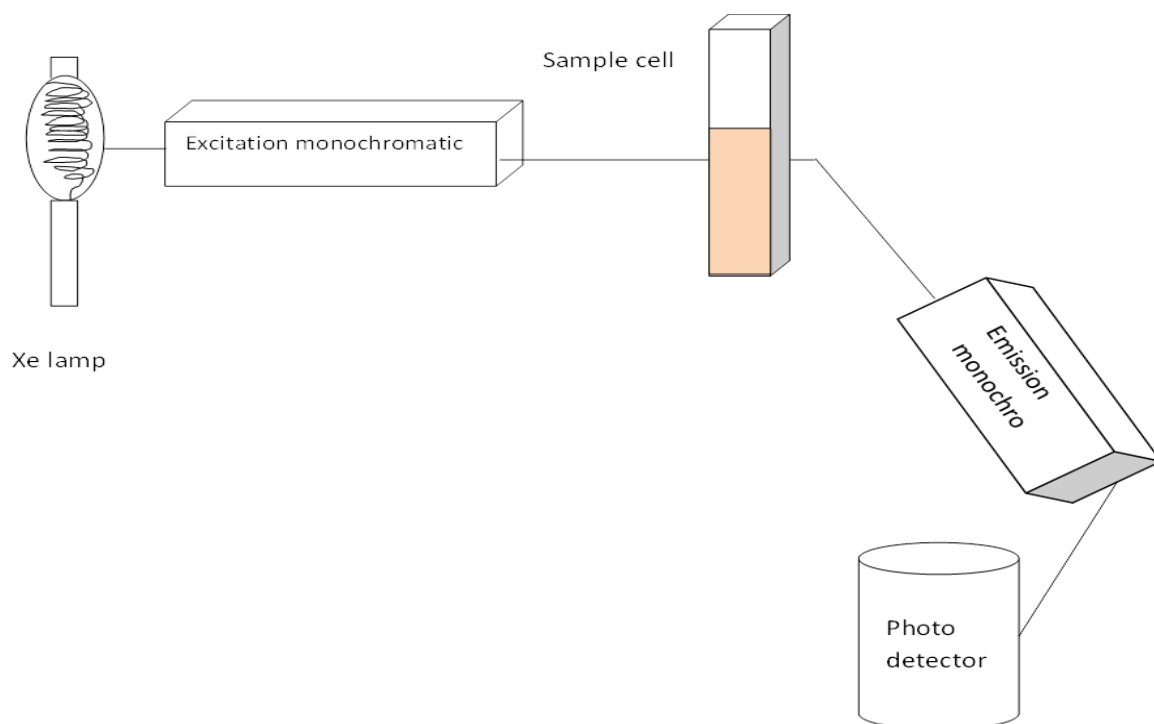


**Figure 3.3:** Schematic diagram of fluorescence spectrophotometer.

Fluorescence spectroscopy is a useful technique in studying the formation of an excimer, which can provide valuable information about the hydrophobicity of

the environment. An excimer is a short lived diatomic complex involving two atoms or molecules with at least one atom/molecule in their excited state (Birks, 1975). The formation of the excimer causes changes in the fluorescent emitted spectra of the fluorophore. Some fluorescent molecules i.e. pyrene (Figure 3.4) form excimers upon moving to the non-polar environment, this enables the use of these probes to investigate the polarity of the core and the CAC of the SA (Kalyanasundaram & Thomas, 1977). Pyrene is a commonly used fluorophore in determining the CAC of SA.

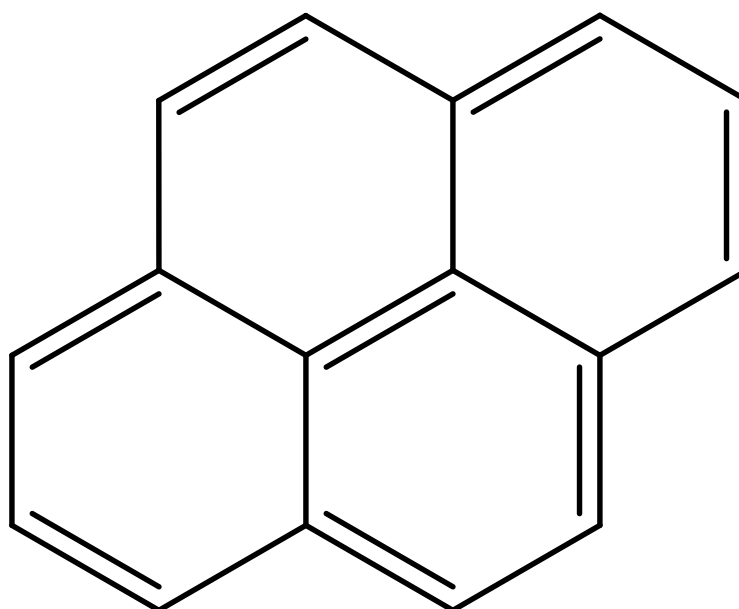


**Figure 3.4:** The chemical structure of pyrene.

The vibrational fine structure fluorescence peaks of a pyrene monomer and excimer are highly dependent on the polarity of the surrounding environment. The most apparent change in the fine structure pattern of pyrene occurs at the 373 and 383 nm peaks (Figure 3.5). In non-polar surroundings, the 383 nm peak dominates the pyrene spectrum (excimer), whereas at a higher polarity environment, the 373 nm peak is the most intense (monomer). Expressing the relative emission intensities at 383 and 373 nm as a ratio is a useful parameter to determine the

environment polarity of the hydrophobic domain (Matsui, Nakazawa & Morisaki, 1991).

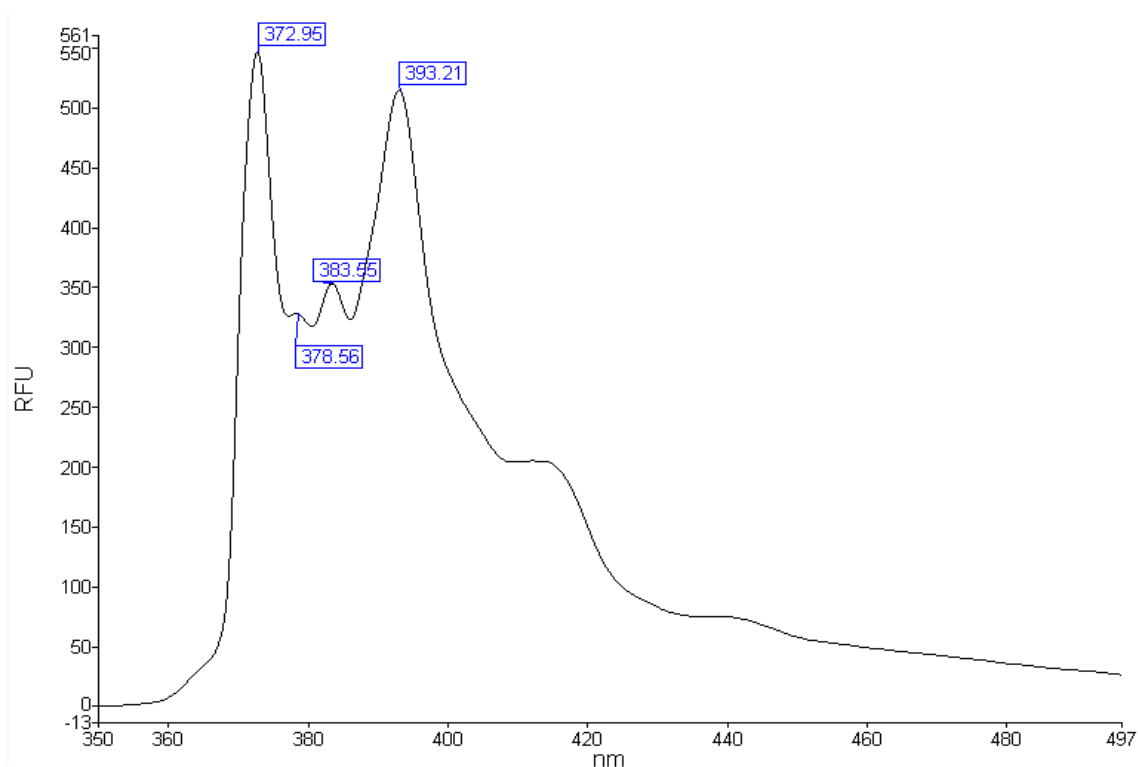


**Figure 3.5:** The fluorescence vibronic peaks of pyrene in aqueous medium (polar environment).

### 3.1.3 Transmission Electron Microscopy

Transmission electron microscopy (TEM) is widely used in studying nano-sized SA providing detailed information about the size, size distribution and the type of the SA (Bakkour, Darcos, Coumes, Li & Coudane, 2013). TEM in principle works in a similar way to a slide projector, however instead of using light, the TEM uses a beam of high energy electrons accelerated to nearly the speed of light (typically 60-120 kV). This beam of electrons is passed through a thin layer (nano-scale) of the sample. The un-scattered electrons are collected on a fluorescent screen or CCD camera providing a shadow image (dark image) of the sample. The darker areas of the image represent the areas of the sample that had fewer electrons transmitted through it (thicker or denser areas). On the contrary, the

brighter areas of the image represent the sample areas that had more electrons transmitted through it (thinner or more penetrable areas) (Amelinckx, Gevers & Landuyt, 1978). The main component of TEM is illustrated in Figure 3.6.

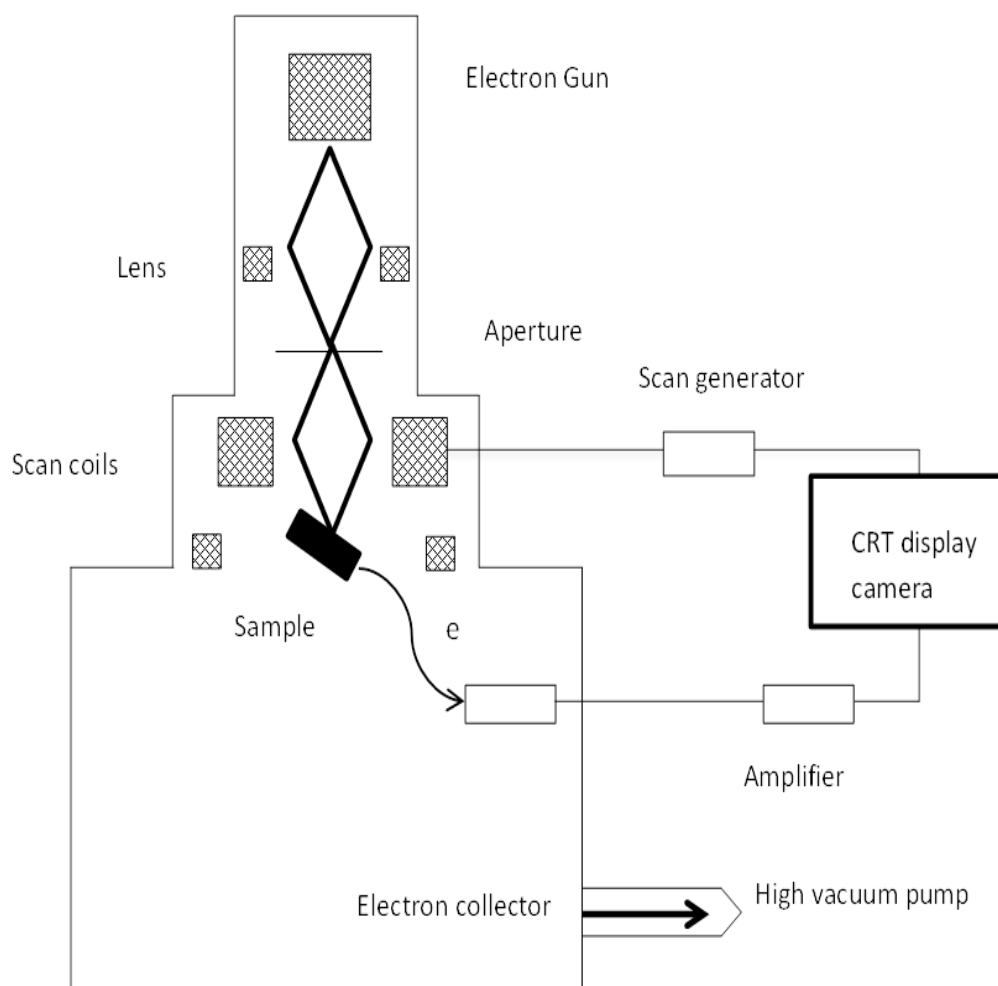
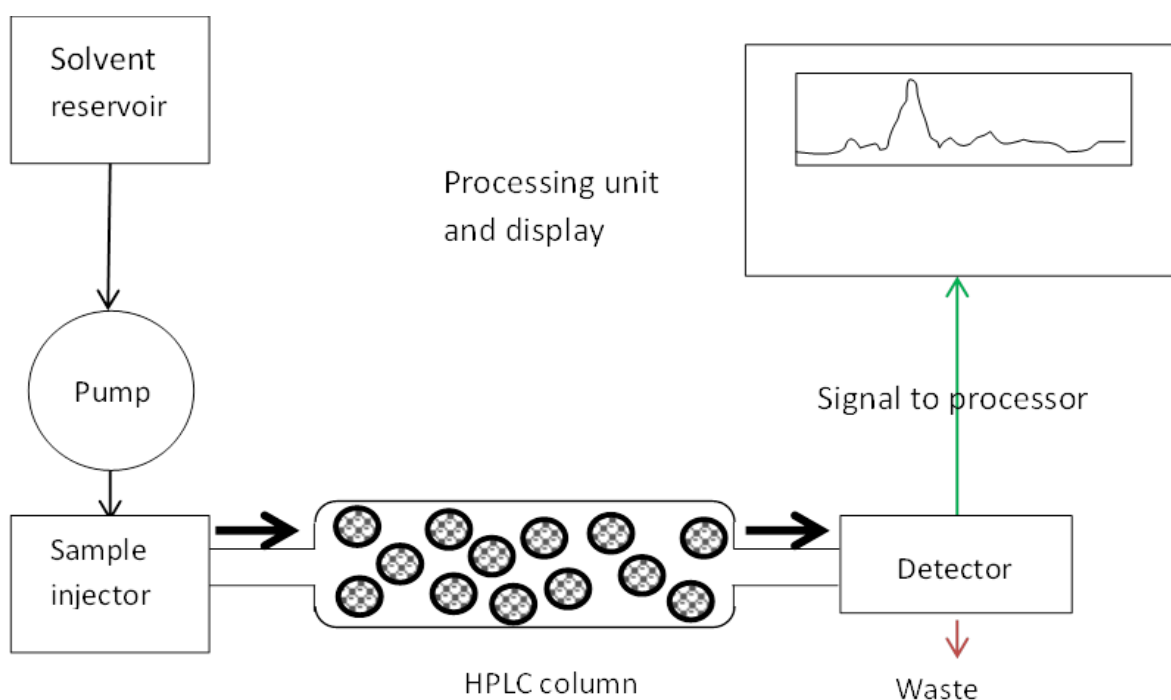


Figure 3.6: Schematic diagram of a transmission electron microscope.

### 3.1.4 High Performance Liquid Chromatography

High performance liquid chromatography (HPLC) is an analytical technique in which a mixture of compounds in a solution are separated for the purpose of quantifying and identifying individual compounds (Kazakevich & LoBrutto, 2007). The types of HPLC vary according to the principle of separation. The most common type is reversed phase HPLC. Reversed phase HPLC involves the use of a non-polar stationary phase such as silica, in which the surface has been

modified with alkyl groups such as  $C_{18}H_{37}$ , and a relatively polar mobile phase (Figure 3.7). The partitioning of the molecules between the mobile and stationary phase is the main principle responsible for the separation of compounds. The retention time is the time elapsed from the injection of the sample to the elution from the column, and dependent mainly on the hydrophobicity of the molecules and the polarity of the mobile phase. A shorter retention time means smaller polar molecules eluting faster due to preferential partition into the polar mobile phase, in contrast to the larger and less polar compounds. A HPLC chromatogram typically shows separated peaks against time, where the area under the peak is used to quantify the studied molecules.



**Figure 3.7:** Schematic diagram of a HPLC.

### 3.1.5 Model Hydrophobic Drug

Triamcinolone acetonide (TA) was used as hydrophobic drug in the drug solubilisation studies for this project (Figure 3.8). TA is a corticosteroid anti-

inflammatory drug, which has been used as an off-label drug to treat many posterior eye diseases such as diabetic macular oedema and AMD (Jonas, Kreissig & Degenring, 2002). TA has a Mw of 434.5, logP of 2.53 (Goundalkar & Mezei, 1984; Steckel, Thies & Müller, 1997) and 21  $\mu\text{g mL}^{-1}$  aqueous solubility at 28 °C (Block & Patel, 1973).

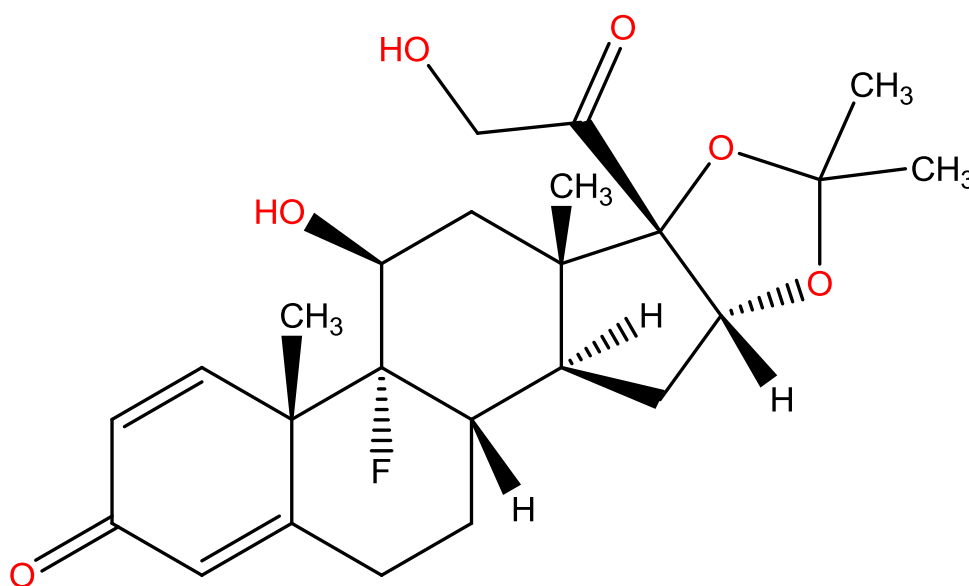


**Figure 3.8:** Triamcinolone acetonide structure (434.5 Mw, 21  $\mu\text{g mL}^{-1}$  solubility in water at 28 °C, logp = 2.53).

Many commercial preparations of TA exist as an injectable suspension for ophthalmic use, such as Kenalog, Flutex and Kenacort-A. Kenalog-40 for example, is a 40  $\text{mg mL}^{-1}$  TA suspension consisting of sodium chloride for isotonicity, 0.99% (w/v) benzyl alcohol as a preservative and 0.75% v/v carboxymethylcellulose sodium and 0.04% w/v polysorbate 80 as stabilisers ("KENALOG<sup>®</sup>-40 INJECTION," 2013). The suspension has a particle distribution size of 69.5% in the 1-5  $\mu\text{m}$  range, 16% in the 5-10  $\mu\text{m}$  range, 2.5% in the 10-20  $\mu\text{m}$  range and 7.6% greater than 20  $\mu\text{m}$  (Jermak, Dellacroce, Heffez & Peyman,

2007). The main route of delivery of TA to the posterior segment of the eye is through an intravitreal injection (Danis, Ciulla, Pratt & Anliker, 2000).

### 3.1.6 Aim and Objectives

The aim of this study was to prepare and characterise the SA formed by the amphiphilic polymers synthesised in chapter 2 and to determine the TA content entrapped within these SA. The objectives were:

- To prepare and characterise SA formed by four different amphiphilic polymers, namely: Pa<sub>5</sub>, Pa<sub>5</sub>-MPEG, Ch<sub>5</sub> and Da<sub>10</sub>.
- To determine the CAC of the SA
- To prepare and characterise TA-SA formulations from four different amphiphilic polymers.
- To study the *in-vitro* drug release profiles of the four TA-SA formulations

## 3.2 Materials and Methods

Pa<sub>5</sub>, Pa<sub>5</sub>-MPEG, Ch<sub>5</sub>, Da<sub>10</sub> were synthesised as described in chapter two (sections 2.2.1.2 – 2.2.1.5). Acetonitrile, methanol and formic acid (HPLC grade) were all purchased from Fisher, United Kingdom. Syringe filters (0.45 µm GDX PVDF, Whatman, United Kingdom), nylon filter membranes (0.2 µm, Whatman, United Kingdom), cremophor<sup>®</sup> EL, tween<sup>®</sup> 80 and pyrene were obtained from Sigma-Aldrich, United Kingdom. Dialysis tubing membrane (Mw cut-off = 12-14 kDa) was supplied by Medicell International Ltd, United Kingdom. Triamcinolone Acetonide micronized powder was acquired from Fagron, United Kingdom. Strata<sup>™</sup> -X-C polymeric solid phase extraction (SPE) tubes were purchased from

Phenomenex<sup>®</sup>, United Kingdom. Highly purified water (deionised) were obtained using a Milli Q<sup>®</sup> integral water purification system.

### **3.2.1 Preparation and Characterisation of SA**

#### **3.2.1.1 Preparation of SA**

SA were formed by probe sonicating the modified polymer (50 mg) in deionised filtered water (10 mL, 0.2  $\mu\text{m}$ , Whatman, United Kingdom) using an ultrasonic processor (Hielscher UP200S, Germany) for 15 min at 100% amplitude on full cycle. The colloidal solution was left to cool down for 15 min and then filtered using a syringe filter (0.45  $\mu\text{m}$  filter). The filtrate was collected for further analysis.

#### **3.2.1.2 Characterisation of SA using PCS**

Hydrodynamic diameters, polydispersity indices (PDI) and zeta potentials of SA in aqueous medium (5 mg mL<sup>-1</sup>) were determined at 25 °C using photon correlation spectroscopy (Zetasizer Nano-ZS, Malvern Instruments, United Kingdom). Analysis was performed at a measurement angle of 173° and equilibration time of 120 s. The collected data were processed using multiple narrow modes (Zetasizer software v6.12). Analysis was performed in triplicate for each sample using a zeta potential cell for both size and zeta potential measurements.

#### **3.2.1.3 Characterisation of SA using TEM**

Samples were sent to the School of Pharmacy, at Keele University for TEM analysis. The method performed was as follows: A glass microscope slide was dipped into 5% formvar in chloroform solution and dried under a heating lamp. The edges of the film were liberated from the glass slide using a fresh razor blade. The

slide was gently lowered into a reservoir filled with deionised water. The film became dissociated from the slide and floated on top of the water. Copper grids were washed in chloroform and dried onto filter paper. The dry grids were placed gently with forceps onto the film surface dull side facing downwards. The film was 'scooped' up by a clean glass slide and dried for 24 h under a heating lamp. The grids were dislodged from the main film using a razor blade and were placed on parafilm ready for use. SA were dried onto the formvar coated copper grids for 8 h under the heating lamp. The grids were imaged using a JEOL JEM-1230 microscope (JEOL, Japan) using anaLYSIS software.

#### **3.2.1.4 Determination of SA CAC**

The CAC of SA in aqueous solution was determined using pyrene as a hydrophobic probe. Pyrene stock solution was prepared by dissolving pyrene (40 mg) in ethanol (100 mL), 100  $\mu$ L of the solution was then transferred to a volumetric flask (100 mL) and the solvent was dried off under a stream of nitrogen gas. The pyrene was subsequently dissolved in 100 mL of deionised water to produce a 2  $\mu$ M stock solution.

SA (5 mg mL<sup>-1</sup>) were prepared in the pyrene stock solution (2  $\mu$ M) and probe sonicated as described in section 3.2.1.1 but without the filtration step. Subsequently, a concentration range of 0.005 to 3 mg mL<sup>-1</sup> polymer solutions were diluted using pyrene stock solution (2  $\mu$ M) as the diluent.

The pyrene fluorescence emission spectrum (350 - 500 nm) was measured using a fluorescence spectrophotometer (Perkin Elmer Precisely, LS 55, United State). The fluorescence emission spectrum was obtained by exciting the sample at 340 nm. The  $I_3/I_1$  intensity values were calculated from the intensity of the third (383 nm) and first (375 nm) peaks in the pyrene emission spectra (Figure 3.5) and

plotted against polymer concentration and 2  $\mu\text{M}$  pyrene stock solution to determine the CAC. The CAC was calculated as the intersection of the tangent to the curve of  $I_3/I_1$  against polymer concentrations at the inflection with the horizontal line passing through the points at low polymer concentration (Figure 3.11).

### **3.2.2 Preparation and Characterisation of TA-SA Formulations**

#### **3.2.2.1 Preparation of TA-SA Formulations**

SA were prepared as described in section 3.2.1.1 without the filtration step. TA (100 mg) was added to the SA colloidal solution (4 mL, 5 mg mL<sup>-1</sup>) in 1:5 polymer to TA weight ratio. The TA-polymer suspension was probe sonicated (Hielscher UP200S, Germany) for 5 min at 100% amplitude on full cycle. The TA-polymer suspension was then left to cool to room temperature before centrifugation at 1008 G force (3000 rpm) for 5 min. The supernatant was transferred into eppendorf tubes and the centrifugation process was repeated two more times to remove any excess drug. Finally the colloidal solution was filtered with a 0.45  $\mu\text{m}$  PVDF syringe filter (Whatman, United Kingdom) to ensure complete removal of any un-encapsulated TA above filter cut-off size. The first 5 drops of the filtrate was discarded while the rest of the TA-SA formulation was collected for further analysis.

#### **3.2.2.2 Characterisation of TA-SA Formulations using PCS and TEM**

The characterisation of TA-SA formulations was carried out using PCS and TEM analysis as described in sections 3.2.1.2 and 3.2.1.3 respectively.

### 3.2.2.3 LC of TA-SA Formulations

The LC of TA was calculated directly by determining the encapsulated TA within the SA using HPLC method (3.2.5) and applying Equation 3.2 (Araujo, Nikolic, Egea, Souto & Garcia, 2011).

$$LC = \frac{[\text{TA}] \text{ measured by HPLC}}{[\text{Polymer}]}$$

Equation 3.2

### 3.2.3 TA Solubility

The solubility of TA in water and in three conventional solubilising agents was performed by the addition of TA (4 mg) to 4 mL of either 1 ) water, 2) 0.1% tween<sup>®</sup> 80, 3) 0.2% cremophor<sup>®</sup> EL or 4) 30% ethanol (v/v). All TA suspensions were sealed in glass vials and left under constant agitation for 24 h (at room temperature approximately 22 °C) before filtering (0.45 µm GDX PVDF, Whatman, United Kingdom) and determining the amount of dissolved TA using the HPLC method (section 3.2.5).

### 3.2.4 *In-vitro* TA Release from TA-SA Formulations

Dialysis tubing with a 12-14 kDa MW cut-off were soaked and washed four times in deionised water. The TA-SA formulations (2 mL) prepared as described in section 3.2.2.1 and TA aqueous suspension (2 mL, 1 mg mL<sup>-1</sup>) were pipetted into the dialysis tubes. The dialysis tubes were tied and immersed in a receiver fluid (200 mL of deionised water) and incubated at 37 °C under magnetic stirring.

The experimental work flow was as follows:

During the first 3-8 h of the experiment, samples (1 mL) were taken at hourly intervals from the receiver fluid (t = 3-8 h), and replenished with 1 mL of receiver fluid at 37 °C. Following the eight hour sample, the receiver fluid was

completely removed and replenished with 37 °C deionised water (200 mL) in order to maintain sink conditions. Subsequent measurements and receiver fluid replacement (complete withdraw of receiver fluid) were taken at regular intervals, to yield samples at t = 23, 32, 47, 56, 71, 80, 97, 121 and 145 h. All withdrawn samples were analysed using the HPLC assay described in section 3.2.5 without the solid phase extraction step.

### **3.2.5 HPLC Analysis Methods**

The amount of TA encapsulated within and released from the TA-SA formulations was determined using HPLC. Due to the relatively high entrapment of TA within the TA-SA formulation in comparison to the low amount of TA released from TA-SA formulations, two HPLC methods were required to ensure sensitivity and linearity across the wide concentration range required to this study. The HPLC system suitability was assessed in compliance with United States Food and Drug Administration (FDA) regulations (US Food and Drug Administration, 1994). The partial validation of the two methods was performed in accordance with the International Conference of Harmonisation (ICH) guidelines (International Conference of Harmonisation, 1995) for analytical methods as detailed below in section 3.2.5.6. The first method was used to determine the relatively high amount of TA entrapped within the TA-SA formulations, whereas the second method was used to determine the low amount of TA released from the TA-SA formulations.

#### **3.2.5.1 Solid Phase Extraction**

The polymers were found to interfere with the HPLC column, resulting in an increased pressure due to partial blockage of the column. This problem was eliminated by extracting TA from the TA-SA formulation using solid a phase

extraction (SPE) method. The extracted TA from the SA was quantified using the TA loading HPLC method (section 3.3.4). The SPE of TA work flow was as follows:

SPE tubes (Strata™ -X-C, 6 mg sorbent, 3 mL) were conditioned by adding methanol (1 mL) to each tube before drying the tubes under low pressure (10-15 inches Hg below ambient pressure) using a vacuum manifold. The tubes were then activated by adding HCl (1 mL, 0.1 M), followed by drying the tubes under low pressure. Prior to the loading step, TA-SA formulation samples were diluted 20 fold in HCl (0.1 M) and mixed thoroughly, before the diluted sample (2 mL) was transferred onto the SPE tube. The samples were left to pass freely under ambient pressure through the SPE tube, followed by drying the tubes under low pressure. TA was eluted using 5% formic acid in methanol (2 ml, v/v) and analysed using the TA loading HPLC method.

### **3.2.5.2 TA Extraction Recovery from TA-SA**

The percentage of TA recovered after extraction using SPE tubes was determined for standards at three concentrations, low ( $5 \mu\text{g mL}^{-1}$ ), medium ( $50 \mu\text{g mL}^{-1}$ ) and high ( $100 \mu\text{g mL}^{-1}$ ) and one TA-SA formulation (Da<sub>10</sub>). TA was extracted from four replicates of each standard concentration and TA-SA formulation. The results were reported as the mean recovery percentage of the four measurements at each concentration level.

### **3.2.5.3 Chromatographic System**

Chromatographic measurements were performed using a Waters HPLC system consisting of Waters 2487 Dual  $\lambda$  Absorbance Detector, Waters In-Line Degasser AF, Waters 717Plus Autosampler, Waters™ 600S controller and Waters™ 616 Pump.

#### 3.2.5.4 Chromatographic Conditions

The mobile phase used was 40: 60 v/v acetonitrile: water. The injection volume and wavelength of detection were 20  $\mu\text{L}$  and 240 nm, respectively. The analysis was carried out isocratically at room temperature on a Gemini 5  $\mu\text{m}$  C18 (250 mm x 4.6 mm x 5  $\mu\text{m}$ ) column (Phenomenex<sup>®</sup>, United Kingdom) and at a flow rate of 1  $\text{mL min}^{-1}$ .

#### 3.2.5.5 Calibration Standards

TA (10 mg) was weighed and then transferred into volumetric flask (100 mL) to which 40 mL of acetonitrile was added. Following complete dissolution of TA, the solution was made up to volume with deionised water, resulting in a stock concentration of 100  $\mu\text{g mL}^{-1}$ . Working standards were prepared by serial dilution using 40: 60 v/v acetonitrile: water solution as the diluent. The standard concentration range for the TA loading and TA *in-vitro* release HPLC methods were 0.5-100  $\mu\text{g mL}^{-1}$  and 0.25-10  $\mu\text{g mL}^{-1}$ , respectively.

#### 3.2.5.6 Validation and Suitability of HPLC Methods

The HPLC system suitability parameters such as theoretical plate number ( $N$ ), capacity factor and tailing factor were assessed for the TA peak. Theoretical plate number is a measure of column efficiency; it is a dimensionless number fairly constant for each peak on a chromatogram.  $N$  was determined using Equation 3.3.

$$N = 16 \left( \frac{t_r}{t_w} \right)^2 \quad \text{Equation 3.3}$$

Where  $t_r$  is the retention time of the peak and  $t_w$  is the peak width at half peak height.

Capacity factor ( $K$ ) is a measure of the peak of interest position with respect to the void volume.  $K$  was calculated according to Equation 3.4.

$$k = \frac{t_r - t_0}{t_0} \quad \text{Equation 3.4}$$

Where  $t_0$  is the retention time of non-retained compounds.

Tailing factor ( $T$ ) is a dimensionless unit which determines when and where the peak of interest ends and therefore a lower  $T$  value results in more accurate calculation of the area under the peak.  $T$  was calculated according to Equation 3.5.

$$T = \frac{w_x}{2f} \quad \text{Equation 3.5}$$

Where  $w_x$  is the width of the peak at  $x\%$  from the baseline of the peak and  $f$  is the distance between the peak maximum and peak front at  $w_x$ .

The linearity, accuracy, precision, range, detection and quantitation limits were assessed to demonstrate the validity of the method (Shabir, 2003). A calibration curve was constructed by plotting the area of the TA peak in the integrated chromatogram versus corresponding concentration. The linearity of the methods was investigated at seven concentration levels in a range between 0.25 and 10  $\mu\text{g mL}^{-1}$  and 0.5 and 100  $\mu\text{g mL}^{-1}$  for the TA loading and TA *in-vitro* release methods, respectively. Six replicates were prepared at each concentration. The accuracy of an analytical method expresses the closeness of the experimental value to the true (reference) concentration. The accuracy of the method was determined by analysing three different standard concentrations levels; low, medium and high for the *in-vitro* TA release (0.25, 5 and 10  $\mu\text{g mL}^{-1}$ ) and for TA loading HPLC methods (0.5, 50 and 100  $\mu\text{g mL}^{-1}$ ), and comparing the measured values to the true value using Equation 3.6. Four replicates were prepared at each concentration. The accuracy was presented as percentage recovery.

$$\text{Accuracy} = \frac{\text{Measured concentration}}{\text{Theoretical concentration}} \times 100\% \quad \text{Equation 3.6}$$

Precision expresses the closeness of measured values between multiple sampling of the same sample under the same analytical conditions. Precision was considered at three levels: repeatability (intra-day), intermediate precision (inter-day) and reproducibility. The repeatability of three standard concentrations (low, medium and high) was assessed by measuring six injections per sample. The inter-day precision was evaluated for three independently prepared standards (low, medium and high) on three different days ( $n = 4$ ). The reproducibility was not assessed as all sample analysis was performed on the same HPLC system. The precision was expressed as relative standard deviation (RSD) percentage. The detection limit (DL) and quantitation limit (QL) were calculated based on the standard deviation of the response and the slope in accordance with Equations 3.7 and 3.8, respectively.

$$\text{Detection limit} = \frac{\sigma}{S} \times 3.3 \quad \text{Equation 3.7}$$

$$\text{Quantification limit} = \frac{\sigma}{S} \times 10 \quad \text{Equation 3.8}$$

Where  $\sigma$  = the standard deviation of the response,  $S$  = the slope of the calibration curve.

### 3.2.6 Statistical Evaluation

Statistical analysis was performed using SPSS program version 19. The normality of the data was assessed using the Shapiro-Wilk test. Experimental difference between groups was compared with the control using the independent student's  $t$ -test. Differences were regarded as significant, with  $P \leq 0.05$ .

### 3.3 Results

#### 3.3.1 Photon Correlation Spectroscopy

The hydrodynamic size of the SA ranged from 114 nm (Da<sub>10</sub>) to 314 nm (Pa<sub>5</sub>-MPEG) as shown in Table 3-1. The Pa<sub>5</sub>, Ch<sub>5</sub> and Pa<sub>5</sub>-MPEG SA all had a low polydispersity index (PDI) indicating a uniform single size population (Table 3-1). A representative size distribution of Pa<sub>5</sub> SA is illustrated in Figure 3.9. On the other hand, Da<sub>10</sub> had a high PDI and is attributed to the multi-size population distribution present in the sample. Figure 3.10 shows the bimodal size distribution for Da<sub>10</sub>, where a small peak appears at around 15-45 nm and a larger peak appears at around 100-400 nm. The Da<sub>10</sub>, Pa<sub>5</sub> and Pa<sub>5</sub>-MPEG SA had similar zeta potential values, in contrast to the higher value associated with Ch<sub>5</sub> SA (Table 3-1).

**Table 3-1:** Average hydrodynamic size, PDI and zeta potential of the SA (Data represented as mean and standard deviation (S.D.), n = 5).

SA ID	Hydrodynamic Diameter (nm), mean ± S.D.	Polydispersity Index (PDI), mean ± S.D.	Zeta Potential (mV), mean ± S.D.
Da <sub>10</sub>	114 ± 8	0.68 ± 0.03	+19.4 ± 0.5
Pa <sub>5</sub>	184 ± 5	0.12 ± 0.01	+20.7 ± 0.9
Ch <sub>5</sub>	232 ± 9	0.22 ± 0.01	+39.5 ± 2.1
Pa <sub>5</sub> -MPEG	314 ± 7	0.12 ± 0.01	+23.6 ± 1.6

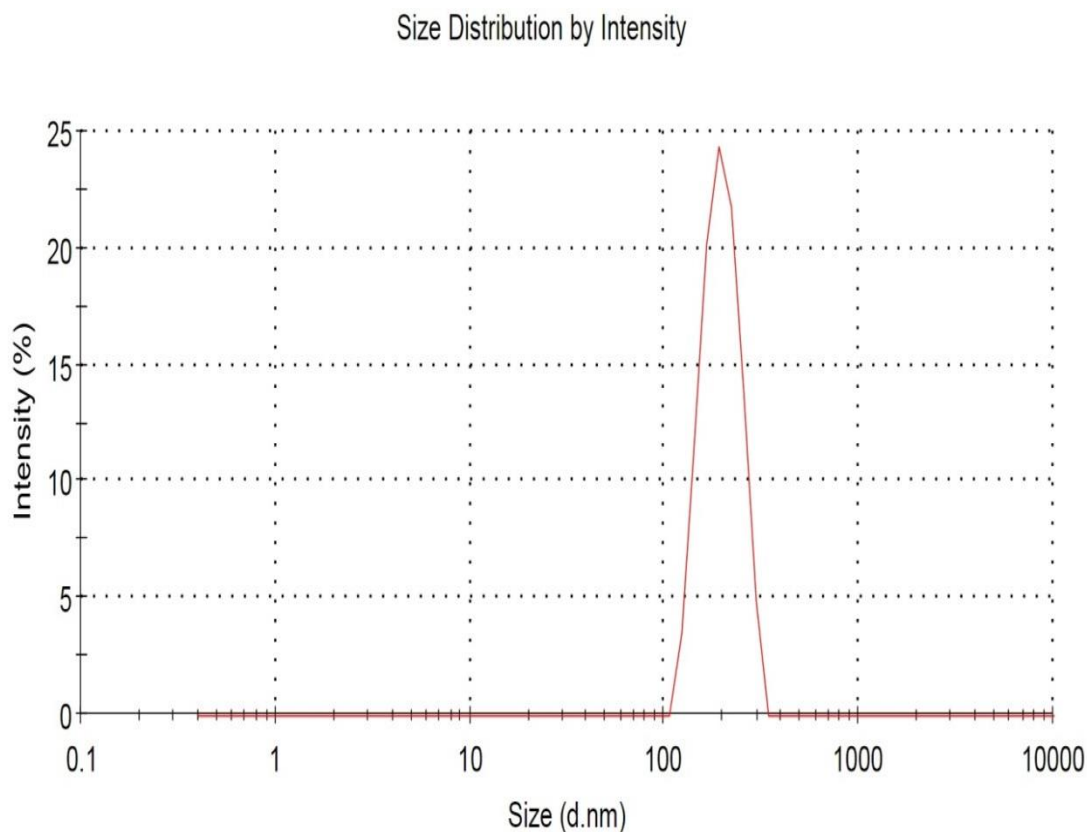


**Figure 3.9:** Photon correlation spectroscopy size correlation chart for Pa<sub>5</sub> SA.

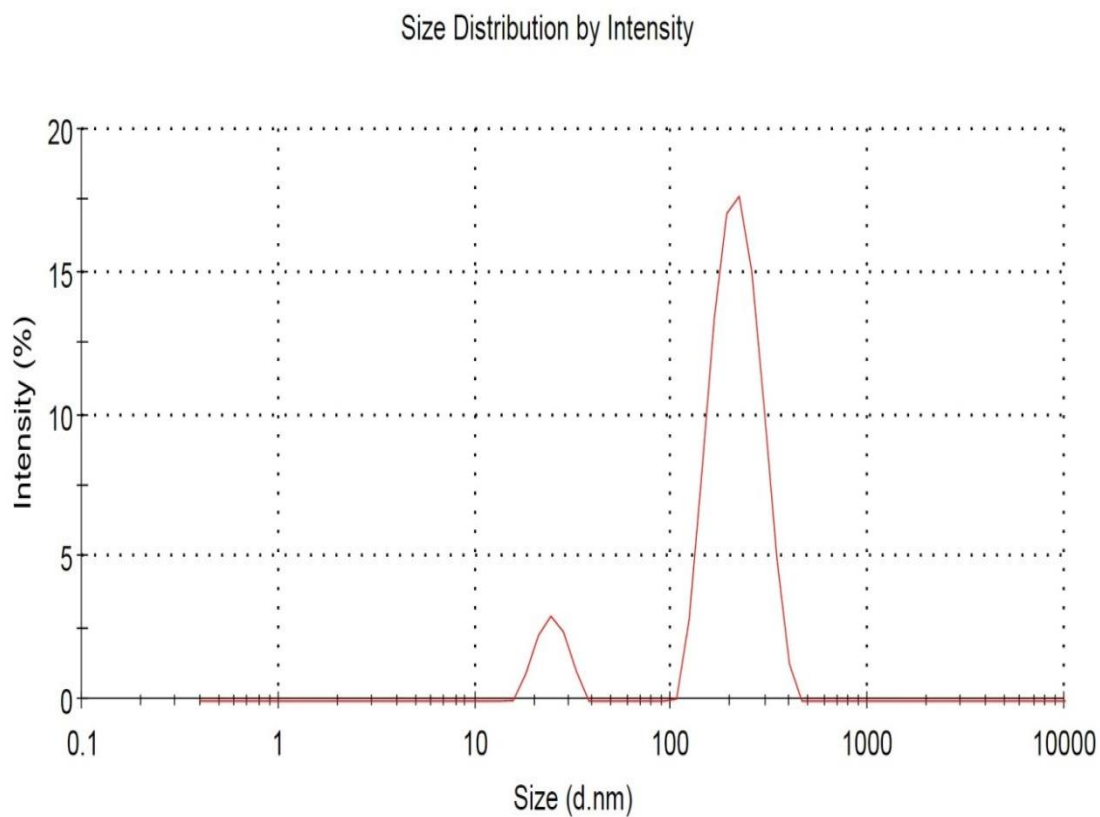


**Figure 3.10:** Photon correlation spectroscopy size correlation chart for Da<sub>10</sub> SA.

The hydrodynamic size of the TA-SA formulations ranged from 200 nm (Da<sub>10</sub>) to 334 nm (Pa<sub>5</sub>-MPEG) as shown in Table 3-2. All TA-SA formulations showed low PDI and single mode size distributions. Apart from Ch<sub>5</sub> SA, the addition of TA did not affect the zeta potential of the SA where TA-SA formulations had similar zeta potentials to the unloaded SA. However, as a whole, addition of TA has an impact on the hydrodynamic size of TA-SA formulations. The hydrodynamic size of all TA-SA formulations was higher than the size of their counterpart SA. The Da<sub>10</sub> TA-SA formulation had the highest increase in hydrodynamic size (*t*-test, *p* < 0.05) from 114 (Da<sub>10</sub> SA) to 200 nm (approximately 80 nm), whereas the rest of the TA-SA formulations had approximately 20 nm increase in hydrodynamic size (*t*-test, *p* < 0.05) in comparison to their counterpart SA. Interestingly, loaded TA-SA formulations resulted in a decrease in PDI in comparison to their unloaded counterparts, with Da<sub>10</sub> having the most significant drop in PDI (from 0.68 to 0.1). This indicates that the addition of TA led to a mono-dispersed size population.

**Table 3-2:** Average hydrodynamic size, PDI and zeta potential of TA-SA formulations (Data represented as mean and standard deviation (S.D.), n = 5).

<b>TA-SA Formulation ID</b>	<b>Hydrodynamic Diameter (nm), mean ± S.D.</b>	<b>Polydispersity Index (PDI), mean ± S.D.</b>	<b>Zeta Potential (mV), mean ± S.D.</b>
<b>Da<sub>10</sub></b>	200 ± 1	0.10 ± 0.01	+20.5 ± 1.0
<b>Pa<sub>5</sub></b>	204 ± 3	0.09 ± 0.01	+21.3 ± 0.4
<b>Ch<sub>5</sub></b>	253 ± 4	0.13 ± 0.02	+45.7 ± 1.0
<b>Pa<sub>5</sub>.MPEG</b>	334 ± 3	0.09 ± 0.01	+22.4 ± 0.5

### 3.3.2 Determination of SA CAC

Figure 3.11, shows the CAC for the Pa<sub>5</sub>, Pa<sub>5</sub>-MPEG and Ch<sub>5</sub> polymers, the CAC for the Da<sub>10</sub> could not be obtained due to the interference between the dansyl absorptivity and the pyrene fluorescent signal. The dansyl group has high absorptivity between 300-450 nm, which masks the hydrophobic probe fluorescent signal (350-450 nm). The Ch<sub>5</sub> polymer had CAC of 0.0052 mg mL<sup>-1</sup>, the lowest CAC value in comparison to Pa<sub>5</sub> (0.011 mg mL<sup>-1</sup>) and Pa<sub>5</sub>-MPEG (0.027 mg mL<sup>-1</sup>). The I<sub>3</sub>/I<sub>1</sub> values for the Ch<sub>5</sub> SA were higher than Pa<sub>5</sub> and the latter had higher I<sub>3</sub>/I<sub>1</sub> values than Pa<sub>5</sub>-MPEG. This observation indicates that the core polarity is in the order of Pa<sub>5</sub>-MPEG > Pa<sub>5</sub> > Ch<sub>5</sub> (*t*-test, *p* < 0.05).

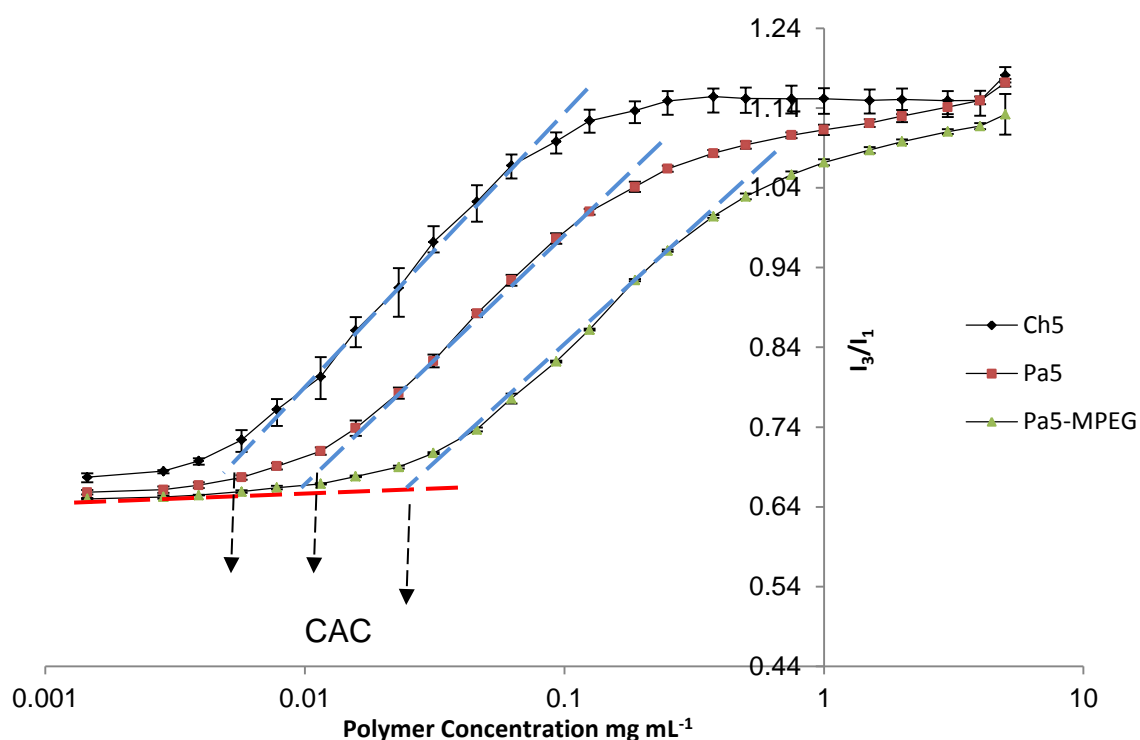


**Figure 3.11:** The fluorescence vibronic peak ratio ( $I_3/I_1$ ) of pyrene at various Pa<sub>5</sub>, Pa<sub>5</sub>-MPEG and Ch<sub>5</sub> concentrations (Data represented as mean, error bars represent range, *n* = 3).

### 3.3.3 TEM of SA and TA-SA Formulations

The TEM micrographs of SA in water are shown in Figures 3.12 to 3.15. The Pa<sub>5</sub>, Ch<sub>5</sub> and Pa<sub>5</sub>-MPEG SA had an approximate size of 100, 100-200 and 150 nm, respectively. The TEM images revealed an irregular shape for Pa<sub>5</sub>; spherical for Pa<sub>5</sub>-MPEG and Da<sub>10</sub>; and cuboid-like for Ch<sub>5</sub> SA (Figures 3.12 to 3.15). The Da<sub>10</sub> SA TEM images (Figure 3.15) showed small spherical SA aggregated into larger clusters. The size of the individual small Da<sub>10</sub> SA was approximately 40 nm and the larger clusters were approximately 200 nm.

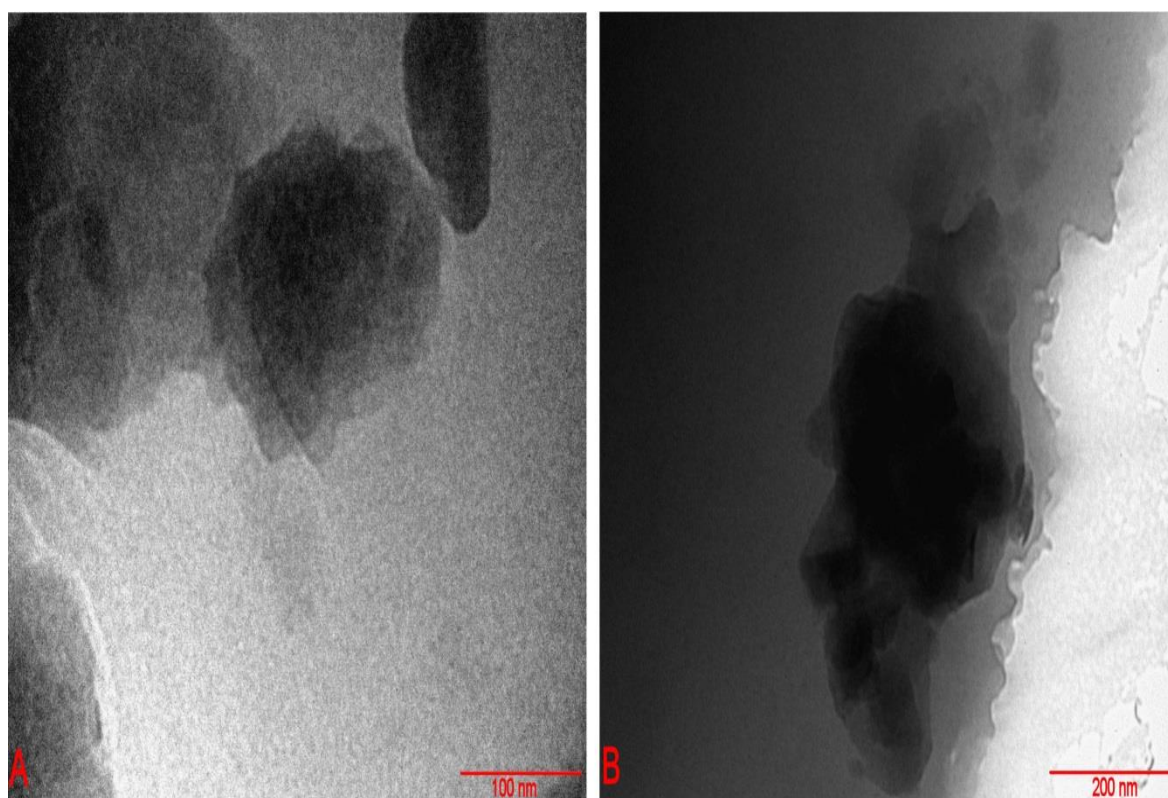


**Figure 3.12:** TEM micrographs of Pa<sub>5</sub> SA (Scale bar A = 100 nm, B = 200 nm).

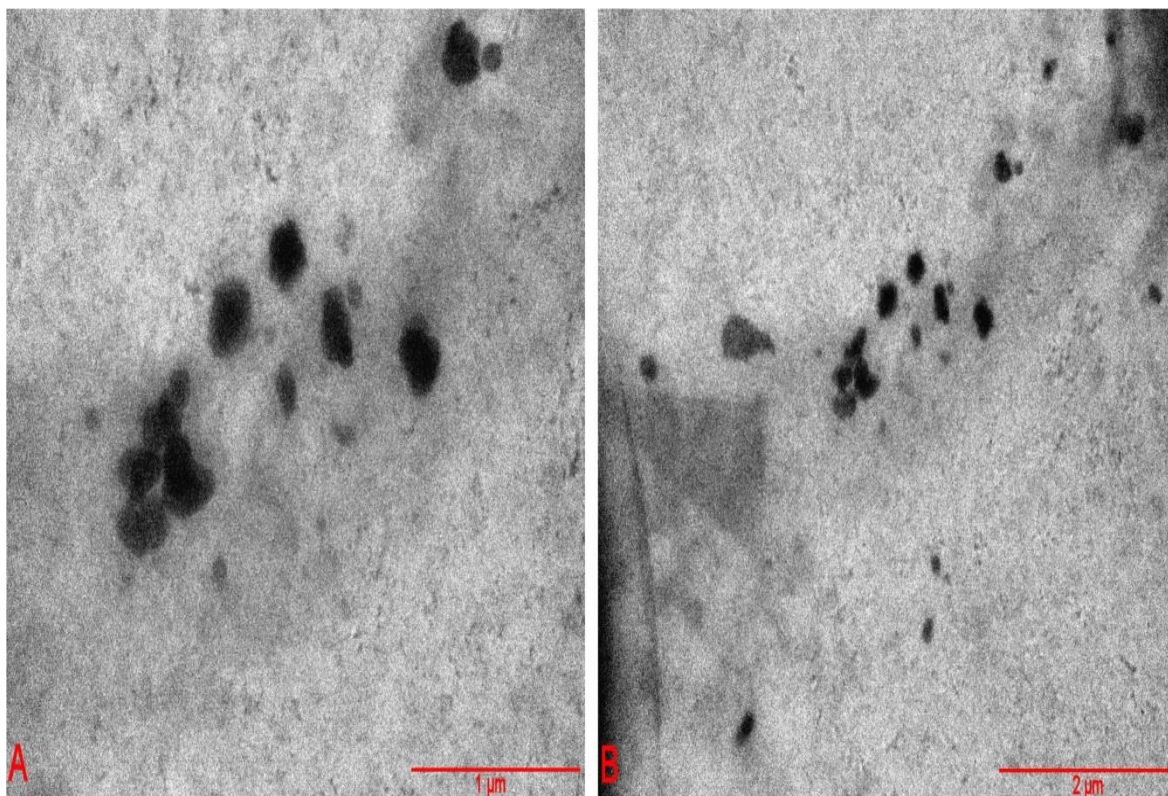


**Figure 3.13:** TEM micrographs of Pa<sub>5</sub>-MPEG SA (Scale bar A = 1 μm, B = 2 μm).

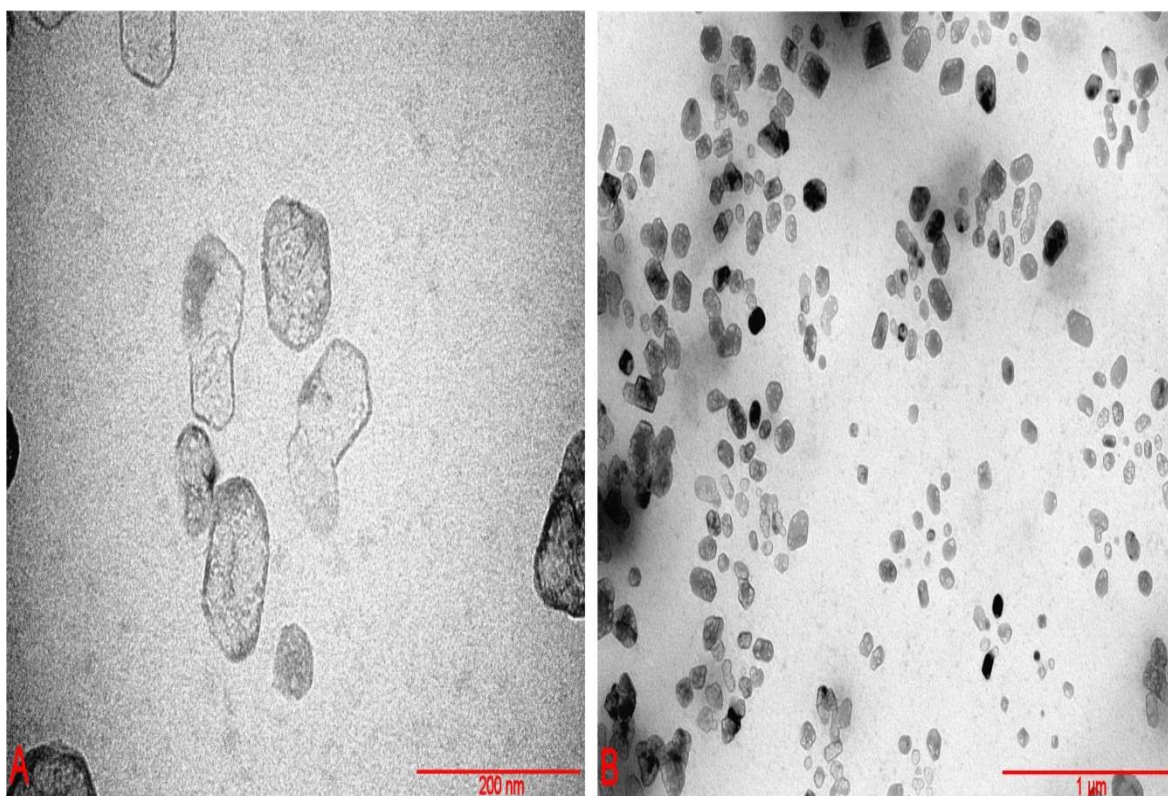


**Figure 3.14:** TEM micrographs of Ch<sub>5</sub> SA (Scale bar A = 200 nm, B = 1 μm).

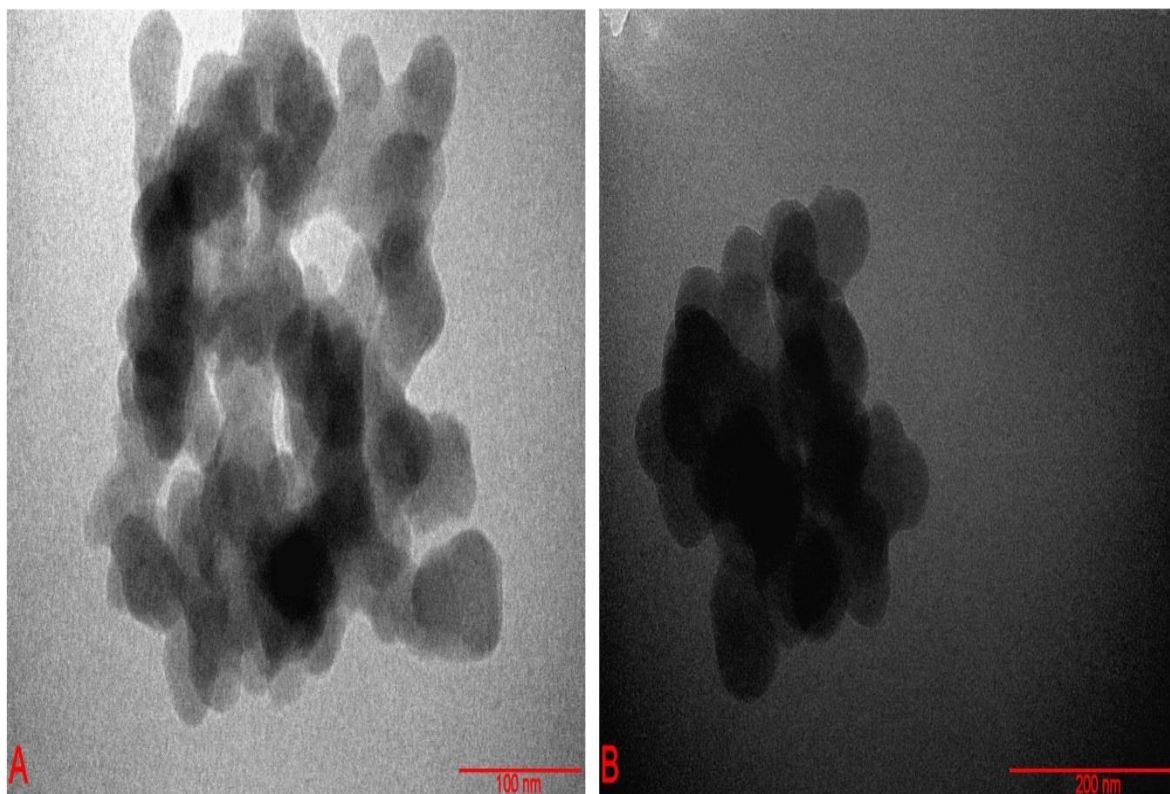


**Figure 3.15:** TEM micrographs of Da<sub>10</sub> SA (Scale bar A = 100 nm, B = 200 nm).

The TEM micrographs of the TA-SA formulations (Figures 3.16 to 3.19) showed that for all formulations, addition of TA led to the formation of spherical particles. The size of the TA-SA formulations varied considerably with the smallest about 100 nm (Pa<sub>5</sub>) (Figure 3.16) and the largest around 400 nm (Pa<sub>5</sub>-MPEG) (Figure 3.17). The Ch<sub>5</sub>-TA and Da<sub>10</sub>-TA SA had an approximate size of 250 and 200 nm, respectively (Figures 3.18 and 3.19). Interestingly, TA loaded Da<sub>10</sub> resulted in the disappearance of the large clusters of small aggregates (Figure 3.15) but instead consisted of discrete, individual spherical particles.

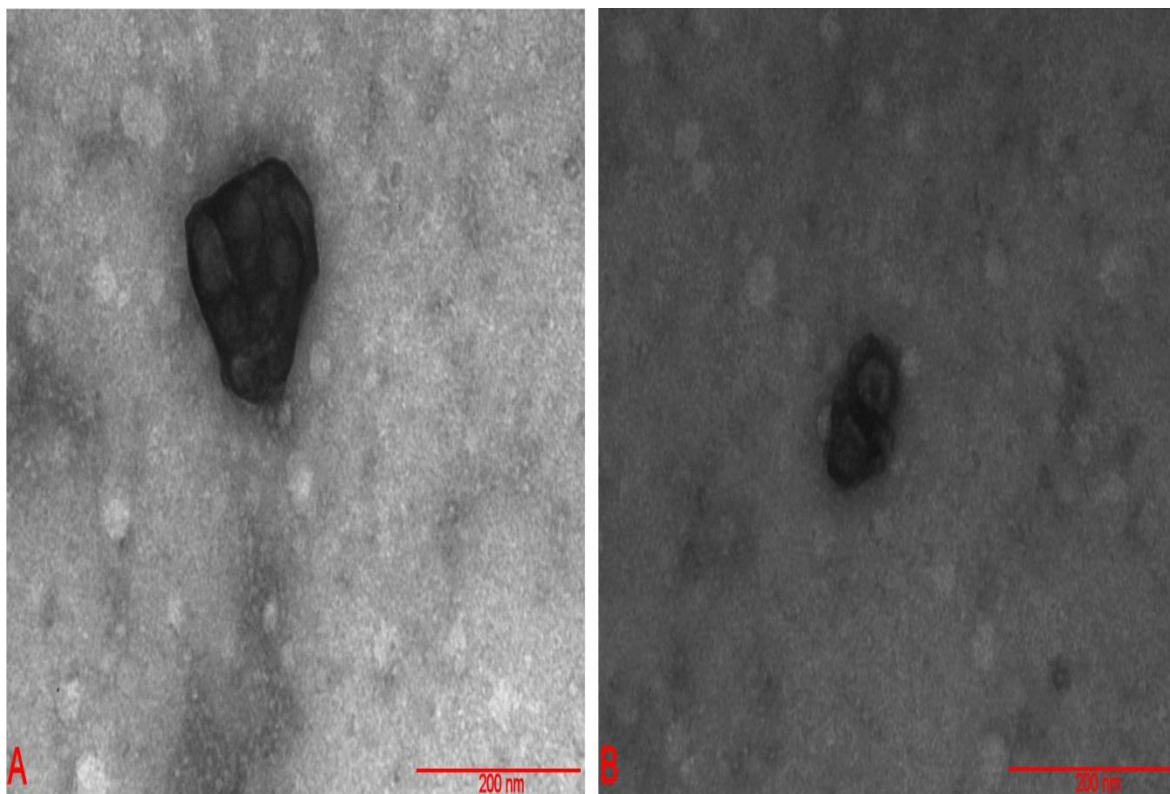


**Figure 3.16:** TEM micrographs of Pa<sub>5</sub> TA-SA formulation (Scale bar A = 200 nm, B = 200 nm).

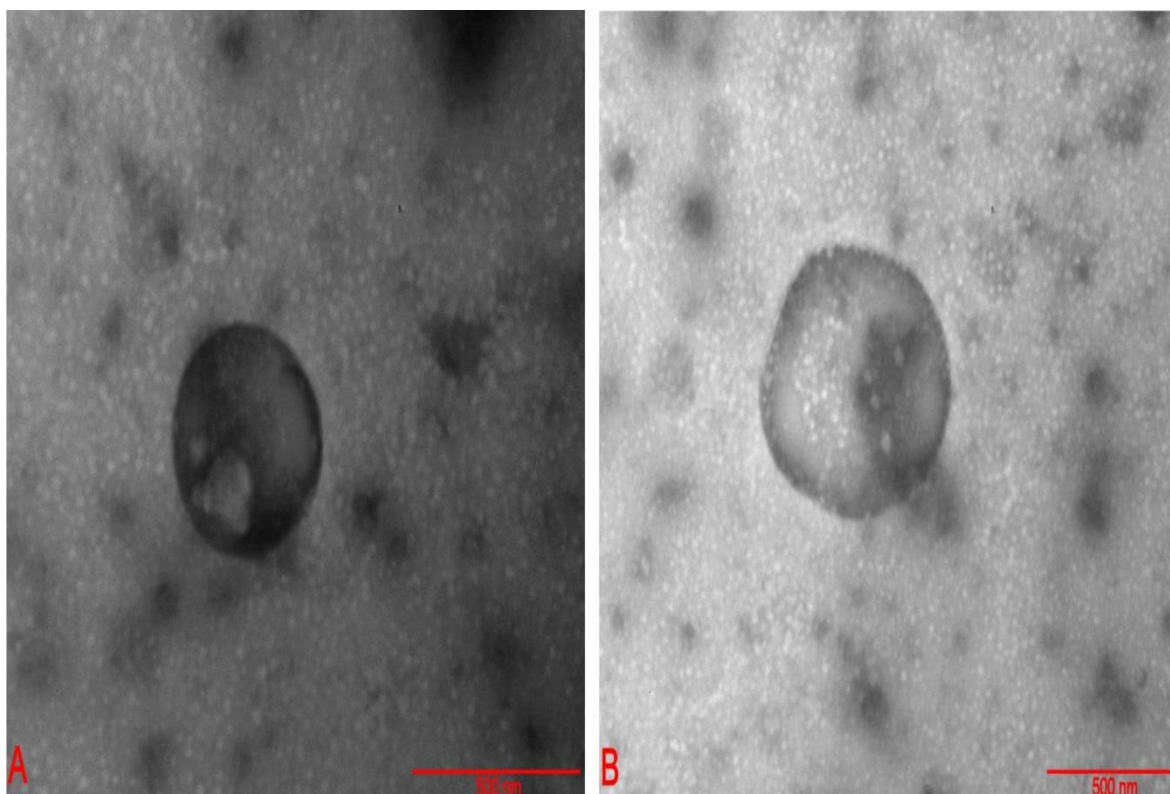


**Figure 3.17:** TEM micrographs of Pa<sub>5</sub>-MPEG TA-SA formulation (Scale bar A = 500 nm, B = 500 nm).

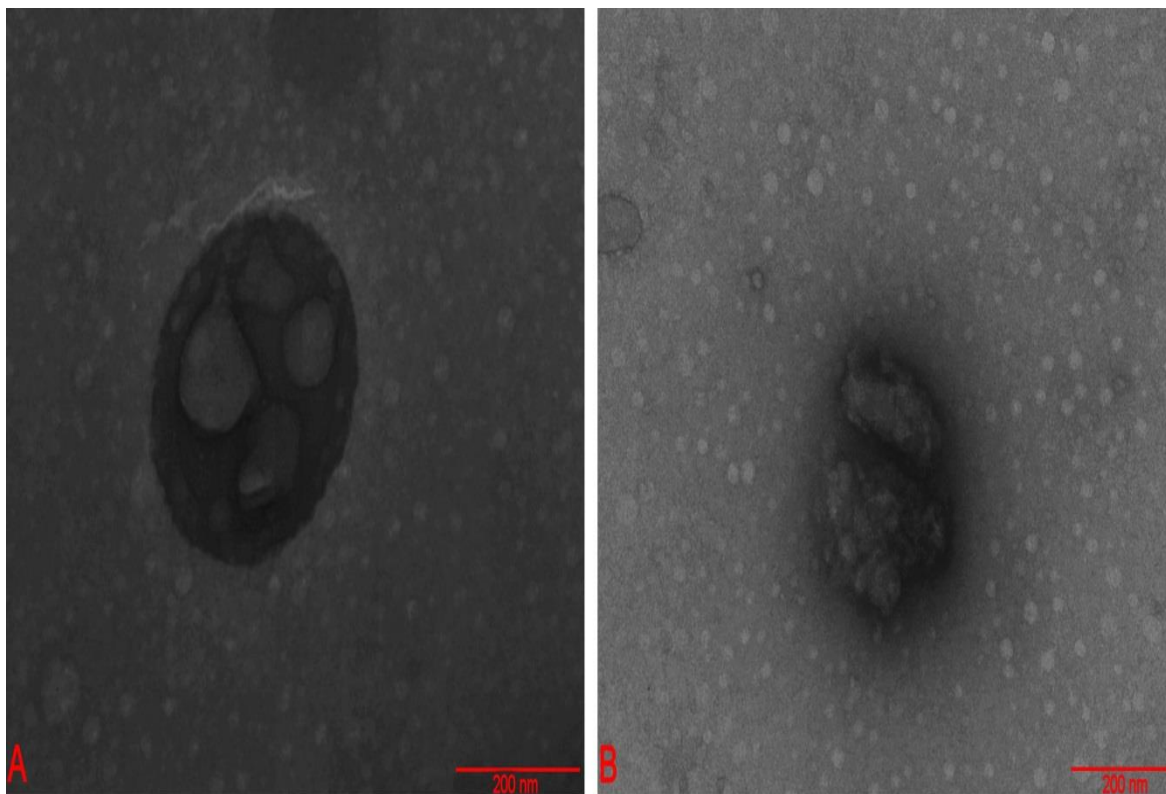


**Figure 3.18:** TEM micrographs of Ch<sub>5</sub> TA-SA formulation (Scale bar A = 200 nm, B = 200 nm).

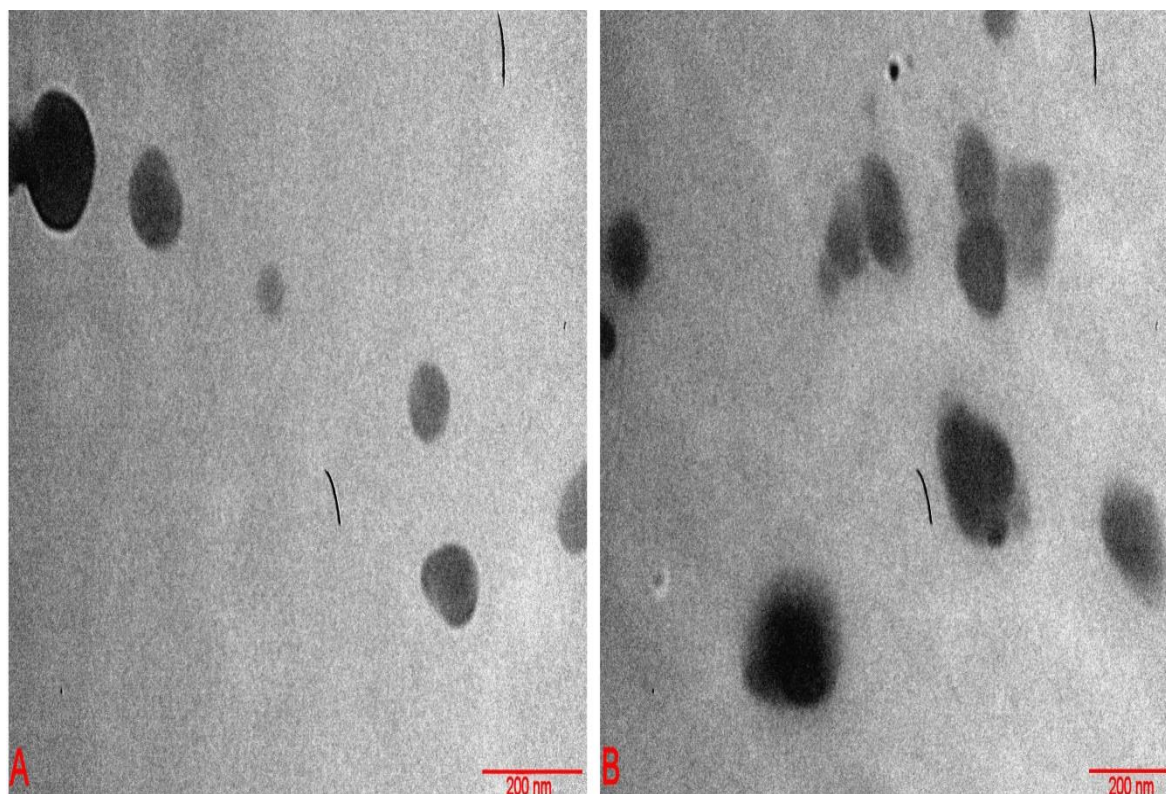


**Figure 3.19:** TEM micrographs of Da<sub>10</sub> TA-SA formulation (Scale bar A = 100 nm, B = 200 nm).

### 3.3.4 Partial Validation and Suitability of HPLC methods

A well resolved TA peak at retention time ( $t_r$ ) of 10.8 min was obtained, as depicted in Figure 3.20. The constructed calibration curves based on the peak area gave excellent linearity ( $R^2 > 0.999$ ) in the range of 0.5-100  $\mu\text{g mL}^{-1}$  for the TA loading method and 0.25-10  $\mu\text{g mL}^{-1}$  for the *in-vitro* release method (Figures 3.21 and 3.22).

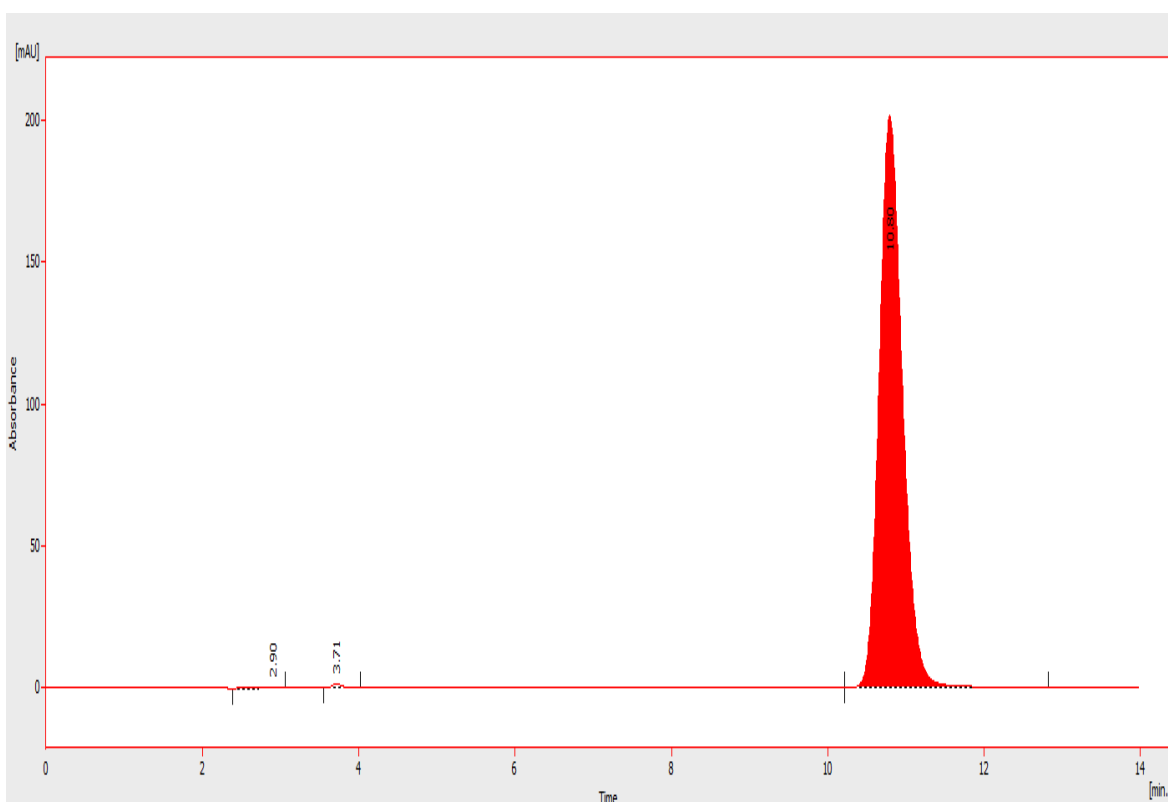


**Figure 3.20:** High performance liquid chromatogram of TA ( $50 \mu\text{g mL}^{-1}$ ) in 40: 60 v/v acetonitrile: water.

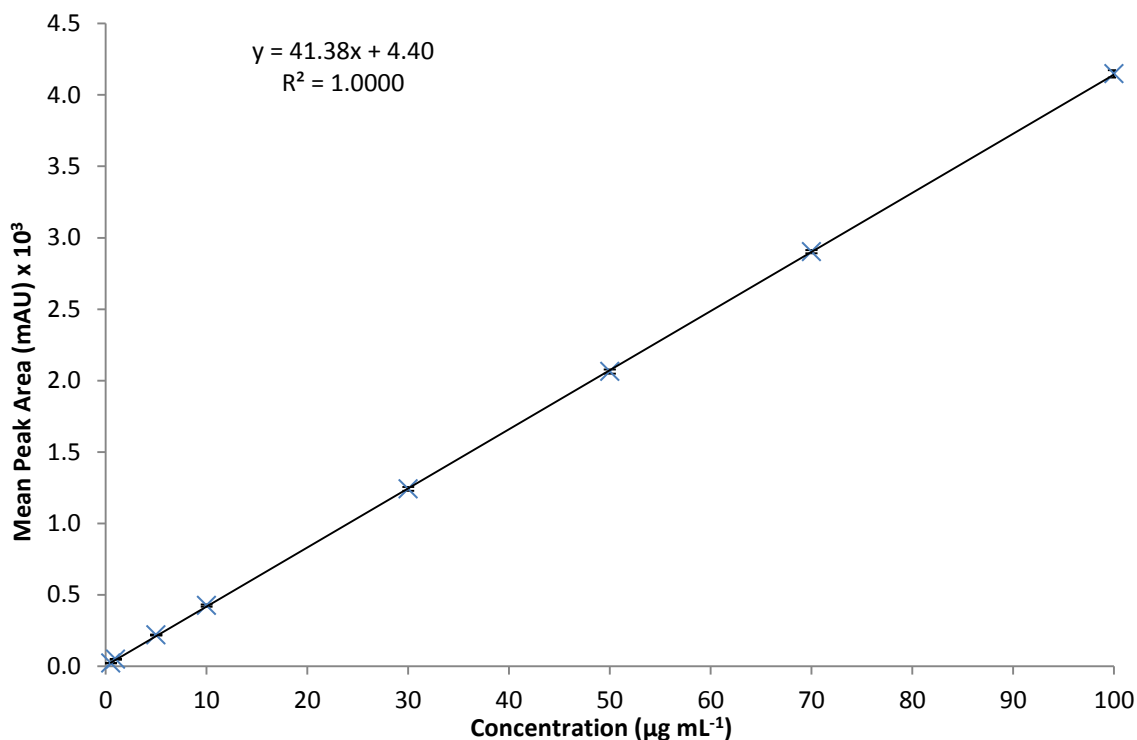


**Figure 3.21:** High performance liquid chromatography calibration curve for triamcinolone acetonide in 40: 60 v/v acetonitrile: water for drug loading studies (Data represented as mean, error bars represented as S.D., n = 6).

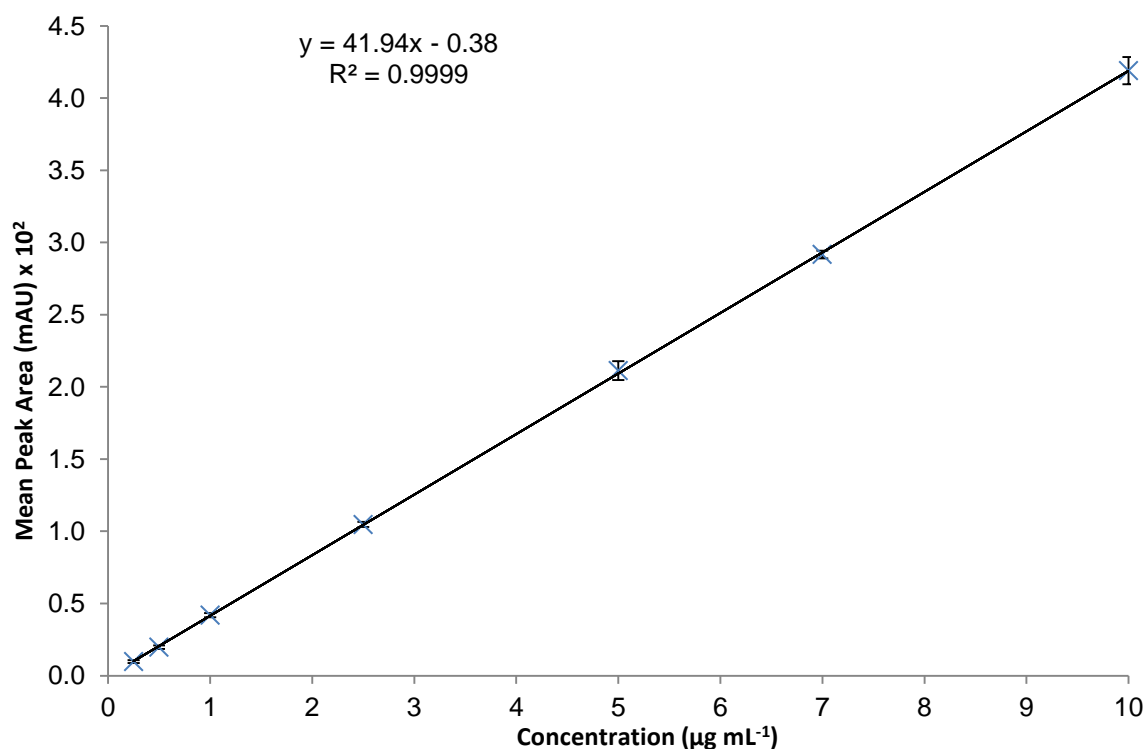


**Figure 3.22:** High performance liquid chromatography calibration curve for triamcinolone acetonide in 40: 60 v/v acetonitrile: water for drug release studies (Data represented as mean, error bars represented as S.D., n = 6).

An optimized reversed-phase HPLC method for the assessment of TA entrapped within and released from the SA carriers was developed and found to be fit for purpose. All suitability and validation parameters of the two methods (Table 3-3) were within the limits proposed by the guidelines of ICH and US FDA, indicating that this method was precise and accurate with low detection and quantification limits.

An optimized SPE method used to extract TA entrapped within the SA was developed. The TA percentage recovered from the SPE tubes for the low, medium and high standards were  $98 \pm 2\%$ ,  $99 \pm 1\%$  and  $100 \pm 1\%$ , respectively (n=4). The TA percentage recovered from the Da<sub>10</sub> TA-SA was  $98 \pm 2\%$  (n=4), indicating the suitability of this method.

**Table 3-3:** HPLC TA methods validation and suitability for the both TA loading and *in-vitro* release methods.

Parameter	HPLC Method		Limits (ICH, US FDA)
	TA Loading	TA <i>In-vitro</i> Release	
Capacity Factor K	4.2	4.2	> 2
Tailing factor T	1.2	1.1	$T \leq 2$
Theoretical plate number	16452	14325	$N > 2000$
Accuracy (low, med & high) (%)	99, 99 & 100	99, 100 & 100	$X = 100 \pm 2\%$
Intra-day precision (low, med & high conc) (R.S.D)	0.26, 0.18 & 0.03	0.6, 0.3 & 0.12	R.S.D < 2%
Inter-day precision (low, med & high conc) (R.S.D)	0.54, 0.38 & 0.34	0.82, 0.61 & 0.23	R.S.D < 2%
Limit of detection ( $\mu\text{g mL}^{-1}$ )	0.53	0.10	-
Limit of quantitation ( $\mu\text{g mL}^{-1}$ )	1.69	0.30	-

### 3.3.5 TA Entrapped and Solubility

The amount of TA entrapped within SA and TA solubility in conventional solubilisers (tween 80, cremophor EL and ethanol) is shown in Figure 3.23. The solubility of TA in water, 0.1% tween 80, 0.2% cremophor EL and 30% ethanol were  $13.58 \pm 0.45$ ,  $18.52 \pm 1.19$ ,  $29.93 \pm 1.94$  and  $241.13 \pm 12.26 \mu\text{g mL}^{-1}$  ( $n = 4$ ), respectively. The TA entrapped within the TA-SA's for Pa<sub>5</sub>, Ch<sub>5</sub>, Pa<sub>5</sub>-MPEG and Da<sub>10</sub> were  $453 \pm 10$ ,  $729 \pm 78$ ,  $910 \pm 92$  and  $1282 \pm 100 \mu\text{g mL}^{-1}$  ( $n = 4$ ), respectively. The Da<sub>10</sub>, Pa<sub>5</sub>-MPEG, Ch<sub>5</sub> and Pa<sub>5</sub> TA-SA enhanced the TA aqueous solubility by 92, 65, 52 and 32-fold, respectively.

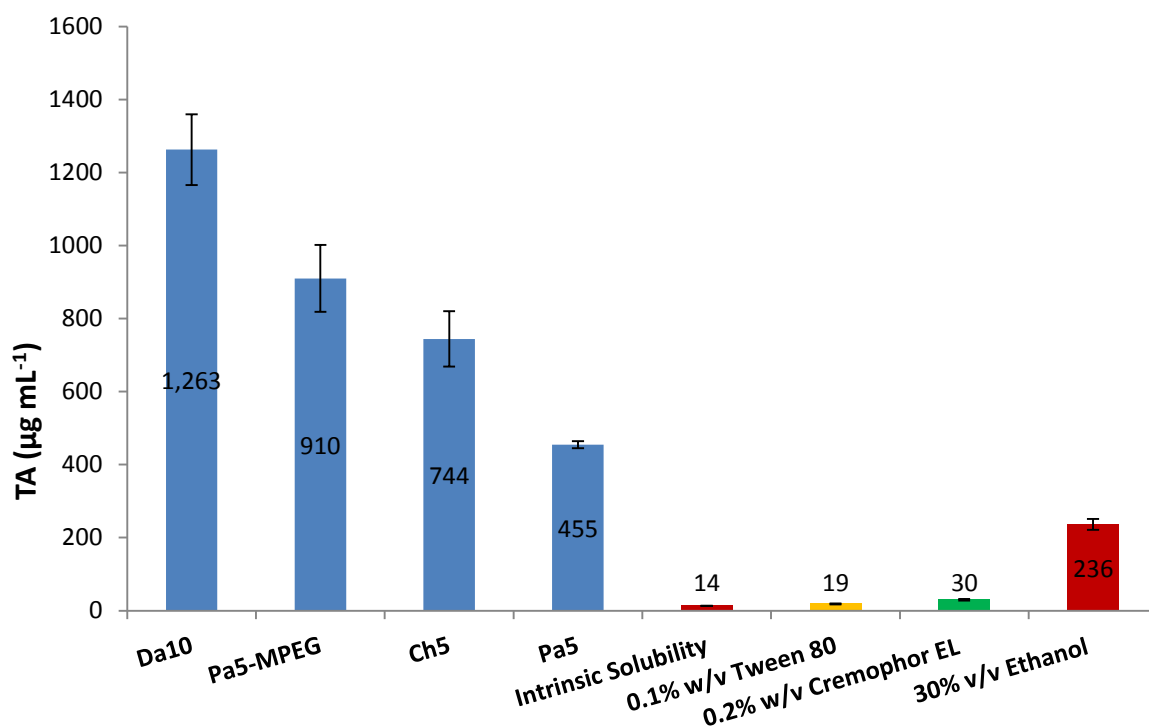


**Figure 3.23:** Maximum TA concentration solubilised by TA-SA formulations at 1:5 initial TA: polymer loading ratio determined by HPLC, compared to the intrinsic solubility and other solubilising agents (Data represented as mean, error bars represent S.D.,  $n = 5$ . All TA solubility and loading experiment were carried out at room temperature at approximately 22 °C).

All TA-SA formulations exhibited higher TA entrapment than the conventional solubilisers as illustrated in Figure 3.23 and Table 3-4. The Da<sub>10</sub> TA-SA formulation had the highest LC (25.3%) and highest TA entrapment compared to the other TA-SA formulations, small molecular weight surfactants and 30% ethanol co-solventol (Table 3-4). The Da<sub>10</sub> TA-SA formulation was able to encapsulate TA up to 66, 42 and 5-fold higher than the 0.1% w/v tween 80, 0.2% cremophor EL and 30% v/v ethanol, respectively (Table 3-4). In contrast, the Pa<sub>5</sub> TA-SA formulation had the lowest LC (9.1%) and lowest TA entrapment amongst the TA-SA formulations. The Pa<sub>5</sub> TA-SA formulation was able to encapsulate TA up to 24, 15 and 2-fold higher than the 0.1% w/v tween 80, 0.2% cremophor EL and 30% v/v ethanol, respectively ( $t$ -test,  $p < 0.05$ ) (Table 3-4).

**Table 3-4:** Loading capacity of TA-SA formulations and number of folds of TA entrapped within the TA-SA formulations in comparison to conventional solubilisers.

TA-SA Formulation	No. of fold increase in TA in comparison to 0.1% tween 80	No. of fold increase in TA in comparison to 0.2% cremophor EL	No. of fold increase in TA in comparison to 30% ethanol	LC%
Da <sub>10</sub>	66	42	5	25.3
Pa <sub>5</sub> -MPEG	48	30	4	18.2
Ch <sub>5</sub>	39	25	3	14.8
Pa <sub>5</sub>	24	15	2	9.1

### 3.3.6 *In-Vitro* TA Release from TA-SA Formulation

The *in-vitro* TA release profiles of the four TA-SA formulations and a TA control (TA suspension) are presented in Figure 3.24. A 100% drug release from the Pa<sub>5</sub>-MPEG, Pa<sub>5</sub> and Ch<sub>5</sub> TA-SA formulations were obtained in approximately two days (47 h). In contrast, the Da<sub>10</sub> TA-SA formulation showed a prolonged release as it took approximately six days (145 h) for 100% release of the TA. In contrast to the Pa<sub>5</sub>, Pa<sub>5</sub>-MPEG and Ch<sub>5</sub> TA-SA formulations, the Da<sub>10</sub> TA-SA formulation showed a lower cumulative TA percentage release in comparison to the aforementioned formulations (Pa<sub>5</sub>-MPEG, Pa<sub>5</sub> and Ch<sub>5</sub> TA-SA).

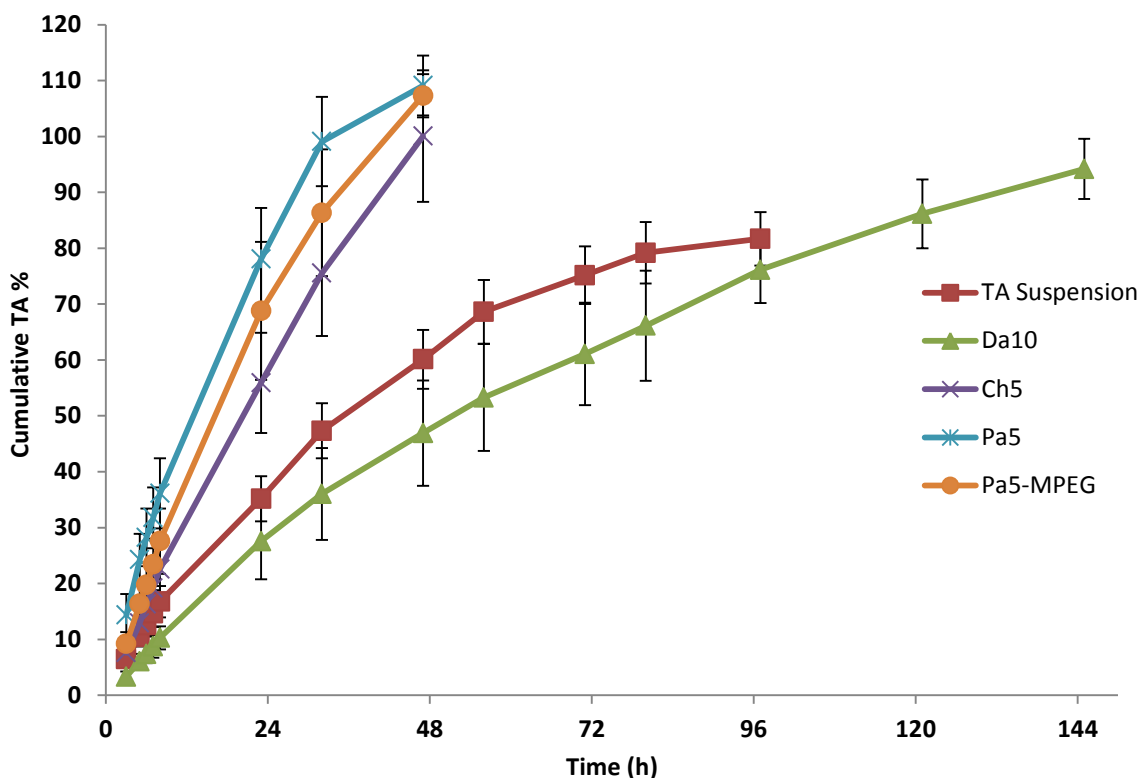


**Figure 3.24:** Release profiles of TA from TA suspension ( $1000 \mu\text{g mL}^{-1}$ ), Da<sub>10</sub> ( $1238 \mu\text{g mL}^{-1}$ ), Pa<sub>5</sub>-MPEG ( $830 \mu\text{g mL}^{-1}$ ), Pa<sub>5</sub> ( $468 \mu\text{g mL}^{-1}$ ), and Ch<sub>5</sub> ( $762 \mu\text{g mL}^{-1}$ ) TA-SA formulations (Data represented as mean, error bars represent range, n = 4).

Table 3-5 summarises the TA *in-vitro* release data fit to kinetic models. The kinetic models best fit for all TA-SA formulations and TA control were obtained using the Higuchi model ( $R^2 > 0.99$ ). The zero order ( $R^2 > 0.95$ ) and Hixon-Crowell ( $R^2 < 0.93$ ) models had the second and third best fit, respectively. The first order model had the least best fit for all TA-SA formulations ( $R^2 < 0.88$ ).

**Table 3-5:** *In-vitro* release data fit to kinetic models.

Kinetic Model	Equation	Parameter	TA Suspension	Ch <sub>5</sub>	Da <sub>10</sub>	Pa <sub>5</sub>	Pa <sub>5</sub> -MPEG
Zero order	$Q_t = k_0 t$	R <sup>2</sup>	0.95	0.99	0.96	0.95	0.98
		k <sub>0</sub>	17.4	30.6	16.6	21.0	38.1
First order	$\ln Q_t = -k_1 t$	R <sup>2</sup>	0.82	0.88	0.76	0.84	0.86
		K <sub>1</sub>	0.03	0.05	0.02	0.04	0.05
Higuchi	$Q_t = k_{HT} t^{1/2}$	R <sup>2</sup>	0.99	1.00	1.00	1.00	1.00
		K <sub>H</sub>	201.4	283.5	224.7	202.2	330.0
Hixson-Crowell	$Q_0^{1/3} - Q_t^{1/3} = k_{HC} t$	R <sup>2</sup>	0.87	0.93	0.85	0.89	0.92
		k <sub>HC</sub>	-0.07	-0.13	-0.06	-0.11	-0.15

$Q_t$  is the cumulative amount of drug release at time  $t$ ;  $Q_0$  is the initial amount of drug in the formulation;  $k_0$ ,  $k_1$ ,  $k_H$  and  $k_{HC}$  are the release rate constants for zero order, first order, Higuchi and Hixson-Crowell, respectively.

### 3.4 Discussion

The formation of SA in an aqueous environment, their CAC, TA solubilising capacity and *in-vitro* TA release were characterised and determined during the work described in this chapter.

The formations of SA in aqueous medium were confirmed using TEM and PCS techniques. The PCS results showed the formation of mono-dispersed nano-sized populations for Pa<sub>5</sub>, Pa<sub>5</sub>-MPEG and CH<sub>5</sub> aqueous SA. In contrast to the mono-dispersed populations of the SA, Da<sub>10</sub> SA had bimodal nano-sized populations. Different size populations (bimodal) phenomenon has been reported in the literature and was attributed to the existence of large loose assemblies in dynamic equilibrium with smaller more compact assemblies (Chiu, Chern, Lee & Chang, 1998; Wang, Tan, Huang, Che & Du, 2009). Others have attributed the bimodal distribution to the existences of unimers (typically few nm in size) coexisting with the multipolymer aggregates (Yusa, Hashidzume & Morishima,

1999). The size (approximately 40 nm) of the small aggregates in the Da<sub>10</sub> TEM micrographs indicates the existence of small compact assemblies alongside large loose assemblies. The Da<sub>10</sub> SA were found to have the lowest hydrodynamic size (114 nm) followed by Pa<sub>5</sub> (184 nm), Ch<sub>5</sub> (232 nm) and Pa<sub>5</sub>-MPEG (314 nm) SA. The lower mean hydrodynamic diameter of Da<sub>10</sub> SA in comparison to the rest of the SA was due to the relatively high hydrophobically modification percentage of Da<sub>10</sub> polymer and the presence of small compact assemblies. The higher modification percentage in Da<sub>10</sub> (10%) results in greater hydrophobic interactions between the hydrophobic groups in the SA and it is these that are likely to have produced smaller compact SA (Yuan, Li & Yuan, 2006). Hoskins *et al* reported smaller hydrodynamic sizes for three hydrophobically modified PAA (10%, dansyl, fluorenylmethoxy carbonyl and naphthalene) in comparison to their lower hydrophobically modified counterparts (5%) (Hoskins, Lin, Tetley & Cheng, 2012a, 2012b). Likewise, Chen *et al.* has reported a decrease in the hydrodynamic size of SA of grafted cholesterol moiety onto poly(amidoamine) by increasing the modification percentage (Chen *et al.*, 2013). The Pa<sub>5</sub> SA had a lower hydrodynamic size than Ch<sub>5</sub> SA despite having similar hydrophobic modification percentages. The bigger size of the Ch<sub>5</sub> SA was attributed to the steric hindrance of the cholesteryl moiety and the longer chain length of the cholesteryl moiety in comparison to the palmitoyl moiety (Thompson *et al.*, 2008; Thompson, Tetley & Cheng, 2010). The addition of the hydrophilic moiety MPEG (3.5%) to the Pa<sub>5</sub> polymer altered the hydrophilic-lipophilic balance and resulted in larger hydrodynamic size SA. The increase in hydrodynamic size of nanoparticles due to the addition of polyethylene glycol (PEG) has been previously reported in the literature (Bagheri & Bigdeli, 2013). The size of nanoparticles increases with an

increase in the molecular weight of the PEG group and the relative content of the hydrophilic attached PEG groups (Bagheri & Bigdeli, 2013; Minimol, Paul & Sharma, 2013; Papadimitriou, Achilias & Bikiaris, 2012).

The mean hydrodynamic diameters of the TA-SA formulations obtained via PCS were in the range of 200–334 nm and larger than their unloaded SA counterparts. Interestingly, the hydrodynamic diameters of Da<sub>10</sub> SA increased by approximately 80 nm upon entrapping TA, whereas the Pa<sub>5</sub>-MPEG, CH<sub>5</sub> and Pa<sub>5</sub> TA-SA formulation had increased by approximately 20 nm, in comparison to their counterpart SA. More interestingly, the Da<sub>10</sub> TA-SA formulation transformed to a mono-disperse population with a low polydispersity index (0.1). The accommodation of TA molecules inside the core of the SA resulted in the expansion of the core and consequently an increase in the hydrodynamic size of the SA. This trend agrees with the findings reported elsewhere, in which loaded SA had bigger hydrodynamic size compared to unloaded SA (Hoskins, Lin, Tetley & Cheng, 2012b; Yang *et al.*, 2012).

The zeta potential of the Pa<sub>5</sub>, Pa<sub>5</sub>-MPEG and Da<sub>10</sub> SA and their corresponding TA-SA formulations did not significantly change (*t*-test, *p* > 0.05). However, the zeta potential of the Ch<sub>5</sub> SA and TA-SA formulations (approximately 40 and 45 mV) was significantly (*t*-test, *p* < 0.05) higher than the rest of the SA and their corresponding TA-SA formulations (approximately 20 mV). Although precise stability thresholds of nanoparticles vary according to the particle type and composition, reports show the stability of colloidal dispersions with zeta potentials above (+/-) 30 mV (Mukherjee, Santra, Pattnaik & Ghosh, 2008; Yue *et al.*, 2008). The stability of the colloids emanates from the highly repulsive surface charge which prevents aggregation. The colloids stability also affected by the ions and

their concentration in the solution; opposite ions charge of the amphiphilic polymer counter the surface charge of the colloid and hence reduce stability. Furthermore, divalent ions cross link two opposite charge polymer strands, resulting in polymer precipitation and increase in CAC, the divalent crosslinking explains the precipitation of amphiphilic polymer in PBS buffer in this work. The increase in the surface charge of the of Ch<sub>5</sub> SA may be due to the amino groups on the PAA backbone being forced out from the hydrophobic domains of the SA to interact with solvent molecules (Thompson *et al.*, 2008). This observation was supported by the pyrene results which indicated lower polarity of the Ch<sub>5</sub> SA core in comparison to the Pa<sub>5</sub> and PA<sub>5</sub>-MPEG SA (Figure 3.11).

In contrast to the PCS technique, TEM analysis also provides additional information about the shape of SA. TEM micrographs of Da<sub>10</sub> SA showed agglomeration of smaller spherical SA into larger agglomerates. The smaller SA had a size of approximately 40 nm, whereas the larger agglomeration had an approximate size of 150-200 nm. This finding is in agreement with the bimodal distribution obtained from the PCS result (Figure 3.10). The Pa<sub>5</sub> TEM micrographs revealed an irregular shape SA with an approximate size of 100 nm, whereas Pa<sub>5</sub>-MPEG had spherical SA with an approximate size between 100-150 nm. Interestingly, the Ch<sub>5</sub> SA TEM micrographs revealed unusual cuboid-like shaped SA with a particle size of approximately 100-200 nm (Figure 3.18). Similar findings were reported by Liu *et al.* in which cubic and cuboid-like shaped SA formed from an amphiphilic polymer consists of approximately 6% mole modification of cholesteryl moieties onto poly(N-isopropylacrylamide-co-N-hydroxymethylacrylamide) (Liu, Pramoda, Yang, Chow & He, 2004). The author also reported changes in the shape of the SA from well-organized cubic and

cuboid-like to roughly spherical when the amphiphilic polymer concentration was increased from 0.1 to 0.6%. The formation of spherical shaped SA was attributed to the increasing hydrophobic–hydrophobic associations between the hydrophobic moieties. TEM micrographs revealed similar findings when the cuboid-like shape of the Ch<sub>5</sub> SA transformed to spherical in the Ch<sub>5</sub> TA-SA formulation. All TA-SA formulation TEM micrographs revealed a spherical shape with comparable sizes to the PCS data. The size of the SA and TA-SA formulation acquired using TEM was smaller than the size obtained from PCS. This is due to the fact that TEM reveals the size of SA in their dry state rather than the hydrodynamic diameter which have larger values because of the solvent effect (hydration double layer).

The CAC values obtained in this work were comparable to the values quoted in the literature for comb shaped amphiphilic polymers (Yuan, Li & Yuan, 2006). The CAC values for CH<sub>5</sub>, Pa<sub>5</sub> and Pa<sub>5</sub>-MPEG were 0.0052, 0.011 and 0.027 mg mL<sup>-1</sup>, respectively. The obtained CAC value for the Ch<sub>5</sub> polymer was comparable to the CAC value (0.004 mg mL<sup>-1</sup>), obtained using a pyrene probe, for a similar cholesterol grafted comb shaped amphiphilic polymer (Liu, Pramoda, Yang, Chow & He, 2004). The lower CAC value of the Ch<sub>5</sub> polymer compared to Pa<sub>5</sub> is in agreement with the previously reported results of Thompson *et al.* (Thompson *et al.*, 2008). The author reported CAC values of 0.02 and 0.08 mg mL<sup>-1</sup>, using a methyl orange probe, for Ch<sub>5</sub> and Pa<sub>5</sub> polymers, respectively. The higher CAC values reported by Thompson *et al.* are thought to be due to different techniques used in measuring the CAC. Lin *et al.* reported CAC values of 0.05 and 0.002 mg mL<sup>-1</sup> for amphiphilic siloxane graft copolymer using methyl orange and pyrene, respectively (Lin & Alexandridis, 2002). The lower CAC value of Ch<sub>5</sub> in comparison to Pa<sub>5</sub> was due to the higher hydrophobicity of the cholesteryl group.

A decrease in the CAC was reported with an increase in the hydrophobicity of the modified group (Wu, Qiao, Yang & Wang, 2010). Unlike the palmitoyl group the cholesteryl moiety is a bulky group with a near planar conformation (Liu, Pramoda, Yang, Chow & He, 2004), which upon self-assembly had restricted mobility. This restricted mobility observation was supported by the NMR results (Chapter two, section 2.3.3.2.3) and by the lower core microviscosity (rigidity) of the Ch<sub>5</sub> SA in comparison to Pa<sub>5</sub> SA as reported by Thompson *et al.* (Thompson *et al.*, 2008). The core rigidity of the Ch<sub>5</sub> SA limits the entry of the flexible PAA backbone into the core of the SA. This explains the lower core polarity (Figure 3.11) and the higher zeta potential (Table 3-1) of Ch<sub>5</sub> SA in comparison to Pa<sub>5</sub> SA. The addition of a hydrophilic MPEG groups to the Pa<sub>5</sub> polymer increases the overall hydrophilicity of the polymer (Lin, Zhang, Kumar & Mark, 2009). This alteration in the hydrophilic-lipophilic balance results in an increased size, CAC and core polarity of the SA (Figure 3.11).

The four SA described in this work possessed the ability to encapsulate TA at high concentrations within their hydrophobic cores. The LC of TA within the SA ranged from 9% for Pa<sub>5</sub> to 25% for Da<sub>10</sub>. The values are similar to the reported LC of amphiphilic polymers which normally range between 5 and 30% (Bagheri & Bigdeli, 2013; Bagheri & Motirasoul, 2013; Chang *et al.*, 2012; Gaucher, Satturwar, Jones, Furtos & Leroux, 2010; Gu *et al.*, 2011).

The SA had superior solubilizing capacity of TA in comparison to conventional solubilisers such as surfactants and co-solvents (Figure 3.23). The Da<sub>10</sub> had the highest TA entrapment followed by Pa<sub>5</sub>-MPEG, Ch<sub>5</sub> and Pa<sub>5</sub> TA-SA formulations. The higher LC of Da<sub>10</sub> is mainly due to the higher modification percentage and better TA-hydrophobic moiety compatibility. Higher

hydrophobically modified polymers have been shown to exhibit higher LC than their lower modified counterparts (Chang *et al.*, 2012; Hoskins, Lin, Tetley & Cheng, 2012b). Moreover, polymers modified with drug-like hydrophobic moieties have been shown to have higher LC as a result of improved compatibility between the drug and the hydrophobic moiety (Gu *et al.*, 2011; Mahmud, Xiong & Lavasanifar, 2008). The higher TA LC by Ch<sub>5</sub> SA compared to Pa<sub>5</sub> was due to a better TA-cholesteryl compatibility in comparison to palmitoyl, as the cholesteryl moiety has a steroid like structure whereas palmitoyl has a hydrocarbon chain. Similar results were reported by Gu *et al.* where poly-L-lysine (PLL) modified by the cholate moiety encapsulated significantly higher levels of sterol drugs (prednisolone and estradiol) than palmitoyl modified PLL (Gu *et al.*, 2011). The addition of the hydrophilic moiety MPEG to Pa<sub>5</sub> resulted in increased TA LC, the reason for this increase is not well understood and could be due simply to the bigger size of the Pa<sub>5</sub>-MPEG SA as a result of altering the hydrophilic-lipophilic balance of the Pa<sub>5</sub> SA.

The TA release profile from the TA-SA formulations (Figure 3.24) showed Ch<sub>5</sub>, Pa<sub>5</sub> and Pa<sub>5</sub>-MPEG TA-SA formulation were able to achieve sustained TA release over 47 h, whilst the Da<sub>10</sub> TA-SA formulation achieved sustained release over 145 h. Interestingly, the Da<sub>10</sub> TA-SA formulation had a lower cumulative percentage released in comparison to the Ch<sub>5</sub>, Pa<sub>5</sub> and Pa<sub>5</sub>-MPEG TA-SA at any time point. This can be explained by high drug affinity to the hydrophobic domain (dansyl group). Similar findings have been reported by Chang *et al.* in which he found introducing hydroxyl groups to the core of nanoparticles resulted in higher doxorubicin LC and a lower cumulative release percentage (Chang *et al.*, 2012). The author related the higher LC and lower release to the formation of

hydrogen bonding between the doxorubicin and hydroxyl group. TA can potentially form hydrogen bonds through two hydroxyl groups (Figure 3.8) with either the sulfonyl group or with the nitrogen atom on the dansyl moiety. In contrast, TA can form hydrogen bonds with the cholesterol or palmitoyl moieties only through the single carbonyl group which is sterically hindered. The predicted hydrogen bonding between TA and the dansyl group may explain both the slower TA release and the higher LC for Da<sub>10</sub> TA-SA in comparison to other TA-SA's. Although  $\pi$  (a type of non-covalent interaction that involves  $\pi$  systems) binding between the aromatic naphthalene ring (dansyl) with TA might be another explanation for the higher LC and lower TA release.

The best mathematical fit for the *in-vitro* release of TA from TA-SA formulations was obtained using Higuchi ( $R^2 > 0.95$ ) and zero order ( $R^2 > 0.99$ ) models. The two mathematical models tell a great deal about the way TA is released from the TA-SA formulation. The Higuchi mathematical model describes drug release from a matrix or porous system. This model is only valid for systems in which erosion or swelling of the matrix does not significantly contribute to drug release. A good fit to the zero order model indicates that the TA release rate is independent of the initial TA concentration within the TA-SA formulation. The deduced information from both models (Higuchi and zero order) leads to the conclusion that TA diffuses away from the matrix of the SA without a significant change in volume (no erosion or swelling) and at constant rate (Brophy & Deasy, 1987). The previous assumptions (TA diffusion from SA matrix at a constant rate) were supported with the low mathematical fit of the first order model ( $R^2 < 0.88$ ) and the Hixson-Crowell model ( $R^2 < 0.93$ ). Hixson and Crowell recognized that particle area is proportional to the cube root of its volume (Dash, Murthy, Nath &

Chowdhury, 2010); accordingly the model describes the release from particles where there is a change in surface area and diameter.

### 3.5 Conclusion

This study showed that a poorly water soluble drug (TA) can be loaded into SA in a higher concentration than aqueous solubility of the drug. The study also showed that the type of pendant group grafted on the polymer has a significant impact on the SA size, surface charge, TA LC and drug release profile. The control of the previously mentioned parameters has significant importance in developing ocular formulations. The solubilisation of TA within the described SA in this work resulted in particles having a diameter of 200-334 nm and positive surface charge (21-46 mV). The positive charge should increase the residence time in the eye through mucoadhesion with the negatively charged cornea, whereas the nano-size should minimise potential vision blurring.

In chapter four the TA-SA formulations prepared in this chapter were tested using an *in-vitro* eye model to assess if the size, surface charge and TA LC and release time influence TA permeation through ocular tissues.

**Chapter Four: The Development of a Porcine *In-Vitro* Eye  
Model for Investigating Potential Ophthalmic Formulation**

---

## 4.1 Introduction

Novel delivery systems such as nanoparticles (Nair, Vidyanand, James & Kumar, 2012), liposomes (Li, Zhuang, Wang, Sui & Pan, 2012), dendrimers (Vandamme & Brobeck, 2005) and polymeric micelles (Di Tommaso *et al.*, 2012) have been explored to enhance the delivery of therapeutic agents to the anterior and posterior eye segments. These delivery systems have in general been assessed using *in-vivo* animal models, despite ethical concerns for animal wellbeing and criticism of the validity and the precision of the animal models (Kirk, 2001). This chapter explores the possibility of developing an *in-vitro* eye model to reduce, refine and replace the number of animals used when developing and testing ocular formulations.

### 4.1.1 Existing *In-Vitro* Eye Models

For many years the *in-vivo* Draize eye test has been the standard method for evaluating the safety of materials which might be in contact with the eye (Kirk, 2001). In recent years, the ethical concerns of animal wellbeing and criticism of the validity and the precision of the test have led many researchers and governments to look for an alternative (Kirk, 2001; Vinardell & Mitjans, 2008). The alternative approaches can be categorised in four groups; *in-vitro* artery perfused eye model, organotypic animal models cell (i.e. isolated animal cornea), culture models and Franz type eye model.

The artery perfused eye model is the closest to the *in-vivo* situation, as the perfusate provides oxygen and vital nutrients necessary to maintain cell viability *ex vivo* (Wilson, Shahidullah & Millar, 1993). Furthermore, the perfusate circulation mimics the blood circulation in the choroidal tissue and hence acts as a dynamic

barrier for the periocular drug delivery route mimicking the *in-vivo* conditions. This model also provides the benefit of instilling the material under study via any of the four drug delivery routes (topical, systemic, periocular and intravitreal). However, this model suffers many draw backs. The perfusion process of the artery/arteries is a technical challenge due to the difficulty in keeping the cannula secured inside the artery (De Coo, Zonnenberg & Trap, 1993). A further problem is monitoring the viability of the cells and the barrier integrity parameters. Additionally, this model also suffers the possibility of having fluctuated arterial perfusion pressure (APP) due to blood vessel occlusions (strokes), air bubbles and collapse of the structural integrity of the blood vessels. This fluctuation in APP affects the secretion of aqueous humour which ultimately affects the intra ocular pressure (IOP) (De Coo, Zonnenberg & Trap, 1993; Koeberle, Hughes, Skellern & Wilson, 2006; Niemeyer, 2001; Wilson, Shahidullah & Millar, 1993). Elevated IOP can result from deterioration or damage to the trabecular meshwork (Koeberle, Hughes, Skellern & Wilson, 2006), affecting inversely the permeability of the drug under study (Cruysberg *et al.*, 2005; Rudnick, Noonan, Geroski, Prausnitz & Edelhauser, 1999).

The organotypic animal tissue models are mainly used as an *in-vitro* toxicological test assessing potential irritants and corrosives (Vinardell & Mitjans, 2008). The most common organotypic animal models are, the isolated rabbit eye (IRE), the isolated chicken eye (ICE), the bovine corneal opacity and permeability (BCOP) and the hen's egg test-chorioallanoic membrane (HET-CAM) (Barile, 2010; Hammer, Richter, Kobuch, Mata & Schweitzer, 2008; Kobuch *et al.*, 2008). The four previously mentioned methods are not considered to be replacements for the Draize eye test. However, they are considered to be screens for the

identification of potential ocular corrosives and irritants in a tiered testing approach. These methods have the disadvantage of maintaining the normal physiological conditions of the cornea in an isolated system for a short time. Also the results from these models typically suffers from an over prediction of human response (Barile, 2010), due to the absence of reflux mechanism and the high dose of test material used. On the other hand, organotypic tissue models are easy to setup, cost effective and avoid unnecessary sacrifice of animals,

Cell culture models are a promising alternative for drug permeability studies and irritancy tests. Despite the difficulties in obtaining natural environmental conditions, many cell culture models of the ocular barriers have been established. In recent years a promising three dimension (3D) cell culture of the whole cornea was constructed (Reichl, Döhring, Bednarz & Müller-Goymann, 2005). The constructed multilayered corneal tissue was built step by step with fibroblast cells embedded in a matrix of collagen cultivated on an underlying layer of endothelial cells covered by corneal epithelial (Reichl, Döhring, Bednarz & Müller-Goymann, 2005). Reichl *et al.* (Reichl, Döhring, Bednarz & Müller-Goymann, 2005) studied the permeability of six drugs in both the human donor cornea and the human cornea construct model. Their results showed similar permeation behaviour in both for all six drugs (Reichl, Döhring, Bednarz & Müller-Goymann, 2005). A 3D human corneal epithelium construct (3D HCEC) model has been studied as an alternative irritancy test by Jung *et al.* (Jung *et al.*, 2011). The latter workers studied 25 reference chemicals with known eye irritancy potential on the 3D HCEC model. The results obtained from the 3D HCEC model had 88% accuracy when compared with the chemical classification for the studied references obtained from the globally harmonised system (GHS). Despite the accuracy this model offers, it has

a few drawbacks. The process of assembling the 3D structure requires time and expertise, it is relatively expensive and it requires certain laboratory settings (i.e. sterility).

An *in vitro* eye model utilising excised tissue in a Franz type diffusion cell provides a simple method, which enables researchers to investigate the permeability of drugs through ocular tissues. This type of *in-vitro* eye model (Franz cells) has been used to test the permeability of many compounds (hydrophilic and hydrophobic) utilising both anterior (cornea) and posterior ocular tissues (mainly sclera) (Araujo, Garcia, Mallandrich, Souto & Calpena, 2012; Mora *et al.*, 2005; Ostacolo *et al.*, 2013; Pescina *et al.*, 2010; Reichl, Döhning, Bednarz & Müller-Goymann, 2005). The Franz type model has the advantages of being well established, cost effective and relatively quick to set up. The model also can be used to study either mono-tissue layer or multi-tissue layers.

#### **4.1.2 Human, Porcine and Rabbit Ocular Tissues**

Porcine ocular tissues are the closest to humans after primate; this is due to the absence of the tapetum layer in porcine eyes, which is present in many other animals such as cows, sheep and rabbits (Prince, 1960). Other similarities are that both human and porcine eyes have a similar retinal pigment epithelium, photoreceptors cells and comparable scleral thickness and water content (Nicoli *et al.*, 2009; Olsen, Aaberg, Geroski & Edelhauser, 1998; Olsen, Sanderson, Feng & Hubbard, 2002). Human, porcine and rabbit scleral tissue vary in thickness. For both human and porcine the sclera tends to have maximum thickness at the posterior pole region decreasing to minimum near the equator and then increasing again towards the limbus, whereas rabbit has maximum thickness at the limbus region decreasing to a minimum thickness near the optic nerve. The reported

mean human sclera thickness was found to be  $0.53 \pm 0.14$  mm at the limbus,  $0.39 \pm 0.17$  mm near the equator and 0.9-1.0 mm near the optic nerve (Olsen, Aaberg, Geroski & Edelhauser, 1998). The reported mean porcine sclera thickness were found to be dependent on the size of the animal, the thickness of large sized pigs were  $1.12 \pm 0.23$  mm at the limbus,  $0.43 \pm 0.16$  mm at its thinnest (6 mm posterior to the limbus),  $0.86 \pm 0.18$  at the equator and approximately 0.9 mm near the optic nerve (Olsen, Sanderson, Feng & Hubbard, 2002). The reported average rabbit sclera thickness at the limbus has been found to be 0.5 mm and 0.2 mm near the optic nerve (Prince, 1960; Tsonis, 2008). Nicoli *et al.* (Nicoli *et al.*, 2009) reported similarity in histology and scanning electron microscope (SEM) images of porcine and human scleral tissues. The rabbit scleral tissue also has a similar extracellular matrix composition to human scleral tissues (Boubriak, Urban, Akhtar, Meek & Bron, 2000; Young, 1985). The water content of human, porcine and rabbit scleral tissues is approximately 70% (Boubriak, Urban, Akhtar, Meek & Bron, 2000; Nicoli *et al.*, 2009).

Human, porcine and rabbit scleral tissues are vascular, opaque tissues consisting of interwoven dense collagen fibre bundles (lamellae) with scattered elastic fibres present between the collagen bundles (Nicoli *et al.*, 2009; Watson & Young, 2004; Young, 1985). Conversely, the cornea is an avascular transparent tissue comprising five layers, where the epithelium and the stroma are the main barrier for drug delivery (section 1.2.1.2).

The horizontal and vertical diameters of adult human, porcine and rabbit corneas are approximately 11.5 and 10.5 mm, 14.9 and 12.4 mm, 13.4 and 13.0 mm, respectively (Bozkir, Bozkir, Dogan, Aycan & Guler, 1997; Faber, Scherfig, Prause & Sorensen, 2008; Willoughby *et al.*, 2010). The corneal thickness of adult

human, porcine and rabbit cornea are approximately 535  $\mu\text{m}$ , 666  $\mu\text{m}$  and 407  $\mu\text{m}$ , respectively (Chan, Payor & Holden, 1983; Doughty & Zaman, 2000; Faber, Scherfig, Prause & Sorensen, 2008).

The analytical methods used in this chapter were HPLC, fluorescence spectroscopy and liquid scintillation counting (fluorescence spectroscopy and HPLC are explained in chapter three sections 3.1.2 and 3.1.4, respectively).

### 4.1.3 Liquid Scintillation Counting

Liquid scintillation counting (LSC) is a widely used method in the biological sciences for measuring  $\beta$ -emitting radioactive isotopes such as tritium and carbon-14. In the LSC procedure the radioactive sample is mixed with compounds in solution (liquid scintillation cocktails), these compounds (phosphors or scintillators) are capable of absorbing the emitted energy from the  $\beta$ -emitting radioactive and re-emitting the energy as light. The re-emitted light is then detected by a photomultiplier tube, which converts the photons to an electrical signal. The intensity of the re-emitted light corresponds to the emission energy of  $\beta$ -emitting isotope and the number of re-emitted light photons per second corresponds to the number of radioactive emissions (disintegrations per minute (DPM)) (Glick, 2009). The SI unit for radiation is Becquerel (Bq), which corresponds to 60 DPM.

## 4.2 Aims and Objectives

In this study, the aims were to develop, and partially validate an *in-vitro* porcine eye model in order to test the permeability of hydrophobic and hydrophilic penetrants from solutions, suspensions or polymeric formulations (TA-SA's) across ocular tissues using the developed model. As such the objectives were:

- To develop an *in-vitro* porcine eye model

- To partially validate the developed eye model
- To evaluate and compare tissue barrier integrity of fresh and stored porcine ocular tissues using tritiated water as a rapid and inexpensive method, in order to use stored tissues as an alternative practical and more convenient option to using fresh tissues
- To compare the permeability of four markers across porcine corneal and scleral tissues with permeability across human counterpart tissue
- To study and compare the permeability of human, porcine and rabbit corneal tissues, in order to evaluate differences or similarities in corneal permeation between the three species
- To assess TA permeation through posterior porcine ocular tissues (sclera, choroid and retina) and human scleral tissue from the TA self-assemblies (TA-SA) developed in chapter three and a TA suspension
- To study the effect of potential permeation enhancers on marker permeation across human and porcine corneal and scleral tissues

### **4.3 Materials and Methods**

#### **4.3.1 Materials**

Fluorescein sodium salt (MW 376.27), fluorescein isothiocyanate–Dextran (FITC-Dextran) average MW 3-5 kDa, FITC-Dextran average MW 10 kDa, FITC-Dextran average MW 20 kDa, tris(hydroxymethyl)aminomethane, tween 80, L-glutamic acid, chitosan (low MW), poly(vinylpyrrolidone)–iodine complex, minimum essential medium eagle (Earle’s salts, 25 mM HEPES and sodium bicarbonate,

without L-glutamine, Sigma M7278), antibiotic antimycotic solution (10,000 units penicillin, 10 mg streptomycin and 25 µg amphotericin B per mL, Sigma A5955), fetal bovine serum (Sigma F0804), penicillin-streptomycin (10,000 units penicillin and 10 mg streptomycin per mL in 0.9% NaCl, Sigma P0781) and dextran from leuconostoc spp average Mw 500 kDa were all purchased from Sigma Aldrich, United Kingdom. Phosphate buffer saline (PBS) tablets, soluene, scintillation cocktail high performance (ScintiSafe 2), sodium chloride, potassium chloride, sodium phosphate dibasic, sodium dihydrogen phosphate monohydrate, calcium chloride, magnesium sulphate, glucose, ethanol, acetonitrile, acetic acid and all solvents (HPLC grade) were acquired from Fisher, United Kingdom. Triamcinolone Acetonide micronized powder (TA) was purchased from Fagron, United Kingdom. Tritiated water ( $^3\text{H}_2\text{O}$ ) was purchased from GE Healthcare, United Kingdom at a specific activity of 37 MBq mL<sup>-1</sup>.

### 4.3.2 Franz Cells Setup

Ocular tissue (human, porcine and rabbit cornea; human and porcine sclera; posterior porcine ocular tissues) was positioned between the two compartments of a Franz cell with the corneal epithelium or the episclera (the outer layer of the sclera) facing the donor compartment as shown in Figure 4.1. The two compartments were wrapped with parafilm<sup>®</sup> and clamped together. A small magnetic stirrer was inserted into the receptor compartment of the Franz cell which was then filled with an appropriate receiver fluid (RF, section 4.4.3.1) suitable for the experiment (i.e. PBS). The Franz cells were then placed in a water bath maintained at either 37 °C (to mimic the *in-vivo* temperature of the eye) or at 45 °C (to study the effect of elevated temperature on permeation) for 15 min to

equilibrate. The donor solution (1 mL of TA suspension/marker solution or 0.1 mL  $^3\text{H}_2\text{O}$ ) was added into the donor compartment before sealing with parafilm<sup>®</sup>.

At pre-determined time points, the receiver fluid was mixed, manually three times using a sampling syringe, prior to the withdrawal of sample aliquots (0.3 mL for permeation and enhancer studies or 0.1 mL for  $^3\text{H}_2\text{O}$  study). Instantly after sampling, the receiver fluid was replenished with pre-warmed receiver fluid. Samples were analysed using HPLC (Triamcinolone Acetonide), a fluorescence microplate reader (fluorescein sodium salt, 4, 10 and 20 kDa FITC-Dextran) or liquid scintillation counting ( $^3\text{H}_2\text{O}$ ).

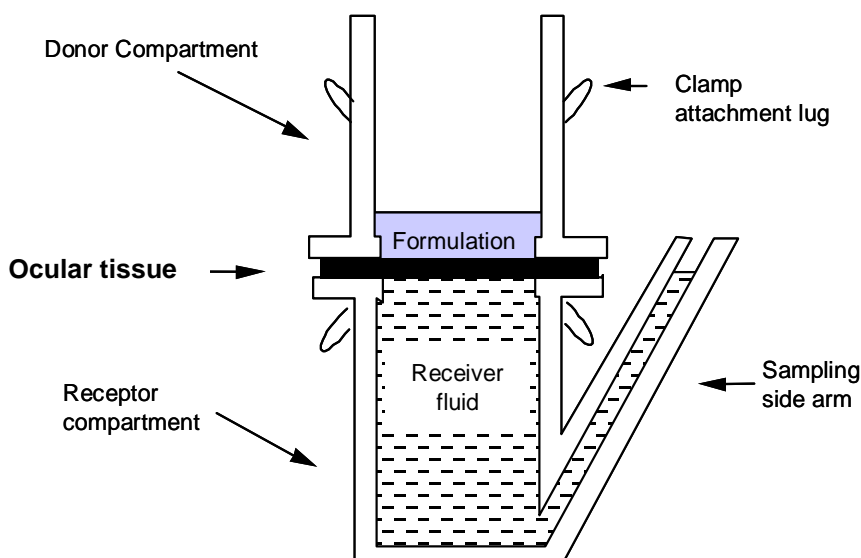


**Figure 4.1:** Schematic representation of Franz cell set-up.

#### 4.3.2.1 Franz Cell Size

The limited availability of human and rabbit ocular tissues required performing experiments on as little tissue as possible, especially corneas. The different areas of the tissue exposed to the donor solutions were investigated using large, medium and small Franz cells having an approximate aperture area of 0.9, 0.6 and 0.1  $\text{cm}^{-2}$ , respectively. The receptor compartment volume of the large, medium and small size cells were approximately 3, 2.6 and 1 mL, respectively.

The large and medium Franz cells were used in studying the posterior ocular tissues, whereas the medium and small cells were used in studying the corneal tissue. Each Franz cell were individually calibrated for volume and diameter in triplicate.

### **4.3.3 Ocular Tissues Preparation and Storage**

#### **4.3.3.1 Porcine Tissue Preparation**

Scoped out porcine eyes were freshly collected from a local farm (Evans and Sons, Bedfordshire). The eye globes were immersed in a 0.9% saline solution within 2 h of slaughter and upon arrival at the laboratory, all extraocular tissues attached to the sclera were removed using surgical scissors and tweezers. The cornea was excised from the globe by carving a small incision using a scalpel approximately 1-3 mm away from the pars plana (the sclera-cornea intersection); a circumferentially cut separated the cornea from the eye globe. This was followed by complete separation of the cornea from the pars plana using a 7 mm radius cork borer. The separated corneas were transferred into PBS buffer (10 mM) after which they were either used immediately or stored as described in section 4.3.3.2.

The lens capsule and vitreous humour were gently separated from the retinal tissue. A straight cut through the equator of the globe was made towards the optic nerve, cutting the eye globe in half. A maximal area where the three posterior tissues remain intact (sclera, choroid and retina) were excised approximately 1-3 mm from the optic nerve. To obtain bare sclera, the intraocular tissues were removed, including retina and choroid tissues. The prepared tissues were kept moist by placing in PBS buffer (10 mM) awaiting mounting onto Franz cells or stored as described in follow section 4.3.3.2.

#### 4.3.3.2 Porcine Tissue Storage

The scleral cuts were gently dried using tissue paper and wrapped in aluminium foil before storing in a freezer at - 20 °C for two weeks.

The storage and de-swelling of the fresh porcine corneas was performed in accordance with the Moorfields Eye Hospital standard operating procedure – organ culture storage of corneas (Appendix B). The porcine corneal buttons (dissected corneas) were transferred from the PBS solution immediately after tissue preparation (Section 4.3.3.1) into 5% poly(vinylpyrrolidone) iodine complex solution (w/v) and left to soak for 5 min. The corneas were then transferred into a sterile saline 0.9% solution and immersed for 5 min, before submerging into 0.5% penicillin-streptomycin solution for 5 min. The corneal storage medium was prepared by adding 0.5% (v/v) antibiotic antimycotic solution and 5% (v/v) fetal bovine serum to minimum essential medium eagle. The sterilised corneas were stored in 50 mL corneal storage medium (two corneas per 50 mL) at 31 °C in an oven for either 4 or 11 d. The corneal storage medium was changed every 2-3 d for the duration of the storage. Nevertheless such corneal storage for between 4 or 11 d resulted in an increase in the thickness of the cornea (swelling). As such a corneal de-swelling medium was made by the addition of 5% 500 kDa dextran (w/v) to the corneal storage medium. The 4 and 11 d stored corneas were then transferred into 50 mL of the de-swelling medium (two corneas per 50 mL) before storing in the dark at room temperature for further 3 d. As the 4 and 11 d stored corneas were de-swelled for 3 d they are referred to as one and two weeks stored corneas, respectively.

An alternative method of porcine corneal storage was also investigated, in which sterilised corneas were stored in sterile PBS buffer at - 80 °C for one month.

#### **4.3.3.3 Human Corneal Tissue Preparation**

The human cadaver corneal-scleral tissues were obtained from Moorfields eye hospital and Manchester royal eye hospital; the tissue was transferred and stored in CorneaJet<sup>®</sup> de-swelling medium at room temperature. The human corneal-scleral tissues were removed from the de-swelling medium and placed on a Petri dish, with the corneal epithelium layer facing upward. Visual inspection of the tissue integrity was performed before aligning a 7 mm radius cork borer at the circumference of the cornea. Continuous pressure and twisting movement was applied until the corneal tissue was separated from the pars plana region. The dissected corneas were immediately immersed in PBS buffer whilst waiting to be mounted onto Franz cells.

#### **4.3.3.4 Human Scleral Tissue Preparation**

The human cadaver globes were obtained from Moorfields eye hospital and Manchester royal eye hospital; the tissue was transferred and stored in 70% ethanol at room temperature. The human globes were then removed from the preserving medium to a Petri dish. Visual inspection of the outer sclera was performed followed by removal of the detached choroidal-retinal tissues using forceps. A 7 mm radius cork borer was inserted inside the eye globe through the corneal aperture. A continuous pressure and twisting movement were applied to obtain four scleral punches; three punches were taken from a semi consecutive arc 1-2 mm away from the optic nerve, and a fourth punch was taken as close as possible to the formed arc.

#### **4.3.3.5 Human and Rabbit Corneal Tissue Preparation**

The human and rabbit corneal tissues were a gift from MedPharm, United Kingdom. The corneal tissue was transferred in Optisol GS de-swelling medium

and stored at 4 °C in a fridge. Both tissues were prepared similar to human cornea as described in section 4.3.3.3. The dissected corneas were divided into four quarters and immediately immersed in PBS buffer whilst waiting to be mounted onto small Franz cells.

#### **4.3.4 Thickness Measurement of Posterior Porcine Ocular**

##### **Tissues**

The thickness of the posterior porcine ocular tissue was measured using a micrometre (MITUTOYO, Japan). The middle of the measured tissue was placed on top of the bottom micrometre plate (anvil) before carefully lowering the spindle of the micrometre; the readings were recorded at the first sign of resistance observed in the ratchet knob. The reported thickness was an average of triplicate measurements around the middle of the tissue.

#### **4.3.5 Development of Suitable Receiver Fluids**

Although it is desirable to have a receiver fluid which mimic the physiological condition of the eye, it is also crucial to ensure that the chosen receiver fluid has no effect on the stability of the drug over the duration of the experiment, the tissue barrier integrity or the actual amount of drug permeating through the tissue during the experiment. Due to the very low solubility of TA in modified Dulbecco's buffer solution ( $13.7 \pm 0.5 \mu\text{g mL}^{-1}$  at room temperature approximately 22 °C), receiver fluids with 0, 5, 10 and 30% (v/v) ethanol were investigated, in order to maintain sink conditions (drug concentration in the receiver compartment of Franz cell not to exceed 10% of the drug solubility in the receiver fluid (Aulton & Cooper, 1988)) over the duration of the experiment. The modified Dulbecco's buffer solution consisted of  $\text{MgSO}_4$  ( $89 \text{ mg L}^{-1}$ ) and glucose

(9008 mg L<sup>-1</sup>) added to Dulbecco's buffer solution ((NaCl (8000 mg L<sup>-1</sup>), KCl (200 mg L<sup>-1</sup>), Na<sub>2</sub>HPO<sub>4</sub> (1150 mg L<sup>-1</sup>), NaH<sub>2</sub>PO<sub>4</sub> (200 mg L<sup>-1</sup>), CaCl<sub>2</sub> (111 mg L<sup>-1</sup>)).

The considerable swelling of the corneal tissues over the period of 24 h in PBS buffer solution required the use of a de-swelling medium for performing longer duration experiments. Both PBS buffer solution and 5% 500 kDa dextran (w/v) in PBS were used as receiver fluid for testing the permeation through porcine corneal tissues.

#### **4.3.6 TA and Marker Stability in Receiver Fluids**

The stability of TA in 30% ethanol receiver fluid was studied by incubating three concentrations (10, 30 and 50 µg mL<sup>-1</sup>) at 4 °C and room temperature for two weeks and at 45 °C for two days. The stability of the fluorescein sodium salt (FSS) and FITC-dextran in PBS solution and 5% (w/v) 500 kDa dextran was evaluated for three standards concentrations (low, medium and high) at -20 °C, 4 °C and at room temperature (in the dark) for two weeks. Similarly, the stability of the FSS and FITC-dextran in PBS and 5% 500 kDa dextran was evaluated at 45 °C (in the dark) for two days.

The stabilities of the analytes were determined by comparing the measured concentration after incubation to the original control concentration and expressed as recovery percentage of the initial concentration. All measurements were performed in quadruplicate.

#### **4.3.7 Tritiated Water Studies**

The <sup>3</sup>H<sub>2</sub>O studies were investigated as a measure of tissue barrier integrity and as a potential way of normalising the drug permeation data as an alternative to using tissue thickness.

Ocular tissue was mounted on to Franz diffusion cells as previously described in section 4.3.2. The receptor compartment was filled with de-ionised water, whereas the donor chamber was dosed with 100  $\mu\text{L}$  of  $^3\text{H}_2\text{O}$  (14.8 kBq). The Franz cells were then placed in a water bath maintained at 37 °C. Sample aliquots (0.1 mL  $^3\text{H}_2\text{O}$ ) were withdrawn at pre-determined time after the receiver fluid was mixed. Instantly after sampling, the receiver fluid was replenished with pre-warmed de-ionised water. The surface of the ocular tissues and both the donor and receptor compartments of the Franz cells were washed five times with de-ionised water after the  $^3\text{H}_2\text{O}$  diffusion experiment and prior to the start of TA or FSS permeation studies.

#### **4.3.8 Tritiated Water Correlation with TA and FSS**

The permeation of TA and FSS were conducted as described in sections 4.3.10.1 and 4.3.9 after the completion of the  $^3\text{H}_2\text{O}$  study as described in the previous section (section 4.3.7). The percentage of the permeated  $^3\text{H}_2\text{O}$  at 15 min (% applied dose) was plotted against the flux rate of the permeated TA or FSS and the correlation was expressed using Pearson correlation coefficient (r).

#### **4.3.9 Marker Permeation Studies**

The donor solutions of the four markers used in the corneal and scleral (human and porcine) marker permeation studies were composed of 5 mg of FSS, 50 mg of 4 kDa FITC-dextran, 100 mg of 10 kDa FITC-dextran and 200 mg of 20 kDa FITC-dextran in 1 ml of PBS buffer (10 mM, pH 7.4). PBS buffer (10 mM, pH 7.4) was used as the receiver fluid. The donor solution used in the FSS porcine scleral permeation correlated to the  $^3\text{H}_2\text{O}$  permeation at 15 min was composed of

1 mg of FSS in 1 mL of PBS buffer (10 mM, pH 7.4). All marker permeation studies were performed at 37 °C.

### 4.3.10 TA Permeation Studies

#### 4.3.10.1 TA Permeation Study across Posterior Porcine Ocular Tissues

The permeation of TA from a range of donor vehicles (shown in Table 4-1) was determined in order to investigate the effect of ethanol and polymeric SA on TA permeation across posterior porcine ocular tissues. The TA permeation study was performed at 37 °C using 0, 5, 10 and 30% ethanol receiver fluids.

**Table 4-1:** The TA donor vehicles used in permeation studies.

TA Vehicle	TA Concentration ( $\mu\text{g mL}^{-1}$ )	Solution/Suspension Composition
TA	500	ethanol: water mixture (50: 50 v/v)
TA	500	water
Pa <sub>5</sub>	450	Water (5 mg mL <sup>-1</sup> polymer)
Pa <sub>5</sub> <sup>-</sup>	450	Water (5 mg mL <sup>-1</sup> polymer)
Ch <sub>5</sub>	450	Water (5 mg mL <sup>-1</sup> polymer)
Da <sub>10</sub>	450	Water (5 mg mL <sup>-1</sup> polymer)

#### 4.3.10.2 TA Permeation Study through Human Scleral Tissue

The donor solution for the TA permeation study using human scleral tissue was composed of Da<sub>10</sub> polymeric self-assembled formulation (1 mg L<sup>-1</sup> TA) and aqueous TA suspension (1 mg mL<sup>-1</sup>). Tris buffer (10 mM) was used as a receiver fluid in this experiment as Da<sub>10</sub> precipitate in PBS buffer. The TA permeation study was performed at 37 °C.

### 4.3.11 Permeation Enhancer Studies

The donor solution for the potential permeation enhancer studies were composed of 10 kDa FITC-Dextran (100 mg) or FSS (5 mg) dissolved in one of the following solutions:

- 1) 0.1% L-glutamic acid in 1 mL PBS buffer solution (10 mM)
- 2) 0.001% tween 80 in 1 mL PBS buffer solution (10 mM)
- 3) 0.01% tween 80 in 1 mL PBS buffer solution (10 mM)
- 4) 5% w/v Pa<sub>5</sub> polymer in 1 mL tris buffer solution (10 mM, pH 7.4)
- 5) 1 mL acetate buffer (0.1 M, pH 5)
- 6) 0.5% (w/v) chitosan in 1 mL acetate buffer solution (0.1 M, pH 5)

The donor solutions of the controls consisted of 10 kDa FITC-Dextran (100 mg) or FSS (5 mg) in 1 mL PBS buffer solution (10 mM, pH 7.4). All the chemical permeation enhancer studies were performed at 37 °C. The effect of elevated temperature (45 °C) was studied as a potential permeation enhancer by replicating the donor and receiver fluids of the controls in a second experiment conducted at 45 °C. The receiver fluid for all Franz cells in the this study consisted of 10 mM PBS buffer, except the Pa<sub>5</sub> experiment in which the receiver fluid consisted of 10 mM tris buffer (Pa<sub>5</sub> precipitate in PBS buffer).

### 4.3.12 Analytical Methods

The analytical methods used in assessing the ocular tissue permeability and integrity were HPLC, fluorescence microplate reader and liquid scintillation counting.

#### **4.3.12.1 HPLC Analytical Method**

The TA content in the receiver fluids was determined using a fit for purpose validated *in-vitro* TA release HPLC method (Chapter three, section 3.3.4). None of the biological matrices or chemical materials used in this study interfered with the HPLC assay.

#### **4.3.12.2 Fluorescence Analysis Method**

Samples containing FSS and FITC-dextran were diluted accordingly with PBS to fit within the range of the corresponding calibration curve. The range of the calibration curves of the four markers are shown in Table 4-2 (Section 4.4.1). Diluted samples were analysed using a fluorescence microplate reader (BMG LABTECH, United Kingdom). The excitation and emission wavelengths were 485 and 520 nm, respectively. Calibration graphs were constructed from known standard concentrations of each marker, and the linearity, limit of detection and limit of quantification were determined as previously explained in chapter three (section 3.2.5.6). Corneal and scleral tissues were incubated with PBS to examine the fluorescence of the tissues at 485 nm and to check for interference with the markers. None of the biological matrices or chemical materials used in this study interfered with the fluorescence assay.

#### **4.3.12.3 Liquid Scintillation Counter Method**

Receiver fluid samples (0.1 mL) from the  $^3\text{H}_2\text{O}$  experiments were transferred to scintillation vials to which 4 mL of liquid scintillation cocktail (ScintiSafe 2) was added. The scintillation vials were sealed and the contents mixed by vortexing before analysis using an LS 6500 multipurpose liquid scintillation counter (Beckman Coulter<sup>TM</sup>, Buckinghamshire, United Kingdom).

### 4.3.13 Permeation Parameters

The cumulative amount of TA or marker compounds ( $Q_t$ ) permeated through the scleral and corneal tissues per unit area was calculated, at each time point, from the TA and marker concentrations in the receiver fluids. The flux ( $J$ ,  $\mu\text{g}\cdot\text{cm}^{-2}\cdot\text{h}^{-1}$ ) across the ocular tissues was calculated by plotting the cumulative amount per  $\text{cm}^2$  of TA or markers that permeated through the tissue against time and determining the slope of the regression line at steady state. The permeability coefficient ( $k_p$ ,  $\text{cm}\cdot\text{h}^{-1}$ , Equation 4.1) at steady state was calculated by dividing the flux ( $J$ ) by the initial concentration ( $C_0$ ) in the donor solution:

$$\text{Permeability coefficient } (k_p) = \frac{\text{Flux } (J)}{C_0} \quad \text{Equation 4.1}$$

### 4.3.14 Statistical Evaluation

All statistical analysis was performed using SPSS program version 20. The normality and the homogeneity of variances of the data were assessed using Shapiro-Wilk and Levene's tests, respectively. Experimental differences between groups were compared with each other or with controls using the independent student's  $t$ -test or analysis of variance (one way ANOVA). Differences were regarded as significant, with  $p \leq 0.05$ . The correlation between tritiated water percentage permeation at 15 min and TA, FSS flux and porcine posterior ocular tissue thickness were calculated using the Pearson test, a correlation was regarded as significant, with  $p < 0.01$ .

## 4.4 Results

### 4.4.1 Analytical Methods

The TA solubility in the 0, 5, 10 and 30% (v/v) ethanol receiver fluids were  $13.7 \pm 0.5$ ,  $23.5 \pm 1.2$ ,  $29.9 \pm 1.9$  and  $243.3 \pm 14.6 \mu\text{g mL}^{-1}$  ( $n = 5$ , measurements were performed at room temperature at approximately 22 °C), respectively. The summary of the validation values for the markers analytical fluorescence assays are show in Table 4-2. All analytical methods were partially validated similar to section 3.2.5.6 (data not shown) and was found to be fit for purpose to determine the concentration of markers understudy.

**Table 4-2:** Parameters of FSS and FITC-dextran calibration graphs.

Parameter	Fluorescein Sodium Salt	4 kDa FITC-dextran	10 kDa FITC-dextran	20 kDa FITC-dextran
Range ( $\mu\text{g mL}^{-1}$ )	0.0047 - 0.37	0.5 - 32	0.31 - 12.5	0.16 - 10.0
Linearity ( $R^2$ )	0.99	0.99	0.99	0.99
L.D ( $\mu\text{g mL}^{-1}$ )	0.05	2.20	1.27	0.86
L.Q ( $\mu\text{g mL}^{-1}$ )	0.14	6.68	3.85	2.59

### 4.4.2 Porcine Ocular Tissue Thickness

The thickness of fresh corneal tissues increased significantly ( $t$ -test,  $p < 0.05$ ) after 24 h in PBS buffer from  $0.60 \pm 0.04$  mm ( $n = 6$ ) at  $t = 0$  h to  $1.35 \pm 0.21$  mm at  $t = 24$  h (37 °C). Following de-swelling treatment the corneas then had a mean thickness of  $0.76 \pm 0.09$  mm ( $n = 8$ ) which was significantly different ( $t$ -test,  $p < 0.05$ ) from the thickness of fresh corneal tissue ( $t = 0$  h). On the other hand, the thickness of scleral, choroidal and retinal tissues (will be referred to as posterior tissues) did not change significantly ( $t$ -test,  $p > 0.05$ ) after 28 h in 0% ethanol receiver fluid. The average thickness of the fresh posterior tissues was 0.8

$\pm 0.13$  mm (n = 11), whereas the average thickness after 28 h was  $0.9$  mm  $\pm 0.18$  mm (n = 11).

### 4.4.3 *In-Vitro* Porcine Eye Model Development

#### 4.4.3.1 Development of Suitable Receiver Fluids

Receiver fluids with 0, 5, 10 and 30% ethanol in modified Dulbecco's buffer solution were investigated, with a view to maintaining sink conditions over the duration of the experiment. The cumulative permeation profiles of TA across porcine posterior tissues from an aqueous TA suspension ( $500 \mu\text{g mL}^{-1}$ ) using four receiver fluids are shown in Figure 4.2. The flux for TA was significantly higher ( $2.1 \mu\text{g. cm}^{-2}.\text{h}^{-1}$ ) when using 30% v/v ethanol as the receiver fluid compared to all the others investigated (0.5 and 10% v/v ethanol;  $0.7 \mu\text{g. cm}^{-2}.\text{h}^{-1}$ ).

The enhancing effect of ethanol on the TA permeation was confirmed using TA solution (ethanol: water (50: 50),  $500 \mu\text{g mL}^{-1}$ ) in the donor compartment (Figure 4.3) which produced a TA flux statistically comparable (one way ANOVA,  $p > 0.05$ ) to the TA flux of the TA suspension using 30% (v/v) ethanol as R.F (Figure 4.2) despite having lower ethanol percentages in the receiver fluids (0, 5 and 10%).

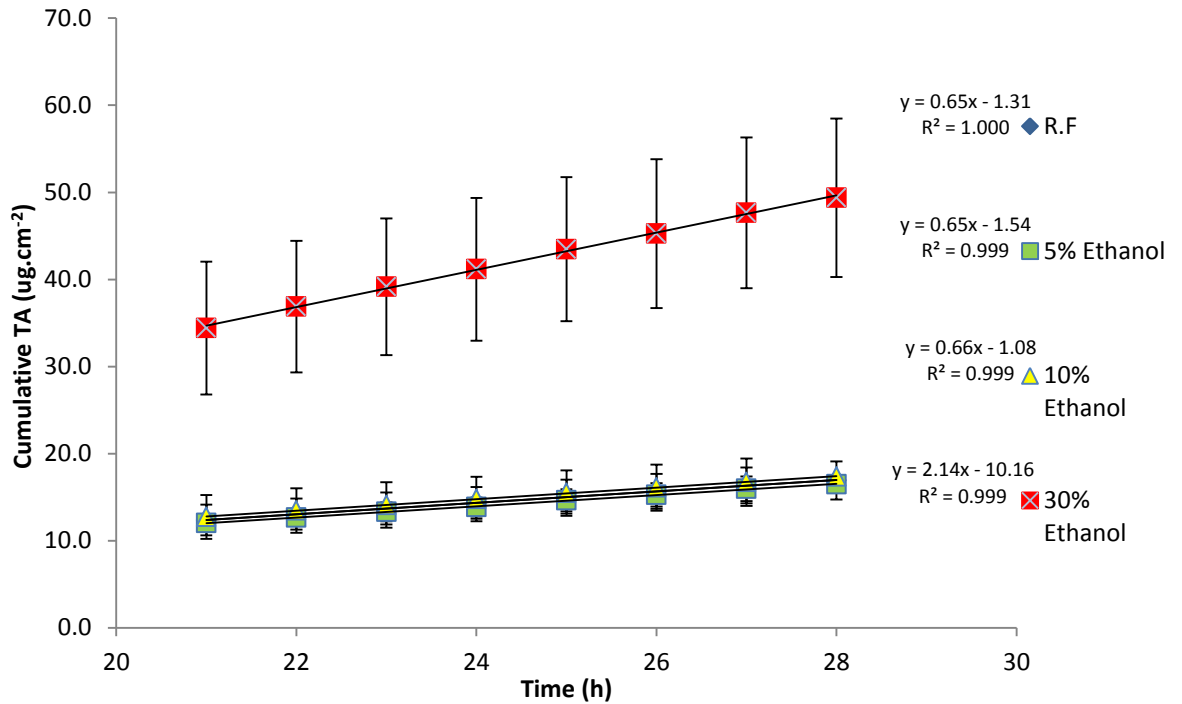


**Figure 4.2:** TA permeation profiles from TA suspension (donor solution,  $500 \mu\text{g mL}^{-1}$ ) across posterior porcine ocular tissues using 0, 5, 10 and 30 v/v % ethanol receiver fluids (Data represented as mean, error bars represented as S.D.,  $n = 6$ ).

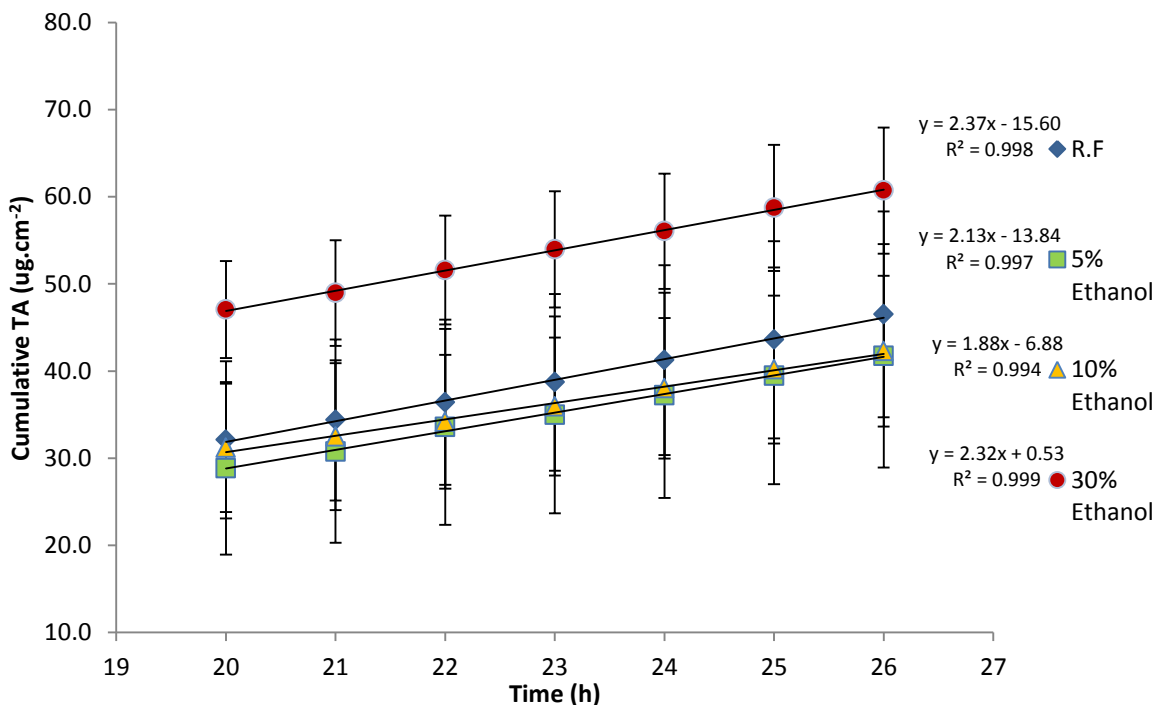


**Figure 4.3:** TA permeation profiles from TA solution (ethanol: water (50: 50),  $500 \mu\text{g mL}^{-1}$ ) across posterior porcine ocular tissues using 0, 5, 10 and 30% ethanol receiver fluids (Data represented as mean, error bars represented as S.D.,  $n = 6$ ).

The suitability of two receiver fluids (PBS and 5% 500 kDa dextran in PBS) for marker permeation across corneal tissues were investigated using fluorescein sodium salt as shown in Figure 4.4. The flux rates of fluorescent sodium salt in either receiver fluid were not significantly different (*t*-test,  $p > 0.05$ ).

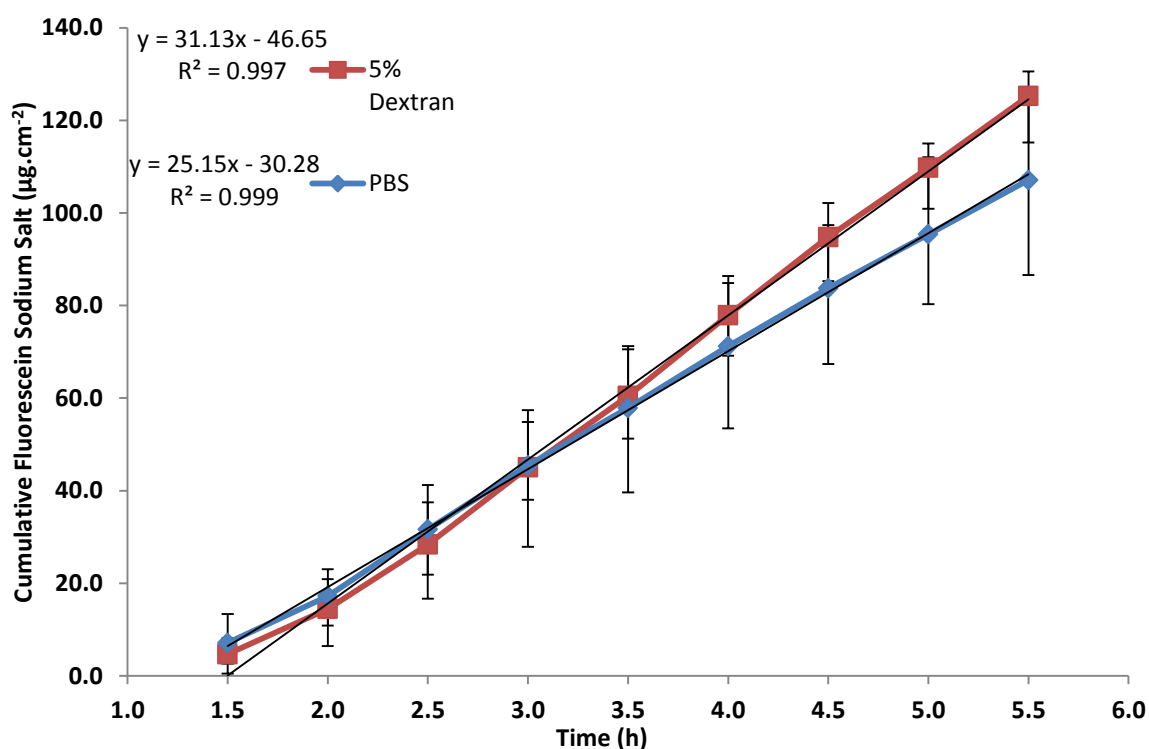


**Figure 4.4:** Fluorescein sodium salt ( $5 \text{ mg mL}^{-1}$ ) permeation profiles through one week stored porcine corneal tissues using PBS and 5% 500 kDa Dextran in PBS as receiver fluids. (Data represented as mean, error bars represent range,  $n = 4$ )

#### 4.4.3.2 TA and Marker Stability in Receiver Fluid

The 30% ethanol (v/v), PBS and the 5% 500 kDa dextran (w/v) receiver fluids showed no influence on the stability of TA nor the markers over two weeks and no interference with the analytical methods. Also, both TA and the markers were stable at  $45 \text{ }^\circ\text{C}$  for two days.

#### 4.4.4 Partial Validation of the In-Vitro Porcine Eye Model

##### 4.4.4.1 Franz Cell Size Effect

Due to the limited availability of the corneal tissue and the continual variation in the scleral tissue thickness (Olsen, Aaberg, Geroski & Edelhauser, 1998; Olsen, Sanderson, Feng & Hubbard, 2002), different size Franz cells were used in investigating the permeability of ocular tissues. The flux of FSS through two week stored corneas using medium and small cells (Figure 4.5) resulted in no significant difference (*t*-test,  $p > 0.05$ ) in the values obtained between the two cells. Similarly, there was no significant difference (*t*-test,  $p > 0.05$ ) between the flux of the TA from the TA suspension using large and medium cells (Figure 4.6).

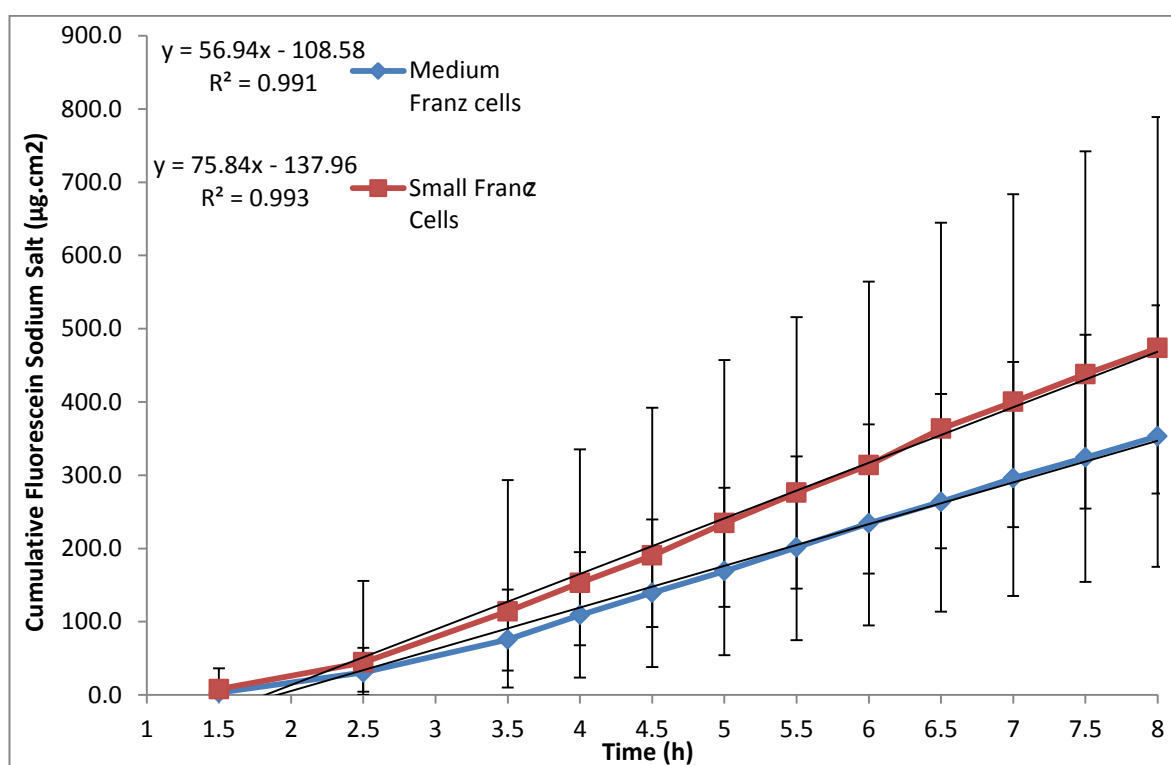


**Figure 4.5:** Fluorescein sodium salt ( $5 \text{ mg mL}^{-1}$ ) permeation profiles through two week stored porcine corneal tissues using 5% (w/v) 500 kDa Dextran as receiver fluids. (Data represented as mean, error bars represent range,  $n = 4$ ).

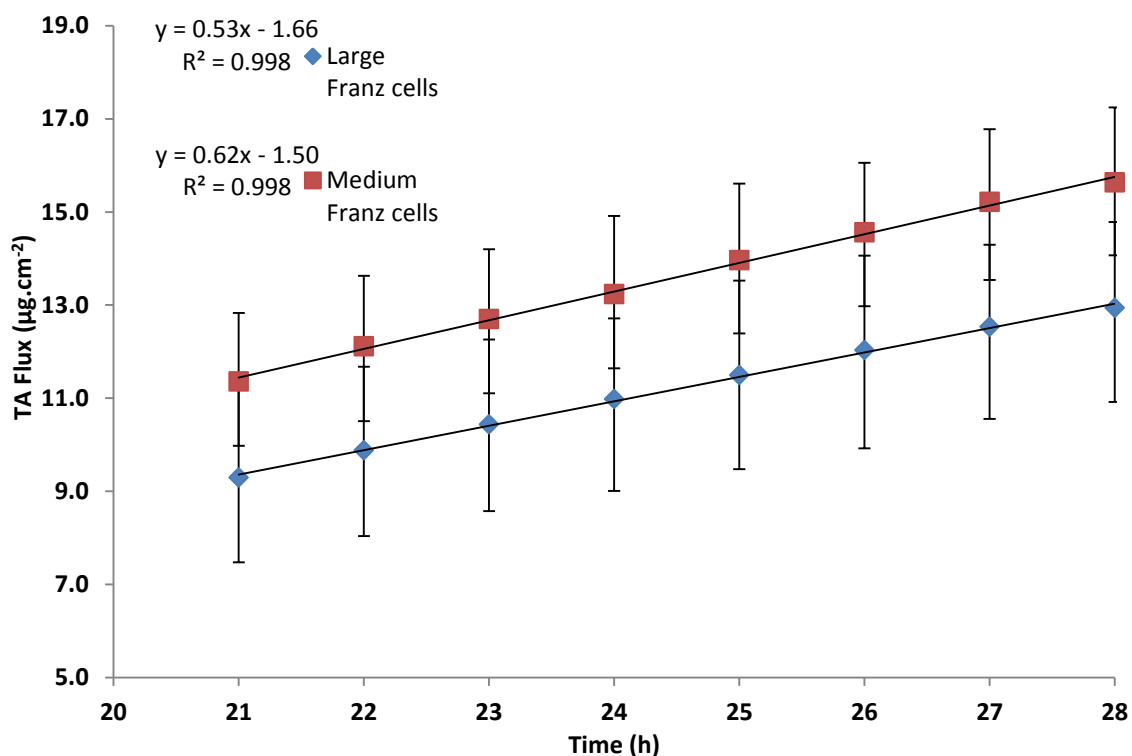


**Figure 4.6:** TA suspension ( $500 \mu\text{g mL}^{-1}$ ) permeation profiles through posterior porcine ocular tissues using 5% (v/v) ethanol as receiver fluids (Data represented as mean, error bars represent range,  $n = 4$ ).

#### 4.4.4.2 Ocular Tissue Integrity

##### 4.4.4.2.1 Tritiated Water Permeation

Tritiated water permeation across porcine posterior tissues was measured at 15, 30, 45 and 60 min (Figure 4.7) with the percentage of the applied  $^3\text{H}_2\text{O}$  permeating after 60 min being  $51.1 \pm 11.9\%$  ( $n = 14$ ). Conversely, the  $^3\text{H}_2\text{O}$  permeates at a slower rate through porcine corneal tissues (Figure 4.7); the percentage of  $^3\text{H}_2\text{O}$  after 60 min was  $17.4 \pm 3.0\%$  ( $n = 9$ ).

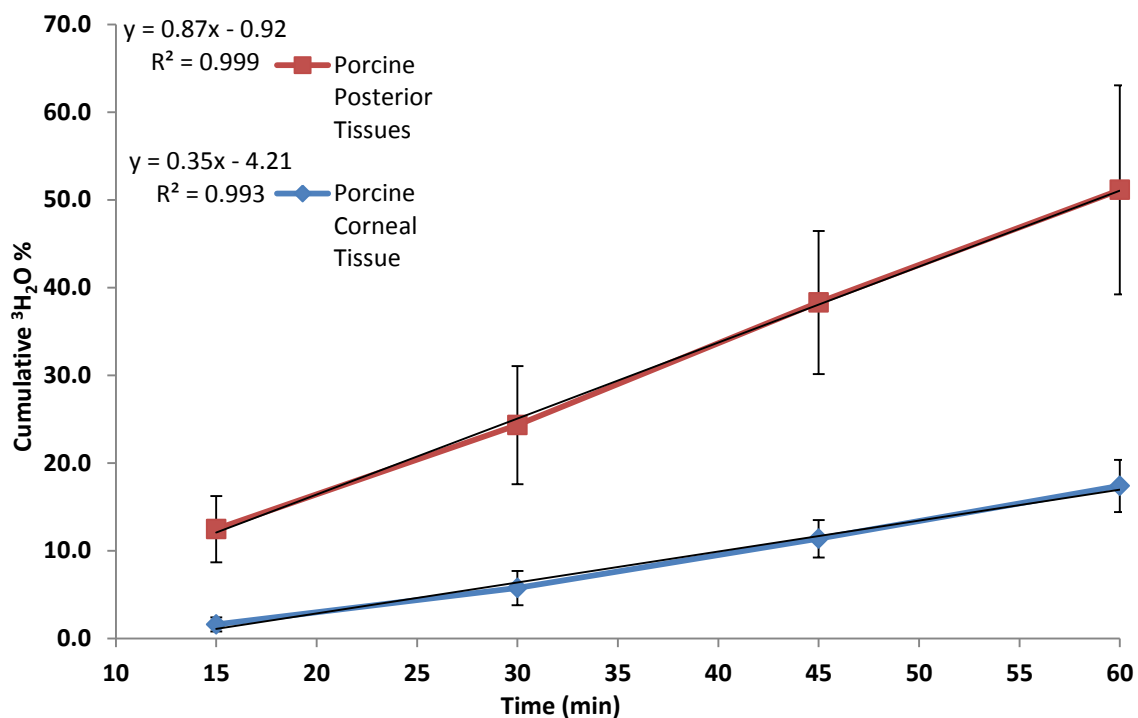


**Figure 4.7:**  $^3\text{H}_2\text{O}$  permeation profiles across porcine posterior tissues (n=14) and corneal tissue (n=9) (Data represented as mean, error bars represent S.D.).

The percentage of the applied  $^3\text{H}_2\text{O}$  permeating across porcine corneal and posterior tissues after 15 minutes was compared for fresh and stored (- 20 °C, two weeks) tissues and no significant difference (*t*-test,  $p > 0.05$ ) was found (Table 4-3 & Table 4-4).

Chapter 4: The Development of a Porcine *In-Vitro* Eye Model for Investigating Potential Ophthalmic Formulations

**Table 4-3:**  $^3\text{H}_2\text{O}\%$  permeating at 15 minutes through fresh and frozen posterior porcine ocular tissues.

	Fresh posterior Tissue	Frozen posterior Tissue
Tissue ID	$^3\text{H}_2\text{O}\%$ (15 min)	
Tissue1	5.0	7.7
Tissue2	12.9	12.1
Tissue3	15.4	6.7
Tissue4	14.8	9.2
Tissue5	7.5	12.7
Tissue6	21.5	16.5
Tissue7	19.3	17.0
Tissue8	5.9	12.0
Tissue9	11.5	13.6
Tissue10	22.8	11.1
Tissue11	15.0	9.1
Tissue12	8.6	7.2
Mean $\pm$ S.D.	13.4 $\pm$ 5.9	11.2 $\pm$ 3.4

**Table 4-4:**  $^3\text{H}_2\text{O}\%$  permeating at 15 minutes through fresh and one week stored porcine corneal tissues.

	Fresh Cornea	Stored Cornea
Tissue ID	$^3\text{H}_2\text{O}\%$ (15 min)	
Tissue1	1.3	1.1
Tissue2	1.9	0.8
Tissue3	1.6	1.0
Tissue4	2.1	1.7
Tissue5	2.8	1.8
Tissue6	1.7	0.7
Tissue7	2.1	3.2
Tissue8	1.8	2.2
Tissue9	3.0	2.0
Mean $\pm$ S.D.	2.0 $\pm$ 0.6	1.6 $\pm$ 0.8

#### 4.4.4.2.2 TA and FSS Permeation across Fresh and Stored Tissues

The barrier integrity in both fresh and frozen (- 20 °C, two weeks) posterior porcine ocular tissues was compared, the TA fluxes are shown in Table 4-5. The TA flux did not change significantly (*t*-test,  $p > 0.05$ ) between the two tissues. On the other hand the FSS flux rates through fresh and stored corneas increased significantly (*t*-test,  $p < 0.05$ ) and were dependent on the storage time and conditions as illustrated by Figure 4.8.

**Table 4-5:** TA flux through fresh and frozen posterior porcine ocular tissues.

	Fresh Posterior Tissue	Frozen Posterior Tissue
Tissue ID	TA Flux ( $\mu\text{g}\cdot\text{cm}^{-2}\cdot\text{h}^{-1}$ )	
Tissue1	2.8	3.3
Tissue2	2.6	2.6
Tissue3	2.9	1.7
Tissue4	2.4	2.9
Tissue5	2.8	3.0
Tissue6	2.7	1.8
Tissue7	2.8	1.9
Tissue8	2.9	2.2
Tissue9	3.3	2.0
Tissue10	2.2	2.0
Tissue11	2.7	
Mean $\pm$ S.D.	2.7 $\pm$ 0.3	2.3 $\pm$ 0.6

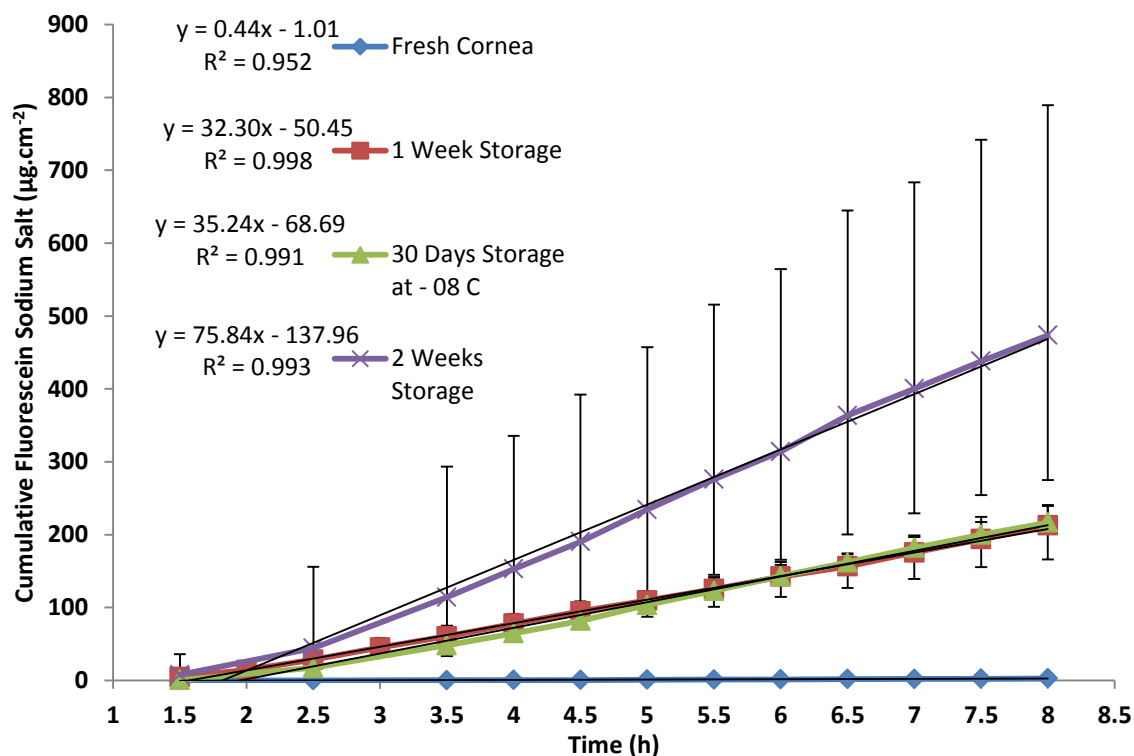


**Figure 4.8:** FSS (5% w/v) permeation profiles across fresh porcine corneal tissue, stored corneal tissues for one and two weeks and at -80 °C (Data represented as mean, error bars represent range., n = 4).

#### 4.4.4.3 Tritiated Water Correlation with TA and FSS Flux

The permeation of FSS and TA over an 8 and 28 h period was measured through posterior porcine ocular tissues and the results correlated with tritium permeation at 15 min (Figures 4.9 & 4.10). The permeability of TA across porcine corneal tissues was not possible to determine due to corneal swelling and high TA lag time. Unlike the corneal tritium permeation at 15 min, the FSS corneal permeability was dependent on the storage conditions (Figure 4.8), and hence correlation with tritium permeation at 15 min was unfeasible. The correlation between the  $^3\text{H}_2\text{O}$  percentage permeation through porcine scleral tissue at 15 min and both the hydrophobic drug (TA) and the hydrophilic marker (FSS) flux were significant (Pearson test,  $p < 0.01$ ), with correlation coefficients of  $r = 0.93$  and  $0.88$ , respectively (Figures 4.9 & 4.10). Both TA and FSS fluxes correlated directly

with the  $^3\text{H}_2\text{O}$  percentage permeation at 15 min. No correlation could be calculated between the FSS flux rates and the  $^3\text{H}_2\text{O}$  percentage permeation at 15 min (or at any other time points) through corneal tissues (data not shown).

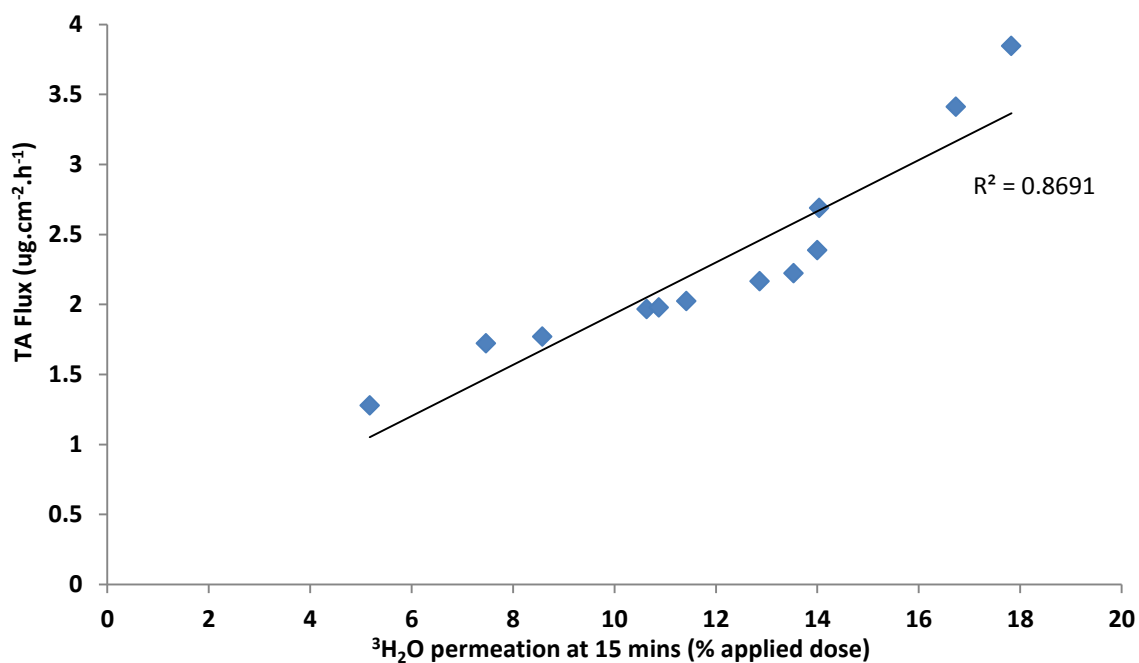


**Figure 4.9:** Correlation between TA flux and  $^3\text{H}_2\text{O}$  percentage permeation (15 min) across posterior porcine ocular tissues.

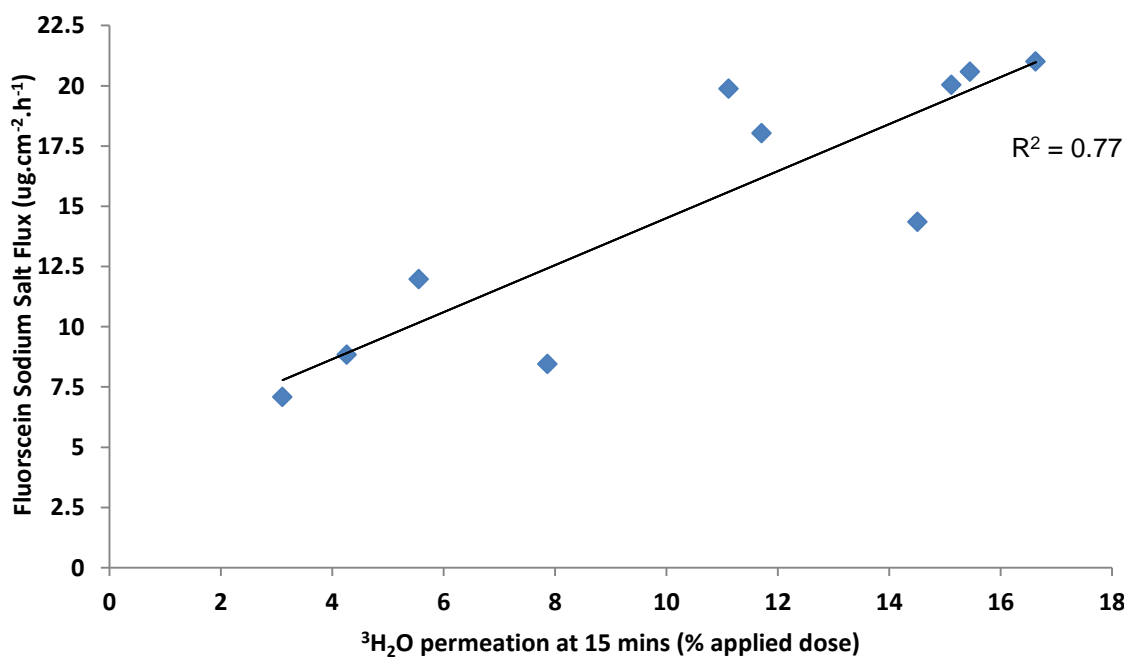


**Figure 4.10:** Correlation between FSS ( $1\text{ mg mL}^{-1}$ ) flux and  $^3\text{H}_2\text{O}$  percentage permeation (15 min) across posterior porcine ocular tissues.

#### 4.4.4.4 Tritiated Water Permeation and Posterior Porcine Ocular Tissue Thickness

The  $^3\text{H}_2\text{O}$  percentage permeation at 15 min was correlated to the posterior porcine ocular tissue thickness (Figure 4.11). The correlation between the  $^3\text{H}_2\text{O}$  percentage permeation at 15 min and porcine posterior ocular tissue thickness were significant (Pearson test,  $p < 0.01$ ), with a correlation coefficient of  $r = 0.81$ . The  $^3\text{H}_2\text{O}$  percentage permeation at 15 min was inversely related to the tissue thickness.

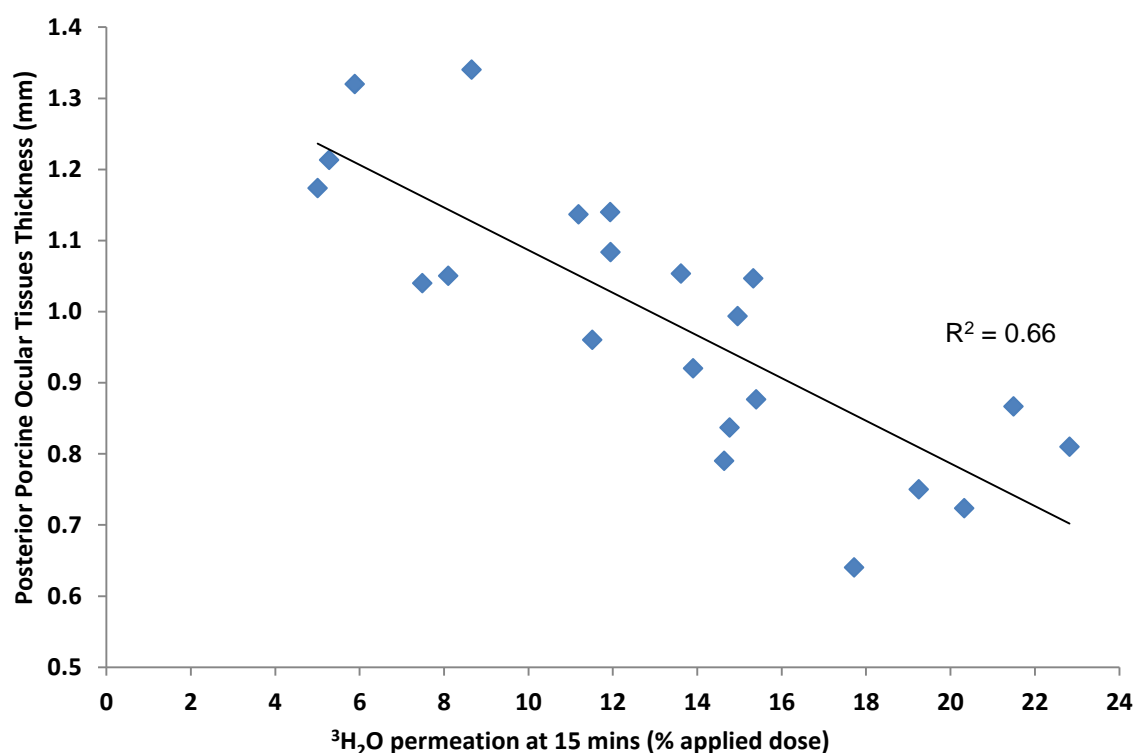


**Figure 4.11:** Correlation between posterior porcine ocular tissues thickness and  $^3\text{H}_2\text{O}$  percentage permeation (15 min) across the tissues.

#### 4.4.4.5 *In-Vitro* Marker Permeability Studies

In order to better understand the permeability of the ocular tissues, it was decided to compare the permeability of porcine and human ocular tissues and to investigate the effect of increasing molecular weight on the permeability of the marker. Four markers were tested through porcine and human corneal and scleral

tissues. For the purpose of comparing the permeability of the markers, the figures have been presented with the permeability coefficient rather than the flux, as the four markers were applied in different concentration in the donor solutions and the saturated solubilities were not determined. Figures 4.12 and 4.13 show the permeability coefficient of the four markers for scleral and corneal human and porcine tissues, respectively. Both figures show a similar trend, in which the permeability decreases with an increase in molecular weight of the marker. The permeability coefficients of FSS and 4 kDa FITC-Dextran permeating across porcine scleral and corneal tissues were lower than their counterpart in the human tissue ( $t$ -test,  $p > 0.05$ ), whereas the permeability coefficients of 10 and 20 kDa FITC-Dextran permeating across porcine scleral and corneal tissues were similar to their counterpart human tissue ( $t$ -test,  $p < 0.05$ ). The fluxes of the permeation and enhancer studies are tabulated in the appendix A.

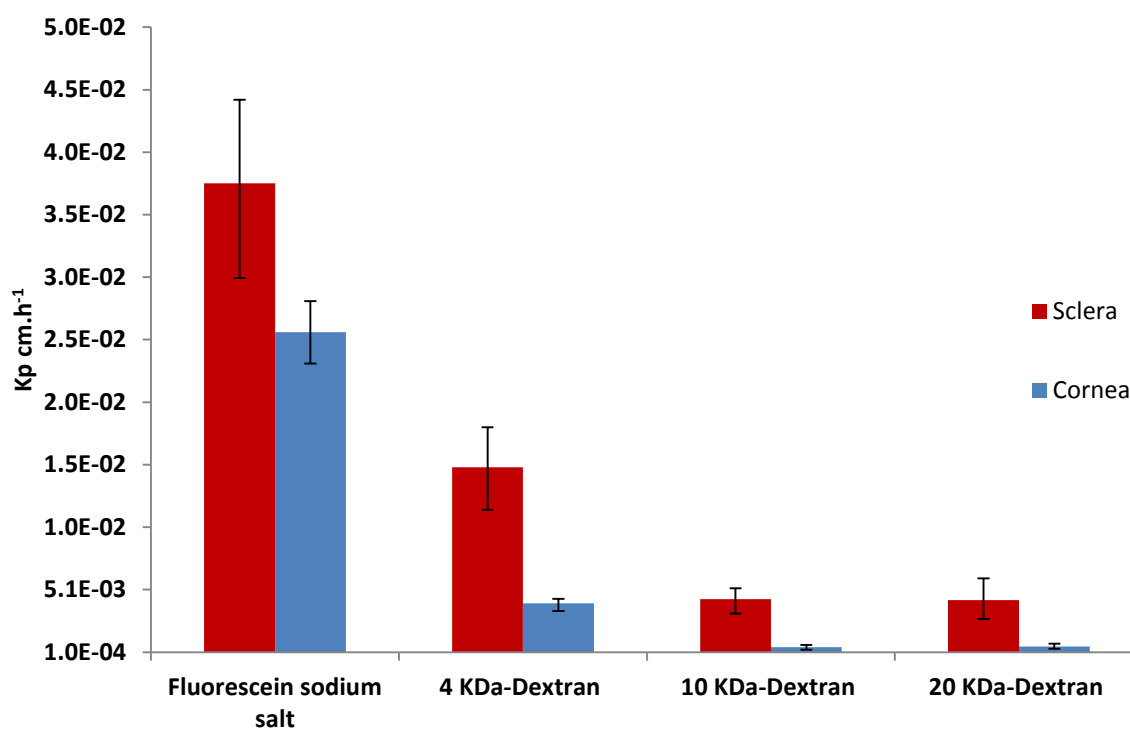


**Figure 4.12:** The permeability coefficients of FSS, 4, 10 and 20 kDa FITC-Dextran across human corneal and scleral tissues (Data represented as mean, error bars represent range,  $n = 4$ ).

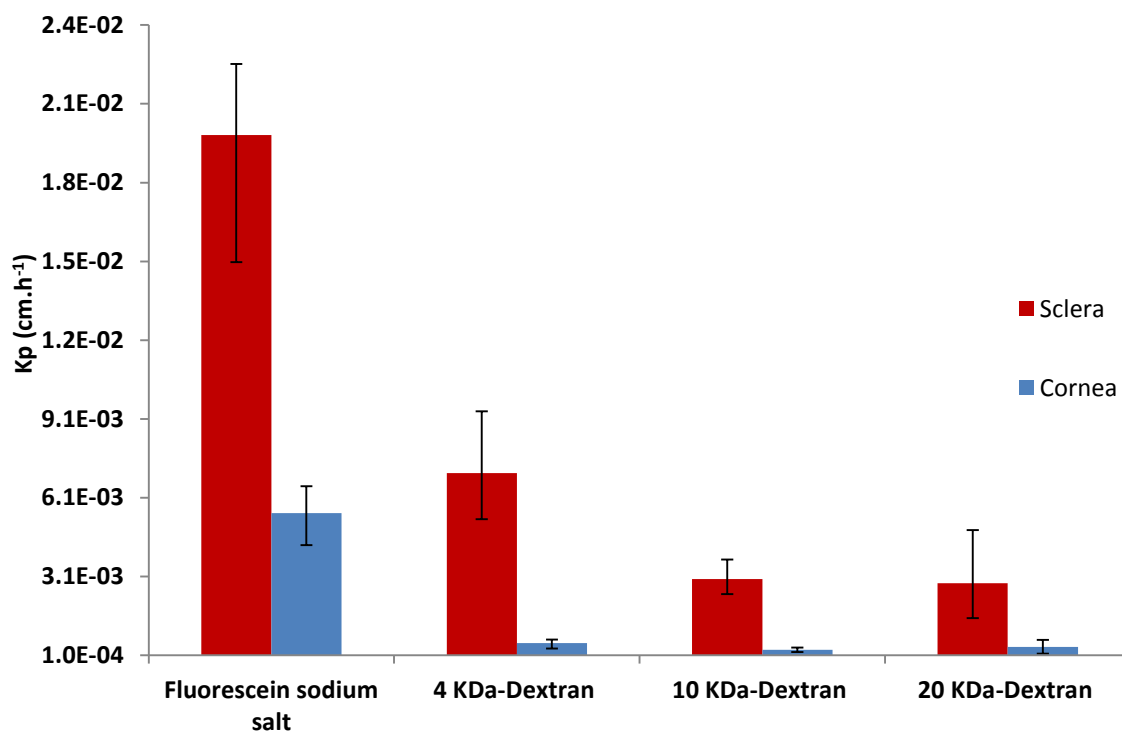


**Figure 4.13:** The permeability coefficients of fluorescein sodium salt, 4, 10 and 20 kDa FITC-Dextran across porcine scleral and corneal tissues (Data represented as mean, error bars represent range, n= 4).

#### 4.4.4.6 Human, Rabbit and Porcine FSS Corneal Tissues Permeability Comparison

The permeability of FSS across stored human, porcine and rabbit cornea was compared (Figure 4.14). Although the rabbit cornea appeared to have a higher FSS permeability than porcine and human corneal tissues (Figure 4.14), there was no significant difference (one way ANOVA,  $p > 0.05$ ) in the FSS permeability between the three species.

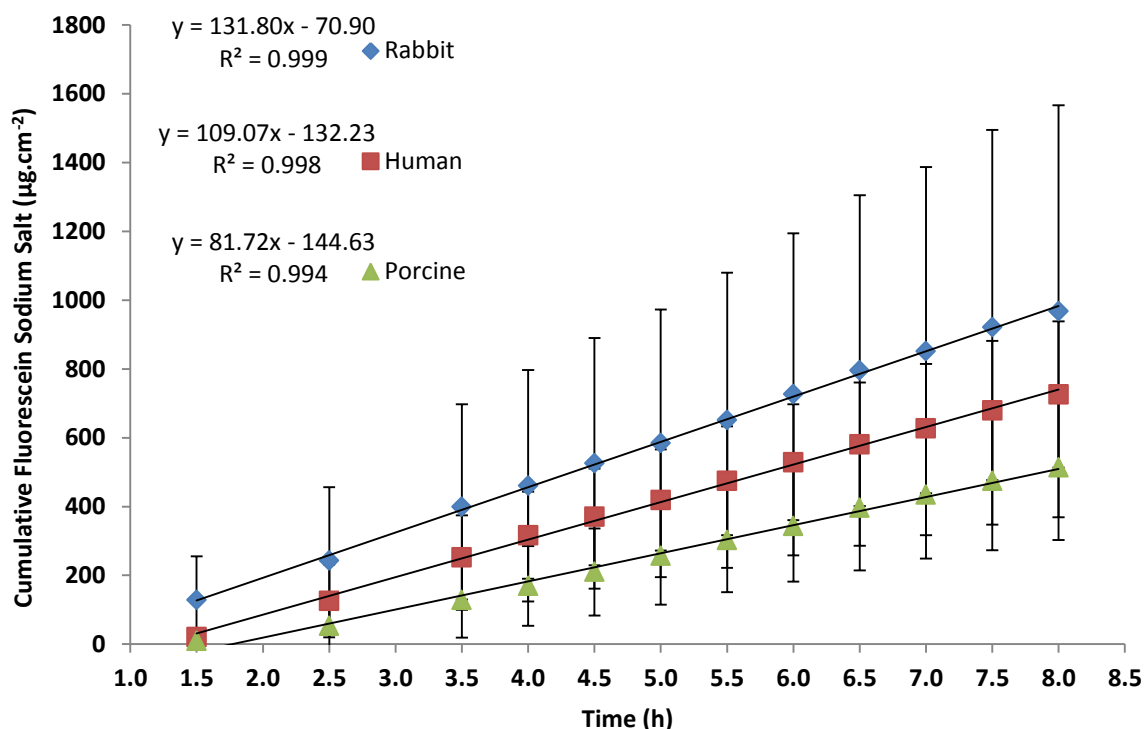


**Figure 4.14:** Comparative permeation profiles of FSS (5% w/v) across human, porcine and rabbit corneal tissues (Data represented as mean, error bars represent S.D., n = 6).

#### 4.4.5 *In-Vitro* TA-SA Permeability Studies

The permeability of the hydrophobic drug TA from a TA suspension and Da<sub>10</sub> TA-SA were tested on human scleral tissues. The use of only one TA-SA (Da<sub>10</sub>) from those developed in chapter three was due to the limited availability of human ocular tissues. Da<sub>10</sub> TA-SA was chosen due to it is high TA solubilisation compared to other TA-SA. The results shown in Figure 4.15 did not show any significant difference (*t*-test,  $p > 0.05$ ) in permeation between the control and the polymeric formulation. Similarly, there were no significant differences (one way ANOVA,  $p > 0.05$ ) in TA permeation from the four polymeric formulations (Pa<sub>5</sub>, Pa<sub>5</sub>-MPEG, Ch<sub>5</sub> and Da<sub>10</sub>) and TA suspension across posterior porcine ocular tissues (Figure 4.16).

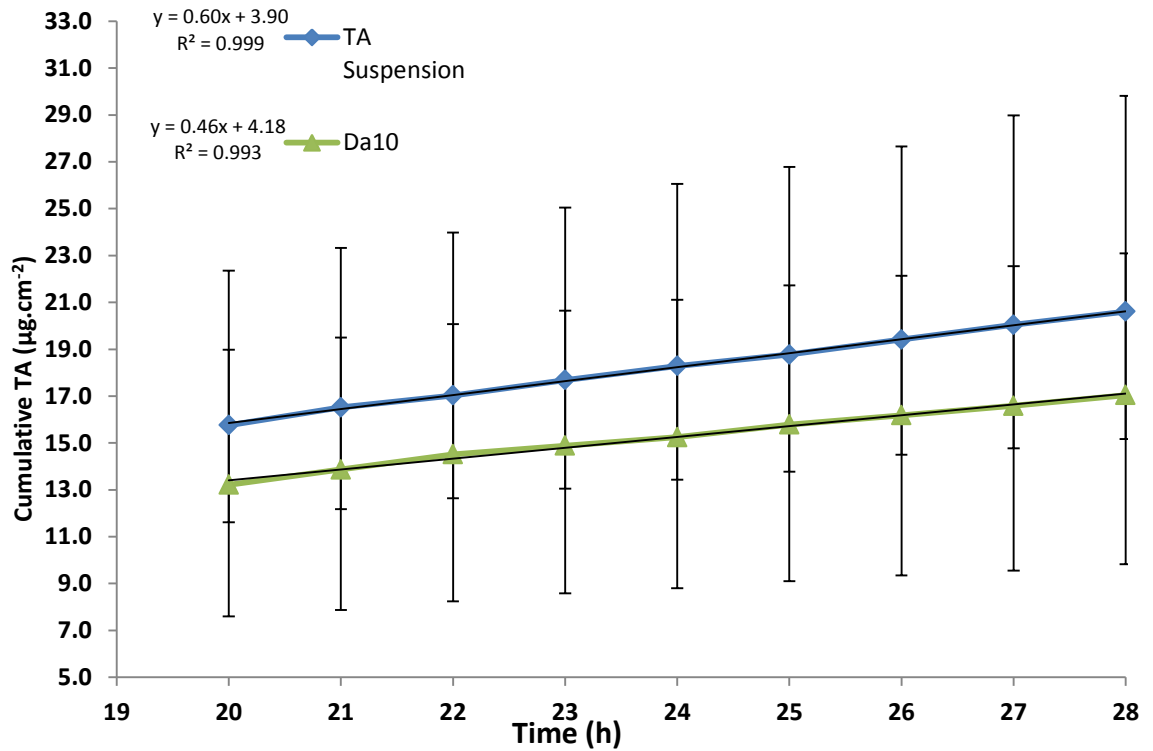


**Figure 4.15:** TA suspension ( $1000 \mu\text{g mL}^{-1}$ ) and Da<sub>10</sub> TA-SA permeation profiles through human scleral tissue (Data represented as mean, error bars represent range. n = 4).

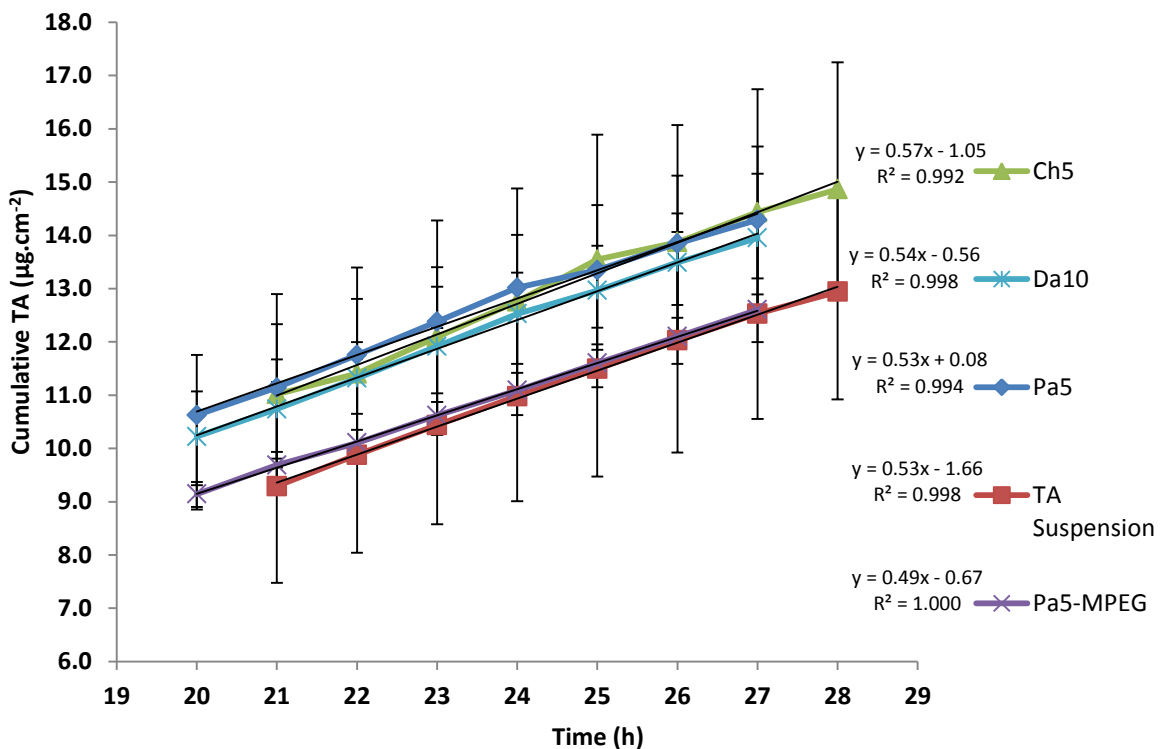


**Figure 4.16:** TA suspension ( $500 \mu\text{g mL}^{-1}$ ) and TA-SA permeation profiles through posterior porcine ocular tissues (Data represented as mean, error bars represent range, n = 4).

#### 4.4.6 Enhancer Permeation Studies

As the permeability of the markers decreased considerably with the increasing molecular weight and the polymeric SA did not significantly increase TA flux through human or porcine scleral tissues, it was appropriate to investigate the use of enhancers with a view to increasing the permeability of the penetrant and to possibly lower potential formulations applied dosage. It was not possible to determine the permeability of TA across corneal tissue due to the corneal swelling and long lag time, hence the enhancer permeation studies were carried out on two markers (FSS and 10 kDa FITC-Dextran) instead. Four potential chemical enhancers and one thermal approach (elevated temperature 45 °C) were investigated using porcine and human tissues. None of the potential enhancers produced a significant difference ( $t$ -test,  $p > 0.05$ ) in the permeation of the 10 kDa FITC-Dextran across porcine or human scleral and corneal tissues (Figures 4.17 and 4.18). The enhancing effect of the aforementioned promoters was also explored using a smaller marker (FSS) more representative of the molecular weight of more commonly used drugs. The FSS enhancer permeation study was performed on porcine scleral tissues as human scleral tissues were unavailable (Figure 4.19). There was no significant difference in the flux between the control and the 0.1% (w/v) glutamic acid, 0.01 and 0.001% (w/v) tween 80, 45 °C and Pa<sub>5</sub> polymer ( $t$ -test,  $p > 0.05$ ). However there was a considerable reduction ( $t$ -test,  $p < 0.05$ ) in the FSS flux when using the acetate buffer and the 0.5% (w/v) chitosan. This reduction was due to the precipitation of the FSS in the former solution and the formation of a gel in the latter solution.

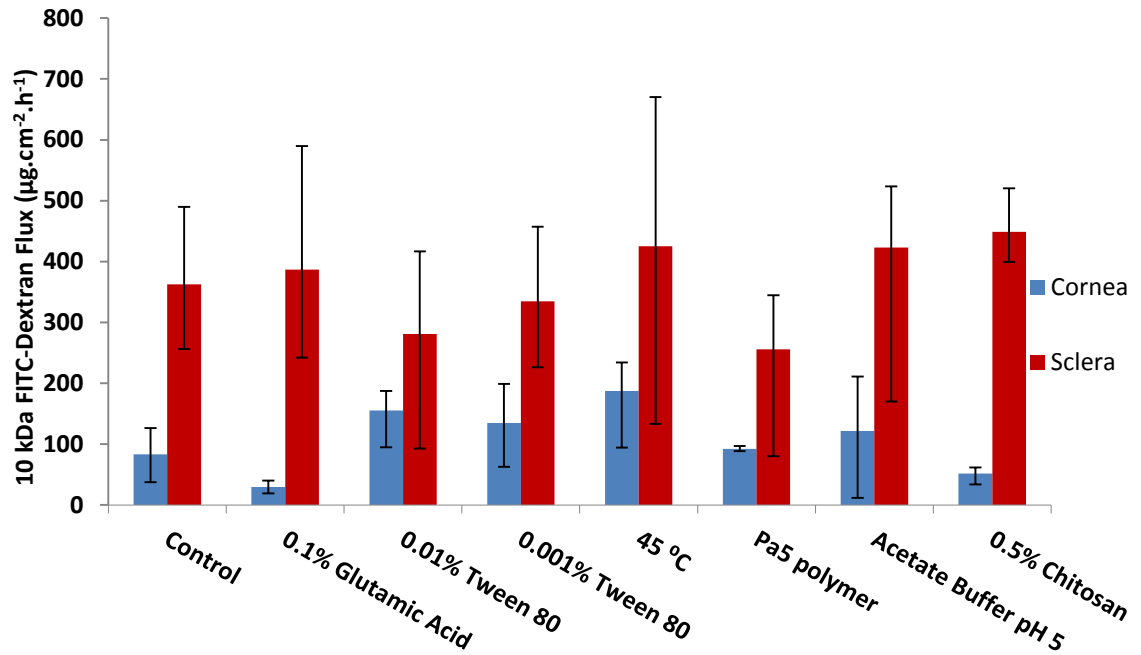


**Figure 4.17:** The flux of 10 kDa FITC-Dextran added to various enhancers and at elevated temperature through human corneal and scleral tissues (Data represented as mean, error bars represent range, n = 4). All percentages in the figure are w/v.

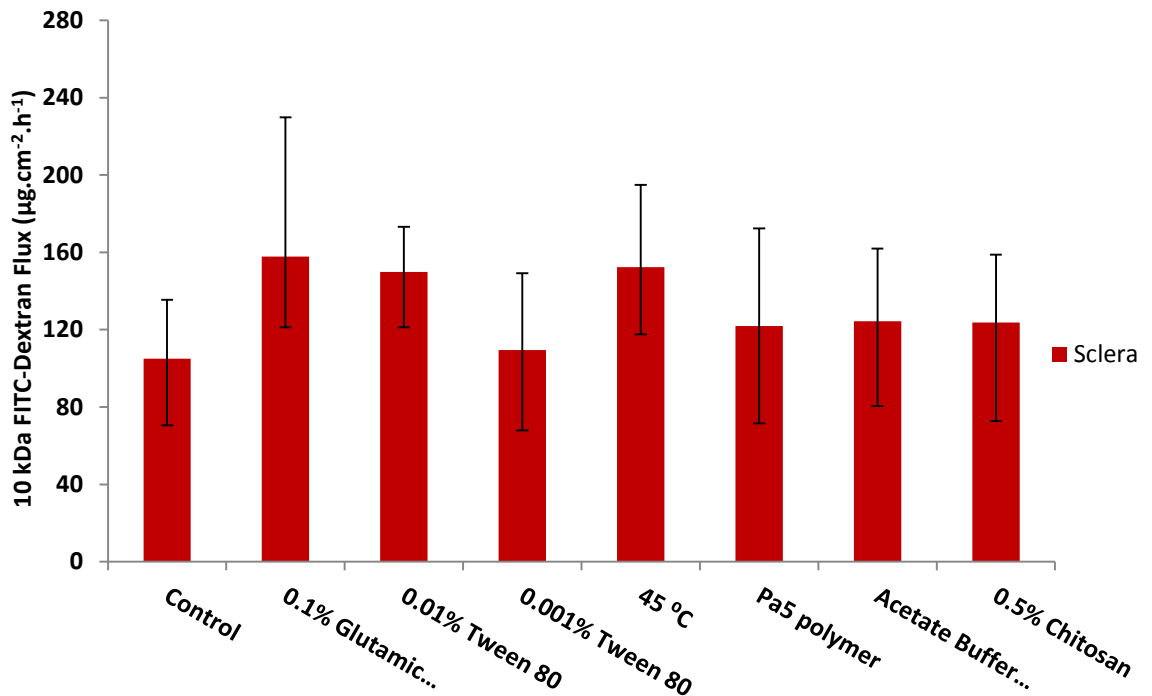


**Figure 4.18:** The flux of 10 kDa FITC-Dextran added to various enhancers and at elevated temperature across porcine scleral tissues (Data represented as mean, error bars represent range, n = 4). All percentages in the figure are w/v.

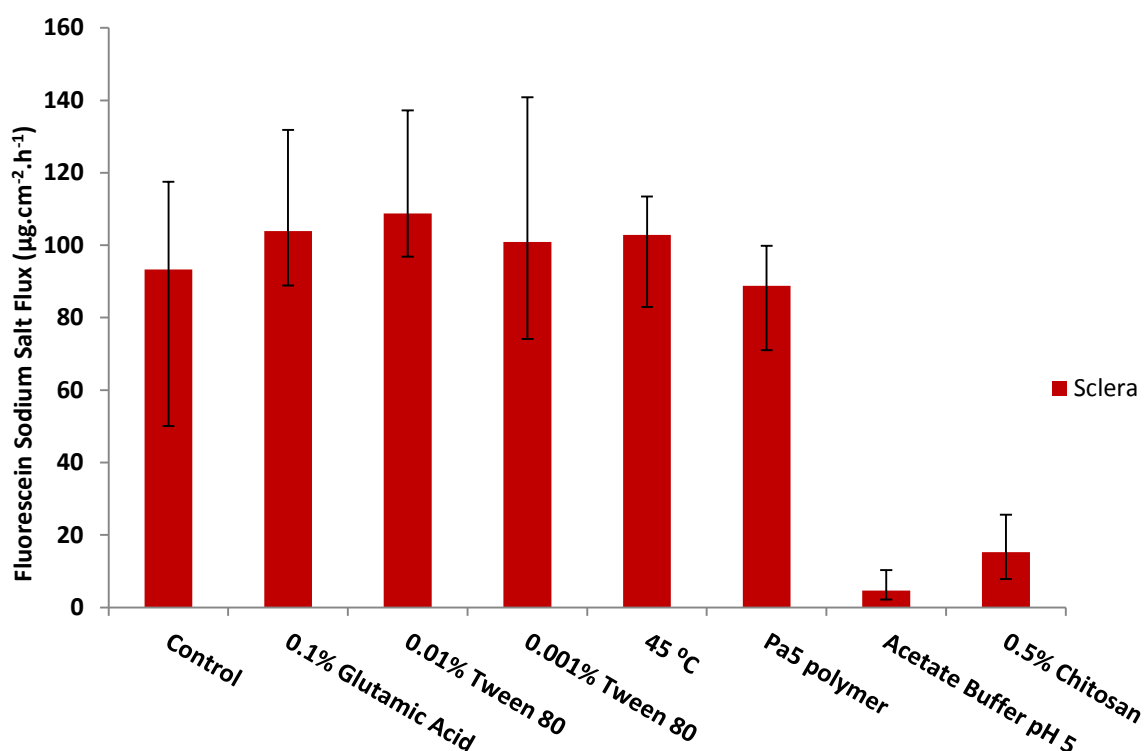


**Figure 4.19:** The flux of fluorescein sodium salt added to various enhancers and at elevated temperature across porcine scleral tissues (Data represented as mean, error bars represent range, n = 4). All percentages in the figure are w/v.

## 4.5 Discussion

In chapter three, the simplicity of preparing different self-assembled nanoparticles as a drug carrier was demonstrated. However, testing the release profiles of these formulations in conditions similar to those *in-vivo* is very difficult. An eye model which correlates well with that of the human clinical setting is necessary to investigate the delivery properties of potential formulations destined for human use. This chapter focused on developing a porcine *in-vitro* eye model where potential formulations could be evaluated without the huge financial burden of *in-vivo* studies or the use of sacrificed animals. The model developed also offers instant availability within almost any laboratory and correlates well to results obtained from human tissues.

The similarities between porcine and human eyes in terms of anatomy and scleral thickness were studied by Olsen *et al.* (Olsen, Aaberg, Geroski & Edelhauser, 1998; Olsen, Sanderson, Feng & Hubbard, 2002). These similarities are absent in other animal models, in particular rabbits, the animal most used in testing ophthalmic formulations. Furthermore, porcine eye globes are easily obtained from slaughterhouses in large numbers and can efficiently substitute for rabbit. In this work, the porcine posterior ocular tissues and corneal tissue were investigated as an alternative to human tissue. The posterior tissue model is of interest to ocular drug delivery to the posterior segment of the eye, whereas the corneal model is of interest to topical drug delivery to the anterior chamber of the eye. The lipophilicity and permeability of different molecular size penetrants across scleral and corneal tissues (mainly rabbit and bovine, occasionally human and porcine) has been investigated by many researchers, in which they found optimal corneal permeability (rabbit) in the range of 1-3 log partition coefficient of the penetrant and scleral tissue (human) allowing large penetrant (up to 120 kDa) to transverse across (Lee, 1990; Mitra, 2003; Mosher & Mikkelsen, 1979; Myung *et al.*, 2006; Nicoli *et al.*, 2009; Pescina *et al.*, 2012; Qi *et al.*, 2013). However, little has been done to directly compare the permeability of human and porcine ocular tissues and to develop and validate an *in-vitro* eye model fit for the purpose of permeation studies (Kadam, Cheruvu, Edelhauser & Kompella, 2011; Nicoli *et al.*, 2009). In this work, a human alternative porcine *in-vitro* eye model was developed and partially validated, in order to investigate the TA-SA formulations developed in chapter three.

TA is a hydrophobic corticosteroid drug widely used in ophthalmology as off-label treatment of many posterior ocular diseases such macular oedema

(Jonas, Kreissig & Degenring, 2002). In recent years, many TA formulations were formulated aiming to deliver the drug to the posterior tissues for a prolonged period of time in comparison to the previously marketed TA suspensions (Araujo, Nikolic, Egea, Souto & Garcia, 2011; Kim, Lim, Kim, Kim & Shin, 2008). The permeation of hydrophobic drugs from a suspension or potential ophthalmic formulations is typically tested *in-vitro* across scleral or sclera-choroida-RPE tissues using buffer solutions as receiver fluids in a diffusion cell (i.e. Ussing chambers or Franz cells) (Araujo, Garcia, Mallandrich, Souto & Calpena, 2012; Kadam, Cheruvu, Edelhauser & Kompella, 2011; Loch *et al.*, 2012; Mora *et al.*, 2005; Olsen, Edelhauser, Lim & Geroski, 1995; Thakur, Kadam & Kompella, 2011). Araújo *et al.* reported that sink conditions for TA in HEPES buffer could not be obtained after 12 h (Araujo, Garcia, Mallandrich, Souto & Calpena, 2012).

In this work, TA permeation studies across porcine posterior tissues were carried out using modified Dulbecco's buffer solution with different levels of ethanol (0, 5, 10 and 30%). The TA permeation through porcine corneal tissues were not studied due to the severe swelling of the corneal tissues over a prolonged period of time and the high lag time of TA. TA permeation across posterior porcine ocular tissues showed that the TA flux in the presence of 30% ethanol, or more, in either the donor or receiver solution is approximately 3 fold higher than the TA flux from TA suspension where no or low ethanol (<30%) is present in the receiver fluid (Figure 4.2). There are two suggested mechanisms in the literature which might explain the increase of TA permeability. The first is, which has been interpreted from skin diffusion studies, ethanol is known to extract lipids and hence lower the skin barrier function and render the membrane more permeable (Lachenmeier, 2008; Van der Merwe & Riviere, 2005). This mechanism

of action is irrelevant to the ocular tissues in particular the sclera as it lacks the presence of lipids, hence no ethanol extraction occurs and no corresponding increase in tissue permeability should occur. The second mechanism is due to the permeation of the ethanol through the membrane which increases the co-permeation of the drug by the effect of solvent drag without affecting the barrier integrity. The solvent drag effect was reported by Ungphaiboon & Maitani (Ungphaiboon & Maitani, 2001) in which a significant increase in the cumulative amount of TA penetrating a synthetic membrane to the receiving fluid was observed with increasing ethanol content in the donor solution (10, 20 and 30%).

In the current study, the difference in the thickness of porcine posterior tissues before and after TA permeation studies was found to be insignificant. Reports have shown scleral thickness is affected by the hydration level of the scleral tissue (Boubriak, Urban, Akhtar, Meek & Bron, 2000; Lee, Geroski, Prausnitz & Edelhauser, 2004). A study by Olsen *et al.* found no significant difference between the hydration of human scleral tissue stored in balance salt solution for 3 h and scleral tissue stored in moist chamber for two days (Olsen, Edelhauser, Lim & Geroski, 1995). Ambati *et al.* also have reported no significant difference between scleral hydration of fresh rabbit scleral tissues and tissues exposed to Hanks' balanced salt solution for 4 h (Ambati *et al.*, 2000). The unchanged thickness of the porcine posterior tissue indicates the unaffected hydration level of the tissue, and hence no alteration in scleral permeability over the duration of the experiment.

Furthermore, to compare the barrier function of freshly excised and frozen porcine posterior tissues (- 20 °C, two weeks), TA and  $^3\text{H}_2\text{O}$  permeation studies were performed. These studies have shown that there is no significant difference

in permeability of TA or  $^3\text{H}_2\text{O}$  percentage permeating through fresh and frozen posterior porcine ocular tissues demonstrating that freezing the porcine posterior tissue does not alter the barrier properties (Table 4-3 & Table 4-5). This outcome is in agreement with the reported literature, in which cryotherapy had no effect on permeability of human and porcine sclera was observed (Nicoli *et al.*, 2009; Oh *et al.*, 2009; Olsen, Edelhauser, Lim & Geroski, 1995).

Commonly the barrier integrity of tissues used in *in-vitro* models are assessed by monitoring the permeation of a marker compound, either concurrently, before or after the permeation of the drug. The limitations of this technique are that it is time consuming, costly and might alter the permeation profile of the drug. Tritiated water has previously been used in monitoring the barrier integrity of tissues, in particular human skin (Lawrence, 1997). In most skin studies  $^3\text{H}_2\text{O}$  permeation is measured over a 2 to 6 h period, in order to determine barrier integrity prior to lengthy drug studies or to normalise permeation data (Chilcott, Dalton, Emmanuel, Allen & Bradley, 2002; Dugard, Walker, Mawdsley & Scott, 1984). The skin is a semi-impermeable natural barrier which has a structure akin to a bricks and mortar model (Brown, Martin, Jones & Akomeah, 2006; Williams, 2003) whereas the sclera tissues have collagen and elastic fibres with a few cells imbedded in-between. Due to the difference in structure between the two tissues, the permeability of water through porcine scleral tissue ( $51.1 \pm 11.9\%$  after 1 h) was found to be much higher in comparison to the skin (less than 10% of the applied dose of  $^3\text{H}_2\text{O}$  permeated within 2 h through full-thickness human abdominal skin ( $n = 42$ , kps were lower than  $20 \times 10^{-4}$  cm.h) (Lawrence, 1997)). The  $^3\text{H}_2\text{O}$  permeation at 15 min could be potentially exploited as a rapid screening test to determine ocular tissue integrity prior to commencing the time consuming

drug permeation studies. As the tritiated water studies have shown that approximately no more than 25% of the applied dose of  $^3\text{H}_2\text{O}$  can permeate through posterior tissues in 15 min (Table 4-3), this value has been considered as a cut-off limit for integrity check of the porcine posterior tissues (the 25% value is an arbitrary value approximately two standard deviations above the mean value percentage of  $^3\text{H}_2\text{O}$  permeating through fresh posterior porcine ocular tissue at 15 min). This methodology has previously been used in other tissue types, for example Brown *et al.* rejected human nails which allowed the permeation of 20% and 40% higher than the average mean nails that had undergone the same treatment at 1 and 20 h, respectively (Brown *et al.*, 2009). A similar approach was reported by Lawrence who used an upper cut off limit of approximately 3 x SEM above the mean  $k_p$  value of  $^3\text{H}_2\text{O}$  for human skin (Lawrence, 1997). The  $^3\text{H}_2\text{O}$  percentage permeating at 15 min of the porcine corneal tissues was much lower in comparison to the posterior tissues  $^3\text{H}_2\text{O}$  percentage permeating at 15 min. This is expected due to the presence of tight junctions between corneal epithelial cell layers which hinders the transport of hydrophilic molecules via the paracellular pathway (section 1.5.1). An arbitrary cut-off limit of  $^3\text{H}_2\text{O}$  percentage permeating at 15 min was set at 3.5% of the applied dose.

Additionally, the  $^3\text{H}_2\text{O}$  percentage permeating at 15 min provided a valuable method to normalise penetrant flux, as porcine posterior tissue thickness inversely related to  $^3\text{H}_2\text{O}$  percentage permeating at 15 min (Figure 4.11). This confers an advantage as the exact thickness of the scleral tissue is hard to measure, due to the sclera not having a uniform thickness across the entire eye and this therefore makes it impractical to cut a uniform section. The TA and FSS fluxes correlated well with  $^3\text{H}_2\text{O}$  percentage permeating at 15 min through frozen porcine posterior

tissues (Figures 4.9 & 4.10). As the  $^3\text{H}_2\text{O}$  percentage permeating at 15 min increased the permeability of TA and FSS increased as well, suggesting that the two molecules (the hydrophobic TA and the hydrophilic FSS) may traverse through the tissue using the same route as water. This can be largely explained by the structure of the scleral tissue where the penetrant molecules diffuse through the spaces between the collagen bundles (fibre matrix pores) (Edwards & Prausnitz, 1998; Haghjou, Abdekhodaie & Cheng, 2013; Maza, Tauber & Foster, 2012) and therefore the penetrant permeation is affected by the collagen architecture. The collagen fibres are loose interwoven in the posterior sclera in comparison to the anterior scleral tissue (Curtin, 1969), this difference in the scleral architecture results in higher penetrant permeation through the posterior scleral tissue (Boubriak, Urban & Bron, 2003).

Little has been done to evaluate the effect of storage time and conditions on the permeability of the corneal tissues. Gratieri *et al.* recently showed the structure integrity and barrier function of porcine epithelial corneal tissue was maintained throughout the duration of the experiment (6 h), without the need of gassing  $\text{CO}_2$  into the receiver solution (HEPES buffer) (Gratieri, Gelfuso, Thomazini & Lopez, 2010). Similarly, Majumdar *et al.* assessed rabbit cornea permeability after storing overnight in phosphate-buffered saline (PBS) or Hanks balanced salt solution (HBSS) in wet ice. They found no difference in transcellular and paracellular passive diffusion between the fresh and the overnight stored corneas (Majumdar, Hingorani & Srirangam, 2010).

The data presented in this thesis shows significant swelling of the porcine corneas after storage in PBS buffer at 37 °C for 24 h. This does significantly affects the permeability of penetrants, in particular hydrophobic drugs as the

corneal stroma is the main limiting barrier. The swelling is due to the presence of four-fold higher glycosaminoglycans (GAG, water binding molecules) concentration in the cornea (4-4.5% GAG) than the sclera (Akhtar *et al.*, 2002; Huang & Meek, 1999; Watson, Hazleman, McCluskey & Pavesio, 2012). Interestingly, the FSS corneal permeability increased with time and was dependent on storage conditions (Figure 4.8). The increase in corneal permeability is mainly due to the change of tight junctions between the epithelial cell layers or the death of the tightly packed epithelium cell, especially in the superficial layer. The change in tight junctions can be confirmed using transepithelial electrical resistance (technique before and after storage). The increase in FSS permeability with the increasing storage time is an important finding indicating the gradual decline in barrier function of the epithelium layers, and to the best knowledge of the author this has not been reported before. Nevertheless FSS permeability in rabbit and two weeks stored porcine corneal tissues (Figure 4.14) were not significantly different from human (one way ANOVA,  $p > 0.05$ ). The porcine *in-vivo* eye results may relate more accurately to human *in-vivo* than the *in-vivo* rabbit results, due to rabbits having a higher corneal area, lower tear turnover and lower blinking rate than humans (Edelhauser & Maren, 1988; Rathbone, Hadgraft & Roberts, 2003). Therefore, a porcine *in-vitro* eye model is more appropriate than rabbit *in-vitro* model to screen potential formulations.

The *in-vitro* permeability of human and porcine tissues was compared with a series of hydrophilic markers with increasing molecular weights. FSS was selected to represent the molecular weights of more commonly used drugs, whereas the larger FITC-dextran polymers have similar molecular weights as larger molecules, such as peptides, growth factors and ribonucleic acid (RNA).

The data obtained revealed an inverse relationship between the permeability through scleral and corneal tissues of both species (human and porcine) and the molecular weight of the markers. The inverse relationship and the abrupt decline in the permeability of various compounds and their molecular weights has been reported using bovine scleral tissue by Maurice and Polgar (Maurice & Polgar, 1977) and human sclera tissue by Olsen *et al.* (Olsen, Edelhauser, Lim & Geroski, 1995). The latter authors suggested the permeability data from the human scleral tissue can be compared to the bovine if the thickness of the bovine sclera is considered (bovine sclera thickness is approximately 0.92 mm at the limbus, 0.65 mm at the equator and more than 1 mm at the optic nerve region (Cheruvu & Kompella, 2006)). Loch *et al.* also found the permeability of three drugs (ciprofloxacin hydrochloride, lidocaine hydrochloride, timolol maleate) were higher in rabbit posterior tissues, followed by porcine and then bovine (Loch *et al.*, 2012). Similarly Kadam *et al.* found the cumulative percentage of eight beta-blockers transported through posterior ocular tissues followed the trend rabbit > human > porcine > bovine. The workers also found upon normalization to scleral thickness the species differences in scleral transport were abolished (Kadam, Cheruvu, Edelhauser & Kompella, 2011). A similar trend to the one observed by Kadam *et al.* in which human scleral tissue was more permeable than porcine was observed in the findings of this work (Figures 4.12 & 4.13). The  $k_p$  values of FSS and 4 kDa FITC-dextran were nearly two fold higher in human scleral tissue in comparison to porcine and this is probably due to the thicker porcine scleral tissue. Interestingly if the tissue thickness at the equator of both species (porcine and human scleral thickness at the equator are approximately 0.86 and 0.39 mm, respectively) were to be considered the difference in the permeability between the two species

diminishes (the  $k_p$  values of FSS normalised by the equator thickness of human and porcine scleral tissue were  $1.47$  and  $1.63 \times 10^{-5} \text{ cm.h}^{-1}$ , respectively, whereas the normalised  $k_p$  values for the 4 kDa FITC-dextran were  $0.58$  and  $0.61 \times 10^{-5} \text{ cm.h}^{-1}$ ).

The permeability of the corneal tissues had the same inverse relationship and abrupt decline in permeability with increasing molecular weight observed in the human and porcine sclera (Figures 4.12 & 4.13). Interestingly, there was a large difference ( $t$ -test,  $p > 0.05$ ) in the permeation of FSS and 4 kDa FITC-dextran between human corneal tissues and one week stored porcine corneal tissues. The porcine corneal tissue was less permeable than human tissue (5 and 7 folds lower for FSS and 4 kDa FITC-dextran, respectively). The lower permeability of the porcine corneal tissue in comparison to human tissue is likely to be due to the difference in thickness (human cornea thickness  $535 \mu\text{m}$ , porcine cornea thickness  $666 \mu\text{m}$ ) and to the undamaged corneal epithelium and endothelium cells in the porcine corneal tissues which were stored for a shorter period of time in comparison to the human corneal tissues (no more than 4 weeks). The percentage of damaged corneal endothelial cells in organ culture medium and dextran containing medium increases with storage time and is affected by the storage and transport media (Borderie, Baudrimont, Lopez, Carvajal & Laroche, 1997; Pels, Beele & Claerhout, 2008). The presence of 500 kDa dextran (macromolecule de-swelling agent) has been shown to cause 8.4% loss in the number of endothelial cells after two days and severe epithelial injuries and lysis of keratinocytes after four days (Borderie, Baudrimont, Lopez, Carvajal & Laroche, 1997). The increase in corneal permeability due to the more damaged epithelial cells can also be deduced from the reported literature, in which de-epithelialized human cornea had

the same  $k_p$  as the sclera (Edelhauser & Maren, 1988), and from the finding of this work in which the permeability of the porcine corneal tissues increased with increased duration of storage (Figure 4.8). The fresh porcine corneal tissue were impermeable (below limit of quantification, data not shown) to the 4 kDa marker, whereas the 20 kDa marker did permeate through stored porcine corneal tissue (one week) indicating an alteration in the corneal epithelium layers. A molecular weight cut-off for the permeability of fresh and stored corneal tissues has not previously been reported, further marker permeation studies with various molecular weights are necessary to determine the highest molecular weight which can permeate through the cornea.

The calculated TA permeability coefficient ( $k_p$  of TA suspension) through human sclera was  $1.23 \times 10^{-5} \text{ cm.s}^{-1}$  and is in good agreement with a previously reported value ( $1.47 \times 10^{-5} \text{ cm.s}^{-1}$ ) (Mora *et al.*, 2005). The TA  $K_p$  value ( $1.32 \times 10^{-5} \text{ cm.s}^{-1}$ ) in porcine posterior tissues was similar to that obtained in human tissue, demonstrating the similarity in permeability between the two tissues and hence the suitability of porcine posterior tissues as an alternative model to human posterior tissues. The TA-SA (TA polymeric nanoparticles), did not significantly increase (*t*-test,  $p > 0.05$ ) TA flux through human or porcine scleral tissues (Figures 4.15 & 4.16). This suggested the SA did not pass through the scleral tissue, and only TA molecules released from the SA traversed across the tissue. This finding is supported by the *in-vitro* permeability of 20 and 200 nm nanoparticles across bovine sclera and posterior tissues over 24 h (Amrite, Edelhauser, Singh & Kompella, 2008). The latter workers reported no quantifiable permeation of the 200 nm nanoparticles across either tissue, whereas only  $0.46\% \pm 0.06\%$  of the 20 nm nanoparticles crossed through the sclera. The observed and reported results in

which large nanoparticles could not penetrate the scleral tissue might be explained by scleral structure and the passive diffusion of penetrants through the scleral aqueous pathways in between the free spaces of the collagen bundles (Ambati *et al.*, 2000; Edwards & Prausnitz, 1998; Komai & Ushiki, 1991a; Thakur, Kadam & Kompella, 2011). As a result the porosity of the collagen fibre matrix is the main determinant of the rate and size of the penetrants traversing across the sclera.

Increasing the permeability of ocular tissue is highly desirable, as the applied dosage encounters many static and dynamic barriers before reaching the targeted tissue in very low concentrations. The potential permeation enhancer studies showed there were no significant difference in  $k_p$  values of the FSS and 10 kDa FITC-Dextran in the presence of penetration enhancers compared to standard solutions through both human and porcine tissues (Figures 4.17, 4.18 & 4.19). The corneal chemical enhancers assist drug delivery via two mechanisms; the first is through the alteration of the tight junction of the epithelium cells (paracellular) whereas the second is via the transcellular route. The chemical enhancers did not have any significant difference on the 10 kDa marker permeating through human cornea (Figure 4.17), due to the loosened tight junctions between the corneal epithelial cells as a result of the storage conditions. In addition, the 10 kDa FITC-dextran traverses paracellular route and acts as a paracellular marker (Kikuchi, Suzuki, Kusai, Iseki & Sasaki, 2005; Krug *et al.*, 2013).

Chemical enhancers might not be sufficient to enhance permeation through the scleral and corneal stroma, due to limited viable cells and lipids in the structure of these tissues. This might necessitate the use of active permeation techniques, such as iontophoresis, electroporation and sonophoresis (Cheung *et al.*, 2010; Hao, Li, Liu & Kao, 2009). Despite the hypocellular nature of the scleral tissue,

thermoperturbation is unlikely to be used in the eye as the scleral tissue is rich in nerves. Other aggressive forms of active permeation techniques such as the use of needleless injections might possibly enable delivering drugs to the posterior segment of the eye. Despite recent reports showing heat facilitated drug transport through human skin by reversible lipid fluidisation at 37 - 45 °C (Akomeah, Nazir, Martin & Brown, 2004; Brown, Martin, Jones & Akomeah, 2006; Wood, Brown & Jones, 2012), the elevated temperatures (45 °C) have did not improve the permeation of the 10 kDa marker through the sclera, which can be explained by the absence of lipids in the scleral tissue.

## 4.6 Conclusion

A porcine *in-vitro* eye model was developed; the results showed that a percentage of ethanol up to 10% v/v in modified Dulbecco's buffer solution can be used as a receiver fluid without significantly altering the permeability of the tissue. The integrity of porcine ocular tissue was checked by monitoring the permeation of tritiated water, this study has shown that it is possible to ensure the membrane is intact after 15 min. This technique may also be used as a method to normalise drug flux to reduce the inherent variability between tissue samples thus increasing the accuracy of the *in-vitro* eye model. Furthermore, the results of this work have shown the validity of using frozen posterior tissues as an alternative practical and more convenient option to using fresh tissues.

*In-vitro* permeation studies were performed with four markers having different molecular weights. The results showed the permeation of the markers reduced with increasing molecular weight in both corneal and scleral tissues in both human and porcine tissue. The four markers had similar permeability in both

human and porcine tissues strengthening the suitability of the porcine eye model as an alternative to human tissue.

Enhancer permeation studies showed for a range of chemical enhancers and the use of nano-self assemblies no enhancement was found in the delivery of marker compounds to the eye. However, the corneal permeability from tissues stored for one or two week revealed an important finding, where fresh corneas might be susceptible to permeation enhancement in comparison to stored corneas due to the undamaged epithelium layers in fresh corneas. Ultimately this finding can lead to the development of an *in-vitro* corneal model mimicking the *in-vivo* response at a fraction of the cost of *in-vivo* studies and in conventional laboratory settings.

In conclusion, a porcine *in-vitro* eye model was developed to assess hydrophobic and hydrophilic drug permeation through anterior and posterior ocular tissues. The porcine *in-vitro* eye model shows good correlation with the human *in-vitro* model providing strong evidence that the porcine *in-vitro* eye model can be used to screen potential formulations before testing *in-vivo* using the porcine model which ultimately might correlate well with the *in-vivo* human responses. The development of an *in-vitro* eye model for permeation studies is crucial for screening of potential formulations. However, this type of models can provide only limited information about the effect of the formulation components on the ocular tissue, hence in the next chapter two methods were investigated to determine the toxicity of formulations components.

**Chapter Five: *In-Vitro* Cytotoxicity of Modified Amphiphilic  
Polymers**

---

## 5.1 Introduction

Today, a plethora of emerging novel drug delivery systems such as nanoparticles and polymeric implants have been developed to deliver drugs to the anterior and posterior ocular tissues (Bourges *et al.*, 2006; Yang *et al.*, 2013). These systems might offer many advantages over marketed formulations such as prolonged drug release and less frequent dose application (Bhatta *et al.*, 2012; Kompella & Edelhauser, 2011). However, it is essential to evaluate the *in-vitro* biocompatibility of these formulations to determine whether these formulations can progress further to *in-vivo* testing and ultimately be introduced to the market as a commercial product.

*In-vitro* cell culture studies allow the screening of potential formulations before performing expensive *in-vivo* experiments. Some of the most common used *in-vitro* ocular cell culture models are listed in Table 5-1.

**Table 5-1:** Most common *in-vitro* ocular cell culture models

<b><i>In-vitro</i> Model</b>	<b>Cell Type</b>	<b>Applications</b>	<b>Advantages / Disadvantages</b>	<b>Reference</b>
<b>EpiOcular™</b>	Human derived epidermal keratinocytes	Ocular irritation determination	Cornea like 3D tissue structure. Excellent correlation <i>in-vivo</i> to <i>in-vitro</i> test Results. Unsurpassed long term tissue reproducibility Lot to lot, year to year	(Kolle, Kandárová, Wareing, van Ravenzwaay & Landsiedel, 2011; Pfannenbecker <i>et al.</i> , 2013)
<b>TMC</b>	Primary human trabecular meshwork cells	Toxicity and permeability studies	culture time 3-4 weeks	(Kernt <i>et al.</i> , 2009)
<b>HCE</b>	Primary human corneal epithelial cells	Toxicity and ocular irritation determination	culture time 3-4 weeks	(Geerling, Daniels, Dart, Cree & Khaw, 2001; Hornof, Toropainen & Urtti, 2005)
<b>HCE-T</b>	Transfected immortalised human corneal epithelial cells	Toxicity, permeability studies and prediction of ocular pharmacokinetics	HCE-T cells form a stratified culture when grown at the air-liquid interface on a collagen membrane in serum free medium. Similar barrier properties to isolated corneal tissue. Higher TEER values in	(Hornof, Toropainen & Urtti, 2005; Kruszewski, Walker & DiPasquale, 1997)
<b>HCE-S</b>	Spontaneously immortalised human corneal epithelial cells	Cell biology and gene regulation studies	HCE-S can be cultured in a simple DMEM and only serum-based media. expression of characteristic markers similar to primary cells such as cytokeratin 3, PAX 6, integrins $\beta 1$ and $\gamma 9$	(Notara & Daniels, 2010)
<b>H1RPE7</b>	Transfected immortalised human retinal pigment epithelial cells	Toxicity, permeability studies and transplantation studies	Expression of cytokeratins, and displaying junctional distribution of ZO-1, p100-p120 and beta-catenin. Exhibit a strong growth potential	(Kanuga <i>et al.</i> , 2002)
<b>ARPE-19</b>	Spontaneously immortalised human retinal pigment epithelial cells	Toxicity and permeability studies	Time course of tight-junction formation reached a maximum of 50-100 $\Omega \text{cm}^2$ after 4 weeks	(Dunn, Aotaki-Keen, Putkey & Hjelmeland, 1996)

Although *in-vitro* analysis is able to provide basic information about the interaction between the cell and the delivery system, it might not be a true representation of the *in-vivo* results. Unlike *in-vivo* studies, *in-vitro* cell culture studies have typically homogenous cells and a controlled physiochemical environment. For example, corneal epithelia cells grown *in-vitro* lack the morphological diversity of those observed *in-vivo*. The latter consists of five to seven layers of superficial, wing and basal cells with tight junctions (Hao, Li, Kao & Liu, 2010). The superficial cells are flat cells with surface microvilli, whereas wing and basal cells have no surface microvilli and adapt wing-like and cuboidal shapes, respectively (Holland, Mannis & Lee, 2013). The tight junction complexes also differ between the superficial, wing and basal cells. The controlled *in-vitro* physiological environment is also lacking of the complex physiological conditions present *in-vivo*. One example is the tear film covering the corneal epithelial cells (Ohashi, Dogru & Tsubota, 2006) which is not recreated in any current *in-vitro* model.

*In-vitro* biocompatibility tests have been developed to predict biological reactions to materials/excipients when they are in contact with cells in the body. The determination of the toxicity and biocompatibility of new emerging formulations can be examined using a number of *in-vitro* biocompatibility tests. The most common *in-vitro* biocompatibility tests are the haemolysis assay, histological examination and cytotoxicity assays. The haemolysis assay is irrelevant to ocular formulations as the majority of formulations are applied topically or through intravitreal injections (no direct contact between the formulation and blood cells). Histological examination of ocular tissues has previously been used to determine the toxic effect of materials or formulations

(Bourges *et al.*, 2003; Huhtala *et al.*, 2009; Prow, 2010). However this approach is limited by the complex tissue preparation methods which might alter the structure of the tissue under study or introduce artifacts such as uneven shrinkage, wrinkles and folds and dye precipitates (Cormack, 2001; Dartt, Dana, D'Amore & Niederkorn, 2011). The most common methods of assessing the toxicity of materials or formulations are cytotoxicity assays such as trypan blue, lactate dehydrogenase (LDH) and methylthiazole tetrazolium (MTT) based assays (Chang, Wu, Tseng, Kuo & Tseng, 2007; Huhtala *et al.*, 2009; Spitzer *et al.*, 2006). In the trypan blue method, dead cells which are unable to maintain an intact cell membrane are stained with trypan blue. In contrast, viable cells with an intact cell membrane are able to prevent trypan blue uptake and therefore appear clear under light microscopy. The unstained cells reflect the total number of viable cells, whereas the stained cells reflect the total number of dead cells. Trypan blue strongly binds to proteins which results in a high false value of viability, and thus, there should not be proteins in the medium when analysing cell viability (Picot, 2004). Also this method suffers from the subjective manual counting of cells, and therefore it requires the use of flow cytometry which is not available in all laboratory settings (Katsares *et al.*, 2009; Stone, Johnston & Schins, 2009). LDH is a soluble enzyme that is normally found within the cell cytoplasm, it serves as an indicator of cell death as it is released into the extracellular medium subsequent to cellular membrane damage. The LDH assay is a less sensitive method than the MTT and in some cases it can produce false positive result (Fotakis & Timbrell, 2006; Hillegass *et al.*, 2010). The MTT assay is based on reduction of MTT into formazan in active mitochondria within viable cells by mainly mitochondrial succinate dehydrogenase or similar reducing molecules (i.e. NADH) that transfer

electrons to MTT (Marshall, Goodwin & Holt, 1995). The reduced water insoluble formazan is subsequently solubilized by dimethyl sulfoxide (DMSO) and quantified using a visible light spectrophotometer. The absorbance value is representative of both cell number and the metabolic activity of cells. It is worth mentioning that the metabolic activity of cells may vary by different conditions or chemical treatments (the chemical nature of the supplements) which might cause significant variation in results obtained from this assay (Riss *et al.*, 2004; Wang, Henning & Heber, 2010). The MTT assay has been used in investigating proliferation as well as material toxicity (Berridge, Herst & Tan, 2005; Organisation for Economic Co-operation and Development, 2009).

The selection of the assays to be used will depend on many factors such as the desired endpoint (i.e. material toxicity, cell viability, cell proliferation or damage to the cell membrane), the cost, simplicity, reproducibility and the time required to perform the assay. Despite the limitations of the MTT assay, such as the multi-step protocol (i.e. removal of culture medium) and the use of organic solvent (DMSO), MTT is still one of the most commonly used cytotoxicity assays in biological sciences (Riss *et al.*, 2004). Da Costa *et al.* compared MTT to the aforementioned assays (trypan blue and LDH) in human cultured epithelial cells and found MTT was the most sensitive assay alongside other advantages such as speed and simplicity (Da Costa, de Assis, de Andrade Marques & Plotkowski, 1999).

In recent years, many cytotoxicity assays have been investigated with the aim of establishing a rapid and robust assay without the limitations associated with the MTT assay. AlmarBlue is resazurin based assay used in measuring cell viability. Similar to MTT, the non-fluorescent resazurin dye penetrates cells where

it is converted by the intracellular enzymes into a fluorescent dye (resorufin). AlmarBlue is easy to use and has been shown to be more sensitive than the MTT assay (Hamid, Rotshteyn, Rabadi, Parikh & Bullock, 2004). Furthermore, this assay was shown to have better linearity with cell number, its activity was not cell line dependent, non-destructive, easy to handle, and less time consuming in comparison to MTT assay (Bopp & Lettieri, 2008; Patel, Zaveri, Zaveri, Shah & Solanki, 2013). PrestoBlue<sup>®</sup> is a new dye reagent based on the resazurin dye introduced by Invitrogen; the new reagent enables a more rapid cellular uptake of the dye (Hamalainen-Laanaya & Orloff, 2012; "Invitrogen," 2013). PrestoBlue<sup>®</sup> is quickly reduced by metabolically active cells, providing a quantitative measure of viability and cytotoxicity in a time frame of only 10 min. The manufacturer of this reagent listed PrestoBlue<sup>®</sup> as the most sensitive viability assay from a panel consisting of MTT, XTT, AlmarBlue and Resazurin ("Invitrogen," 2013). The sensitivity of this reagent is 12 cells per well compared to 1000 cell per well for MTT assay ("Invitrogen," 2013). This reagent has not yet been reported as being used as a viability test for ocular subcultures, and hence PrestoBlue<sup>®</sup> was used to determine the viability of corneal epithelium cell line as a proof of concept in this work.

Due to the unique structure of the eye, the *in-vitro* biocompatibility of materials used in ocular drug delivery can mainly be performed on two types of cells, namely corneal epithelial cells; representing the anterior segment of the eye, and retinal pigment epithelial (RPE) cells; representing the posterior segment of the eye. In this work, two cytotoxicity assays namely MTT and PrestoBlue<sup>®</sup> have been used to assess the toxicity of the modified polymers in eye cell cultures (H1RPE7 and HCE-S).

### 5.1.1 Human Retinal Pigment Epithelial Cell line

The H1RPE7 cell line is an immortalized RPE cell line derived from primary human retinal pigment epithelial cells acquired from a 50-year-old female Caucasian donor (Lund *et al.*, 2001). This is an adherent cell line and the morphology of the cells are polygonal (Figure 5.1). The H1RPE7 cell line was obtained by genetically modifying the primary cells (cells taken directly from living tissue) with a construct encoding SV40 large T antigen to extend the cell line *in-vitro* lifespan (Lund *et al.*, 2001). This cell line retains many of the morphologic and biochemical characteristics of primary cells and expresses cytokeratins and junctional protein zonula occludens-1 (ZO-1). Therefore, it is similar to RPE cells *in-vivo* and other RPE cell lines such as ARPE-19 (Kanuga *et al.*, 2002). This cell line has the advantage of a short culture time (typically 3 d) and is easy to maintain compared to primary RPE cells. Additionally, it has an extended lifespan and maintains unaltered characteristics with high number of passages (Hahne & Reichl, 2011). The P-glycoprotein efflux pump has recently been identified in the apical and basolateral cell membranes of human RPE and in pig RPE (Constable, Lawrenson, Dolman, Arden & Abbott, 2006; Pitkänen, Ranta, Moilanen & Urtti, 2005). The H1RPE7 cell line has the advantage of having P-Glycoprotein (P-gp) efflux pump unlike the ARPE-19, making this cell line more suitable for *in-vitro* drug transport studies (Constable, Lawrenson, Dolman, Arden & Abbott, 2006).

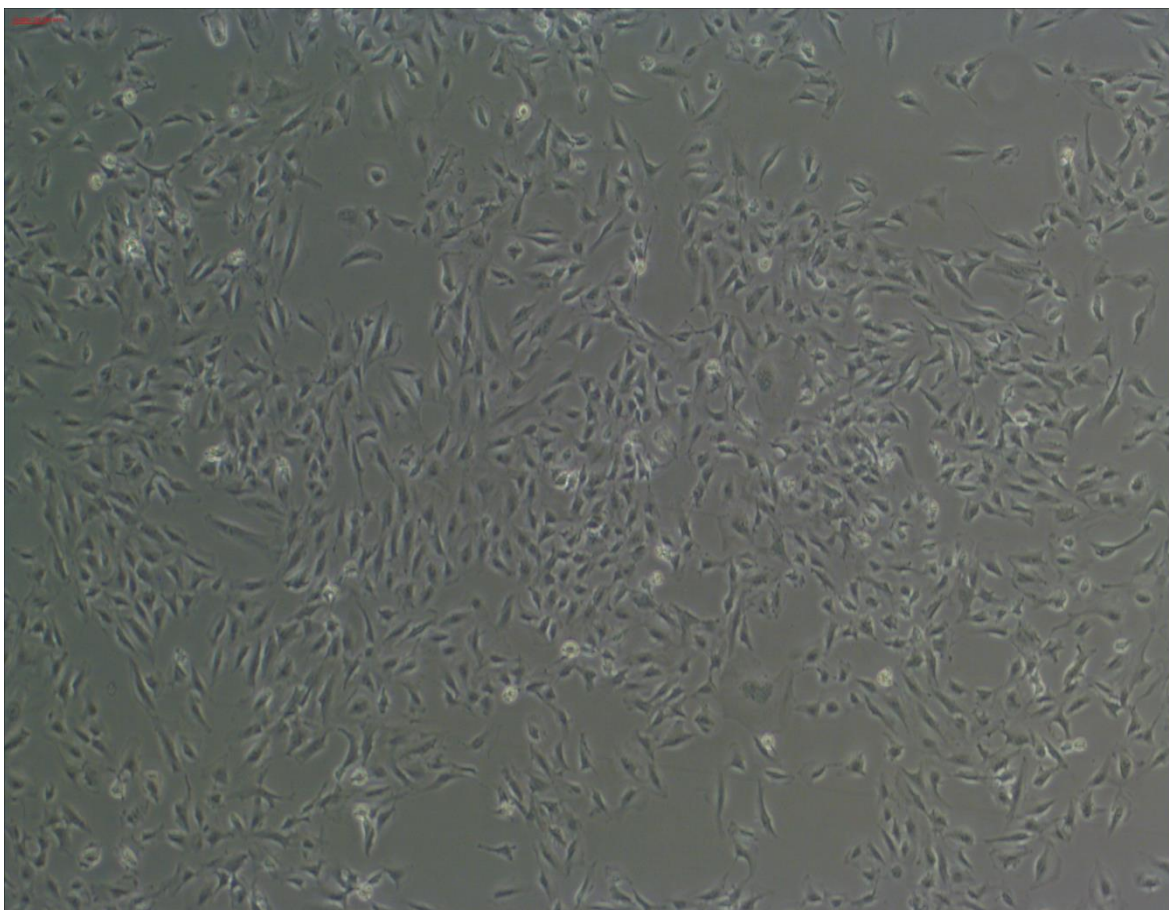


**Figure 5.1:** Phase contrast image of H1RPE7 cells grown in culture medium at day three.

### **5.1.2 Human Corneal Epithelial Cell Line**

The HCE-S cell line is a new immortalized adherent corneal epithelial cell line which was passaged spontaneously until reaching over 100 cell duplications (Notara & Daniels, 2010). The cell line was derived from primary human corneal epithelial (HCE) cells and it has similar morphology (hexagonal cells, Figure 5.2) to the primary corneal epithelial cells (Notara & Daniels, 2010). The HCE-S cell line expresses cytokeratin and has tightly packed cells mimicking the tight junctions in the corneal epithelium layer (Notara & Daniels, 2010). The cell line has advantages over other HCE cell lines, including the fact that they can be cultured in a simple Dulbecco's Modified Eagle Medium (DMEM) without the need for supplements such as insulin. Additionally, it can also be cultured without

extracellular matrix (ECM) coating on tissue culture plastic (Notara & Daniels, 2010). HCE cell lines have been used in corneal epithelial wound healing and as an eye irritation test to toxicologically assess chemicals (Cho *et al.*, 2012; Li *et al.*, 2013).

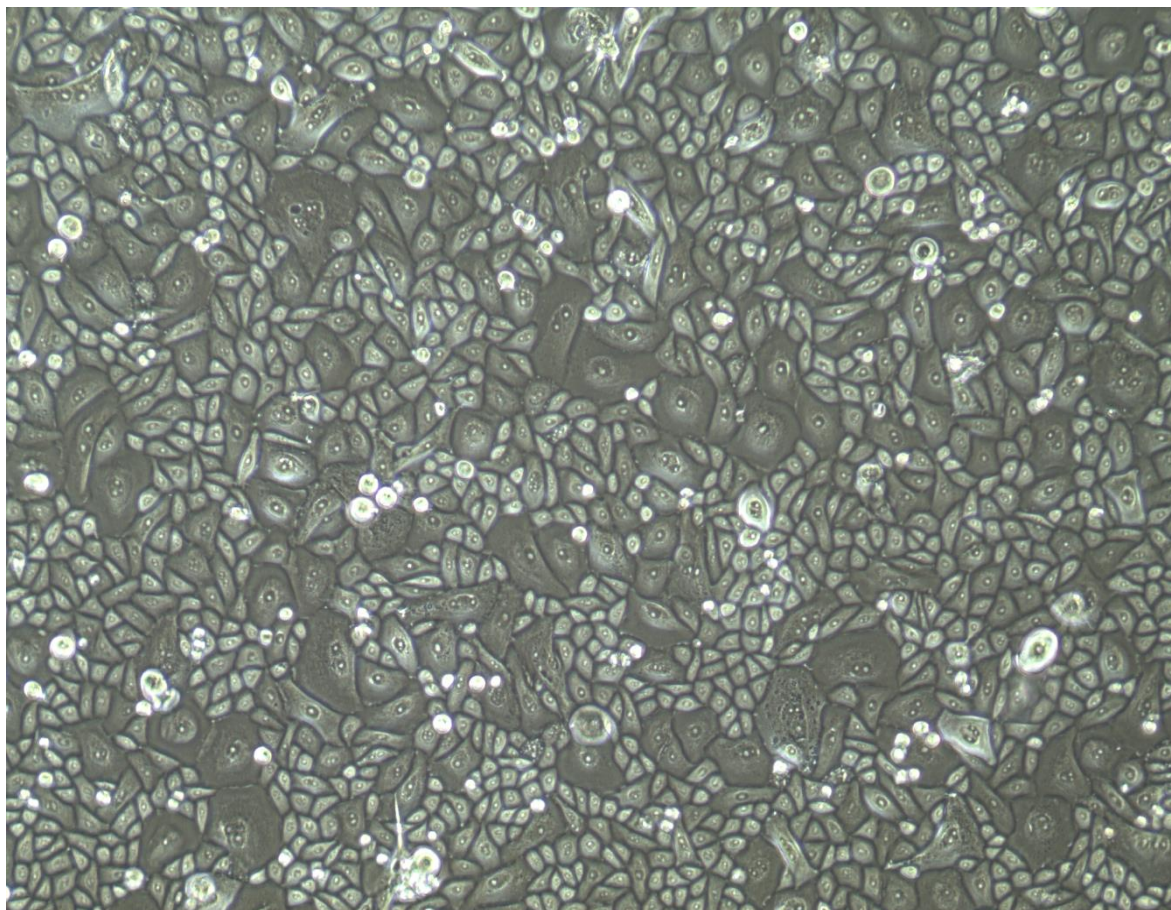


**Figure 5.2:** Image of HCE-S cells grown in culture medium at day two.

### 5.1.3 MTT Assay

The MTT assay is a modified method adapted from Mosmann *et al.* (Mosmann, 1983). The assay is based on the reduction of the water soluble yellow tetrazolium salt (MTT) by mitochondrial dehydrogenase into a blue water insoluble formazan dye (Vega-Avila & Pugsley, 2011). The formazan crystals are soluble in dimethyl sulfoxide (DMSO) so can be recovered at the end of the assay and

formazan concentration quantified measuring absorbance at 550 nm. The measured values are directly proportional to the number of living cells (Gerlier & Thomasset, 1986; Mosmann, 1983). The IC<sub>50</sub> value (the polymer concentration at which 50% of the cells is viable) can be calculated by plotting the determined cell viability (as a percentage of the total cells) versus polymer concentration.

#### 5.1.4 PrestoBlue<sup>®</sup> Assay

PrestoBlue<sup>®</sup> is a non-fluorescent blue dye reagent based on resazurin (7-Hydroxy-3H-phenoxazin-3-one-10-oxide). The PrestoBlue<sup>®</sup> reagent is a cell permeant dye, upon entering the cytosol of active cells it is converted from resazurin form to resorufin which exhibit fluorescence property and it is red in colour (O'Brien & Pognan, 2001). The assay can be quantified by measuring either the absorbance at 570 or 600 nm or by fluorescence, measuring the excitation and emission wavelengths at 560 and 590 nm, respectively. The rate at which PrestoBlue<sup>®</sup> is reduced is proportional to the number of viable cells.

#### 5.1.5 Aims and Objectives

The aim of the work described in this chapter was to assess the *in-vitro* cytotoxicity of PAA and hydrophobically modified PAA polymers described in chapter two on RPE and corneal epithelial cell lines. The objectives were:

- To compare the cytotoxicity of the Pa<sub>5</sub>, Pa<sub>5</sub>-MPEG, Ch<sub>5</sub> and Da<sub>10</sub> polymers to the unmodified PAA
- To establish the IC<sub>50</sub> for the aforementioned polymers in the RPE cell lines
- To assess the viability of corneal epithelium cell line using new assay (PrestoBlue<sup>®</sup>) as a proof of concept.

## 5.2 Materials and Methods

### 5.2.1 Materials

Nutrient mixture F-10 ham (with sodium bicarbonate, without L-glutamine), heat inactivated fetal bovine serum, L-glutamine solution (200 mM), 3-[4,5-dimethylthiazol-2-yl]-2,5-diphenyltetrazolium bromide (thiazolyl blue tetrazolium blue (MTT), glycine, sodium chloride, tween<sup>®</sup> 80, L-glutamic acid, penicillin-streptomycin (10,000 units penicillin and 10 mg streptomycin per mL in 0.9% w/v NaCl) and trypsin-EDTA solution 10X (0.5% v/v) were all purchased from Sigma Aldrich, United Kingdom. Phosphate buffer saline (PBS) tablets, dimethyl sulfoxide, triton X (10x) and all solvents (HPLC grade) were supplied by Fisher, United Kingdom. PrestoBlue<sup>®</sup> cell viability reagent, Dulbecco's modified eagle medium (Gibco<sup>®</sup> DMEM), adult bovine serum (Gibco<sup>®</sup>) and penicillin/streptomycin (Gibco<sup>®</sup>) were acquired from Invitrogen, United Kingdom. Triamcinolone Acetonide micronized powder (TA) was obtained from Fagron, United Kingdom. Human retinal pigment epithelial cell line (H1RPE7) was purchased from the health protection agency (HPA, United Kingdom). The HCE-S cells used in this work were courtesy of Dr. Moore, University of Ulster.

### 5.2.2 Cell Resuscitation and Freezing

The frozen cell stock was heated in a water bath for 1-2 min at 37 °C until fully thawed. The ampoule was cleaned by tissue soaked with 70% (v/v) alcohol prior to opening. The whole content of the ampoule was pipetted in 25 cm<sup>2</sup> flask containing 10 ml of pre warmed culture medium. Cells were grown for three days at 37 °C in a humidified atmosphere containing 5% v/v CO<sub>2</sub>. The grown cells were

sub-cultured in three 75 cm<sup>2</sup> flask (15 ml of culture medium) as described in section 5.2.4.1.

The establishment of a cell line bank were made as follows. Cells from 75 cm<sup>2</sup> flask were trypsinized as described in section 5.2.4.1. The detached cells were thoroughly dispersed in 15 mL of culture medium and counted before transferred to centrifuge tube (15 ml sterile centrifuge tube). The tube was span at 5004 G force (1500 rpm) for 5 min. The supernatant was decanted using pipette, the cells pellet was then re-suspend in freezing medium (10% (v/v) DMSO in cell culture medium) before transferring into cryovials. The cryovials were transferred immediately to -80 °C overnight before permanent storage in liquid nitrogen.

### **5.2.3 Heat-inactivation of Fetal Bovine Serum**

The fetal bovine serum was thawed in a water bath for 1-2 h at 37 °C and gently mixed. The serum was then immersed in 56 °C water bath and incubated for 1 h. The heat inactivated serum were then transferred into 50 mL sterile centrifuge tube and stored at 4 °C in a fridge.

### **5.2.4 H1RPE7 Cell Growth Medium**

The H1RPE7 culture medium was prepared under aseptic conditions. The culture medium consisted of nutrient mixture F-10 ham (500 mL) supplemented with 20% v/v heat-inactivated fetal bovine serum (125 mL), 2 mM L-Glutamine solution (6.4 mL) and 100 U mL<sup>-1</sup> penicillin, 100 µg mL<sup>-1</sup> streptomycin (6.4 mL).

#### **5.2.4.1 H1RPE7 Cell Growth and Sub-culture**

The H1RPE7 cells were grown in 15 mL of the culture medium for three days in 75 cm<sup>2</sup> cell culture flasks at 37 °C in a humidified atmosphere containing 5% v/v CO<sub>2</sub>. The culture medium was aspirated after two days and replaced with

fresh medium. On the third day post-seeding, the cells were sub-cultured when approximately 90% confluent. This was achieved by washing the cells three times with sterilised PBS pH 7.4 buffer (5 mL, 10 mM) followed by one wash with trypsin-EDTA (3 mL, 0.05% w/v) to dislodge the cells attached to the surface of the flask. The detached cells were thoroughly dispersed in 15 mL of culture medium and sub-divided into three 75 cm<sup>2</sup> cell culture flasks before adding 10 mL of culture medium to each flask. Cells between passages 15 and 18 were used for cell viability test experiments.

### **5.2.5 MTT and Glycine Buffer Preparation**

MTT (50 mg) was dissolved in 10 mL of sterile PBS buffer, the solution was then filtered and stored immediately in the fridge for further use. Glycine (3.75 g) and 2.93 g of NaCl was dissolved in 450 mL of sterile water; the pH of the solution was then adjusted by the addition of sodium hydroxide solution (1 M) until pH 10.5 (pH meter 209, HANNA<sup>®</sup> Instruments, United Kingdom) was reached, before topping the solution volume to 500 mL.

### **5.2.6 L-glutamic acid and tween 80 Solution Preparation**

L-glutamic acid (20 mg) was dissolved in 10 mL of H1RPE7 culture medium. From this stock solution, five concentrations (0.06 - 1 mg mL<sup>-1</sup>) were prepared by serial dilution using H1RPE7 culture medium as the diluent. Tween 80 (40 mg) was dissolved in 40 mL H1RPE7 culture medium. From this stock solution seven concentrations (0.01 - 0.5 mg mL<sup>-1</sup>) were prepared by serial dilution using H1RPE7 culture medium as the diluent.

### 5.2.7 H1RPE7 Cell Viability Test

PAA and hydrophobically modified polymers, namely Pa<sub>5</sub>, Pa<sub>5</sub>-MPEG, Ch<sub>5</sub> and Da<sub>10</sub> were dissolved separately in sterile water (4 mg mL<sup>-1</sup>) and sonicated for 5 min. The polymeric colloidal solutions (0.5 mL) were then diluted in culture media (4.5 mL) to form a 0.4 mg mL<sup>-1</sup> solution. From the stock solutions, ten concentrations (0.2-3.9 x 10<sup>-4</sup> mg mL<sup>-1</sup>) were prepared by serial dilution using culture medium as a diluent. The H1RPE7 cells were seeded in exponential growth phases in 96-well plates at 1x10<sup>4</sup> cells per well in 200 µL of culture medium. The 96-well plate was then incubated for two days at 37 °C in 5% v/v CO<sub>2</sub> humidified atmosphere.

On the second day, the culture medium was aspirated and replaced with one of the polymers at a concentration as prepared above (200 µL, 3.9 x 10<sup>-4</sup> - 0.4 mg mL<sup>-1</sup>). Untreated cells cultured in medium were the negative control whereas cells treated with triton X (1:5 PBS) were the positive control. The 96-well plate was incubated for a further 24 h. The following day MTT (50 µL, 5 mg mL<sup>-1</sup>) was added to the 96-well plate before incubation in the dark for 4 h (37 °C with 5% CO<sub>2</sub>). The medium in the wells were carefully aspirated before dissolving any purple formazan complexes in DMSO (200 µL) and adding glycine buffer (25 µL, pH 10.5) to enhance the sensitivity of the MTT (Plumb, Milroy & Kaye, 1989). The 96-well plates were shaken gently for 10 min to ensure the dissolution of formazan before the absorbance was measured using an ELISA reader (Ascend Lab-Systems, United Kingdom) at 570 nm. The cell percentage viability was calculated relative to the positive controls.

## 5.2.8 HCE-S Cell Growth Medium

The HCE-S culture medium was prepared under aseptic conditions. The culture medium consisted of Dulbecco's modified eagle medium (DMEM) (500 mL) supplemented with 10% v/v fetal bovine serum (55 mL) and 1% v/v penicillin/streptomycin (5.5 mL).

### 5.2.8.1 HCE-S Cell Growth and Cell Viability Test

The HCE-S cells were grown in 5 mL of the culture medium in 25 cm<sup>2</sup> cell culture flasks for six days, the cells were maintained at 37 °C in a humidified atmosphere containing 5% v/v CO<sub>2</sub>. Hydrophobically modified polymers (50 mg) were dissolved in sterile water (10 mL) and sonicated for 5 min. The polymeric colloidal solutions (0.5 mL) were then diluted in culture media (4.5 mL) to form 0.5 mg mL<sup>-1</sup> solution. From the stock solutions, five concentrations (0.25 - 1.25 x 10<sup>-2</sup> mg mL<sup>-1</sup>) were prepared by serial dilution using culture medium as a diluent. The HCE-S cells were seeded in 96-well plates at 6x10<sup>3</sup> cells per well in 100 µL of medium. The 96-well plate was then incubated for 24 h at 37 °C in a 5% v/v CO<sub>2</sub> humidified atmosphere. The medium was then aspirated and replaced with one of the polymers at a concentration as prepared above (100 µL, 0.5 - 1.25x10<sup>-2</sup> mg mL<sup>-1</sup>) and incubated for a further 24 h. Untreated cells cultured in medium were the negative control whereas cells treated with triton X (1:5 PBS) were the positive control. PrestoBlue<sup>®</sup> reagent (15 µL) was then added to each well before incubating for 30 min in a 5% v/v CO<sub>2</sub> humidified atmosphere at 37 °C. The fluorescence of the PrestoBlue<sup>®</sup> was measured using a fluorescence microplate reader (BMG LABTECH). The excitation and emission wavelengths were 560 and 590 nm, respectively.

### 5.2.9 Statistical Evaluation

Statistical analysis was performed using SPSS program version 19. The normality of the data was assessed using the Shapiro-Wilk test. Experimental difference between groups was compared with the control using the independent student's *t*-test. Differences were regarded as significant, with  $p \leq 0.05$ .

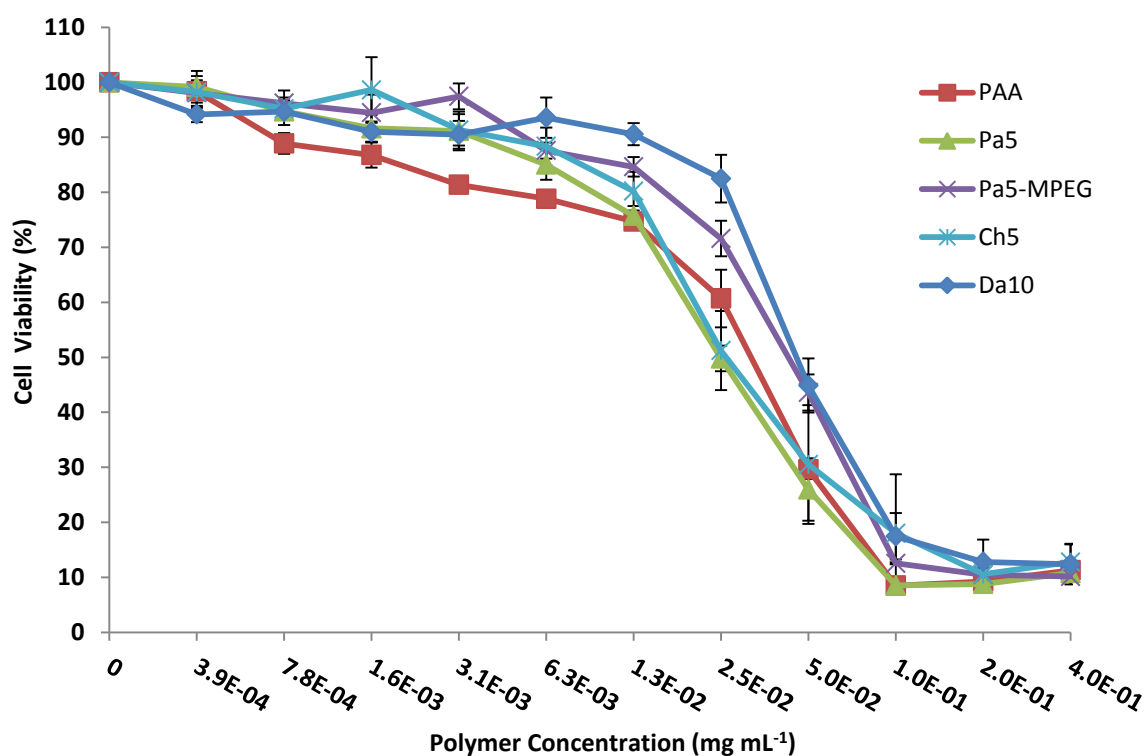
## 5.3 Results

### 5.3.1 Polymer Cytotoxicity Studies

The MTT assay was carried out on RPE cells treated with PAA or PAA modified polymers to determine the polymer concentration at which 50% of the cells population were viable ( $IC_{50}$ ). Polymers with higher  $IC_{50}$  values have a lower cytotoxic effect. The cytotoxicity profiles of all polymers are shown in Figure 5.3. All polymers showed cell viability higher than 75% at  $1.3 \times 10^{-2}$  mg mL<sup>-1</sup> or lower, and less than 15% cell viability at  $1.0 \times 10^{-1}$  mg mL<sup>-1</sup> or higher. The  $IC_{50}$  of RPE cells treated with PAA and modified PAA is shown in Table 5-2. The  $IC_{50}$  values of Da<sub>10</sub> and Pa<sub>5</sub>-MPEG were significantly higher (*t*-test,  $p < 0.05$ ) when compared to the  $IC_{50}$  of PAA.

**Table 5-2:** IC<sub>50</sub> values for RPE cells treated with PAA and modified PAA polymers ( $3.9 \times 10^{-4}$  -  $0.4 \text{ mg mL}^{-1}$ ) for 24 h.

Polymer	IC <sub>50</sub> value on RPE cells ( $\text{mg mL}^{-1}$ ) $\times 10^{-2}$ (mean $\pm$ S.D., n = 4)	IC <sub>50</sub> of modified PAA / IC <sub>50</sub> of PAA
PAA	$3.4 \pm 0.5$	-
Pa <sub>5</sub>	$2.9 \pm 0.5$	0.85
Pa <sub>5</sub> -MPEG	$4.5 \pm 0.4$	1.32
Ch <sub>5</sub>	$3.7 \pm 1.2$	1.09
Da <sub>10</sub>	$4.9 \pm 0.6$	1.4

**Figure 5.3:** MTT results for percentage cell viability of RPE cells exposed to PAA, Pa<sub>5</sub>, Pa<sub>5</sub>-MPEG, Ch<sub>5</sub> and Da<sub>10</sub> (Data represented as mean, error bars represent range, n = 4).

The PrestoBlue<sup>®</sup> toxicity studies showed cell viability of at least 54% for all studied polymers at  $1.3 \times 10^{-2} \text{ mg mL}^{-1}$  (Figure 5.4). This finding is comparable to the result obtained from the RPE cells using MTT assay at  $2.5 \times 10^{-2} \text{ mg mL}^{-1}$ . The PrestoBlue<sup>®</sup> toxicity test also showed Pa<sub>5</sub>-MPEG had higher cell viability (80%) than all other polymers (<20%) at  $2.5 \times 10^{-2} \text{ mg mL}^{-1}$ . A comparison between the

IC<sub>50</sub> of PAA and PAA modified polymers obtained using MTT and PrestoBlue® tests are shown in Table 5-3. The IC<sub>50</sub> of PAA and PAA modified polymers obtained using PrestoBlue® test were similar to the values obtained using the MTT assay.

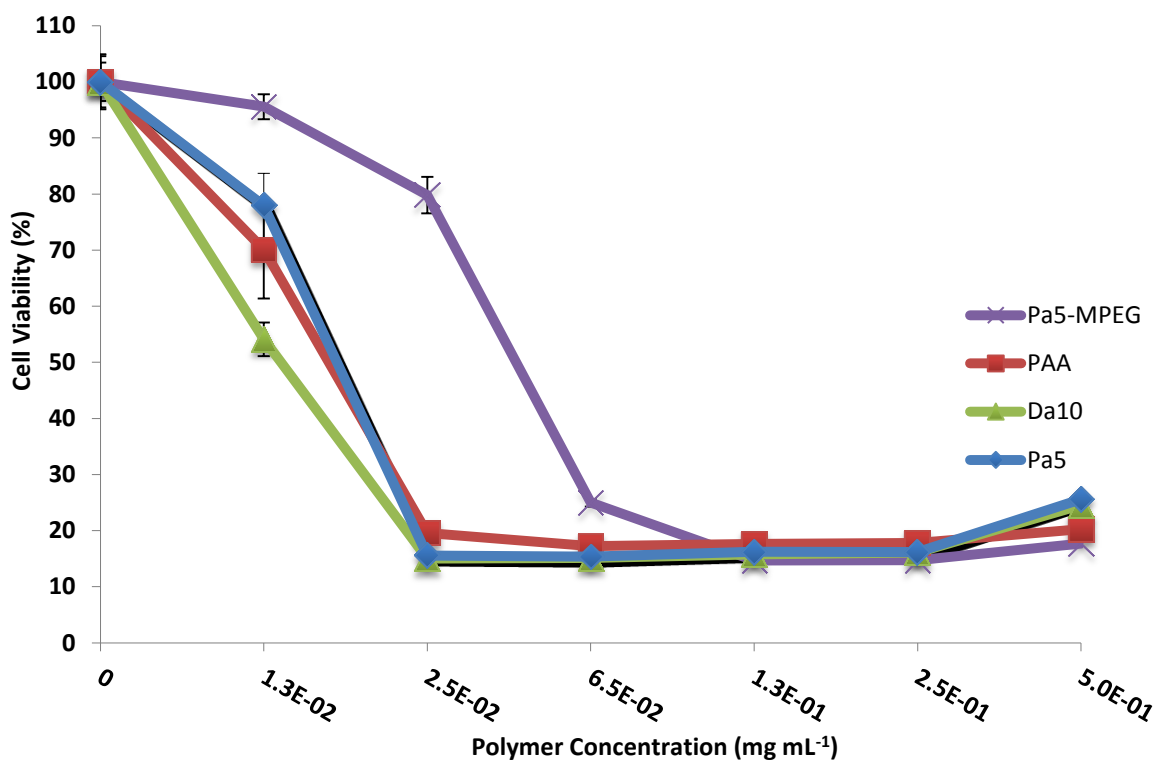


**Figure 5.4:** PrestoBlue® results for percentage cell viability of corneal epithelial cells (HCE-S) exposed to PAA, Pa<sub>5</sub>, Pa<sub>5</sub>-MPEG and Da<sub>10</sub> (Data represented as mean, error bars represent range, n = 4).

**Table 5-3:** IC<sub>50</sub> values for RPE and HCE cells treated with PAA and modified PAA polymers.

Polymer	IC <sub>50</sub> value on RPE cells (mg mL <sup>-1</sup> ) x 10 <sup>-2</sup> (mean ± S.D., n = 4)	IC <sub>50</sub> value on HCE cells (mg mL <sup>-1</sup> ) x 10 <sup>-2</sup> (mean ± S.D., n = 4)
PAA	3.4 ± 0.5	1.9 ± 0.3
Pa <sub>5</sub>	2.9 ± 0.5	2.0 ± 0.3
Pa <sub>5</sub> -MPEG	4.5 ± 0.4	4.7 ± 0.2
Ch <sub>5</sub>	3.7 ± 1.2	-
Da <sub>10</sub>	4.9 ± 0.6	1.4 ± 0.1

### 5.3.2 Permeation Enhancer Cytotoxicity Studies

The toxicity of two enhancers used in chapter four was tested on RPE using the MTT assay, the results of tween 80 and L-glutamic acid are shown in Figure 5.5. The cytotoxicity of the chitosan could not be performed due to it being poorly soluble in cell culture medium pH 7.4. The acetate buffer (pH5) used to dissolve chitosan was not a suitable medium since cells were not viable in an acidic medium after 24 h. Tween 80 at a concentration of  $0.13 \text{ mg mL}^{-1}$  allowed 51% cell viability, whereas higher concentrations resulted in less than 10% cell viability at all concentrations tested. L-glutamic acid showed cell viability of 86% or more at any of the concentrations tested.

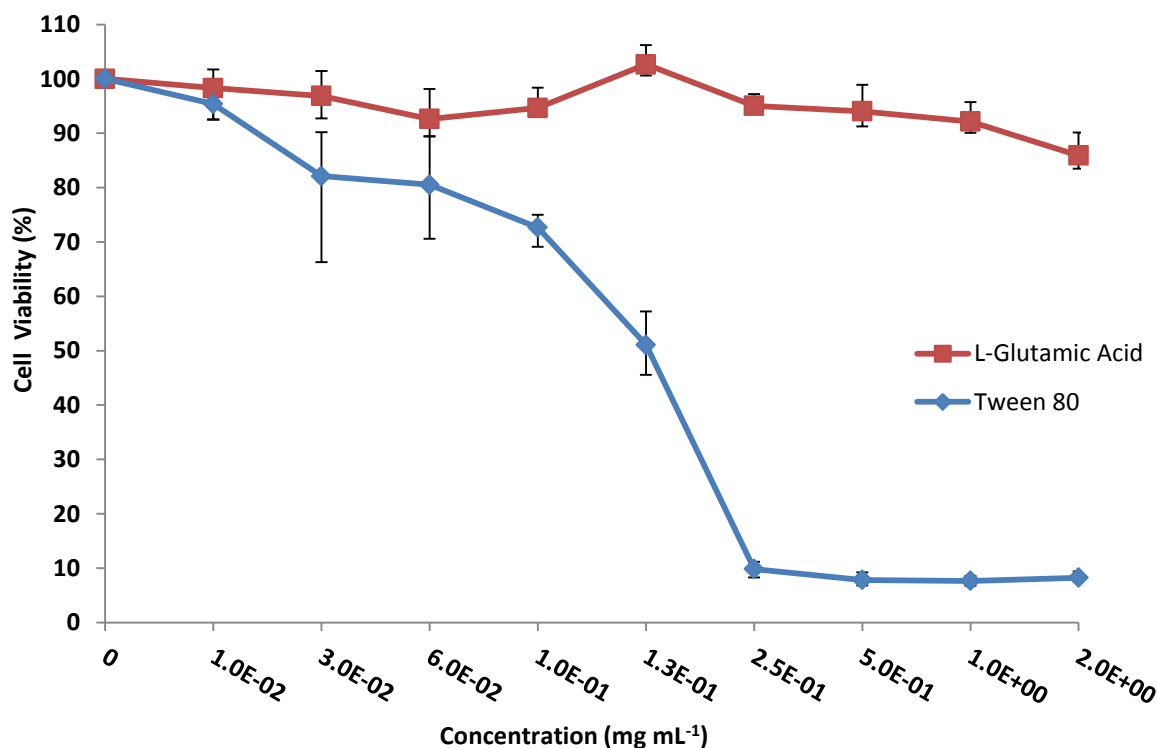


**Figure 5.5:** MTT results for percentage cell viability of RPE cells exposed to Tween 80 and L-Glutamine acid (Data represented as mean, error bars represent range, n = 4).

## 5.4 Discussion

The toxic effect of PAA and hydrophobically modified PAA were tested on HCE-S and RPE cell lines using two cell viability assays.

The MTT assay showed the modification of PAA had minute impact on the cytotoxicity of the polymers to RPE cells. Nevertheless, both Da<sub>10</sub> and Pa<sub>5</sub>-MPEG had higher IC<sub>50</sub> values (i.e. are less cytotoxic) than PAA. The PAA and PAA modified polymers were highly toxic in comparison to other common polymers used in ocular drug deliver such as chitosan (no toxicity up to 2 mg mL<sup>-1</sup>) or poly(D,L-lactide-co-glycolide) (PLGA) which have been found to be nontoxic in ocular tissues (Kompella & Edelhauser, 2011; Sarmiento & das Neves, 2012). The increase in IC<sub>50</sub> of Pa<sub>5</sub>-MPEG might be due to the presence of polyethylene glycol, which is known for its low toxicity (Fruijtier-Pölloth, 2005) and has been used to decrease the cytotoxicity of other polymers via conjugation of polyethylene glycol (PEGylation). Mao *et al.* reported that the PEGylation of different molecular weight trimethyl chitosan (TMC) polymers decreased the cytotoxicity of TMC in a L929 cell line to a great extent. The authors also reported lower toxicity of TMC with the increase in the PEG molecular weight and grafting percentage (Mao *et al.*, 2005). The increase in IC<sub>50</sub> of Da<sub>10</sub> on the other hand might be due to the higher modification percentage in comparison to the rest of the polymers. The modification percentage is directly linked to the number of primary amine groups in the polymer; the higher modification percentage the lower the number of primary amine groups. Reports have shown modification of the primary amines on the polymer backbone results in a lower toxicity than the parent polymer (Aravindan, Bicknell, Brooks, Khutoryanskiy & Williams, 2009; Thomas & Klibanov, 2002). Thompson *et al.* (Thompson, Tetley, Uchegbu & Cheng, 2009) also reported that

modification of the primary amine groups on PAA polymer with palmitoyl decreased its cytotoxicity in Caco-2 cells by 2-3 fold compared to the parent polymer. The authors explained that the lower toxicity of the palmitoyl modified PAA polymers (Pa<sub>2.5</sub> and Pa<sub>5</sub>) is due to the fact it has fewer primary amine groups in comparison to unmodified PAA. They further supported this finding by converting primary amine groups to tertiary amine groups via methyl quaternisation, resulting in a 15 fold increase in the IC<sub>50</sub>. The different trend observed in this study (minute impact on the cytotoxicity profile) compared to Thompson *et al.* (2-3 fold increase in the IC<sub>50</sub>) is possibly due to the different cell lines used in the two experiments. Yeung *et al.* has shown human glial (SVG) cells were 11 times more sensitive than RPE (ARPE19) cells when cells were exposed to TA for one day (Yeung, Chan, Chiang, Pang & Lam, 2003). Similar findings were reported by Nastiti in which he revealed that BALB/c 3T3 cell line was more sensitive than RPE cell line (ARPE 19) in response to 24 h exposure to TA (Nastiti, 2007).

The presence of water (up to 10% v/v) in the culture medium as a consequence of diluting the polymer solution (sections 5.2.7 and 5.2.8.1) would change the osmolality of the medium, and hence this might have an effect on cell viability. The particle size and the stability of the formulation in culture medium were not tested in this work. Proteins deposition on the particulate surface might have impact on the surface charge and hence particle stability.

The low impact of hydrophobic modification on the IC<sub>50</sub> of RPE cells found in this work is in good agreement with the findings of Hoskins (Hoskins, 2010). Hoskins observed little difference between the IC<sub>50</sub> of PAA modified polymer (Ch<sub>5</sub> and Da<sub>10</sub>) and the unmodified PAA backbone when assessed in Caco-2 cell line.

The PAA, Da<sub>10</sub> and Ch<sub>5</sub> had IC<sub>50</sub> values of 2.3x10<sup>-2</sup>, 2.5x10<sup>-2</sup> and 3.7x10<sup>-2</sup> mg mL<sup>-1</sup>, respectively. Although the author used different cell line, the IC<sub>50</sub> values were comparable to the IC<sub>50</sub> values found in this work.

The MTT assay was also used to study the cytotoxicity effect of the enhancers used in chapter four on the RPE cell line only (due to the limited availability of the human corneal epithelial cells). The results showed that both tween 80 and L-glutamic acid were non-toxic at the concentrations applied in the permeation enhancer studies performed in chapter four. However, RPE percentage cell viability decreased with increasing concentration of tween 80. Although PAA modified polymers were significantly more cytotoxic than tween 80, the latter at 0.01% (w/v) had a very low solubilising capacity (19 µg mL<sup>-1</sup> as demonstrated in chapter three) compared to the PAA modified polymers. In order to achieve comparable solubilising capacity to the PAA modified polymers much higher tween 80 concentrations would have to be used and hence it will result in a higher toxicity, with the RPE cells displaying less than 10% cell viability.

The MTT assay is considered to be a cytotoxic end point assay, as the formazan crystals formed from the reduction of the MTT salt must be solubilized with dimethyl sulfoxide (DMSO) or HCl/isopropanol. The aforementioned solubilisers destroy the cells under investigation and therefore time course experiments cannot be carried out (Rampersad, 2012). PrestoBlue® reduced by dehydrogenases and reductases and does not require an intermediate electron acceptor; this might be the reason behind the reported higher sensitivity of resazurin based assays. Unlike MTT, PrestoBlue® is a non-toxic dye (Larson, Doughman, Gregerson, & Obritsch, 1997) and it is stable in culture media, which enables the continuous *in-vitro* measurement of cell proliferation or delayed cytotoxic effect.

Furthermore, the PrestoBlue® dye does not require a long incubation time in comparison to the MTT assay, a typical incubation time for toxicity test being between 10 min to 2 h (Allen *et al.*, 2013; Baehring *et al.*, 2013; Nikolajski, Wotschadlo, Clement, & Heinze, 2012). The PrestoBlue® assay overcomes the previously mentioned limitations of the MTT assay. In addition, it offers advantages over the MTT assay such as being a one step protocol and having higher sensitivity (Hamid, Rotshteyn, Rabadi, Parikh & Bullock, 2004; "Invitrogen," 2013). The reported PrestoBlue® sensitivity is 12 cells per well in comparison to 1000 cell per well for the MTT assay (Boncler, Różalski, Krajewska, Podśędek & Watała, 2013; "Invitrogen," 2013).

There are a few publications reporting this assay (Allen *et al.*, 2013; Baehring *et al.*, 2013), however none of these reports have used PrestoBlue® on corneal or RPE cell lines, hence the feasibility of using the PrestoBlue® assay in corneal epithelial cells has been demonstrated in this work. In this study the PrestoBlue® assay showed comparable polymer cytotoxicity results to the one obtained using the MTT assay on the RPE cell line at low and high polymer concentrations ( $1.3 \times 10^{-2}$  mg mL<sup>-1</sup> and concentrations higher than  $5 \times 10^{-2}$  mg mL<sup>-1</sup>). However, unlike the MTT assay at  $2.5 \times 10^{-2}$  mg mL<sup>-1</sup> the PrestoBlue® assay showed Pa<sub>5</sub>-MPEG had considerably higher cell viability compared to the other tested polymers. This may be due to the higher sensitivity of the PrestoBlue® assay.

### 5.5 Conclusion

The cytotoxicity of the Pa<sub>5</sub> and Ch<sub>5</sub> polymers were not significantly (*t*-test, *p* > 0.05) changed in comparison to the PAA in both RPE and corneal epithelia cells

lines. Despite the fact that Da<sub>10</sub> and Pa<sub>5</sub>-MPEG had significantly (*t*-test,  $p < 0.05$ ) higher IC<sub>50</sub> the IC<sub>50</sub> of PAA, they had little impact on the safety profile of PAA.

The RPE and corneal epithelial cells are useful cell lines to test the toxicity of new materials or delivery systems targeting the posterior and anterior segment of the eye. Both MTT and PrestoBlue<sup>®</sup> assays can be used to determine the cytotoxicity of the polymers. However, PrestoBlue<sup>®</sup> would appear to offer some advantages over the MTT assay in terms of simplicity and shorter incubation time.

**Chapter Six: General Discussion**

---

## 6.1 Discussion

The first amphiphilic polymers (block copolymers) were prepared in early 1950s (Velichkova & Christova, 1995). In the early 1980s, amphiphilic polymers were shown to form nano sized self-assemblies (SA) and exhibit potential as hydrophobic drug solubilisers (Hoskins, Lin & Cheng, 2012). A decade later in the 1990s, extensive research had been conducted to explore the ability of these nanoparticles to encapsulate ophthalmic drugs and overcome ocular physiological barriers (Alonso, 2004; Liu, Jones & Gu, 2012). Polymeric nanoparticles have been reported to prolong drug residence time in the eye (Bourges *et al.*, 2003; Chaiyasan, Srinivas & Tiyaboonchai, 2013; Nagarwal, Kumar & Pandit, 2012) and to increase corneal drug permeability, through the epithelial uptake of drug loaded nanoparticles and via altering the corneal epithelia cells tight junctions (Contreras-Ruiz *et al.*, 2011; Enriquez de Salamanca *et al.*, 2006). In order to prepare nano sized SA, four amphiphilic polymers (Pa<sub>5</sub>, Pa<sub>5</sub>-MPEG, Ch<sub>5</sub> and Da<sub>10</sub>) were synthesised by attaching three hydrophobic groups namely, palmitoyl, cholesteryl and dansyl (Pa, Ch and Da) and a hydrophilic (MPEG) group onto a poly(allylamine) backbone. The four comb-shaped amphiphilic polymers were synthesised with a high yield (>81%) and good reproducibility. The presence of the attached groups was confirmed and quantified using elemental analysis, DSC and NMR spectroscopy. The DSC thermograms of the Pa<sub>5</sub>, Ch<sub>5</sub> and Da<sub>10</sub> amphiphilic polymers revealed the amorphous nature of the aforementioned polymers, whereas the Pa<sub>5</sub>-MPEG polymer had a crystalline nature. The <sup>1</sup>H NMR and elemental analysis confirmed the presence of the attached Pa, Ch, Da and MPEG groups onto a poly(allylamine) backbone and showed that the percentage mole modification (8.9% Pa, 6.2% Ch, 3.4% MPEG and 9.6% Da) of the attached

moieties was similar to the initial feed ratios (5% initial feed ratio for Pa, Ch and MPEG, 10% initial feed ratio for Da).

The formation of SA of the amphiphiles in aqueous media was confirmed using PCS, TEM and a hydrophobic probe (pyrene). The study demonstrated that the type of moiety attached onto the PAA backbone had a significant influence on the CAC, SA hydrodynamic size and the SA surface charge. In an aqueous environment all four amphiphiles were capable of forming spontaneous nano SA comprising of a hydrophobic inner core (Figure 6.1). The SA were shown to have a hydrodynamic diameter of 114-314 nm. The 5% hydrophobically modified polymers (Pa<sub>5</sub>, Ch<sub>5</sub> and Pa<sub>5</sub>-MPEG) formed uniform single size population aggregates, whereas the 10% modified polymer (Da<sub>10</sub>) had a bimodal size distribution. The bimodal size distribution of Da<sub>10</sub> was due to the presence of small compact assemblies (approximately 40 nm) formed due to greater hydrophobic interactions, alongside larger loose assemblies (100-400 nm) (Chiu, Chern, Lee & Chang, 1998; Wang, Tan, Huang, Che & Du, 2009). The Ch<sub>5</sub> amphiphilic polymer had the lowest CAC (0.0052 mg mL<sup>-1</sup>) and the lowest core polarity in comparison to Pa<sub>5</sub> (0.011 mg mL<sup>-1</sup>) and Pa<sub>5</sub>-MPEG (0.027 mg mL<sup>-1</sup>).

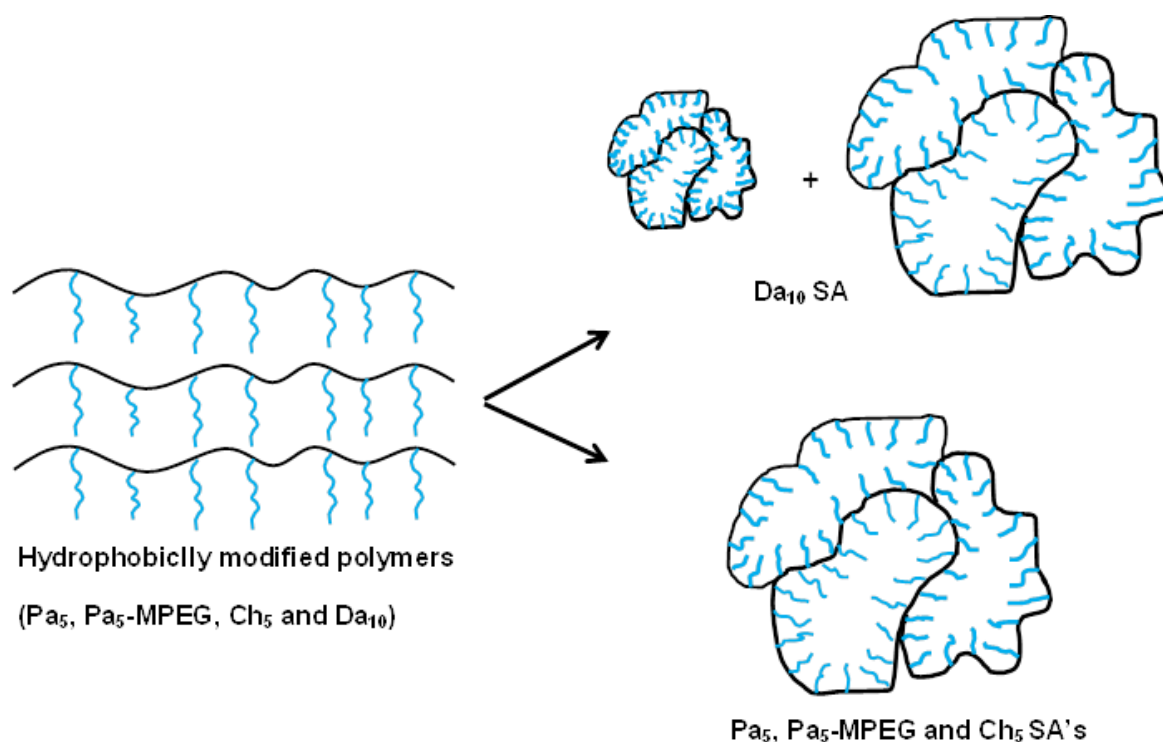


**Figure 6.1:** Schematic diagram showing the formation of the polymeric SA's from amphiphilic polymers in aqueous media.

The SA formed in aqueous media were able to load high concentrations (1263, 910, 744 and 455  $\mu\text{g mL}^{-1}$  for Da<sub>10</sub>, Pa<sub>5</sub>-MPEG, Ch<sub>5</sub> and Pa<sub>5</sub> polymers, respectively) of a poorly water soluble drug (TA) compared to the inherent aqueous solubility of TA and compared to the concentrations achieved using conventional solubilisers. The Da<sub>10</sub>, Pa<sub>5</sub>-MPEG, Ch<sub>5</sub> and Pa<sub>5</sub> TA-SA enhanced the TA aqueous solubility by 92, 65, 52 and 32-fold, respectively. The TA-SA formulations were simple to manufacture in comparison to other polymeric nanoparticles, in which multistep and time consuming preparation methods are required (Rao & Geckeler, 2011), facilitating the possibility of scaling up to industrial scale and most importantly the fabrication avoids the use of organic solvents, eliminating undesirable *in-vivo* effects such as toxicity. The mean hydrodynamic diameters of the TA-SA formulations had a size range of 200–334 nm and a positive surface charge of 21-46 mV. The small size and positive charge

of the TA-SA formulations are ideal for a potential formulation to overcome physiological and anatomical barriers of the anterior and posterior segments of the eye, as the retention and permeation across ocular tissues is reportedly dependent on the size and charge of nanoparticles (Koo *et al.*, 2012; Liu, Jones & Gu, 2012; Pathak & Thassu, 2009). Research on the use of poly(D,L-lactide-co-glycolide) (PLGA) nanoparticles has revealed that the uptake of small size PLGA nanoparticles (100 nm) was found to be higher than larger nanoparticles (800 nm) in primary cultured rabbit conjunctival epithelial cells (Qaddoumi *et al.*, 2004), and thus the higher cellular uptake of smaller nanoparticles resulted in higher drug delivery enhancement. The size of particles also plays a significant role in penetrating the retinal tissues; intravitreal injection of 2  $\mu\text{m}$ , 200 nm and 50 nm polystyrene spheres into rabbit eyes revealed that the 2  $\mu\text{m}$  microspheres were unable to penetrate the retina, while both the 200 and 50 nm nanospheres were capable of penetrating the retinal tissue (Sakurai, Ozeki, Kunou & Ogura, 2001). Hence, utilisation of a nanoparticle size allows the potential to affect potential distribution in the retinal tissue and RPE cells or localisation in the vitreous humour when applied intravitreally. The size of nanoparticles also determines their diffusivity across the vitreous humour. For example, Xu *et al.* have shown that nanoparticles with a diameter of 1190 nm or larger had restricted movement in bovine vitreous humour regardless of their surface chemistry. In contrast smaller nanoparticles (510 nm) were able to freely diffuse across the vitreous humour (Xu *et al.*, 2013). The size of the TA-SA should therefore allow the SA to move freely across the vitreous humour and penetrate the retinal tissue (Sakurai, Ozeki, Kunou & Ogura, 2001; Xu *et al.*, 2013). The positive charge of the TA-SA is desirable in order to increase TA pre-corneal retention time through interactions

with negatively charged mucins at the corneal surface (Li, Zhuang, Wang, Sui & Pan, 2012; Mitra, 2003). Also the movement of nanoparticles in the vitreous humour has been shown to be dependent on the surface charge. Positively charged nanoparticles were found to localise into the three dimensional collagen fibrils network of the vitreous humour when compared to their negatively charged counterparts (Kim, Robinson & Csaky, 2009; Koo *et al.*, 2012). In comparison to negatively charged nanoparticles immobilized positively charged nanoparticles injected in the vitreous humour stay suspended for a longer period before migrating to the retina and aqueous humour (Mains & Wilson, 2013; Sakurai, Ozeki, Kunou & Ogura, 2001). Consequently cationic nanoparticles cleared slower than anionic nanoparticles via the trabecular meshwork, blood vascular system (i.e. ciliary body (Kim & Csaky, 2010)) and cells capable of engulfing and clearing the nanoparticles (i.e. phagocytes by the astrocytes of the internal limited membrane of the retina (Mains & Wilson, 2013)).

The ability of the SA to encapsulate TA and the *in-vitro* release of TA from the TA-SA formulations were dependent on the type of hydrophobic group attached onto PAA backbone and the modification percentage. The Ch<sub>5</sub>, Pa<sub>5</sub> and Pa<sub>5</sub>-MPEG TA-SA's formulations were able to achieve sustained *in-vitro* release of TA over 47 h, whilst the Da<sub>10</sub> TA-SA formulation achieved sustained release over 145 h. The higher TA entrapment and longer release time of Da<sub>10</sub> TA-SA formulation in comparison to the 5% hydrophobically modified TA-SA formulations (Pa<sub>5</sub>, Ch<sub>5</sub> and Pa<sub>5</sub>-MPEG) was due to the higher modification percentage of the dansyl moiety and better TA-dansyl moiety compatibility. Unlike Pa<sub>5</sub>, Pa<sub>5</sub>-MPEG and Ch<sub>5</sub> polymers modified with alkyl or cyclic ring pendant groups, Da<sub>10</sub> consists of an aromatic pendant group which can potentially form two hydrogen bonds and

$\pi$  binding with TA. As a result of the high TA affinity to the hydrophobic domain (dansyl group) (Chang *et al.*, 2012), the Da<sub>10</sub> formulation had the highest TA solubilisation and was capable of releasing TA in a sustained manner for a longer period of time. The drug release from the SA formulations can potentially be controlled by selecting the appropriate pendant groups grafted onto the polymers. The variation in TA release time is beneficial as it allows drug release profiles to be tailored according to the targeted site. Ocular formulations applied topically and targeting the anterior segment should be retained at the ocular surface long enough to ensure sustained drug release but should also release the drug at a rate faster than the drug clearance rate. In addition, topical ocular formulations should not interfere with vision or cause irritation. On the other hand, to minimise the application frequency of formulations applied through invasive injections, it would be preferred that the posterior formulations release drugs at a slow rate to maintain prolonged therapeutic activity. The Da<sub>10</sub> TA-SA formulation is more suitable than Pa<sub>5</sub>, Pa<sub>5</sub>-MPEG and Ch<sub>5</sub> TA-SA formulations for posterior drug delivery, as the Da<sub>10</sub> TA-SA formulation prolonged TA release. In contrast, Pa<sub>5</sub>, Pa<sub>5</sub>-MPEG and Ch<sub>5</sub> TA-SA formulations (release approximately 100% of TA load in two days) are more suitable for topically applied formulations targeting the anterior segment of the eye, as the Da<sub>10</sub> formulation released approximately 100% of TA load in six days, which is much higher than the residence time of a topically instilled formulation in the eye (typically less than 24 h).

In order to test the ocular permeability of the developed TA-SA formulations and other potential formulations a porcine *in-vitro* eye model was developed and was found fit for purpose. The developed eye model mimicked the posterior segment of the eye by employing posterior porcine ocular tissues, and is based on

the well-established *in-vitro* permeation system, the Franz cell, which is cost-effective and relatively quick to set up in comparison to other *in-vitro* eye models such as the perfused eye model or cell culture model (De Coo, Zonnenberg & Trap, 1993; Reichl, Döhning, Bednarz & Müller-Goymann, 2005). Little has been done to develop and validate an *in-vitro* eye model fit for the purpose of permeation studies. Typically *in-vitro* permeation eye models test the permeability of ocular tissues using buffer solutions as receiver fluids in a diffusion cell such as Ussing chambers or Franz cells (Araujo, Garcia, Mallandrich, Souto & Calpena, 2012; Kadam, Cheruvu, Edelhauser & Kompella, 2011; Loch *et al.*, 2012; Mora *et al.*, 2005; Olsen, Edelhauser, Lim & Geroski, 1995; Thakur, Kadam & Kompella, 2011). Sink conditions for poorly water soluble drugs could not be maintained in these models over long experimental durations using buffer solutions alone. The development process included selecting a suitable receiver fluid in order to maintain sink conditions for TA over the duration of the experiment. TA permeation studies performed on porcine posterior ocular tissues using various receiver fluids showed that up to 10% of ethanol in modified Dulbecco's buffer solution could be used as a receiver fluid without significantly altering the permeability of the tissue, through the co-permeation of TA by the effect of solvent drag. Partial validation of the developed *in-vitro* porcine eye model included assessing tissues barrier integrity using tritiated water and assessing and comparing the permeability of four hydrophilic markers across human and porcine scleral tissues. The barrier integrity of frozen porcine posterior ocular tissue was found to be similar to the barrier integrity of fresh tissue as demonstrated by the TA and  $^3\text{H}_2\text{O}$  permeation studies. Hence, the use of frozen tissue is a practical alternative and more convenient option to using fresh tissue (fresh tissue typically has limited availability due to it

not being easily obtained from slaughterhouses in large amounts and it requires controlled transport conditions which are time consuming and costly). It was found that determining the permeation of tritiated water through porcine ocular tissue over a 15 min period can be used to assess the tissue barrier integrity, and can be used to normalise the flux of model compounds across porcine posterior tissues. Tritiated water has previously been used in monitoring the barrier integrity of tissues, in particular human skin and nails (Brown *et al.*, 2009; Lawrence, 1997). The normalisation allows the compensation of the inherent variability due to non-uniformity thickness between tissue samples and thus this increases the reliability of the *in-vitro* eye model. The normalisation has a significant advantage as the exact thickness of the scleral tissue is hard to measure, due to the sclera not having a uniform thickness across the entire eye and therefore makes it impractical to cut a uniform section. The four markers had similar permeability in both human and porcine scleral tissues when the scleral thickness at the equator was considered (the  $k_p$  values of FSS, 4, 10 and 20 kDa FITC-dextran normalised by the equator thickness of human scleral tissues were  $1.5 \times 10^{-5}$ ,  $0.6 \times 10^{-5}$ ,  $5.0 \times 10^{-6}$  and  $4.9 \times 10^{-6}$   $\text{cm}\cdot\text{h}^{-1}$ , respectively, whereas the normalised  $k_p$  values of porcine scleral tissues were  $1.6 \times 10^{-5}$ ,  $0.6 \times 10^{-5}$ ,  $7.7 \times 10^{-6}$  and  $7.3 \times 10^{-6}$   $\text{cm}\cdot\text{h}^{-1}$ , respectively) and permeability decreased with increasing molecular weight of the marker. The inverse relationship and the abrupt decline in the permeability of various compounds and their molecular weights has been reported using bovine scleral tissue by Maurice *et al.* (Maurice & Polgar, 1977) and human sclera tissue by Olsen *et al.* (Olsen, Edelhauser, Lim & Geroski, 1995). The similarity in permeability of the markers between the two species (human and porcine)

indicates the suitability of porcine scleral tissues as an alternative to human scleral tissue.

The nano size TA-SA formulations were tested on the *in-vitro* porcine eye model described above to study and compare the permeability of TA from TA-SA's and a TA suspension. The TA-SA formulations did not significantly increase TA flux (approximately  $0.6 \mu\text{g}\cdot\text{cm}^{-2}\cdot\text{h}^{-1}$ ) across posterior porcine ocular tissues and human scleral tissue when compared to TA suspension (approximately  $0.5 \mu\text{g}\cdot\text{cm}^{-2}\cdot\text{h}^{-1}$ ), indicating that the nano sized TA-SA did not permeate across the scleral tissues. This finding can be explained by the passive diffusion of penetrants in between the free spaces of the collagen bundles (intracollagen pathways), which is the main determinant of the rate and size of the penetrants traversing across the sclera. The distance between human scleral fibres (intracollagen pathways, centre to centre) is approximately 60 nm (Edwards & Prausnitz, 1998; Fatt & Weissman, 1992) and hence the TA-SA (200–334 nm) were unable to traverse across the sclera. This is supported by the results published by Amrite *et al.* (Amrite, Edelhauser, Singh & Kompella, 2008), in which the workers reported quantifiable permeation of the 20 nm nanoparticles across bovine sclera, whereas the 200 nm nanoparticles were showing not to penetrate through the scleral tissue. The fact that no enhancement of TA permeation across posterior porcine ocular tissues (sclera, choroid and retina) was observed using the TA-SA was similar to results obtained from the chemical enhancer studies performed on human and porcine scleral tissues. In these studies the enhancers showed no significant enhancement effect on human and porcine scleral tissues permeability. Even though TA-SA formulation could not penetrate the posterior tissues, they might be of interest for ophthalmic topically administered formulations as corneal epithelium

cells uptake nanoparticles and positively charged nanoparticles increase drug retention time when topically applied at the front of the eye (De Campos *et al.*, 2003; De la Fuente *et al.*, 2010). The uptake of nanoparticles by the corneal epithelium cells is reported to improve ocular bioavailability of the drug and prolong the therapeutic action (Aksungur *et al.*, 2011; Hippalgaonkar, Adelli, Hippalgaonkar, Repka & Majumdar, 2013; Nagarwal, Kumar & Pandit, 2012). Such an effect would be useful for treating persistent and chronic diseases such as endophthalmitis and glaucoma.

Testing TA-SA formulations on corneal tissue using buffer solution was not possible due to the severe corneal swelling over the duration of the experiment (24 h). An *in-vitro* anterior eye permeation model was developed by employing porcine corneal tissue in modified Franz cells. A suitable receiver fluid consisting of a de-swelling agent (5% w/v 500 kDa Dextran) was developed for the corneal model so as to prevent swelling of the cornea and to maintain the thickness of the corneal tissue over the duration of the experiment. The storage conditions had an impact on the corneal permeability in that the permeability of stored corneas increased with the increase in duration of storage time (the flux rate of FSS across fresh corneal tissue increased from  $0.44 \mu\text{g}\cdot\text{cm}^{-2}\cdot\text{h}^{-1}$  to 32.2 and  $75.84 \mu\text{g}\cdot\text{cm}^{-2}\cdot\text{h}^{-1}$  after one and two weeks storage, respectively). This finding (increased corneal permeability with the increase in duration of storage time) might explain the lack of difference in marker permeability across stored corneas in the presence of permeation enhancers. The stored corneas might not be susceptible to permeation enhancement in comparison to fresh corneas due to the damaged epithelium layers or loosen corneal tight junctions as a result of storage. The percentage of damaged corneal endothelial cells in organ culture medium and dextran containing

medium increases with storage time and is affected by the storage and transport media employed (Borderie, Baudrimont, Lopez, Carvajal & Laroche, 1997; Pels, Beele & Claerhout, 2008). The presence of de-swelling agent (500 kDa dextran) has been shown to cause an 8.4% loss in the number of endothelia cells after two days and severe epithelial injuries and lysis of keratinocytes after four days (Borderie, Baudrimont, Lopez, Carvajal & Laroche, 1997). This highlights the importance of developing an *in-vitro* corneal model using fresh corneas which is able to mimic the *in-vivo* response at a fraction of the cost of *in-vivo* studies.

Two ocular cell lines (RPE and HCE) and two cytotoxicity assays (MTT and PrestoBlue<sup>®</sup>) were investigated in order to determine the toxicity of potential formulations or excipients. The hydrophobically modified polymers used in the TA-SA had similar toxicity profiles in the RPE cells as the unmodified PAA. The IC<sub>50</sub> of the modified polymers were relatively low ( $2.9 \times 10^{-2}$  -  $4.9 \times 10^{-2}$  mg mL<sup>-1</sup>) which suggest a higher toxicity of these polymers in comparison to other common polymers used in ophthalmic drug deliver such as PLGA (nontoxic (Kompella & Edelhauser, 2011)) or chitosan (no toxicity up to 2 mg mL<sup>-1</sup> (Sarmiento & das Neves, 2012)). The two cytotoxicity assays were able to determine the toxicity of the polymers in the ocular cell lines. However, the PrestoBlue<sup>®</sup> method is simpler than the MTT method and has a shorter incubation time.

The importance of this work relies on providing a partial validated eye model to test potential ocular formulation. The developed eye model has significance to the pharmaceutical industry and can be refined and further validated to produce precise and accurate prediction of *in-vivo* the potential formulation permeability

## 6.2 Future Work

The hydrophobic drug (TA) was not tested on corneal tissue due to severe corneal swelling and high lag time. The corneal swelling was resolved by the addition of 5% dextran 500 kDa to the receiver fluid; however an analysis method quantifying the hydrophobic drug in the de-swelling medium was not been developed. In the future, it would be desirable to investigate various separation techniques such as liquid extraction, solid phase extraction or centrifugation to separate the hydrophobic drug from the matrix of the receiver fluid especially the 500 kDa Dextran (the 500 kDa interferes with the HPLC column, resulting in an increased pressure due to partial blockage of the column). Once a quantification assay of the hydrophobic drug has been developed and validated, polymeric SA entrapping the hydrophobic drug should be tested on corneal tissues.

In this work, TA (hydrophobic drug) was used to study the loading capacity of the polymeric SA, it would be beneficial to encapsulate other hydrophobic drugs and determine their loading capacity and their *in-vitro* release. In the future it would be desirable to carry out short and long term stability tests on aqueous and freeze dried formulations, in order to determine the shelf life of these formulations. Nanoparticles have previously been shown to facilitate penetrant permeation across corneal tissue by altering the tight junctions between the epithelia cells or by promoting cellular uptake of nanoparticles (Hippalgaonkar, Adelli, Hippalgaonkar, Repka & Majumdar, 2013; Tiyaboonchai, 2003). Testing the drug-SA on corneal tissue is crucial as these formulations might enhance the drug permeability across the corneal tissue and provided different results from the posterior tissues.

A longer experiment duration in the developed *in-vitro* corneal model is required to investigate drugs with high corneal lag time. The developed *in-vitro* eye model did not examine the effect of long experiment duration on the viability of the corneal epithelia cells or the looseness of the tight junctions after permeation studies. The corneal tissue should be examined and compared to a control at the end of the permeation study. Furthermore the effect of any anatomical change on the permeation should be determined.

This study showed prolonged corneal storage time might either decrease cell viability or loosen tight junctions between the epithelia cells as indicated by the increase in marker permeation with the increase in storage time. Further work should determine whether the increase in corneal permeability is due to damage in epithelia cells or due to loose tight junctions. Other corneal storage conditions should be investigated in order to minimise changes in corneal barrier integrity and maintain cell viability and tight junctions.

The toxicity of the amphiphilic polymers was determined on RPE cell lines; however neither the toxicity of the hydrophobic drug nor the formulations was determined in this study. Performing *in-vitro* intracellular localisation studies to determine the mechanism of cellular uptake in the cell would be useful as this might provide information about the fate of the drug and polymer.

In conclusion, four pendant groups were attached to a PAA backbone resulting in four amphiphilic polymers. These amphiphilic polymers formed spontaneous nano-polymeric SA in aqueous media. A poorly-water soluble drug (TA) was loaded into the nano-polymeric SA with a significantly higher drug loading than its saturated aqueous solubility or that achieved through the use of conventional solubilisers such as cremophor<sup>®</sup> EL and tween<sup>®</sup> 80. The solubilising

capacity, SA size and surface charge and drug release can be controlled by selecting the appropriate pendant groups to graft onto the polymers. A porcine *in-vitro* eye model was developed and found to have good correlation with the human *in-vitro* model providing strong evidence that the porcine *in-vitro* eye model can be used to screen potential formulations. The *in-vitro* model can assess hydrophobic and hydrophilic drug permeation through posterior ocular tissues and hydrophilic drugs through the corneal tissue. The drug loaded SA (TA-SA) did not significantly increase TA flux through human or porcine scleral tissues. However these SA might be of interest for ophthalmic topically administered formulations due to their small size and positive charge. In future, the developed *in-vitro* porcine eye model can be used to screen various formulations or enhancers targeting both the anterior and the posterior segment of the eye before testing *in-vivo*.

## References

- Akhtar, S., Tullo, A., Catterson, B., Davies, J. R., Bennett, K. & Meek, K. M. (2002). Clinical and morphological features including expression of  $\beta$ ig-h3 and keratan sulphate proteoglycans in Maroteaux-Lamy syndrome type B and in normal cornea. *British Journal of Ophthalmology*, 86(2), 147-151.
- Akomeah, F., Nazir, T., Martin, G. P. & Brown, M. B. (2004). Effect of heat on the percutaneous absorption and skin retention of three model penetrants. *European Journal of Pharmaceutical Sciences*, 21(2-3), 337-345.
- Aksungur, P., Demirbilek, M., Denkbaşı, E. B., Vandervoort, J., Ludwig, A. & Ünlü, N. (2011). Development and characterization of cyclosporine a loaded nanoparticles for ocular drug delivery: cellular toxicity, uptake, and kinetic studies. *Journal of Controlled Release*, 151(3), 286-294.
- Albani, J. R. (2007). *Principles and applications of fluorescence spectroscopy*. Oxford ; Ames, Iowa: Blackwell Science.
- Allen, E. H. A., Atkinson, S. D., Liao, H., Moore, J. E., Pedrioli, D. M. L., Smith, F. J. D., et al. (2013). Allele-specific siRNA silencing for the common keratin 12 founder mutation in meesmann epithelial corneal dystrophy. *Investigative Ophthalmology & Visual Science*, 54(1), 494-502.
- Alonso, M. (2004). Nanomedicines for overcoming biological barriers. *Biomedicine & Pharmacotherapy*, 58(3), 168-172.
- Ambati, J., Canakis, C. S., Miller, J. W., Gragoudas, E. S., Edwards, A., Weissgold, D. J., et al. (2000). Diffusion of high molecular weight compounds through sclera. *Investigative ophthalmology & visual science*, 41(5), 1181-1185.
- Amelinckx, S., Gevers, R. & Landuyt, J. v. (1978). *Diffraction and imaging techniques in material science* (2d, rev. ed.). Amsterdam ; New York: North-Holland Pub. Co. : sole distributors for the U.S.A. and Canada, Elsevier North-Holland.
- Amos, A. F., McCarty, D. J. & Zimmet, P. (1997). The rising global burden of diabetes and its complications: estimates and projections to the year 2010. *Diabet Med*, 14(5), S1-85.
- Amrite, A. C., Edelhauser, H. F., Singh, S. R. & Kompella, U. B. (2008). Effect of circulation on the disposition and ocular tissue distribution of 20 nm nanoparticles after periocular administration. *Molecular Vision*, 14(19-23), 150-160.
- Antonetti, D. A., Barber, A. J., Bronson, S. K., Freeman, W. M., Gardner, T. W., Jefferson, L. S., et al. (2006). Diabetic retinopathy: seeing beyond glucose-induced microvascular disease. *Diabetes*, 55(9), 2401-2411.
- Araujo, J., Garcia, M. L., Mallandrich, M., Souto, E. B. & Calpena, A. C. (2012). Release profile and transscleral permeation of triamcinolone acetonide loaded nanostructured lipid carriers (TA-NLC): in vitro and ex vivo studies. *Nanomedicine: Nanotechnology, Biology and Medicine*, 8(6), 1034-1041.
- Araujo, J., Nikolic, S., Egea, M. A., Souto, E. B. & Garcia, M. L. (2011). Nanostructured lipid carriers for triamcinolone acetonide delivery to the posterior segment of the eye. *Colloids Surf B Biointerfaces*, 88(1), 150-157.
- Aravindan, L., Bicknell, K. A., Brooks, G., Khutoryanskiy, V. V. & Williams, A. C. (2009). Effect of acyl chain length on transfection efficiency and toxicity of polyethylenimine. *International Journal of Pharmaceutics*, 378(1-2), 201-210.
- Aulton, M. E. & Cooper, J. W. (1988). *Pharmaceutics : the science of dosage form design* (1st ed.). Edinburgh ; New York: Churchill Livingstone.

- Avery, R. L., Pearlman, J., Pieramici, D. J., Rabena, M. D., Castellarin, A. A., Nasir, M. a. A., *et al.* (2006). Intravitreal bevacizumab (Avastin) in the treatment of proliferative diabetic retinopathy. *Ophthalmology*, *113*(10), 1695.e1691-1615.
- Ayalasomayajula, S. P. & Kompella, U. B. (2004). Retinal delivery of celecoxib is several-fold higher following subconjunctival administration compared to systemic administration. *Pharmaceutical Research*, *21*(10), 1797-1804.
- Baba, K., Tanaka, Y., Kubota, A., Kasai, H., Yokokura, S., Nakanishi, H., *et al.* (2011). A method for enhancing the ocular penetration of eye drops using nanoparticles of hydrolyzable dye. *Journal of Controlled Release*, *153*(3), 278-287.
- Badawi, A., El-Laithy, H., Qidra, R., Mofty, H. & Dally, M. (2008). Chitosan based nanocarriers for indomethacin ocular delivery. *Archives of Pharmacal Research*, *31*(8), 1040-1049.
- Baehring, F., Schlenk, F., Wotschadlo, J., Buske, N., Liebert, T., Bergemann, C., *et al.* (2013). Suitability of viability assays for testing biological effects of coated superparamagnetic nanoparticles. *Ieee Transactions on Magnetics*, *49*(1), 383-388.
- Bagheri, M. & Bigdeli, E. (2013). Preparation of stealth micellar nanoparticles of novel biodegradable and biocompatible brush copolymers with cholesteryl-modified PLA and PEG side chains. *Journal of Polymer Research*, *20*(3), 84-84.
- Bagheri, M. & Motirasoul, F. (2013). Synthesis, characterization, and micellization of cholesteryl-modified amphiphilic poly(L-lactide)-block-poly (glycidyl methacrylate) as a nanocarrier for hydrophobic drugs. *Journal of Polymer Research*, *20*(2).
- Bakkour, Y., Darcos, V., Coumes, F., Li, S. M. & Coudane, J. (2013). Brush-like amphiphilic copolymers based on polylactide and poly(ethylene glycol): Synthesis, self-assembly and evaluation as drug carrier. *Polymer*, *54*(7), 1746-1754.
- Barhoum, S. & Yethiraj, A. (2010). An NMR study of macromolecular aggregation in a model polymer-surfactant solution. *Journal of Chemical Physics*, *132*(2).
- Barile, F. A. (2010). Validating and troubleshooting ocular in vitro toxicology tests. *Journal of Pharmacological and Toxicological Methods*, *61*(2), 136-145.
- Bartlett, J. D. & Jaanus, S. D. (2008). *Clinical ocular pharmacology* (5th ed.). St. Louis, Mo.: Butterworth-Heinemann/Elsevier.
- Berridge, M. V., Herst, P. M. & Tan, A. S. (2005). Tetrazolium dyes as tools in cell biology: New insights into their cellular reduction. In M. R. El-Gewely (Ed.), *Biotechnology Annual Review* (Vol. Volume 11, pp. 127-152): Elsevier.
- Bhagat, N., Grigorian, R. A., Tutela, A. & Zarbin, M. A. (2009). Diabetic macular edema: pathogenesis and treatment. *Surv Ophthalmol*, *54*(1), 1-32.
- Bhatta, R. S., Chandasana, H., Chhonker, Y. S., Rathi, C., Kumar, D., Mitra, K., *et al.* (2012). Mucoadhesive nanoparticles for prolonged ocular delivery of natamycin: In vitro and pharmacokinetics studies. *International Journal of Pharmaceutics*, *432*(1-2), 105-112.
- Birch, D. G. & Liang, F. Q. (2007). Age-related macular degeneration: a target for nanotechnology derived medicines. *Int J Nanomedicine*, *2*(1), 65-77.
- Birks, J. B. (1975). Excimers. *Reports on Progress in Physics*, *38*(8), 903.
- Block, L. H. & Patel, R. N. (1973). Solubility and dissolution of triamcinolone acetonide. *Journal of Pharmaceutical Sciences*, *62*(4), 617-621.
- Boncler, M., Róźalski, M., Krajewska, U., Podsędek, A. & Watała, C. (2013). Comparison of PrestoBlue and MTT assays of cellular viability in the assessment of anti-proliferative effects of plant extracts on human endothelial cells. *Journal of Pharmacological and Toxicological Methods*(0).

- Bonovas, S., Peponis, V. & Filioussi, K. (2004). Diabetes mellitus as a risk factor for primary open-angle glaucoma: a meta-analysis. *Diabetic Medicine*, 21(6), 609-614.
- Bopp, S. K. & Lettieri, T. (2008). Comparison of four different colorimetric and fluorometric cytotoxicity assays in a zebrafish liver cell line. *BMC pharmacology*, 8(1), 8.
- Borderie, V. M., Baudrimont, M., Lopez, M., Carvajal, S. & Laroche, L. (1997). Evaluation of the deswelling period in dextran-containing medium after corneal organ culture. *Cornea*, 16(2), 215-223.
- Bos, K. J., Holmes, D. F., Meadows, R. S., Kadler, K. E., McLeod, D. & Bishop, P. N. (2001). Collagen fibril organisation in mammalian vitreous by freeze etch/rotary shadowing electron microscopy. *Micron*, 32(3), 301-306.
- Boubriak, O. A., Urban, J. P. G., Akhtar, S., Meek, K. M. & Bron, A. J. (2000). The Effect of Hydration and Matrix Composition on Solute Diffusion in Rabbit Sclera. *Experimental Eye Research*, 71(5), 503-514.
- Boubriak, O. A., Urban, J. P. G. & Bron, A. J. (2003). Differential effects of aging on transport properties of anterior and posterior human sclera. *Experimental Eye Research*, 76(6), 701-713.
- Bourges, J. L., Bloquel, C., Thomas, A., Froussart, F., Bochot, A., Azan, F., *et al.* (2006). Intraocular implants for extended drug delivery: therapeutic applications. *Adv Drug Deliv Rev*, 58(11), 1182-1202.
- Bourges, J. L., Gautier, S. E., Delie, F., Bejjani, R. A., Jeanny, J. C., Gurny, R., *et al.* (2003). Ocular drug delivery targeting the retina and retinal pigment epithelium using polylactide nanoparticles. *Investigative Ophthalmology & Visual Science*, 44(8), 3562-3569.
- Bourne, W. M., Nelson, L. R. & Hodge, D. O. (1997). Central corneal endothelial cell changes over a ten-year period. *Investigative Ophthalmology & Visual Science*, 38(3), 779-782.
- Bozkir, G., Bozkir, M., Dogan, H., Aycan, K. & Guler, B. (1997). Measurements of axial length and radius of corneal curvature in the rabbit eye. *Acta Medica Okayama*, 51(1), 9-11.
- Branco, M. C. & Schneider, J. P. (2009). Self-assembling materials for therapeutic delivery. *Acta Biomaterialia*, 5(3), 817-831.
- British National Formulary* (2013). British Medical Association and Royal Pharmaceutical Society of Great Britain.
- British Pharmacopoeia Volume III. (2012). *Formulated Preparations: Specific Monographs* Retrieved 05/07, 2013
- Brophy, M. R. & Deasy, P. B. (1987). Application of the Higuchi model for drug release from dispersed matrices to particles of general shape. *International Journal of Pharmaceutics*, 37(1-2), 41-47.
- Brown, M. B., Khengar, R. H., Turner, R. B., Forbes, B., Traynor, M. J., Evans, C. R. G., *et al.* (2009). Overcoming the nail barrier: a systematic investigation of unguinal chemical penetration enhancement. *International Journal of Pharmaceutics*, 370(1-2), 61-67.
- Brown, M. B., Martin, G. P., Jones, S. A. & Akomeah, F. K. (2006). Dermal and transdermal drug delivery systems: current and future prospects. *Drug Delivery: Journal of Delivery and Targeting of Therapeutic Agents*, 13(3), 175-187.
- Brown, M. D., Schätzlein, A., Brownlie, A., Jack, V., Wang, W., Tetley, L., *et al.* (2000). Preliminary characterization of novel amino acid based polymeric vesicles as gene and drug delivery agents. *Bioconjugate Chemistry*, 11(6), 880-891.

- Brown, R. H. & Lynch, M. G. (1986). Drop size of commercial glaucoma medications. *American Journal of Ophthalmology*, 102(5), 673-674.
- Brown, T. L. (2006). *Chemistry : the central science* (10th ed.). Upper Saddle River, NJ: Pearson Prentice Hall.
- Brydson, J. (1999). *Plastics materials* (Seventh ed.): Butterworth Heinmann.
- Buruiana, E. C., Chibac, A. L. & Buruiana, T. (2010). Polyacrylates containing dansyl semicarbazide units sensitive for some structures in solution and film. *Journal of Photochemistry and Photobiology A: Chemistry*, 213(2-3), 107-113.
- Buttery, R. G., Hinrichsen, C. F. L., Weller, W. L. & Haight, J. R. (1991). How thick should a retina be? a comparative study of mammalian species with and without intraretinal vasculature. *Vision Research*, 31(2), 169-187.
- Cardillo, J. A., Souza-Filho, A. A. & Oliveira, A. G. (2006). Intravitreal bioerudivel sustained-release triamcinolone microspheres system (RETAAC). Preliminary report of its potential usefulness for the treatment of diabetic macular edema. *Archivos de la Sociedad Espanola de Oftalmologia*, 81(12), 675-677, 679-681.
- Cedrone, C., Mancino, R., Cerulli, A., Cesareo, M. & Nucci, C. (2008). Epidemiology of primary glaucoma: prevalence, incidence, and blinding effects *Progress in Brain Research* (Vol. Volume 173, pp. 3-14): Elsevier.
- Chaiyasan, W., Srinivas, S. P. & Tiyaboonchai, W. (2013). Mucoadhesive Chitosan-Dextran Sulfate Nanoparticles for Sustained Drug Delivery to the Ocular Surface. *Journal of Ocular Pharmacology and Therapeutics*, 29(2), 200-207.
- Chan, T., Payor, S. & Holden, B. A. (1983). Corneal thickness profiles in rabbits using an ultrasonic pachometer. *Investigative Ophthalmology & Visual Science*, 24(10), 1408-1410.
- Chang, L., Deng, L., Wang, W., Lv, Z., Hu, F., Dong, A., *et al.* (2012). Poly(ethyleneglycol)-b-Poly(epsilon-caprolactone-co-gamma-hydroxyl-epsilon-caprolactone) Bearing Pendant Hydroxyl Groups as Nanocarriers for Doxorubicin Delivery. *Biomacromolecules*, 13(10), 3301-3310.
- Chang, Y.-S., Wu, C.-L., Tseng, S.-H., Kuo, P.-Y. & Tseng, S.-Y. (2007). Cytotoxicity of triamcinolone acetonide on human retinal pigment epithelial cells. *Investigative Ophthalmology & Visual Science*, 48(6), 2792-2798.
- Chen, C. J., Wang, J.-C., Zhao, E.-Y., Gao, L.-Y., Feng, Q., Liu, X.-Y., *et al.* (2013). Self-assembly cationic nanoparticles based on cholesterol-grafted bioreducible poly(amidoamine) for siRNA delivery. *Biomaterials*, 34(21), 5303-5316.
- Chen, M. H., Kumar, R., Parmar, V. S., Kumar, J., Samuelson, L. A. & Watterson, A. C. (2004). Self-organization of amphiphilic copolymers into nanoparticles: study by H-1 NMR longitudinal relaxation time. *Journal of Macromolecular Science-Pure and Applied Chemistry*, A41(12), 1489-1496.
- Chen, S., Cheng, S.-X. & Zhuo, R.-X. (2011). Self-Assembly Strategy for the Preparation of Polymer-Based Nanoparticles for Drug and Gene Delivery. *Macromolecular Bioscience*, 11(5), 576-589.
- Cheng, W. P., Gray, A. I., Tetley, L., Hang, T. L. B., Schätzlein, A. G. & Uchegbu, I. F. (2006). Polyelectrolyte nanoparticles with high drug loading enhance the oral uptake of hydrophobic compounds. *Biomacromolecules*, 7(5), 1509-1520.
- Cheng, W. P., Thompson, C., Ryan, S. M., Aguirre, T., Tetley, L. & Brayden, D. J. (2010). In vitro and in vivo characterisation of a novel peptide delivery system: Amphiphilic polyelectrolyte-salmon calcitonin nanocomplexes. *Journal of Controlled Release*, 147(2), 289-297.

- Cheruvu, N. P. S. & Kompella, U. B. (2006). Bovine and porcine transscleral solute transport: Influence of lipophilicity and the choroid-bruch's layer. *Investigative Ophthalmology & Visual Science*, 47(10), 4513-4522.
- Cheung, A. C. Y., Yu, Y., Tay, D., Wong, H. S., Ellis-Behnke, R. & Chau, Y. (2010). Ultrasound-enhanced intrascleral delivery of protein. *International Journal of Pharmaceutics*, 401(1-2), 16-24.
- Cheung, N. & Wong, T. Y. (2007). Obesity and eye diseases. *Survey of Ophthalmology*, 52(2), 180-195.
- Chilcott, R. P., Dalton, C. H., Emmanuel, A. J., Allen, C. E. & Bradley, S. T. (2002). Transepidermal water loss does not correlate with skin barrier function in vitro. *Journal of Investigative Dermatology*, 118(5), 871-875.
- Chiu, H.-C., Chern, C.-S., Lee, C.-K. & Chang, H.-F. (1998). Synthesis and characterization of amphiphilic poly(ethylene glycol) graft copolymers and their potential application as drug carriers. *Polymer*, 39(8-9), 1609-1616.
- Cho, S.-A., An, S., Lee, E., Shin, K., Cho, J.-C. & Lee, T. R. (2012). A new cell-based method for assessing the eye irritation potential of chemicals: an alternative to the Draize test. *Toxicology Letters*, 212(2), 198-204.
- Choonara, Y. E., Pillay, V., Danckwerts, M. P., Carmichael, T. R. & Du Toit, L. C. (2010). A Review of implantable intravitreal drug delivery technologies for the treatment of posterior segment eye diseases. *Journal of Pharmaceutical Sciences*, 99(5), 2219-2239.
- Chronopoulos, A., Trudeau, K., Roy, S., Huang, H. & Viores, S. A. (2011). High glucose-induced altered basement membrane composition and structure increases trans-endothelial permeability: implications for diabetic retinopathy. *Curr Eye Res*, 36(8), 747-753.
- Civiale, C., Licciardi, M., Cavallaro, G., Giammona, G. & Mazzone, M. G. (2009). Polyhydroxyethylaspartamide-based micelles for ocular drug delivery. *International Journal of Pharmaceutics*, 378(1-2), 177-186.
- Cogan, D. G. & Hirsch, E. O. (1944). The cornea VII permeability to weak electrolytes. *Archives of Ophthalmology*, 32(4), 276-282.
- Collins, A. M. (2012). *Nanotechnology cookbook : practical, reliable and jargon-free experimental procedures* (1st ed.). Boston ; Oxford: Elsevier.
- Constable, P. A., Lawrenson, J. G., Dolman, D. E. M., Arden, G. B. & Abbott, N. J. (2006). P-Glycoprotein expression in human retinal pigment epithelium cell lines. *Experimental Eye Research*, 83(1), 24-30.
- Contreras-Ruiz, L., de la Fuente, M., Parraga, J. E., Lopez-Garcia, A., Fernandez, I., Seijo, B., *et al.* (2011). Intracellular trafficking of hyaluronic acid-chitosan oligomer-based nanoparticles in cultured human ocular surface cells. *Molecular Vision*, 17(34-35), 279-290.
- Cormack, D. H. (2001). *Essential histology*: Lippincott Williams & Wilkins.
- Cortiject<sup>®</sup>. (2013) Retrieved 11/03/2013, 2013, from <http://www.novagali.com/en/eye-therapy/retinopathies/>
- Costa, V. P., Braga, M. E. M., Duarte, C. M. M., Alvarez-Lorenzo, C., Concheiro, A., Gil, M. H., *et al.* (2010). Anti-glaucoma drug-loaded contact lenses prepared using supercritical solvent impregnation. *The Journal of Supercritical Fluids*, 53(1-3), 165-173.
- Crooke, A., Guzman-Aranguez, A., Peral, A., Abdurrahman, M. K. A. & Pintor, J. (2008). Nucleotides in ocular secretions: their role in ocular physiology. *Pharmacology & Therapeutics*, 119(1), 55-73.

- Cruysberg, L. P. J., Nuijts, R. M. M. A., Geroski, D. H., Gilbert, J. A., Hendrikse, F. & Edelhauser, H. F. (2005). The influence of intraocular pressure on the transscleral diffusion of high-molecular-weight compounds. *Investigative Ophthalmology and Visual Science*, 46(10), 3790-3794.
- Cummings, T. J. (2012). *Ophthalmic pathology : a concise guide*: Springer.
- Cunha-Vaz, J. G. (2010). *Diabetic retinopathy*. Hackensack, NJ: World Scientific.
- Curtin, B. J. (1969). Physiopathologic aspects of scleral stress-strain. *Trans Am Ophthalmol Soc*, 67, 417-461.
- Da Costa, A. O., de Assis, M.-C., de Andrade Marques, E. & Plotkowski, M.-C. (1999). Comparative analysis of three methods to assess viability of mammalian cells in culture. *Biocell*, 23(1), 65-72.
- Danhier, F., Ansorena, E., Silva, J. M., Coco, R., Le Breton, A. & Préat, V. (2012). PLGA-based nanoparticles: an overview of biomedical applications. *Journal of Controlled Release*, 161(2), 505-522.
- Danis, R. P., Ciulla, T. A., Pratt, L. M. & Anliker, W. (2000). Intravitreal triamcinolone acetonide in exudative age-related macular degeneration. *Retina (Philadelphia, Pa.)*, 20(3), 244-250.
- Dartt, D. A., Dana, R., D'Amore, P. & Niederkorn, J. Y. (2011). *Immunology, inflammation and diseases of the eye*: Access Online via Elsevier.
- Das, T., Jalali, S., Gothwal, V. K., Sharma, S. & Naduvilath, T. J. (1999). Intravitreal dexamethasone in exogenous bacterial endophthalmitis: results of a prospective randomised study. *British Journal of Ophthalmology*, 83(9), 1050-1055.
- Dash, S., Murthy, P. N., Nath, L. & Chowdhury, P. (2010). Kinetic modeling on drug release from controlled drug delivery systems. *Acta Pol Pharm*, 67(3), 217-223.
- De Campos, A. M., Diebold, Y., Carvalho, E. L. S., Sanchez, A. & Alonso, M. J. (2004). Chitosan nanoparticles as new ocular drug delivery systems: in vitro stability, in vivo fate, and cellular toxicity. *Pharmaceutical Research*, 21(5), 803-810.
- De Campos, A. M., Sánchez, A., Gref, R., Calvo, P., Alonso, M., amp, *et al.* (2003). The effect of a PEG versus a chitosan coating on the interaction of drug colloidal carriers with the ocular mucosa. *European Journal of Pharmaceutical Sciences*, 20(1), 73-81.
- De Coo, F. A. M., Zonnenberg, B. A. & Trap, N. H. (1993). Prolonged normothermic perfusion of the isolated bovine eye: Initial results. *Current Eye Research*, 12(4), 293-301.
- De la Fuente, M., Ravina, M., Paolicelli, P., Sanchez, A., Seijo, B. & Jose Alonso, M. (2010). Chitosan-based nanostructures: a delivery platform for ocular therapeutics. *Advanced Drug Delivery Reviews*, 62(1), 100-117.
- De la Fuente, M., Seijo, B. & Alonso, M. J. (2008). Novel hyaluronic acid-chitosan nanoparticles for ocular gene therapy. *Investigative Ophthalmology & Visual Science*, 49(5), 2016-2024.
- Del Amo, E. M. & Urtti, A. (2008). Current and future ophthalmic drug delivery systems. a shift to the posterior segment. *Drug Discov Today*, 13(3-4), 135-143.
- Di Tommaso, C., Bourges, J.-L., Valamanesh, F., Trubitsyn, G., Torriglia, A., Jeanny, J.-C., *et al.* (2012). Novel micelle carriers for cyclosporin A topical ocular delivery: In vivo cornea penetration, ocular distribution and efficacy studies. *European Journal of Pharmaceutics and Biopharmaceutics*, 81(2), 257-264.
- Diebold, Y. & Calonge, M. (2010). Applications of nanoparticles in ophthalmology. *Prog Retin Eye Res*, 29(6), 596-609.

- Diebold, Y., Jarrín, M., Sáez, V., Carvalho, E. L. S., Orea, M., Calonge, M., *et al.* (2007). Ocular drug delivery by liposome–chitosan nanoparticle complexes (LCS-NP). *Biomaterials*, 28(8), 1553-1564.
- Doughty, M. J. & Zaman, M. L. (2000). Human corneal thickness and its impact on intraocular pressure measures: a review and meta-analysis approach. *Survey of Ophthalmology*, 44(5), 367-408.
- Douroumis, D. & Fahr, A. (2012). *Drug delivery strategies for poorly water-soluble drugs*. Chichester, West Sussex: John Wiley & Sons.
- Dugard, P. H., Walker, M., Mawdsley, S. J. & Scott, R. C. (1984). Absorption of some glycol ethers through human skin in vitro. *Environmental Health Perspectives*, VOL. 57, 193-197.
- Dunn, K., Aotaki-Keen, A., Putkey, F. & Hjelmeland, L. (1996). ARPE-19, a human retinal pigment epithelial cell line with differentiated properties. *Experimental Eye Research*, 62(2), 155-170.
- Duong, T. Q., Pardue, M. T., Thule, P. M., Olson, D. E., Cheng, H., Nair, G., *et al.* (2008). Layer-specific anatomical, physiological and functional MRI of the retina. *NMR Biomed*, 21(9), 978-996.
- Edelhauser, H. F. & Maren, T. H. (1988). Permeability of human cornea and sclera to sulfonamide carbonic-anhydrase inhibitors. *Archives of Ophthalmology*, 106(8), 1110-1115.
- Edward, D. P. & Vajaranant, T. S. (2012). *Glaucoma*. Oxford: Oxford University Press.
- Edwards, A. & Prausnitz, M. R. (1998). Fibre matrix model of sclera and corneal stroma for drug delivery to the eye. *Aiche Journal*, 44(1), 214-225.
- Enriquez de Salamanca, A., Diebold, Y., Calonge, M., Garcia-Vazquez, C., Callejo, S., Vila, A., *et al.* (2006). Chitosan nanoparticles as a potential drug delivery system for the ocular surface: toxicity, uptake mechanism and in vivo tolerance. *Investigative ophthalmology & visual science*, 47(4), 1416-1425.
- European Commission (2013) Retrieved 25/09/2013, 2013, from [http://ec.europa.eu/environment/chemicals/nanotech/faq/definition\\_en.htm](http://ec.europa.eu/environment/chemicals/nanotech/faq/definition_en.htm)
- Faber, C., Scherfig, E., Prause, J. U. & Sorensen, K. E. (2008). Corneal thickness in pigs measured by ultrasound pachymetry in vivo. *Scandinavian Journal of Laboratory Animal Science*, 35(1), 39-43.
- Fatt, I. & Weissman, B. A. (1992). *Physiology of the eye : an introduction to the vegetative functions* (2nd ed.). Boston: Butterworth-Heinemann.
- Fitzgerald, P., Hadgraft, J., Kreuter, J. & Wilson, C. G. (1987). A  $\gamma$ -scintigraphic evaluation of microparticulate ophthalmic delivery systems: liposomes and nanoparticles. *International Journal of Pharmaceutics*, 40(1–2), 81-84.
- Fogagnolo, P. & Rossetti, L. (2011). Medical treatment of glaucoma: present and future. *Expert Opinion on Investigational Drugs*, 20(7), 947-959.
- Fotakis, G. & Timbrell, J. A. (2006). In vitro cytotoxicity assays: comparison of LDH, neutral red, MTT and protein assay in hepatoma cell lines following exposure to cadmium chloride. *Toxicology Letters*, 160(2), 171-177.
- Fruijtier-Pölloth, C. (2005). Safety assessment on polyethylene glycols (PEGs) and their derivatives as used in cosmetic products. *Toxicology*, 214(1–2), 1-38.
- Gaucher, G., Dufresne, M.-H., Sant, V. P., Kang, N., Maysinger, D. & Leroux, J.-C. (2005). Block copolymer micelles: preparation, characterization and application in drug delivery. *Journal of Controlled Release*, 109(1–3), 169-188.
- Gaucher, G., Satturwar, P., Jones, M.-C., Furtos, A. & Leroux, J.-C. (2010). Polymeric micelles for oral drug delivery. *European Journal of Pharmaceutics and Biopharmaceutics*, 76(2), 147-158.

- Gaudana, R., Ananthula, H., Parenky, A. & Mitra, A. (2010). Ocular drug delivery. *The AAPS Journal*, 12(3), 348-360.
- Gedde, U. W. (2001). *Polymer physics* (First edition ed.): Kluwer Academic Publishers.
- Geerling, G., Daniels, J. T., Dart, J. K., Cree, I. A. & Khaw, P. T. (2001). Toxicity of natural tear substitutes in a fully defined culture model of human corneal epithelial cells. *Investigative Ophthalmology & Visual Science*, 42(5), 948-956.
- Gerlier, D. & Thomasset, N. (1986). Use of MTT colorimetric assay to measure cell activation. *Journal of Immunological Methods*, 94(1-2), 57-63.
- Glick, D. (2009). *Methods of biochemical analysis* (pp. v.). New York,: Wiley-Interscience.
- Goundalkar, A. & Mezei, M. (1984). Chemical modification of triamcinolone acetonide to improve liposomal encapsulation. *Journal of Pharmaceutical Sciences*, 73(6), 834-835.
- Gratieri, T., Gelfuso, G. M., Thomazini, J. A. & Lopez, R. F. V. (2010). Excised porcine cornea integrity evaluation in an in vitro model of Iontophoretic ocular research. *Ophthalmic Research*, 43(4), 208-216.
- Gruen, D. W. R. & Haydon, D. A. (1980). *The hydrophobic effect: formation of micelles and biological membranes: By Charles Tanford*, Wiley, New York, 1979, 2nd ed., \$18.50. *Journal of Colloid and Interface Science*, 77(2), 588.
- Gu, J., Cheng, W.-P., Liu, J., Lo, S.-Y., Smith, D., Qu, X., *et al.* (2007). Ph-triggered reversible “stealth” polycationic micelles. *Biomacromolecules*, 9(1), 255-262.
- Gu, J., Cheng, W. P., Hoskins, C., Lin, P. K. T., Zhao, L., Zhu, L., *et al.* (2011). Nano self-assemblies based on cholate grafted poly-L-lysine enhanced the solubility of sterol-like drugs. *Journal of Microencapsulation*, 28(8), 752-762.
- Gupta, H., Aqil, M., Khar, R. K., Ali, A., Bhatnagar, A. & Mittal, G. (2010). Sparfloxacin-loaded PLGA nanoparticles for sustained ocular drug delivery. *Nanomedicine*, 6(2), 324-333.
- Gupta, M., Agrawal, G. P. & Vyas, S. P. (2013). Polymeric nanomedicines as a promising vehicle for solid tumor therapy and targeting. *Current Molecular Medicine*, 13(1), 179-204.
- Gupta, R. B. & Kompella, U. B. (2006). *Nanoparticle technology for drug delivery*. New York: Taylor & Francis.
- Habot-Wilner, Z. & Belkin, M. (2005). Obesity is a risk factor for eye diseases. *Harefuah*, 144(11), 805.
- Haghjou, N., Abdekhodaie, M. J. & Cheng, Y.-L. (2013). Retina-Choroid-Sclera Permeability for Ophthalmic Drugs in the Vitreous to Blood Direction: Quantitative Assessment. *Pharmaceutical Research*, 30(1), 41-59.
- Hahne, M. & Reichl, S. (2011). Development of a serum-free human cornea construct for in vitro drug absorption studies: the influence of varying cultivation parameters on barrier characteristics. *International Journal of Pharmaceutics*, 416(1), 268-279.
- Halary, J.-L., Lauprêtre, F. & Monnerie, L. (2011). *Polymer materials : macroscopic properties and molecular interpretations*. Hoboken, N.J.: Wiley.
- Hamaguchi, T., Kato, K., Yasui, H., Morizane, C., Ikeda, M., Ueno, H., *et al.* (2007). A phase I and pharmacokinetic study of NK105, a paclitaxel-incorporating micellar nanoparticle formulation. *British Journal of Cancer*, 97(2), 170-176.
- Hamalainen-Laanaya, H. K. & Orloff, M. S. (2012). Analysis of cell viability using time-dependent increase in fluorescence intensity. *Analytical Biochemistry*, 429(1), 32-38.
- Hamalainen, K. M., Kananen, K., Auriola, S., Kontturi, K. & Urtti, A. (1997). Characterization of paracellular and aqueous penetration routes in cornea,

- conjunctiva, and sclera. *Investigative Ophthalmology & Visual Science*, 38(3), 627-634.
- Hamid, R., Rotshteyn, Y., Rabadi, L., Parikh, R. & Bullock, P. (2004). Comparison of alamar blue and MTT assays for high through-put screening. *Toxicology in Vitro*, 18(5), 703-710.
- Hammer, M., Richter, S., Kobuch, K., Mata, N. & Schweitzer, D. (2008). Intrinsic tissue fluorescence in an organotypic perfusion culture of the porcine ocular fundus exposed to blue light and free radicals. *Graefes Archive for Clinical and Experimental Ophthalmology*, 246(7), 979-988.
- Hao, J., Li, S. K., Kao, W. W. & Liu, C. Y. (2010). Gene delivery to cornea. *Brain Res Bull*, 81(2-3), 256-261.
- Hao, J., Li, S. K., Liu, C.-Y. & Kao, W. W. Y. (2009). Electrically assisted delivery of macromolecules into the corneal epithelium. *Experimental Eye Research*, 89(6), 934-941.
- Hathout, R. M., Mansour, S., Mortada, N. D. & Guinedi, A. S. (2007). Liposomes as an ocular delivery system for acetazolamide: in vitro and in vivo studies. *AAPS PharmSciTech*, 8(1), 1.
- Hillegass, J. M., Shukla, A., Lathrop, S. A., MacPherson, M. B., Fukagawa, N. K. & Mossman, B. T. (2010). Assessing nanotoxicity in cells in vitro. *Wiley Interdisciplinary Reviews-Nanomedicine and Nanobiotechnology*, 2(3), 219-231.
- Hippalgaonkar, K., Adelli, G. R., Hippalgaonkar, K., Repka, M. A. & Majumdar, S. (2013). Indomethacin-Loaded Solid Lipid Nanoparticles for Ocular Delivery: Development, Characterization, and In Vitro Evaluation. *Journal of Ocular Pharmacology and Therapeutics*, 29(2), 216-228.
- Hoang-Xuan, T., Baudouin, C. & Creuzot-Garcher, C. (1998). Inflammatory Diseases of the conjunctiva. *Creuzot-Garcher C. Focus*, 3, 12-15.
- Holland, E. J., Mannis, M. J. & Lee, W. B. (2013). *Ocular surface disease: cornea, conjunctiva and tear film: expert consult-online and print*: WB Saunders Company.
- Hornof, M., Toropainen, E. & Urtti, A. (2005). Cell culture models of the ocular barriers. *Eur J Pharm Biopharm*, 60(2), 207-225.
- Hoskins, C. (2010). *The use of novel poly(allylamine) based amphiphilic polymers for drug delivery*. Doctor of Philosophy, The Robert Gordon University, OpenAIR.
- Hoskins, C., Lin, P. K. T. & Cheng, W. P. (2012). A review on comb-shaped amphiphilic polymers for hydrophobic drug solubilization. *Therapeutic delivery*, 3(1), 59-79.
- Hoskins, C., Lin, P. K. T., Tetley, L. & Cheng, W. P. (2012a). Novel fluorescent amphiphilic poly(allylamine) and their supramacromolecular self-assemblies in aqueous media. *Polymers for Advanced Technologies*, 23(3), 710-719.
- Hoskins, C., Lin, P. K. T., Tetley, L. & Cheng, W. P. (2012b). The Use of Nano Polymeric Self-Assemblies Based on Novel Amphiphilic Polymers for Oral Hydrophobic Drug Delivery. *Pharmaceutical Research*, 29(3), 782-794.
- Hoskins, C., Ouaiissi, M., Lima, S. C., Cheng, W. P., Loureiro, I., Mas, E., *et al.* (2010). In vitro and in vivo anticancer activity of a novel nano-sized formulation based on self-assembling polymers against pancreatic cancer. *Pharmaceutical Research*, 27(12), 2694-2703.
- Hsu, J. (2007). Drug delivery methods for posterior segment disease. *Current Opinion in Ophthalmology*, 18(3), 235-239.
- Huang, Y. & Meek, K. M. (1999). Swelling studies on the cornea and sclera: the effects of pH and ionic strength. *Biophysical Journal*, 77(3), 1655-1665.
- Huang, Y., Yu, H., Guo, L. & Huang, Q. (2010). Structure and self-assembly properties of a new chitosan-based amphiphile. *J Phys Chem B*, 114(23), 7719-7726.

- Huhtala, A., Rönkkö, S., Teräsvirta, M., Puustjärvi, T., Sihvola, R., Vehanen, K., *et al.* (2009). The effects of 5-fluorouracil on ocular tissues in vitro and in vivo after controlled release from a multifunctional implant. *Investigative Ophthalmology & Visual Science*, 50(5), 2216-2223.
- Icon Bioscience, Inc. (IBI). (2013) Retrieved 31/10/2013, 2013, from <http://iconbioscience.com/ibi-20089>
- International Conference of Harmonisation. (1995). ICH Topic Q 2 (R1) Validation of analytical procedures: text and methodology. Retrieved from
- Invitrogen. (2013) Retrieved 31/07/2013, 2013, from <http://www.invitrogen.com/site/us/en/home/brands/Molecular-Probes/Key-Molecular-Probes-Products/PrestoBlue-Cell-Viability-Reagent.html>
- Isaac, D. L. C., Abud, M. B., Frantz, K. A., Rassi, A. R. & Avila, M. (2012). Comparing intravitreal triamcinolone acetonide and bevacizumab injections for the treatment of diabetic macular oedema: a randomized double-blind study. *Acta Ophthalmologica*, 90(1), 56-60.
- Jain, D., Carvalho, E. & Banerjee, R. (2010). Biodegradable hybrid polymeric membranes for ocular drug delivery. *Acta Biomaterialia*, 6(4), 1370-1379.
- Jain, G. K., Pathan, S. A., Akhter, S., Jayabalan, N., Talegaonkar, S., Khar, R. K., *et al.* (2011). Microscopic and spectroscopic evaluation of novel PLGA–chitosan Nanoplexes as an ocular delivery system. *Colloids and Surfaces B: Biointerfaces*, 82(2), 397-403.
- Janoria, K. G., Gunda, S., Boddu, S. H. & Mitra, A. K. (2007). Novel approaches to retinal drug delivery. *Expert Opinion on Drug Delivery*, 4(4), 371-388.
- Järvinen, K., Järvinen, T. & Urtti, A. (1995). Ocular absorption following topical delivery. *Advanced Drug Delivery Reviews*, 16(1), 3-19.
- Järvinen, T. & Järvinen, K. (1996). Prodrugs for improved ocular drug delivery. *Advanced Drug Delivery Reviews*, 19(2), 203-224.
- Jermak, C. M., Dellacrose, J. T., Heffez, J. & Peyman, G. A. (2007). Triamcinolone acetonide in ocular therapeutics. *Surv Ophthalmol*, 52(5), 503-522.
- Jiang, G.-B., Quan, D., Liao, K. & Wang, H. (2006). Novel polymer micelles prepared from chitosan grafted hydrophobic palmitoyl groups for drug delivery. *Mol Pharm*, 3(2), 152-160.
- Jiang, J., Moore, J. S., Edelhauser, H. F. & Prausnitz, M. R. (2009). Intrasceral drug delivery to the eye using hollow microneedles. *Pharmaceutical Research*, 26(2), 395-403.
- Jonas, J., Kreissig, I. & Degenring, R. (2002). Intravitreal triamcinolone acetonide as treatment of macular edema in central retinal vein occlusion. *Graefe's Archive for Clinical and Experimental Ophthalmology*, 240(9), 782-783.
- Jung, K.-M., Lee, S.-H., Ryu, Y.-H., Jang, W.-H., Jung, H.-S., Han, J.-H., *et al.* (2011). A new 3D reconstituted human corneal epithelium model as an alternative method for the eye irritation test. *Toxicology in Vitro*, 25(1), 403-410.
- Kadam, R. S., Cheruvu, N. P. S., Edelhauser, H. F. & Kompella, U. B. (2011). Sclera-choroid-RPE transport of eight beta-blockers in human, bovine, porcine, rabbit, and rat models. *Investigative Ophthalmology & Visual Science*, 52(8), 5387-5399.
- Kalyanasundaram, K. & Thomas, J. K. (1977). Environmental effects on vibronic band intensities in pyrene monomer fluorescence and their application in studies of micellar systems. *Journal of the American Chemical Society*, 99(7), 2039-2044.
- Kanuga, N., Winton, H. L., Beauchene, L., Koman, A., Zerbib, A., Halford, S., *et al.* (2002). Characterization of genetically modified human retinal pigment epithelial

- cells developed for in vitro and transplantation studies. *Investigative Ophthalmology & Visual Science*, 43(2), 546-555.
- Kataoka, K., Harada, A. & Nagasaki, Y. (2012). Block copolymer micelles for drug delivery: Design, characterization and biological significance. *Advanced Drug Delivery Reviews*, 64, Supplement(0), 37-48.
- Katsares, V., Petsa, A., Felesakis, A., Pappas, Z., Nikolaidou, E., Gargani, S., *et al.* (2009). A rapid and accurate method for the stem cell viability evaluation: the case of the thawed umbilical cord blood. *Labmedicine*, 40(9), 557-560.
- Kaur, I. P. & Smitha, R. (2002). Penetration enhancers and ocular bioadhesives: two new avenues for ophthalmic drug delivery. *Drug Development and Industrial Pharmacy*, 28(4), 353-369.
- Kazakevich, Y. & LoBrutto, R. (2007). *HPLC for pharmaceutical scientists*. Hoboken, N.J.: Wiley-Interscience.
- Kedar, U., Phutane, P., Shidhaye, S. & Kadam, V. (2010). Advances in polymeric micelles for drug delivery and tumor targeting. *Nanomedicine: Nanotechnology, Biology and Medicine*, 6(6), 714-729.
- KENALOG<sup>®</sup>-40 INJECTION. (2013) Retrieved 09/05/2013, 2013, from [http://www.accessdata.fda.gov/drugsatfda\\_docs/label/2011/014901s039lbl.pdf](http://www.accessdata.fda.gov/drugsatfda_docs/label/2011/014901s039lbl.pdf)
- Kernt, M., Neubauer, A. S., Liegl, R. G., Lackerbauer, C. A., Eibl, K. H., Alge, C. S., *et al.* (2009). Intracameral moxifloxacin: in vitro safety on human ocular cells. *Cornea*, 28(5), 553-561.
- Kikuchi, T., Suzuki, M., Kusai, A., Iseki, K. & Sasaki, H. (2005). Synergistic effect of EDTA and boric acid on corneal penetration of CS-088. *International Journal of Pharmaceutics*, 290(1-2), 83-89.
- Kim, E., Durairaj, C., Kadam, R., Lee, S., Mo, Y., Geroski, D., *et al.* (2009). Human scleral diffusion of anticancer drugs from solution and nanoparticle formulation. *Pharmaceutical Research*, 26(5), 1155-1161.
- Kim, H., Choi, J.-S., Kim, K. S., Yang, J.-A., Joo, C.-K. & Hahn, S. K. (2012). Flt1 peptide-hyaluronate conjugate micelle-like nanoparticles encapsulating genistein for the treatment of ocular neovascularization. *Acta Biomaterialia*, 8(11), 3932-3940.
- Kim, H. & Csaky, K. G. (2010). Nanoparticle-integrin antagonist C16Y peptide treatment of choroidal neovascularization in rats. *Journal of Controlled Release*, 142(2), 286-293.
- Kim, H., Robinson, S. B. & Csaky, K. G. (2009). Investigating the movement of intravitreal human serum albumin nanoparticles in the vitreous and retina. *Pharmaceutical Research*, 26(2), 329-337.
- Kim, Y. M., Lim, J. O., Kim, H. K., Kim, S. Y. & Shin, J. P. (2008). A novel design of one-side coated biodegradable intrascleral implant for the sustained release of triamcinolone acetonide. *Eur J Pharm Biopharm*, 70(1), 179-186.
- Kirk, W. (2001). The Draize eye test. *Survey of Ophthalmology*, 45(6), 493-515.
- Kishida, K. & Otori, T. (1980). A quantitative study on the relationship between transcorneal permeability of drugs and their hydrophobicity. *Japanese Journal of Ophthalmology*, 24(3), 251-259.
- Kleckner, I. R. & Foster, M. P. (2011). An introduction to NMR-based approaches for measuring protein dynamics. *Biochim Biophys Acta*, 8, 942-968.
- Klein, R., Cruickshanks, K. J., Nash, S. D., Krantz, E. M., Javier Nieto, F., Huang, G. H., *et al.* (2010). The Prevalence of age-related macular degeneration and Associated risk factors. *Archives of Ophthalmology*, 128(6), 750-758.

- Klyce, S. D. & Crosson, C. E. (1985). Transport processes across the rabbit corneal epithelium - a review. *Current Eye Research*, 4(4), 323-331.
- Kobuch, K., Herrmann, W. A., Framme, C., Sachs, H. G., Gabel, V. P. & Hillenkamp, J. (2008). Maintenance of adult porcine retina and retinal pigment epithelium in perfusion culture: Characterisation of an organotypic in vitro model. *Experimental Eye Research*, 86(4), 661-668.
- Koeberle, M. J., Hughes, P. M., Skellern, G. G. & Wilson, C. G. (2006). Pharmacokinetics and disposition of memantine in the arterially perfused bovine eye. *Pharmaceutical Research*, 23(12), 2781-2798.
- Kolb, H., Fernandez, E. & Nelson, R. (2007). *Webvision: The Organization of the Retina and Visual System*: National Library of Medicine (US).
- Kolle, S. N., Kandárová, H., Wareing, B., van Ravenzwaay, B. & Landsiedel, R. (2011). In-house validation of the EpiOcular™ eye irritation test and its combination with the Bovine Corneal Opacity and Permeability test for the assessment of ocular irritation. *Alternatives to Laboratory Animals-ATLA*, 39(4), 365.
- Komai, Y. & Ushiki, T. (1991a). The 3-dimensional organization of collagen fibrils in the human cornea and sclera. *Investigative ophthalmology & visual science*, 32(8), 2244-2258.
- Komai, Y. & Ushiki, T. (1991b). The three-dimensional organization of collagen fibrils in the human cornea and sclera. *Investigative Ophthalmology and Visual Science*, 32(8), 2244-2258.
- Kompella, U. B. & Edelhauser, H. F. (2011). *Drug product development for the back of the eye*. New York: Springer.
- Koo, H., Moon, H., Han, H., Na, J. H., Huh, M. S., Park, J. H., *et al.* (2012). The movement of self-assembled amphiphilic polymeric nanoparticles in the vitreous and retina after intravitreal injection. *Biomaterials*, 33(12), 3485-3493.
- Krug, S. M., Amasheh, M., Dittmann, I., Christoffel, I., Fromm, M. & Amasheh, S. (2013). Sodium caprate as an enhancer of macromolecule permeation across tricellular tight junctions of intestinal cells. *Biomaterials*, 34(1), 275-282.
- Kruszewski, F., Walker, T. & DiPasquale, L. (1997). Evaluation of a human corneal epithelial cell line as an in vitro model for assessing ocular irritation. *Toxicological Sciences*, 36(2), 130-140.
- Kuang, Y., Liu, J., Liu, Z. & Zhuo, R. (2012). Cholesterol-based anionic long-circulating cisplatin liposomes with reduced renal toxicity. *Biomaterials*, 33(5), 1596-1606.
- Kuppermann, B. D., Blumenkranz, M. S., Haller, J. A., Williams, G. A., Weinberg, D. V., Chou, C., *et al.* (2007). Randomized controlled study of an intravitreal dexamethasone drug delivery system in patients with persistent macular edema. *Arch Ophthalmol*, 125(3), 309-317.
- Lachenmeier, D. W. (2008). Safety evaluation of topical applications of ethanol on the skin and inside the oral cavity. *Journal of occupational medicine and toxicology (London, England)*, 3, 26-26.
- Landau, D., Schneidman, E. M., Jacobovitz, T. & Rozenman, Y. (1997). Quantitative In Vivo Retinal Thickness Measurements in Healthy Subjects. *Ophthalmology*, 104(4), 639-642.
- Lawrence, J. N. (1997). Electrical resistance and tritiated water permeability as indicators of barrier integrity of in vitro human skin. *Toxicology in Vitro*, 11(3), 241-249.
- Lee, S.-B., Geroski, D. H., Prausnitz, M. R. & Edelhauser, H. F. (2004). Drug delivery through the sclera: effects of thickness, hydration, and sustained release systems. *Experimental Eye Research*, 78(3), 599-607.

- Lee, S. S., Hughes, P., Ross, A. D. & Robinson, M. R. (2010). Biodegradable implants for sustained drug release in the eye. *Pharmaceutical Research*, 27(10), 2043-2053.
- Lee, S. Y., Chee, S. P., Balakrishnan, V., Farzavandi, S. & Tan, D. T. H. (2003). Surodex in paediatric cataract surgery. *British Journal of Ophthalmology*, 87(11), 1424-1426.
- Lee, V. H. & Robinson, J. R. (1986). Topical ocular drug delivery: recent developments and future challenges. *J Ocul Pharmacol*, 2(1), 67-108.
- Lee, V. H. L. (1990). Mechanisms and facilitation of corneal drug penetration. *Journal of Controlled Release*, 11(1-3), 79-90.
- Lee, V. H. L., Carson, L. W. & Takemoto, K. A. (1986). Macromolecular drug absorption in the albino rabbit eye. *International Journal of Pharmaceutics*, 29(1), 43-51.
- Lee, Y. S. (2008). *Self-assembly and nanotechnology : a force balance approach*. Hoboken, N.J.: John Wiley & Sons.
- Lehner, R., Wang, X., Marsch, S. & Hunziker, P. (2013). Intelligent nanomaterials for medicine: Carrier platforms and targeting strategies in the context of clinical application. *Nanomedicine: Nanotechnology, Biology and Medicine*, 9(6), 742-757.
- Lens, A., Nemeth, S. C. & Ledford, J. K. (2008). *Ocular anatomy and physiology*: Slack Incorporated.
- Letchford, K. & Burt, H. (2007). A review of the formation and classification of amphiphilic block copolymer nanoparticulate structures: micelles, nanospheres, nanocapsules and polymersomes. *European Journal of Pharmaceutics and Biopharmaceutics*, 65(3), 259-269.
- Li, H. F., Petroll, W. M., Møller-Pedersen, T., Maurer, J. K., Cavanagh, H. D. & Jester, J. V. (1997). Epithelial and corneal thickness measurements by in vivo confocal microscopy through focusing (CMTF). *Current Eye Research*, 16(3), 214-221.
- Li, J.-M., Chou, H.-C., Wang, S.-H., Wu, C.-L., Chen, Y.-W., Lin, S.-T., *et al.* (2013). Hyaluronic acid-dependent protection against UVB-damaged human corneal cells. *Environmental and molecular mutagenesis*, 54(6), 429-449.
- Li, N., Zhuang, C. Y., Wang, M., Sui, C. G. & Pan, W. S. (2012). Low molecular weight chitosan-coated liposomes for ocular drug delivery: In vitro and in vivo studies. *Drug Delivery*, 19(1), 28-35.
- Li, X., Qian, Y., Liu, T., Hu, X., Zhang, G., You, Y., *et al.* (2011). Amphiphilic multiarm star block copolymer-based multifunctional unimolecular micelles for cancer targeted drug delivery and MR imaging. *Biomaterials*, 32(27), 6595-6605.
- Liaw, J. & Robinson, J. R. (1992). The effect of polyethylene glycol molecular weight on corneal transport and the related influence of penetration enhancers. *International Journal of Pharmaceutics*, 88(1-3), 125-140.
- Liaw, J., Rojanasakul, Y. & Robinson, J. R. (1992). The effect of drug charge type and charge density on corneal transport. *International Journal of Pharmaceutics*, 88(1-3), 111-124.
- Lim, J. I., Fung, A. E., Wieland, M., Hung, D. & Wong, V. (2011). Sustained-release intravitreal liquid drug delivery using triamcinolone acetonide for cystoid macular edema in retinal vein occlusion. *Ophthalmology*, 118(7), 1416-1422.
- Lin, G., Zhang, X., Kumar, S. R. & Mark, J. E. (2009). Improved hydrophilicity from poly(ethylene glycol) in amphiphilic conetworks with poly(dimethylsiloxane). *Silicon*, 1(3), 173-181.
- Lin, Y. & Alexandridis, P. (2002). Self-assembly of an amphiphilic siloxane graft copolymer in water. *The Journal of Physical Chemistry B*, 106(42), 10845-10853.
- Liu, S. Y., Jones, L. & Gu, F. X. (2012). Nanomaterials for ocular drug delivery. *Macromolecular Bioscience*, 12(5), 608-620.

- Liu, X. M., Pramoda, K. P., Yang, Y.-Y., Chow, S. Y. & He, C. (2004). Cholesteryl-grafted functional amphiphilic poly(N-isopropylacrylamide-co-N-hydroxymethylacrylamide): synthesis, temperature-sensitivity, self-assembly and encapsulation of a hydrophobic agent. *Biomaterials*, 25(13), 2619-2628.
- Liu, Y., Wang, Y., Zhuang, D., Yang, J. & Yang, J. (2012). Bionanoparticles of amphiphilic copolymers polyacrylate bearing cholesterol and ascorbate for drug delivery. *Journal of Colloid and Interface Science*, 377(1), 197-206.
- Loch, C., Zakelj, S., Kristl, A., Nagel, S., Guthoff, R., Weitschies, W., *et al.* (2012). Determination of permeability coefficients of ophthalmic drugs through different layers of porcine, rabbit and bovine eyes. *European Journal of Pharmaceutical Sciences*, 47(1), 131-138.
- Lund, R. D., Adamson, P., Sauve, Y., Keegan, D. J., Girman, S. V., Wang, S. M., *et al.* (2001). Subretinal transplantation of genetically modified human cell lines attenuates loss of visual function in dystrophic rats. *Proceedings of the National Academy of Sciences of the United States of America*, 98(17), 9942-9947.
- Macha, S. & Mitra, A. K. (2003). Overview of ocular drug delivery *Ophthalmic Drug Delivery Systems* (2 ed., pp. 847).
- Macoul, K. L. & Pavanlangston, D. (1975). Pilocarpine ocusert system for sustained control of ocular hypertension. *Archives of Ophthalmology*, 93(8), 587-590.
- Mahmud, A., Xiong, X.-B. & Lavasanifar, A. (2008). Development of novel polymeric micellar drug conjugates and nano-containers with hydrolyzable core structure for doxorubicin delivery. *European Journal of Pharmaceutics and Biopharmaceutics*, 69(3), 923-934.
- Mains, J. & Wilson, C. G. (2013). The Vitreous Humor As a Barrier to Nanoparticle Distribution. *Journal of Ocular Pharmacology and Therapeutics*, 29(2), 143-150.
- Majumdar, S., Hingorani, T. & Srirangam, R. (2010). Evaluation of active and passive transport processes in corneas extracted from preserved rabbit eyes. *Journal of Pharmaceutical Sciences*, 99(4), 1921-1930.
- Malik, P., Kadam, R. S., Cheruvu, N. P. & Kompella, U. B. (2012). Hydrophilic prodrug approach for reduced pigment binding and enhanced transscleral retinal delivery of celecoxib. *Mol Pharm*, 9(3), 605-614.
- Mandell, A. I., Stentz, F. & Kitabchi, A. E. (1978). Dipivalyl epinephrine - new pro-drug in treatment of glaucoma. *Ophthalmology*, 85(3), 268-275.
- Mao, S., Shuai, X., Unger, F., Wittmar, M., Xie, X. & Kissel, T. (2005). Synthesis, characterization and cytotoxicity of poly(ethylene glycol)-graft-trimethyl chitosan block copolymers. *Biomaterials*, 26(32), 6343-6356.
- Marshall, N., Goodwin, C. & Holt, S. (1995). A critical assessment of the use of microculture tetrazolium assays to measure cell growth and function. *Growth regulation*, 5(2), 69.
- Matsui, K., Nakazawa, T. & Morisaki, H. (1991). Micellar formation of sodium dodecyl-sulfate in sol-gel glasses probed by pyrene fluorescence. *Journal of Physical Chemistry*, 95(2), 976-979.
- Maurice, D. M. (1973). The dynamics and drainage of tears. *International Ophthalmology Clinics*, 13(1), 103-116.
- Maurice, D. M. & Polgar, J. (1977). Diffusion across the sclera. *Experimental Eye Research*, 25(6), 577-582.
- Maza, M. S. d. l., Tauber, J. & Foster, C. S. (2012). *The sclera* (2nd ed.). New York: Springer.
- McDonald, M., D'Aversa, G., Perry, H. D., Wittpenn, J. R., Donnenfeld, E. D. & Nelinson, D. S. (2009). Hydroxypropyl cellulose ophthalmic inserts (lacrisert) reduce the

- signs and symptoms of dry eye syndrome and improve patient quality of life. *Trans Am Ophthalmol Soc*, 107, 214-221.
- Minimol, P. F., Paul, W. & Sharma, C. P. (2013). PEGylated starch acetate nanoparticles and its potential use for oral insulin delivery. *Carbohydrate Polymers*, 95(1), 1-8.
- Mitra, A. K. (2003). *Ophthalmic drug delivery systems* (2nd ed.). New York: Marcel Dekker.
- Mitra, A. K., Velagaleti, P. R. & Grau, U. M. (2010). Topical drug delivery systems for ophthalmic use: WO Patent 2,010,144,194.
- Molokhia, S. A., Sant, H., Simonis, J., Bishop, C. J., Burr, R. M., Gale, B. K., *et al.* (2010). The capsule drug device: Novel approach for drug delivery to the eye. *Vision Research*, 50(7), 680-685.
- Molokhia, S. A., Thomas, S. C., Garff, K. J., Mandell, K. J. & Wirostko, B. M. (2013). Anterior Eye Segment Drug Delivery Systems: Current Treatments and Future Challenges. *Journal of Ocular Pharmacology and Therapeutics*, 29(2), 92-105.
- Moore, K. L., Dalley, A. F. & Agur, A. M. R. (2009). *Clinically oriented anatomy* (6 ed.): Lippincott Williams & Wilkins, 2009.
- Mora, P., Eperon, S., Felt-Baeyens, O., Gurny, R., Sagodira, S., Breton, P., *et al.* (2005). Trans-scleral diffusion of triamcinolone acetonide. *Current Eye Research*, 30(5), 355-361.
- Mosher, G. L. & Mikkelsen, T. J. (1979). Permeability of the n-alkyl p-aminobenzoate esters across the isolated corneal membrane of the rabbit. *International Journal of Pharmaceutics*, 2(3-4), 239-243.
- Mosmann, T. (1983). Rapid colorimetric assay for cellular growth and survival: application to proliferation and cytotoxicity assays. *Journal of Immunological Methods*, 65(1-2), 55-63.
- Mukherjee, B., Santra, K., Pattnaik, G. & Ghosh, S. (2008). Preparation, characterization and in-vitro evaluation of sustained release protein-loaded nanoparticles based on biodegradable polymers. *Int J Nanomedicine*, 3(4), 487-496.
- Myles, M. E., Neumann, D. M. & Hill, J. M. (2005). Recent progress in ocular drug delivery for posterior segment disease: emphasis on transscleral iontophoresis. *Advanced Drug Delivery Reviews*, 57(14), 2063-2079.
- Myung, D., Derr, K., Huie, P., Noolandi, J., Ta, K. P. & Ta, C. N. (2006). Glucose permeability of human, bovine, and porcine corneas in vitro. *Ophthalmic Research*, 38(3), 158-163.
- Nagarwal, R. C., Kant, S., Singh, P. N., Maiti, P. & Pandit, J. K. (2009). Polymeric nanoparticulate system: A potential approach for ocular drug delivery. *Journal of Controlled Release*, 136(1), 2-13.
- Nagarwal, R. C., Kumar, R. & Pandit, J. K. (2012). Chitosan coated sodium alginate-chitosan nanoparticles loaded with 5-FU for ocular delivery: In vitro characterization and in vivo study in rabbit eye. *European Journal of Pharmaceutical Sciences*, 47(4), 678-685.
- Nair, K. L., Vidyanand, S., James, J. & Kumar, G. S. V. (2012). Pilocarpine-loaded poly(DL-lactic-co-glycolic acid) nanoparticles as potential candidates for controlled drug delivery with enhanced ocular pharmacological response. *Journal of Applied Polymer Science*, 124(3), 2030-2036.
- Nanomedicine. (2005) Retrieved 13/03/2013, 2013, from <http://www.nanopharmaceuticals.org/files/nanomedicine.pdf>
- Nastiti, C. M. R. R. (2007). *Development and evaluation of polymeric nanoparticle formulations for triamcinolone acetonide delivery*. Master of Pharmacy Curtin University of Technology

- National Institute for Health and Care Excellence. (2013) Retrieved 07/07/2013, 2013, from <http://www.nice.org.uk/newsroom/pressreleases/NICESaysYesToRanibizumabForDiabeticMacularOedemaInFinalDraftGuidanceAfterRapidReview.jsp>
- Nicholson, B. P., Singh, R. P., Sears, J. E., Lowder, C. Y. & Kaiser, P. K. (2012). Evaluation of fluocinolone acetonide sustained release implant (retisert) dissociation during Implant removal and exchange surgery. *American Journal of Ophthalmology*, 154(6), 969-973.e961.
- Nicoli, S., Ferrari, G., Quarta, M., Macaluso, C., Govoni, P., Dallatana, D., *et al.* (2009). Porcine sclera as a model of human sclera for in vitro transport experiments: histology, SEM, and comparative permeability. *Molecular vision*, 15, 259-266.
- Niemeyer, G. (2001). Retinal research using the perfused mammalian eye. *Progress in Retinal and Eye Research*, 20(3), 289-318.
- Nimesh, S., Kumar, R. & Chandra, R. (2006). Novel polyallylamine–dextran sulfate–DNA nanoplexes: highly efficient non-viral vector for gene delivery. *International Journal of Pharmaceutics*, 320(1–2), 143-149.
- Nishiyama, N. & Kataoka, K. (2006). Current state, achievements, and future prospects of polymeric micelles as nanocarriers for drug and gene delivery. *Pharmacology & Therapeutics*, 112(3), 630-648.
- Norman, R. E., Flanagan, J. G., Rausch, S. M. K., Sigal, I. A., Tertinegg, I., Eilaghi, A., *et al.* (2010). Dimensions of the human sclera: thickness measurement and regional changes with axial length. *Experimental Eye Research*, 90(2), 277-284.
- Notara, M. & Daniels, J. T. (2010). Characterisation and functional features of a spontaneously immortalised human corneal epithelial cell line with progenitor-like characteristics. *Brain Research Bulletin*, 81(2-3), 279-286.
- O'Brien, J. & Pognan, F. (2001). Investigation of the alamar blue (resazurin) fluorescent dye for the assessment of mammalian cell cytotoxicity. *Toxicology*, 164(1-3), 132-132.
- Organisation for Economic Co-operation and Development. (2009). Skin irritation test protocol using the reconstructed human model "LABCYTE EPI-MODEL 24" Retrieved 09/10, 2013, from <http://www.oecd.org/env/ehs/testing/44302392.pdf>
- Oerlemans, C., Bult, W., Bos, M., Storm, G., Nijssen, J. F. W. & Hennink, W. E. (2010). Polymeric micelles in anticancer therapy: targeting, imaging and triggered release. *Pharmaceutical Research*, 27(12), 2569-2589.
- Office for National Statistics. (2002). Prevalence of diagnosed diabetes mellitus in general practice in England and Wales, 1994 to 1998 Retrieved 26/09/2012, 2012, from <http://www.ons.gov.uk/ons/search/index.html?pageSize=50&sortBy=none&sortDirection=none&newquery=diabetes>
- Oh, J. Y., Kim, M. K., Lee, H. J., Ko, J. H., Wee, W. R. & Lee, J. H. (2009). Comparative observation of freeze-thaw-induced damage in pig, rabbit, and human corneal stroma. *Veterinary Ophthalmology*, 12, 50-56.
- Ohashi, Y., Dogru, M. & Tsubota, K. (2006). Laboratory findings in tear fluid analysis. *Clinica Chimica Acta*, 369(1), 17-28.
- Olsen, T. W., Aaberg, S. Y., Geroski, D. H. & Edelhauser, H. F. (1998). Human sclera: thickness and surface area. *Am J Ophthalmol*, 125(2), 237-241.
- Olsen, T. W., Edelhauser, H. F., Lim, J. I. & Geroski, D. H. (1995). Human scleral permeability - effects of age, cryotherapy, transscleral diode-laser, and surgical thinning. *Investigative ophthalmology & visual science*, 36(4), S159-S159.
- Olsen, T. W., Feng, X., Warner, K., Conston, S. R., Sierra, D. H., Folden, D. V., *et al.* (2006). Cannulation of the suprachoroidal space: a novel drug delivery

- methodology to the posterior segment. *American Journal of Ophthalmology*, 142(5), 777-787.
- Olsen, T. W., Sanderson, S., Feng, X. & Hubbard, W. C. (2002). Porcine sclera: thickness and surface area. *Invest Ophthalmol Vis Sci*, 43(8), 2529-2532.
- Ostacolo, C., Caruso, C., Tronino, D., Troisi, S., Laneri, S., Pacente, L., *et al.* (2013). Enhancement of corneal permeation of riboflavin-5'-phosphate through vitamin E TPGS: A promising approach in corneal trans-epithelial cross linking treatment. *International Journal of Pharmaceutics*, 440(2), 148-153.
- Papadimitriou, S. A., Achilias, D. S. & Bikiaris, D. N. (2012). Chitosan-g-PEG nanoparticles ionically crosslinked with poly(glutamic acid) and tripolyphosphate as protein delivery systems. *International Journal of Pharmaceutics*, 430(1-2), 318-327.
- Patel, H. D., Zaveri, A. D., Zaveri, D. N., Shah, S. & Solanki, A. (2013). Comparison of the MTT and alamar blue assay for in vitro anti cancer activity by testing of various chalcone and thiosemicarbazone derivatives. *International Journal of Pharma & Bio Sciences*, 4(2).
- Patel, P., Shastri, D., Shelat, P. & Shukla, A. (2010). Ophthalmic drug delivery system: Challenges and approaches. *Systematic Reviews in Pharmacy*, 1(2), 113.
- Patel, S. V., McLaren, J. W., Hodge, D. O. & Bourne, W. M. (2001). Normal human keratocyte density and corneal thickness measurement by using confocal microscopy in vivo. *Investigative Ophthalmology & Visual Science*, 42(2), 333-339.
- Pathak, A., Aggarwal, A., Kurupati, R. K., Patnaik, S., Swami, A., Singh, Y., *et al.* (2007). Engineered polyallylamine nanoparticles for efficient in vitro transfection. *Pharm Res*, 24(8), 1427-1440.
- Pathak, Y. & Thassu, D. (2009). *Drug delivery nanoparticles formulation and characterization*. New York: Informa Healthcare.
- Peeters, L., Sanders, N. N., Braeckmans, K., Boussery, K., Van de Voorde, J., De Smedt, S. C., *et al.* (2005). Vitreous: a barrier to nonviral ocular gene therapy. *Invest Ophthalmol Vis Sci*, 46(10), 3553-3561.
- Pels, E., Beele, H. & Claerhout, I. (2008). Eye bank issues: II. preservation techniques: warm versus cold storage. *Int Ophthalmol*, 28(3), 155-163.
- Pepic, I., Hafner, A., Lovric, J., Pirkic, B. & Filipovic-Grcic, J. (2010). A Nonionic Surfactant/Chitosan Micelle System in an Innovative Eye Drop Formulation. *Journal of Pharmaceutical Sciences*, 99(10), 4317-4325.
- Pescina, S., Ferrari, G., Govoni, P., Macaluso, C., Padula, C., Santi, P., *et al.* (2010). In-vitro permeation of bevacizumab through human sclera: effect of iontophoresis application. *Journal of Pharmacy and Pharmacology*, 62(9), 1189-1194.
- Pescina, S., Santi, P., Ferrari, G., Padula, C., Cavallini, P., Govoni, P., *et al.* (2012). Ex vivo models to evaluate the role of ocular melanin in trans-scleral drug delivery. *European Journal of Pharmaceutical Sciences*, 46(5), 475-483.
- Pfannenbecker, U., Bessou-Touya, S., Faller, C., Harbell, J., Jacob, T., Raabe, H., *et al.* (2013). Cosmetics Europe multi-laboratory pre-validation of the EpiOcular™ reconstituted human tissue test method for the prediction of eye irritation. *Toxicology in Vitro*, 27(2), 619-626.
- Picot, J. (2004). *Human cell culture protocols* (Vol. 107): Humana Press.
- Pignatello, R., Bucolo, C., Ferrara, P., Maltese, A., Puleo, A. & Puglisi, G. (2002). Eudragit RS100® nanosuspensions for the ophthalmic controlled delivery of ibuprofen. *European Journal of Pharmaceutical Sciences*, 16(1-2), 53-61.

- Pijl, B. J., Theelen, T., Tilanus, M. A. D., Rentenaar, R. & Crama, N. (2010). Acute endophthalmitis after cataract surgery: 250 consecutive cases treated at a tertiary referral center in the netherlands. *American Journal of Ophthalmology*, 149(3), 482-487.
- Pitkänen, L., Ranta, V.-P., Moilanen, H. & Urtti, A. (2005). Permeability of retinal pigment epithelium: effects of permeant molecular weight and lipophilicity. *Investigative Ophthalmology & Visual Science*, 46(2), 641-646.
- Plumb, J. A., Milroy, R. & Kaye, S. B. (1989). Effects of the ph-dependence of 3-(4,5-dimethylthiazol-2-yl)-2,5-diphenyl-tetrazolium bromide-formazan absorption on chemosensitivity determined by a novel tetrazolium-based assay. *Cancer Research*, 49(16), 4435-4440.
- Prasad, P. S., Schwartz, S. D. & Hubschman, J. P. (2010). Age-related macular degeneration: current and novel therapies. *Maturitas*, 66(1), 46-50.
- Prince, J. H. (1960). *Anatomy and histology of the eye and orbit in domestic animals*: Springfield.
- Prow, T. W. (2010). Toxicity of nanomaterials to the eye. *Wiley Interdisciplinary Reviews: Nanomedicine and Nanobiotechnology*, 2(4), 317-333.
- Qaddoumi, M. G., Ueda, H., Yang, J., Davda, J., Labhasetwar, V. & Lee, V. H. L. (2004). The characteristics and mechanisms of uptake of PLGA nanoparticles in rabbit conjunctival epithelial cell layers. *Pharmaceutical Research*, 21(4), 641-648.
- Qi, H.-P., Gao, X.-C., Zhang, L.-Q., Wei, S.-Q., Bi, S., Yang, Z.-C., *et al.* (2013). In vitro evaluation of enhancing effect of borneol on transcorneal permeation of compounds with different hydrophilicities and molecular sizes. *European journal of pharmacology*.
- Qu, X. Z., Khutoryanskiy, V. V., Stewart, A., Rahman, S., Papahadjopoulos-Sternberg, B., Dufes, C., *et al.* (2006). Carbohydrate-based micelle clusters which enhance hydrophobic drug bioavailability by up to 1 order of magnitude. *Biomacromolecules*, 7(12), 3452-3459.
- Rabinovich-Guilatt, L., Couvreur, P., Lambert, G. & Dubernet, C. (2004). Cationic vectors in ocular drug delivery. *J Drug Target*, 12(9-10), 623-633.
- Rampersad, S. N. (2012). Multiple applications of Alamar Blue as an indicator of metabolic function and cellular health in cell viability bioassays. *Sensors*, 12(9), 12347-12360.
- Ranta, V.-P., Mannermaa, E., Lummeppuro, K., Subrizi, A., Laukkanen, A., Antopolsky, M., *et al.* (2010). Barrier analysis of periocular drug delivery to the posterior segment. *Journal of Controlled Release*, 148(1), 42-48.
- Rao, J. P. & Geckeler, K. E. (2011). Polymer nanoparticles: preparation techniques and size-control parameters. *Progress in Polymer Science*, 36(7), 887-913.
- Rathbone, M. J., Hadgraft, J. & Roberts, M. S. (2003). *Modified-release drug delivery technology* (Vol. 1): CRC Press.
- Reichl, S., Döhring, S., Bednarz, J. & Müller-Goymann, C. C. (2005). Human cornea construct HCC—an alternative for in vitro permeation studies? a comparison with human donor corneas. *European Journal of Pharmaceutics and Biopharmaceutics*, 60(2), 305-308.
- Remington, J. P., Troy, D. B. & Beringer, P. (2006). *Remington: The science and practice of pharmacy* (Vol. 1): Wolters Kluwer Health.
- Riss, T. L., Moravec, R. A., Niles, A. L., Benink, H. A., Worzella, T. J. & Minor, L. (2004). Cell viability assays. In G. S. Sittampalam, N. Gal-Edd, M. Arkin, D. Auld, C. Austin, B. Bejcek, M. Glicksman, J. Inglese, V. Lemmon, Z. Li, J. McGee, O.

- McManus, L. Minor, A. Napper, T. Riss, O. J. Trask & J. Weidner (Eds.), *Assay Guidance Manual*. Bethesda (MD).
- Roberts, M. J., Bentley, M. D. & Harris, J. M. (2002). Chemistry for peptide and protein PEGylation. *Advanced Drug Delivery Reviews*, 54(4), 459-476.
- Rogers, K. (2010). *The eye : the physiology of human perception* (1st ed.). New York: Britannica Educational Pub. in association with Rosen Educational Services.
- Rudnick, D. E., Noonan, J. S., Geroski, D. H., Prausnitz, M. R. & Edelhauser, H. F. (1999). The effect of intraocular pressure on human and rabbit scleral permeability. *Investigative Ophthalmology and Visual Science*, 40(12), 3054-3058.
- Rufer, F., Schroder, A. & Erb, C. (2005). White-to-white corneal diameter: normal values in healthy humans obtained with the Orbscan II topography system. *Cornea*, 24(3), 259-261.
- Sakurai, E., Ozeki, H., Kunou, N. & Ogura, Y. (2001). Effect of particle size of polymeric nanospheres on intravitreal kinetics. *Ophthalmic Research*, 33(1), 31-36.
- Salek, S. S., Leder, H. A., Butler, N. J., Gan, T. J., Dunn, J. P. & Thorne, J. E. (2013). Periocular triamcinolone acetonide injections for control of intraocular inflammation associated with uveitis. *Ocul Immunol Inflamm*, 21(4), 257-263.
- Salminen, L., Urtti, A., Kujari, H. & Juslin, M. (1983). Prolonged pulse-entry of pilocarpine with a soluble drug insert. *Graefes Archive for Clinical and Experimental Ophthalmology*, 221(2), 96-99.
- Sanford, M. (2013). Fluocinolone acetonide intravitreal implant (iluvien()) : in diabetic macular oedema. *Drugs*, 73(2), 187-193.
- Sarkar, D., El Khoury, J. M., Lopina, S. T. & Hu, J. (2007). Grafting poly(t-butyl acrylate) to poly(allylamine) by inverse microemulsion radical polymerization: From comb-polymer to amphiphilic shell crosslinked polymer nanocapsule. *Journal of Applied Polymer Science*, 104(3), 1905-1911.
- Sarmiento, B. & das Neves, J. (2012). *Chitosan-based systems for biopharmaceuticals: delivery, targeting and polymer therapeutics*: Wiley. com.
- Schaeffer, H. E. & Krohn, D. L. (1982). Liposomes in topical drug delivery. *Investigative Ophthalmology & Visual Science*, 22(2), 220-227.
- Schoenwald, R. D. & Huang, H. S. (1983). Corneal penetration behavior of beta-blocking-agents .1. physicochemical factors. *Journal of Pharmaceutical Sciences*, 72(11), 1266-1272.
- Schoenwald, R. D. & Ward, R. L. (1978). Relationship between steroid permeability across excised rabbit cornea and octanol-water partition-coefficients. *Journal of Pharmaceutical Sciences*, 67(6), 786-788.
- Scott, I. U., Loo, R. H., Flynn, H. W., Jr. & Miller, D. (2003). Endophthalmitis caused by enterococcus faecalis: antibiotic selection and treatment outcomes. *Ophthalmology*, 110(8), 1573-1577.
- Shabir, G. A. (2003). Validation of high-performance liquid chromatography methods for pharmaceutical analysis: Understanding the differences and similarities between validation requirements of the US Food and Drug Administration, the US Pharmacopeia and the International Conference on Harmonization. *Journal of Chromatography A*, 987(1-2), 57-66.
- Shen, Y. C., Wang, C. Y., Tsai, H. Y. & Lee, H. N. (2010). Intracameral voriconazole injection in the treatment of fungal endophthalmitis resulting from keratitis. *Am J Ophthalmol*, 149(6), 916-921.
- Shibuya, T., Kashiwagi, K. & Tsukahara, S. (2003). Comparison of efficacy and tolerability between two gel-forming timolol maleate ophthalmic solutions in patients with glaucoma or ocular hypertension. *Ophthalmologica*, 217(1), 31-38.

- Siepmann, J. (2012). *Fundamentals and applications of controlled release drug delivery*: Springer.
- Sihvola, P. & Puustjarvi, T. (1981). Practical problems in the use of ocusert pilocarpine delivery system. *Acta Ophthalmologica*, 58(6), 933-937.
- Sinha, V. R., Bansal, K., Kaushik, R., Kumria, R. & Trehan, A. (2004). Poly- $\epsilon$ -caprolactone microspheres and nanospheres: an overview. *International Journal of Pharmaceutics*, 278(1), 1-23.
- Sivaprasad, S., McCluskey, P. & Lightman, S. (2006). Intravitreal steroids in the management of macular oedema. *Acta Ophthalmol Scand*, 84(6), 722-733.
- Spitzer, M. S., Wallenfels-Thilo, B., Sierra, A., Yoeruek, E., Peters, S., Henke-Fahle, S., *et al.* (2006). Antiproliferative and cytotoxic properties of bevacizumab on different ocular cells. *British Journal of Ophthalmology*, 90(10), 1316-1321.
- Steckel, H., Thies, J. & Müller, B. W. (1997). Micronizing of steroids for pulmonary delivery by supercritical carbon dioxide. *International Journal of Pharmaceutics*, 152(1), 99-110.
- Stone, V., Johnston, H. & Schins, R. P. F. (2009). Development of in vitro systems for nanotoxicology: methodological considerations. *Critical Reviews in Toxicology*, 39(7), 613-626.
- Suen, W.-L. L. & Chau, Y. (2013). Specific uptake of folate-decorated triamcinolone-encapsulating nanoparticles by retinal pigment epithelium cells enhances and prolongs antiangiogenic activity. *Journal of Controlled Release*, 167(1), 21-28.
- Sun, L.-l., Du, Z.-p., Wang, W.-x. & Liu, Y. (2011). Synthesis and Self-Assembly Behavior of Comb-Like Surfactant Polymethyl Methacrylate-g-Methoxy Polyethylene Glycol. *Journal of Surfactants and Detergents*, 14(2), 161-166.
- Tanito, M., Hara, K., Takai, Y., Matsuoka, Y., Nishimura, N., Jansook, P., *et al.* (2011). Topical dexamethasone-cyclodextrin microparticle eye drops for diabetic macular edema. *Investigative Ophthalmology & Visual Science*, 52(11), 7944-7948.
- Thakur, A., Kadam, R. S. & Kompella, U. B. (2011). Influence of drug solubility and lipophilicity on transscleral retinal delivery of six corticosteroids. *Drug Metabolism and Disposition*, 39(5), 771-781.
- Thassu, D. & Chader, G. (2013). *Ocular drug delivery systems : barriers and application of nanoparticulate systems*. Boca Raton: CRC Press/Taylor & Francis.
- The NHS Information Centre, L. S. (2012). Statistics on obesity, physical activity and diet: England, 2012, from [http://www.ic.nhs.uk/webfiles/publications/003\\_Health\\_Lifestyles/OPAD12/Statistics\\_on\\_Obesity\\_Physical\\_Activity\\_and\\_Diet\\_England\\_2012.pdf](http://www.ic.nhs.uk/webfiles/publications/003_Health_Lifestyles/OPAD12/Statistics_on_Obesity_Physical_Activity_and_Diet_England_2012.pdf)
- Thomas, M. & Klibanov, A. M. (2002). Enhancing polyethylenimine's delivery of plasmid DNA into mammalian cells. *Proceedings of the National Academy of Sciences*, 99(23), 14640-14645.
- Thompson, C. J., Cheng, W. P., Gadad, P., Skene, K., Smith, M., Smith, G., *et al.* (2011). Uptake and transport of novel amphiphilic polyelectrolyte-insulin nanocomplexes by caco-2 cells-towards oral insulin. *Pharmaceutical Research*, 28(4), 886-896.
- Thompson, C. J., Ding, C., Qu, X., Yang, Z., Uchegbu, I., Tetley, L., *et al.* (2008). The effect of polymer architecture on the nano self-assemblies based on novel comb-shaped amphiphilic poly(allylamine). *Colloid and Polymer Science*, 286(13), 1511-1526.
- Thompson, C. J., Tetley, L. & Cheng, W. P. (2010). The influence of polymer architecture on the protective effect of novel comb shaped amphiphilic poly(allylamine) against in vitro enzymatic degradation of insulin—Towards oral insulin delivery. *International Journal of Pharmaceutics*, 383(1-2), 216-227.

- Thompson, C. J., Tetley, L., Uchegbu, I. F. & Cheng, W. P. (2009). The complexation between novel comb shaped amphiphilic polyallylamine and insulin—Towards oral insulin delivery. *International Journal of Pharmaceutics*, 376(1–2), 46-55.
- Tiyaboonchai, W. (2003). Chitosan nanoparticles: a promising system for drug delivery. *Naresuan University Journal*, 11(3), 51-66.
- To, C. H., Kong, C. W., Chan, C. Y., Shahidullah, M. & Do, C. W. (2002). The mechanism of aqueous humour formation. *Clin Exp Optom*, 85(6), 335-349.
- Torchilin, V. P. (2006). *Nanoparticulates as drug carriers*. London, Hackensack, N.J.: Imperial College Press
- Touitou, E. & Barry, B. W. (2007). *Enhancement in drug delivery*. Boca Raton: CRC Press.
- Tsonis, A. A. (2008). *Animal models in eye research*: Academic Press.
- Ungphaiboon, S. & Maitani, Y. (2001). In vitro permeation studies of triamcinolone acetonide mouthwashes. *International Journal of Pharmaceutics*, 220(1–2), 111-117.
- Urtti, A. (2006). Challenges and obstacles of ocular pharmacokinetics and drug delivery. *Adv Drug Deliv Rev*, 58(11), 1131-1135.
- US Food and Drug Administration. (1994). Center for Drug Evaluation and Research, Reviewer guidance validation of chromatographic methods. Retrieved from
- Van der Merwe, D. & Riviere, J. E. (2005). Comparative studies on the effects of water, ethanol and water/ethanol mixtures on chemical partitioning into porcine stratum corneum and silastic membrane. *Toxicology in Vitro*, 19(1), 69-77.
- Vandamme, T. F. & Brobeck, L. (2005). Poly(amidoamine) dendrimers as ophthalmic vehicles for ocular delivery of pilocarpine nitrate and tropicamide. *Journal of Controlled Release*, 102(1), 23-38.
- Vannas, S. & Teir, H. (1960). Observations on structures and age changes in the human sclera. *Acta Ophthalmologica*, 38(3), 268-279.
- Vega-Avila, E. & Pugsley, M. K. (2011). An overview of colorimetric assay methods used to assess survival or proliferation of mammalian cells. *Proceedings of the Western Pharmacology Society*, 54, 10-14.
- Velichkova, R. S. & Christova, D. C. (1995). Amphiphilic polymers from macromonomers and telechelics. *Progress in Polymer Science*, 20(5), 819-887.
- Vinardell, M. P. & Mitjans, M. (2008). Alternative methods for eye and skin irritation tests: An overview. *Journal of Pharmaceutical Sciences*, 97(1), 46-59.
- Volker, W., Bärbel, H. & Sibylle, G. (2008). Nanomedicine - drivers for development and possible impacts Retrieved 13/03/2013, 2013, from <http://publications.jrc.ec.europa.eu/repository/handle/111111111/2859>
- Wang, P., Henning, S. M. & Heber, D. (2010). Limitations of MTT and MTS-based assays for measurement of antiproliferative activity of green tea polyphenols. *Plos One*, 5(4), e10202.
- Wang, W., McConaghy, A. M., Tetley, L. & Uchegbu, I. F. (2001). Controls on polymer molecular weight may be used to control the size of palmitoyl glycol chitosan polymeric vesicles. *Langmuir*, 17(3), 631-636.
- Wang, W., Qu, X., Gray, A. I., Tetley, L. & Uchegbu, I. F. (2004). Self-assembly of cetyl linear polyethylenimine to give micelles, vesicles, and dense nanoparticles. *Macromolecules*, 37(24), 9114-9122.
- Wang, Y. X., Tan, Y. B., Huang, X. L., Che, Y. J. & Du, X. (2009). Synthesis of Biodegradable Amphiphilic Thermo-Responsive Multiblock Polycarbonate and Its Self-Aggregation Behavior in Aqueous Solution. *Journal of Applied Polymer Science*, 112(3), 1425-1435.

- Watson, P. G., Hazleman, B. L., McCluskey, P. & Pavesio, C. (2012). *The sclera and systemic disorders*: JP Medical Ltd.
- Watson, P. G. & Young, R. D. (2004). Scleral structure, organisation and disease. A review. *Exp Eye Res*, 78(3), 609-623.
- Williams, A. (2003). *Transdermal and topical drug delivery*: Pharmaceutical Press.
- Willoughby, C. E., Ponzin, D., Ferrari, S., Lobo, A., Landau, K. & Omidi, Y. (2010). Anatomy and physiology of the human eye: effects of mucopolysaccharidoses disease on structure and function – a review. *Clinical & Experimental Ophthalmology*, 38, 2-11.
- Wilson, C. G., Semenova, E. M., Hughes, P. M. & Olejnik, O. (2006). Eye structure and physiological functions *Enhancement in Drug Delivery* (pp. 656 ): CRC Press.
- Wilson, C. G., Zhu, Y. P., Kurmala, P., Rao, L. S. & Dhillon, B. (2001). Ophthalmic drug delivery *Drug Delivery and Targeting For Pharmacists and Pharmaceutical Scientists* (pp. 481): Taylor and Francis.
- Wilson, W. S., Shahidullah, M. & Millar, C. (1993). The bovine arterially-perfused eye: an in vitro method for the study of drug mechanisms on IOP, aqueous humour formation and uveal vasculature. *Current Eye Research*, 12(7), 609-620.
- Wong, V. H. Y., Bui, B. V. & Vingrys, A. J. (2011). Clinical and experimental links between diabetes and glaucoma. *Clinical and Experimental Optometry*, 94(1), 4-23.
- Wood, D. G., Brown, M. B. & Jones, S. A. (2012). Understanding heat facilitated drug transport across human epidermis. *European Journal of Pharmaceutics and Biopharmaceutics*, 81(3), 642-649.
- Wu, X., Qiao, Y., Yang, H. & Wang, J. (2010). Self-assembly of a series of random copolymers bearing amphiphilic side chains. *Journal of Colloid and Interface Science*, 349(2), 560-564.
- Xiong, X.-B., Binkhathlan, Z., Molavi, O. & Lavasanifar, A. (2012). Amphiphilic block co-polymers: preparation and application in nanodrug and gene delivery. *Acta Biomaterialia*, 8(6), 2017-2033.
- Xu, J. K., Li, X. S. & Sun, F. Q. (2011). In vitro and in vivo evaluation of ketotifen fumarate-loaded silicone hydrogel contact lenses for ocular drug delivery. *Drug Delivery*, 18(2), 150-158.
- Xu, J. P., Ji, J., Chen, W. D. & Shen, J. C. (2005). Novel biomimetic surfactant: Synthesis and micellar characteristics. *Macromolecular Bioscience*, 5(2), 164-171.
- Xu, Q., Boylan, N. J., Suk, J. S., Wang, Y.-Y., Nance, E. A., Yang, J.-C., *et al.* (2013). Nanoparticle diffusion in, and microrheology of, the bovine vitreous ex vivo. *Journal of Controlled Release*, 167(1), 76-84.
- Yamamoto, T., Kitazawa, Y., Azuma, I., Tsukahara, S. & Nakashima, M. (1997). Clinical evaluation of a new formula of timolol maleate (WP-934 ophthalmic solution). *Japanese Journal of Ophthalmology*, 41(4), 244-250.
- Yang, C. M., Jiang, L. Q., Bu, S. J., Zhang, L. H., Xie, X. J., Zeng, Q. G., *et al.* (2013). Intravitreal administration of dexamethasone-loaded PLGA-TPGS nanoparticles for the treatment of posterior segment diseases. *Journal of Biomedical Nanotechnology*, 9(9), 1617-1623.
- Yang, Y. Q., Guo, X. D., Lin, W. J., Zhang, L. J., Zhang, C. Y. & Qian, Y. (2012). Amphiphilic copolymer brush with random pH-sensitive/hydrophobic structure: synthesis and self-assembled micelles for sustained drug delivery. *Soft Matter*, 8(2), 454-464.
- Yanoff, M. & Duker, J. S. (2008). *Ophthalmology* (Vol. 3): Mosby.
- Yanoff, M., Duker, J. S. & Augsburger, J. J. (2004). *Ophthalmology* (2nd ed.). St. Louis, MO: Mosby.

- Yao, J., Ruan, Y., Zhai, T., Guan, J., Tang, G., Li, H., *et al.* (2011). ABC block copolymer as “smart” pH-responsive carrier for intracellular delivery of hydrophobic drugs. *Polymer*, 52(15), 3396-3404.
- Yasukawa, T., Ogura, Y., Tabata, Y., Kimura, H., Wiedemann, P. & Honda, Y. (2004). Drug delivery systems for vitreoretinal diseases. *Prog Retin Eye Res*, 23(3), 253-281.
- Yeung, C. K., Chan, K. P., Chiang, S. W., Pang, C. P. & Lam, D. S. (2003). The toxic and stress responses of cultured human retinal pigment epithelium (ARPE19) and human glial cells (SVG) in the presence of triamcinolone. *Invest Ophthalmol Vis Sci*, 44(12), 5293-5300.
- Yorio, T., Clark, A. & Wax, M. B. (2011). *Ocular therapeutics: eye on new discoveries*: Academic Press.
- Young, R. D. (1985). The ultrastructural organization of proteoglycans and collagen in human and rabbit scleral matrix. *Journal of Cell Science*, 74(MAR), 95-104.
- Yu, J.-M., Li, Y.-J., Qiu, L.-Y. & Jin, Y. (2008). Self-aggregated nanoparticles of cholesterol-modified glycol chitosan conjugate: Preparation, characterization, and preliminary assessment as a new drug delivery carrier. *European Polymer Journal*, 44(3), 555-565.
- Yuan, X.-b., Li, H. & Yuan, Y.-b. (2006). Preparation of cholesterol-modified chitosan self-aggregated nanoparticles for delivery of drugs to ocular surface. *Carbohydrate Polymers*, 65(3), 337-345.
- Yue, P. F., Yuan, H. L., Yang, M., You, R. H., Cong, L. B., Zhu, J., *et al.* (2008). Preparation, characterization, and pharmacokinetic evaluation of puerarin submicron emulsion. *PDA J Pharm Sci Technol*, 62(1), 32-45.
- Yusa, S., Hashidzume, A. & Morishima, Y. (1999). Interpolymer association of cholesterol pendants linked to a polyelectrolyte as studied by quasielastic light scattering and fluorescence techniques. *Langmuir*, 15(26), 8826-8831.
- Yusa, S., Kamachi, M. & Morishima, Y. (1998). Hydrophobic self-association of cholesterol moieties covalently linked to polyelectrolytes: Effect of spacer bond. *Langmuir*, 14(21), 6059-6067.
- Zambito, Y., Zaino, C. & Di Colo, G. (2006). Effects of N-trimethylchitosan on transcellular and paracellular transcorneal drug transport. *European Journal of Pharmaceutics and Biopharmaceutics*, 64(1), 16-25.
- Zhang, C. Y., Yang, Y. Q., Huang, T. X., Zhao, B., Guo, X. D., Wang, J. F., *et al.* (2012). Self-assembled pH-responsive MPEG-b-(PLA-co-PAE) block copolymer micelles for anticancer drug delivery. *Biomaterials*, 33(26), 6273-6283.
- Zhang, L., Li, Y., Zhang, C., Wang, Y. & Song, C. (2009). Pharmacokinetics and tolerance study of intravitreal injection of dexamethasone-loaded nanoparticles in rabbits. *International Journal of Nanomedicine*, 4, 175-183.
- Zhang, X., Jackson, J. K. & Burt, H. M. (1996). Development of amphiphilic diblock copolymers as micellar carriers of taxol. *International Journal of Pharmaceutics*, 132(1-2), 195-206.
- Zhu, H., Liu, F., Guo, J., Xue, J., Qian, Z. & Gu, Y. (2011). Folate-modified chitosan micelles with enhanced tumor targeting evaluated by near infrared imaging system. *Carbohydrate Polymers*, 86(3), 1118-1129.
- Zhu, L., Zhao, L., Qu, X. & Yang, Z. (2012). PH-sensitive polymeric vesicles from coassembly of amphiphilic cholate grafted poly(l-lysine) and acid-cleavable polymer–drug conjugate. *Langmuir*, 28(33), 11988-11996.

## Appendix A

### Markers Permeations Fluxes

Table 1: Summary of the flux of 10 kDa FITC-Dextran added to various enhancers and elevated temperature through human corneal and scleral tissues and porcine scleral tissue.

Enhancer	Human Cornea Flux $\pm$ S.D. ( $\mu\text{g}\cdot\text{cm}^{-2}\cdot\text{h}^{-1}$ )	Human Sclera Flux $\pm$ S.D. ( $\mu\text{g}\cdot\text{cm}^{-2}\cdot\text{h}^{-1}$ )	Porcine Sclera Flux $\pm$ S.D. ( $\mu\text{g}\cdot\text{cm}^{-2}\cdot\text{h}^{-1}$ )
Control	83.5 $\pm$ 40.3	362.4 $\pm$ 119.5	105.0 $\pm$ 27.5
0.1% Glutamic Acid	29.6 $\pm$ 10.4	387.0 $\pm$ 156.3	157.8 $\pm$ 62.4
0.001% Tween 80	155.3 $\pm$ 68.5	280.8 $\pm$ 96.2	109.4 $\pm$ 40.8
0.01% Tween 80	134.8 $\pm$ 52.2	334.8 $\pm$ 135.8	150.0 $\pm$ 23.9
45 °C	187.5 $\pm$ 80.6	425.1 $\pm$ 222.1	152.3 $\pm$ 33.1
Pa5 polymer	92.2 $\pm$ 3.8	256.1 $\pm$ 119.1	122.0 $\pm$ 41.9
Acetate Buffer pH 5	121.6 $\pm$ 88.6	423.3 $\pm$ 169.6	124.4 $\pm$ 41.1
0.5% Chitosan	51.7 $\pm$ 13.9	449.0 $\pm$ 65.8	123.7 $\pm$ 42.2

Table 2: Summary of the flux of fluorescein sodium salt, 4, 10 and 20 kDa FITC-Dextran through human and porcine ocular tissues.

Marker	Sclera		Cornea	
	Human Flux $\pm$ S.D. ( $\mu\text{g}\cdot\text{cm}^{-2}\cdot\text{h}^{-1}$ )	Porcine Flux $\pm$ S.D. ( $\mu\text{g}\cdot\text{cm}^{-2}\cdot\text{h}^{-1}$ )	Human Flux $\pm$ S.D. ( $\mu\text{g}\cdot\text{cm}^{-2}\cdot\text{h}^{-1}$ )	Porcine Flux $\pm$ S.D. ( $\mu\text{g}\cdot\text{cm}^{-2}\cdot\text{h}^{-1}$ )
Fluorescein sodium salt	188.0 $\pm$ 35.9	99.5 $\pm$ 15.8	128.5 $\pm$ 10.9	27.5 $\pm$ 5.9
4 KDa FITC-Dextran	745.0 $\pm$ 153.5	352.0 $\pm$ 93.0	201.0 $\pm$ 27.0	28.2 $\pm$ 7.6
10 KDa FITC-Dextran	434 $\pm$ 105	299.6 $\pm$ 55.7	49.4 $\pm$ 19.5	30.6 $\pm$ 9.0
20 KDa FITC-Dextran	426 $\pm$ 164	284.6 $\pm$ 154.9	53.9 $\pm$ 18.4	42.1 $\pm$ 25.8



## Appendix B

### STANDARD OPERATING PROCEDURE (SOP) – ORGAN CULTURE STORAGE OF CORNEAS

#### A. Purpose

Deceased donor selection guidelines for tissue donors allows for the storage of corneas in organ culture media. This is mainly performed for donor eyes where the donor has either recovered from a systemic infection within two weeks of death or suffered from a bacterial infection at the time of death. This procedure defines the steps to be taken when storing corneoscleral buttons in organ culture media.

#### B. Definitions

**Septic** Term used by the eye bank to define the status of a donor that had a bacterial infection at the time of death or within two weeks prior to death. All septic donations must be stored in organ culture media.

#### C. Materials and equipment

Procedure labels

Media thaw label

Corneal storage label

Tissue labels (created by the eye bank database)

1 x bottle of Povidone Iodine 5% w/v (or 3 x bottles of eye drops)

1 x bottle of Normal Saline 0.9% w/v

1 x bottle of Framycetin 0.5% v/v

1x bottle 70% Alcohol for storage of sclera in alcohol (if required)

1 x corneal excision pack containing a trephine, 2 forceps, 2 scissors, scalpel

1 x blue eye bank pack containing a tray, 4 large gallipots, 2 small gallipots (not required for this procedure), gauze swabs

1x sterile suture

2 x organ culture media (defrosted)

2 x sampling caps

1 x sterile microbiology tube

6 x sterile pots (for sclera storage – if required)

4 x TSA settle plates for environmental monitoring

1 x sterile gloves

Donor eyes in containers

Donning gloves, clean room suit, mask, clean room boots, sterile gloves

Sterile alcohol spray.



#### **D. Safety Concerns**

Cornea preparation and transfer and all microbiology testing must be carried out in class two biological cabinets in the GMP Grade B room. Personnel protective equipment provided (cleanroom clothing, gloves and masks) as described in MLEB SOPC 2.2 and C2.3 must be worn during processing of tissue.

Only one donation should be processed at a time. The cabinet and work surfaces should be emptied and cleaned before a second donation is processed.

The tissue label should be applied to the organ culture bottle before they are taken into the grade B room.

#### **E. Responsibilities**

The Eye Bank Technicians for performing the procedure as described and report any deviations. The Eye Bank Manager to ensure that the Technicians are trained to perform the procedure.

#### **F. Procedure**

##### **Corneal button storage - Preparation of media**

The media is stored at -20°C and should be thawed at ambient room temperature (~4hrs) or at 30°C using the water bath (~30mins). Water in water bath should be supplemented with a water bath cleanse solution prior to heating – this will remove any microbes from the water. Sufficient time should be allowed to thaw the media before the processing of tissue begins, as introduction of the cornea to media not thawed sufficiently may cause damage to the endothelial cells.

On removal from the freezer a 'media thaw label' must be applied providing the following information

- Date of removal
- Time of removal
- Operator

The media cannot be refrozen once thawed, but will remain suitable for use for up to five days when stored at +4°C and remains unopened. Media not used within this timeframe must be destroyed

##### **Corneal button dissection**

Prior to entering the cleanroom suite ensure room pressures are within the required range and recorded on the Room Pressure Log (this is a daily activity, the pressure may have already been recorded, but it is good practice to visually check the pressure reading before entering the cleanroom suite).

##### **In preparation room:**



1. Place batch labels from items on the batch record for organ culture storage form
2. Disinfect hands with alcohol gel
3. Put on gloves.
4. Spray alcohol and wipe inside of pass through
5. Place items in lower section of pass through. Spray or wipe with sterile alcohol.
6. Where sterile products are double wrapped – remove the outer packing layer and place into the pass through without touching the inner packaging.

**Move through areas:**

7. Move to entrance of change room 2
8. Change into clean room apparel as per MLEB SOP C2.2

**In the cleanroom**

9. Move into processing room and remove items from clean room pass through.
10. Check safety cabinet pressure is correct and wipe / spray interior surface with sterile alcohol.
11. Wipe area to layout equipment on work surface.
12. Place and expose environmental monitoring settle plates as per MLEB SOP I1.1
13. Open blue pack out into cabinet and create a sterile field.
14. Open all other sterile equipment onto the sterile field.
15. Spray down all non sterile products with ethanol and place into the cabinet adjacent to the sterile field.
16. Open and fill (*non-touch*) gallipots with:
  - i. Framycetin
  - ii. Saline x 2
  - iii. Povidone iodine
17. Put on second pair of sterile gloves to begin the processing session.
18. Transfer globes into the first pot of povidine iodine using forceps.
19. Discard pots and forceps.
20. Eyes soaked as follows:
  - i. Povidone iodine x 3 minutes
  - ii. Then saline wash
  - iii. Framycetin x 3 minutes



iv. Final rinse in saline.

An alarm clock is provided to ensure that time limits are not exceeded, and should be used in all cases.

*Note: Should Framycetin not be available use Gentamycin as alternative or take advice from Pharmacy (Gentamycin dilution – 4 vials (80mg/2ml) per 100mls sterile NaCl). An additional 3 minutes in Framycetin/Gentamycin can be performed if the donor had systemic sepsis prior to death.*

21. Invert the media gently a number of times, remove the tamper proof cap from the organ culture media, leave the cap over the bottle top until the cornea button is ready to be added to the media. *Note – this is a single use cap so will be discarded and replaced with a new cap once the button has been added to the media.*
22. Place a knot in the end of the suture in preparation to suspend the cornea.
23. Remove 1 globe from final saline wash.
24. Wrap a sterile gauze swab round the globe. Hold the globe gently.
25. Dissect off conjunctiva.
26. Incise 360 degrees about 4-5 mm from the limbus with the trephine, and knife and complete with corneal scissors. Adjust tension if ciliary body bulges.

**Important:**

**Maintain the anterior chamber as long as possible.**

**Do not distort the cornea.**

**Do not touch the endothelium**

27. Lift cornea, with minimal distortion, prepare the cornea for suspension in the media using the suture through the sclera. *Note – work from the epithelium side in to ensure the endothelial surface is protected from the suture.*
28. Once the cornea is at the end of the thread use the suture to secure the cornea to the side of the gray sampling cap bung, take the thread from the inside of the cap to the outside close the bung.
29. Lower the cornea in to the media, take care not to touch the outer surface of the bottle. Close container with a sterile sampling cap. Make sure the cornea is suspended half way into the media and is not touching the bottom or too close to the top of the media. Media will be removed as part of the microbiology testing and may lead to exposure of the cornea if suspended too close to the top of the bottle.
30. Take a sample of the sclera for microbiology testing and place into the designated sterile tube.

**Important – sclera storage**



**Sclera can be stored for transplant if infection at the time of death was**

- not eye related
- not systemic
- not viral

31. If sclera is to be stored follow MLEB/SOP E1.5 or E1.7. Place all internal eye structures into a separate container for transfer to research or appropriate discard.
32. Repeat for second eye
33. Place all used equipment, wrappings and materials in bottom shelf of pass through.
34. Place ocular tissue on top shelf of pass through.
35. Remove all rubbish and tidy room and wipe down surfaces and safety cabinet with disinfectant and sterile alcohol spray.
36. Leave corneal storage room and go to second change area to remove clean suit and boots – according to MLEB/SOP C2.4 Leaving grade B and C areas

**In preparation room:**

37. Remove containers with corneas from pass through d (and scleral tissue if prepared).
38. Add the corneal storage label to each of the organ culture bottles and record the following information
  - a. Date of storage
  - b. Time of storage
  - c. Operator
39. Place organ culture bottles into the +31°C incubator designated as the 'quarantine one'.
40. Remove equipment, wrappings and instruments from pass through d. Clean pass through with sterile Alcohol spray and low lint wipes.
41. The labelled tissue containers (sclera and retina if research if applicable) and batch record form is placed on the top shelf of pass through a.
42. Clinical waste should be placed on the lower shelf to be moved into the receiving room for disposal.
43. The preparation room is tidied and the work surface is wiped down with disinfectant and sterile alcohol.
44. The technician then moves to change room 1.

**In the receiving room:**



45. Place labelled sclera containers in quarantine tray into the quarantine refrigerator
46. Remove clinical waste bag and place in clinical waste bin
47. Remove waste fluid bottle and dispose of fluids in trap waste.
48. Clean waste trap, sink and surface areas (including pass through a) using alcohol spray.

#### **In office**

49. Update donor file with time of storage and processing comments.
50. Place notes and batch record form in file and place file in tissue in quarantine (organ culture).
51. Update the donor database and add date of 7 day microbiology test in the lab diary.

#### **Maximum storage period and microbiology testing**

52. Microbiology testing must be carried out on day seven (or later) of storage – see MLEB SOP E1.11 Microbiology testing of corneas in organ culture
53. The maximum storage time for corneas in organ culture is 28 days. This can be extended to 30 days on agreement form the Eye Bank Manager.
54. Corneas must be stored at +31°C +/-2°C whilst in organ culture media. If the temperature exceeds 37°C at any point the graft will no longer be deemed suitable for corneal grafting.

#### **G. Records to be kept**

All records will be kept for 30 years from the use or disposal of the tissue.

#### **H. Copies of forms**

MLEB FORM Batch record for organ culture storage

MLEB/FORM Organ culture processing and microbiology results form

#### **I. References**

HTA Directions

Manufacturer Guidelines – Eurobio

MLEB SOP C2.2 People moving from preparation room to cleanrooms

MLEB SOP C2.3 People moving from receiving room area to preparation area

MLEB SOP I1.1 Sessional monitoring

MLEB SOP E1.11 Microbiology testing of corneas in organ culture



MLEB SOP C2.4 Leaving Grade B and Grade C areas

MLEB SOP E1.5 Preparing and storing sclera in alcohol